# Interactions and S-acylation of Sprouty and SPRED proteins

by

**Liam Butler**

In fulfilment of the requirement for the degree of

**Doctor of Philosophy**

**2023**

**University of Strathclyde**

Strathclyde Institute of

Pharmacy and Biomedical Sciences

## Declaration of authenticity and authors rights

*This thesis is the result of the author's original research. It has been composed by the author and has not been previously submitted for examination which has led to the award of a degree.*

*The copyright of this thesis belongs to the author under the terms of the United Kingdom Copyright Acts as qualified by University of Strathclyde Regulation 3.50. Due acknowledgement must always be made of the use of any material contained in, or derived from, this thesis.*

*Signed:* 

*Date:* ***05/11/2023***

## Acknowledgements

First and foremost, I would like to give the biggest thanks to my supervisor ***Prof. Luke Chamberlain*** for taking a chance on me (twice). I am extremely grateful and could not have wished for a better mentor. Your unwavering patience and support are truly appreciated. If I had to do my PhD again, I would pick your lab every time. Not only for the academic direction you have given me, but also the professional freedom and personal encouragement. Both of which are a big part of why I have succeeded to this point, feel like I have achieved so much, and enjoyed my PhD.

I would also like to give major thanks to **Dr. Christine Salaun.** I would not be half the scientist that I am today without everything you have taught me. I appreciate you and everything you have done for me. Wherever possible I will try to get a Terry's chocolate orange (*made in France*) to you at Christmas. I would also like to thank both **Dr. Carolina Locatelli** and **Dr. Kimon Lemonidis** for their help, guidance, contribution, and previous work that this thesis has built upon.

Special thanks should also go to **Debbie**, I am so lucky that you joined the lab, and I could not have asked for a better friend and squash rival. Thanks also to **Iona, Mohammad, Ash, Carla, Shervone, Filip,** and everyone else who came through the lab. I have been in Strathclyde/SIPBS for quite a while by this point, and every person that I have met over the years has made the experience unique, funny, memorable, worthwhile, and overall, better for having met each person. Thanks to you all!

❖

***To my family,*** you have, you do, and you will, inspire me. Thank you for everything you have done for me, as it has given me everything I have now. I couldn't ask for a better support system from the people who I know believe in me no matter what I do.

***To my friends,*** thank you for being the people I can rely on and for being there when I needed a break. Whether it is a just a day, a weekend, or the odd week abroad, it always feels to me like nothing has changed.

***To my Amie,*** *my best friend, my fiancée, and soon to be my wife.* Every challenge, change, achievement, and joy, which has been mine/ours to face over the past six years would not have been possible without your love and support at every step. Thank you with all my heart.

***- It has been for me, but it is for all of you.***
***Liam***

## Publications

### Research articles

***Butler, L.,*** *Locatelli, C., Allagioti, D., Lousa, I., Lemonidis, K., Tomkinson, N. C. O., Salaun, C., & Chamberlain, L. H. (2023). S-acylation of Sprouty and SPRED proteins by the S-acyltransferase zDHHC17 involves a novel mode of enzyme-substrate interaction. The Journal of Biological Chemistry, 299(1), 102754. https://doi.org/10.1016/j.jbc.2022.102754.*

### Magazine articles

***Butler, L.,*** (2023) *FASEB Protein Lipidation Conference: Enzymology, Signalling, and Therapeutics, 31 July – 5 August 2022. Vermont, USA.* British Society for Cell Biology Magazine, page 25.

### Oral communications

***Butler, L.,*** *Locatelli, C., Allagioti, D., Lemonidis, K., Tomkinson, N. C. O., Salaun, C., & Chamberlain, L. H. (2023). Interactions and S-acylation of Sprouty & SPRED proteins. The Biochemical Society: New Insights into Lipidation in Cell Biology, Liverpool, UK.*

***Butler, L.,*** *Locatelli, C., & Chamberlain, L. H. (2021). Interactions & S-acylation of Spry & SPRED proteins by zDHHC17.* The Biochemical Society: Lipidation in cell biology and disease 2021, virtual, international.

### Poster communications

***Butler, L.,*** *Locatelli, C., Allagioti, D., Lemonidis, K., Tomkinson, N. C. O., Salaun, C., & Chamberlain, L. H. (2023). Interactions and S-acylation of Sprouty & SPRED proteins. The Biochemical Society: New Insights into Lipidation in Cell Biology, Liverpool, UK.*

***Butler, L.,*** *Locatelli, C., Salaun, C., Allagioti, D., & Chamberlain, L. H. (2022). Forming the connection between zDHHC17 and Sprouty/SPRED proteins.* The Federation of American Societies for Experimental Biology Science international research conference. FASEB: The Protein Lipidation Conference: Enzymology, Signalling and Therapeutics 2022, VT, USA.

***Butler, L.,*** *Locatelli, C., & Chamberlain, L. H. (2021). Interactions & S-acylation of Spry & SPRED proteins by zDHHC17.* The Biochemical Society: Lipidation in cell biology and disease 2021, virtual, international.

***Butler, L.,*** *Locatelli, C., & Chamberlain, L. H. (2021). Interactions & S-acylation of Spry & SPRED proteins by zDHHC17.* The Federation of American Societies for Experimental Biology Science international research conference. FASEB: The Protein Lipidation Conference: Enzymology, Signalling and Therapeutics 2021 virtual, international.

***Butler, L.,*** *& Chamberlain, L. H. (2020). Detection of Sprouty-2 protein S-acylation using click chemistry.* Strathclyde Institute of Pharmacy and Biological Sciences PhD research day. University of Strathclyde, Glasgow, UK.

## Table of contents

## List of figures

### Chapter 1



### Chapter 3

**Chapter 5**

**Chapter 6**

## List of tables

### Chapter 1



### Chapter 2

## Abbreviations

| | |
|---|---|
| 2-BP | 2-Bromopalmitate (zDHHC enzymes/S-acylation inhibitor) |
| aa | Amino acid |
| ABE | Acyl-biotin exchange |
| ABHD | α/β hydrolase domain-containing proteins |
| ABHD17 A-C | α/β hydrolase domain-containing proteins 17 A-C |
| ACE2 | Angiotensin-converting enzyme 2 |
| AI | Artificial intelligence |
| AK | Alkyne |
| AK800 | Alkyne conjugated Infrared reporter of 800 nm |
| AMPA | α-amino-3-hydroxy-5-methyl-4-isoxazolepropionic acid |
| ANCL | Adult-onset neuronal ceroid lipofuscinosis |
| Ank | Ankyrin repeat domain |
| ANOVA | Analysis of variance |
| APS | Ammonium persulfate |
| APT1 | Acyl-protein thioesterases 1 |
| APT2 | Acyl-protein thioesterases 2 |
| AR | Ankyrin repeat |
| ATP | Adenosine triphosphate |
| AZ | Azide |
| BAK1 | BRI1-associated receptor kinase 1 |
| Bid | BH3-interacting-domain death agonist |
| BK Channel | Big potassium channels; large conductance calcium-activated potassium channels |

| | |
|---|---|
| Bnl-FGF | Branchless homolog of fibroblast growth factor |
| BRAC1 | Breast cancer type 1 gene/protein |
| BSA | Bovine serum albumin |
| BST-2 | Bone marrow stromal antigen 2; also known as tetherin |
| C14:0 | Myristic acid |
| C16:0 | Palmitic acid |
| C18:0 | Stearic acid |
| CaaX | CaaX box prenylation motif |
| Cas9 | CRISPR associated protein 9 |
| Cav-1 | Caveolin-1 |
| CBL | Casitas B-linage lymphoma protein |
| CCR5 | C-C chemokine receptor type 5 |
| CD61 | Cluster of differentiation 61; also known as integrin beta-3 |
| CHH | Congenital hypogonadotropic hypogonadism |
| CHX | Cycloheximide |
| c-KIT | Receptor tyrosine-protein kinase KIT |
| CoA | Co-enzyme A |
| COVID-19 | Coronavirus disease 2019 |
| CRD | Cysteine-rich domain |
| CRISPR | Clustered regularly interspaced short palindromic repeats |
| CSPα | Cysteine string protein alpha |
| ctBid | BH3-interacting-domain death agonist with exposed C-terminal glycine |
| $_dH_2O$ | Distilled water |

| | |
|---|---|
| DHHC | Aspartic acid – histidine – histidine – cysteine motif |
| DM | C265A/C268A (of mSpry2) |
| DMEM | Dulbecco's modified eagle medium |
| DMSO | Dimethyl sulfoxide |
| DNA | Deoxyribonucleic acid |
| DNAJC5 | DnaJ (Hsp40) homolog, subfamily C, member 5; also known as CSPα |
| dNTPs | Deoxynucleotide Triphosphates |
| DPG | Asp-Pro-Gly motif |
| DRM | Detergent-resistant membranes |
| DTT | Dithiothreitol |
| EDTA | Ethylenediaminetetraacetic acid |
| EGF | Epidermal growth factor |
| EGFP (-tag) | Enhanced green fluorescent protein |
| EGFR | Epidermal growth factor receptor |
| eNOS | Endothelial nitric-oxide synthase |
| EOC | Epithelial ovarian cancer |
| ER | Endoplasmic reticulum |
| ERGIC | Endoplasmic reticulum–Golgi intermediate compartment |
| ERK | Extracellular signal-related kinase |
| ERK1/2 | Extracellular signal-regulated kinases 1/2 |
| EVH1 | Enabled/vasodilator-stimulated phosphoprotein homology 1 domain |
| FBS | Foetal bovine serum |
| FGF | Fibroblast growth factor |

| | |
|---|---|
| FLS2 | Plant receptor kinase flagellin sensing 2 protein |
| FTase | Farnesyltransferase |
| GAB1 | Grb2-associated binding protein 1 |
| GABA | Gamma-aminobutyric acid |
| GAP-43 | Growth associated protein 43 |
| GCP16 | Golgi complex-associated protein of 16 kDa; also known as Golgin subfamily A member 7 |
| GDP | Guanosine diphosphate |
| GEF | Guanine nucleotide exchange factor |
| GGTase | Geranyl-geranyl transferase |
| GnRH | Gonadotropin-releasing hormone |
| GPCR | G-protein coupled receptor |
| GPI | Glycosylphosphatidylinositol |
| GRB2 | Growth factor-bound protein 2 |
| GRIP | Glutamate receptor-interacting protein |
| gRNA | Viral genomic ribonucleic acid |
| GTP | Guanosine triphosphate |
| Gα | G alpha subunit |
| Gβ | G beta subunit |
| Gγ | G gamma subunit |
| HA (-tag) | Human influenza hemagglutinin |
| HD | Huntington’s disease |
| HEK-293T | Human embryonic kidney 293 cells that express a mutant of the SV40 large T antigen |
| HIV | Human immunodeficiency virus |
| HTT | Huntingtin protein |

| | |
|---|---|
| ID | Intellectual disability |
| IFN | Interferon |
| IgG | Immunoglobulin G |
| INCL | Infantile neuronal ceroid lipofuscinosis |
| IP | Immunoprecipitation |
| IR680 | Infrared reporter of 680 nm |
| IR800 | Infrared reporter of 800 nm |
| ITSN1 | Intersectin 1 |
| JAK/STAT | Janus kinases/signal transducer and activator of transcription proteins |
| JNK | C-Jun N-terminal kinase |
| KBD | c-Kit-binding domain |
| kDa | Kilodalton |
| KO | Knockout |
| Kv1 | Associated Type-I voltage-gated potassium channels |
| LRP6 | Lipoprotein-receptor-related protein 6 |
| MAP | Mitogen activated protein |
| MAP3K | Mitogen-activated protein kinase kinase kinase |
| MAP6 | Microtubule-associated protein 6 |
| MAPK | Mitogen-activated protein kinase |
| MAPK2K | Mitogen-activated protein kinase kinase; also known as MEK |
| MCS | Multiple cloning site |
| MDM2 | Mouse double minute 2 homolog |
| METTL13 | Methyltransferase-like protein 13 |
| mHTT | Mutant Huntingtin protein |

| | |
|---|---|
| MnK1 | Mitogen-activated kinase-interacting kinase 1 |
| mPEG | Methoxypolyethylene glycol |
| mRNA | Messenger ribonucleic acid |
| Msh | Metabolic serine hydrolase |
| Na-Pump | Sodium-potassium ATPase |
| NCL | Neuronal ceroid lipofuscinosis |
| NDK | N211A/D214A/K223A (of mSpry2) |
| Nedd4 | Neural precursor cell expressed developmentally down-regulated protein 4 |
| NF1 | Neurofibromin |
| NGF | Nerve growth factor |
| NMT1 | N-myristaltransferease 1 |
| NMT2 | N-myristaltransferease 2 |
| NSP | Non-structural protein |
| Orf3d | Open reading frame protein 3d (57 aa) |
| Orf3d-2 | Open reading frame protein 3d (33 aa) |
| p38 | p38 mitogen-activated protein kinases |
| P53 | Tumour protein P53 |
| PaCCT | Palmitoyltransferase conserved C-terminal motif |
| PAGE | Polyacrylamide gel electrophoresis |
| PBS | Phosphate-buffered saline |
| PBS-T | Phosphate buffered saline containing 0.1 % Tween-20 |
| PC12 | Cell line derived from a pheochromocytoma of the rat adrenal medulla |
| PCR | Polymerase chain reaction |

| | |
|---|---|
| PDZ | Post synaptic density protein, Drosophila disc large tumour suppressor, and Zonula occludens-1 protein domain |
| pEF | pEF-BOS-HA plasmid |
| PEI | Polyethyleneimine |
| p-ERK | Phosphorylated extracellular signal-related kinase |
| PI-3K | Phosphoinositide 3-kinases |
| PIP2 | Phosphatidylinositol 4,5-bisphosphate |
| PKD | Protein kinase D |
| PLCβ | Phospholipase C beta |
| PLM | Phospholemman |
| PM | Plasma membrane |
| PNDK | P154A/N211A/D214A/K223A (of mSpry2) |
| polyQ | Expanded polyglutamine |
| PP2A | Protein phosphatase 2A |
| PPI | Protein-protein interaction |
| PPT1 | Palmitoyl-protein thioesterases 1 |
| PPT2 | Palmitoyl-protein thioesterases 2 |
| PSD93 | Postsynaptic density protein 93 |
| PSD95 | Postsynaptic density protein 95 |
| PTM | Post-translational modifications |
| Rab | Ras analogy in brain protein |
| RAF | Rapidly accelerated fibrosarcoma kinase |
| RAS | Rat sarcoma virus protein |
| Rce1 | CaaX prenyl protease 2 |
| RNA | Ribonucleic acid |

| | |
|---|---|
| RNAi | Ribonucleic acid interference |
| RPMI | Roswell park memorial institute 1640 medium |
| RTK | Receptor tyrosine kinase |
| RT-PCR | Reverse transcription polymerase chain reaction |
| SARS-CoV | Severe acute respiratory syndrome coronavirus |
| SARS-CoV-2 | Severe acute respiratory syndrome coronavirus 2 |
| Scrib | Scribble protein |
| SDS | Sodium dodecyl sulfate |
| SDS-PAGE | Sodium dodecyl sulfate polyacrylamide gel electrophoresis |
| SEM | Standard error mean |
| SH3 | Src homology 3 domain |
| SHP-2 | Src homology-2 domain-containing protein tyrosine phosphatase-2 |
| shRNA | Short hairpin ribonucleic acid |
| siRNA | Small interfering ribonucleic acid |
| SNAP23 | Synaptosomal-associated protein of 23 kDa |
| SNAP25 | Synaptosomal-associated protein of 25 kDa |
| SNARE | Synaptosomal-associated protein receptors |
| SOS | Son of sevenless protein |
| SPR | Sprouty domain |
| SPRED | Sprouty-related EVH1 domain containing protein |
| SPRED1 | Sprouty-related EVH1 domain containing protein 1 |
| SPRED2 | Sprouty-related EVH1 domain containing protein 2 |
| SPRED3 | Sprouty-related EVH1 domain containing protein 3 |
| Spry | Sprouty protein |

| | |
|---|---|
| Spry1 | Sprouty-1 protein |
| Spry2 | Sprouty-2 protein |
| Spry3 | Sprouty-3 protein |
| Spry4 | Sprouty-4 protein |
| STOML2 | Stomatin-like protein 2 |
| STREX | Stress-regulated exon |
| TEM8 | Tumour endothelial marker 8; also known as anthrax toxin receptor 1 |
| TEMED | N,N,N',N'-tetramethylethane-1,2-diamine |
| TESK1 | Dual specificity testis-specific protein kinase 1 |
| TGCT | Testicular germ cell tumours |
| TKBD | Tyrosine kinase binding domain |
| TMD | Transmembrane domain |
| TMPRSS2 | Transmembrane serine protease 2 |
| TNFR | Tumour necrosis factor receptor |
| TPS | Total protein stain |
| TrkA | Tropomyosin receptor kinase A |
| TTxE | Thr-Thr-x-Glu motif |
| W.H.O | World Health Organisation |
| WB | Western blot |
| WT | Wild type |
| XLID | X-Linked intellectual disability |
| zDABM | zDHHC-ankyrin-repeat binding motif |
| zDHHC | Zinc finger DHHC-type acyltransferase |

| Amino acid | Three-letter code | One-letter symbol |
|---|---|---|
| Alanine | Ala | A |
| Cysteine | Cys | C |
| Aspartic Acid | Asp | D |
| Glutamic Acid | Glu | E |
| Phenylalanine | Phe | F |
| Glycine | Gly | G |
| Histidine | His | H |
| Isoleucine | Iso | I |
| Lysine | Lys | K |
| Leucine | Leu | L |
| Methionine | Met | M |
| Asparagine | Asp | N |
| Proline | Pro | P |
| Glutamine | Glu | Q |
| Arginine | Arg | R |
| Serine | Ser | S |
| Threonine | Thr | T |
| Valine | Val | V |
| Tryptophan | Try | W |
| Tyrosine | Tyr | Y |

## Abstract

Sprouty (Spry)/SPRED proteins are important regulators of the MAPK/ERK signalling pathway, and dysregulation of this pathway can contribute to development of cancer. The defining feature of Spry/SPRED proteins is a highly conserved cysteine-rich Sprouty domain, which for Spry2 contains 26 cysteine residues. Recent work has shown that the SPR domain is S-acylated by zDHHC17. The aim of this thesis is to explore the mechanisms of interaction and S-acylation of Spry/SPRED proteins by zDHHC17 and identify downstream effects of these interactions. The approaches used included expression of zDHHC17 and Spry/SPRED mutants in HEK-293T and PC12 cells, followed by analysis of protein interactions by immunoprecipitation and analysis of S-acylation using click chemistry methodologies. Protein localisation was examined using confocal microscopy and protein stability measured in cycloheximide-chase experiments. The use of AlphaFold structural predictions and other bioinformatic tools was used to inform these analyses. The results indicate that the interaction of Spry2 and zDHHC17 has a unique dual-stabilisation effect on both the enzyme and substrate. Furthermore, a novel mechanism of recognition/S-acylation of Spry/SPRED proteins, which is distinct from the mechanism of SNAP25 recognition/S-acylation by zDHHC17 was identified. Specifically, the zDABM sequence of Spry2 which is the major interaction site for zDHHC17 was shown to be dispensable for S-acylation. Analysis of SPRED3, which lacks a zDABM sequence, showed that the highly conserved SPR domain contains a novel zDHHC17 binding site that facilitates S-acylation. This thesis also identifies a potential effect of Spry2 on the S-acylation of the SARS-CoV-2 accessory protein, Orf3d, which should be investigated further in future work. Collectively, the findings in this thesis provide important new information on substrate recognition by zDHHC enzymes. This new knowledge can assist in identifying new zDHHC17 substrates and could also be used to develop peptide-based inhibitors that disrupt specific substrate interactions of zDHHC17.

Words: 297

# CHAPTER 1

# GENERAL INTRODUCTION

# Chapter 1 - General introduction

## Introduction

The International Agency for Research on Cancer, estimates that worldwide in 2020 there were over 19.3 million new cancer cases and almost 10 million cancer deaths (Sung et al., 2021). Nearly half of these cancer cases were breast (11.7%), lung (11.4%), corectal (10%), prostate (7.3%), and stomach (5.6%) cancers (Sung et al., 2021). It is important to identify new biomarkers to improve early diagnosis, patient stratification, and treatment of cancer. These biomarkers can be epigenetic (Herceg and Hainaut, 2007), genetic (Calzone, 2012), metabolic (Aizpurua-Olaizola et al., 2018), or proteomic. An example protein biomarker is the tumour supressing breast cancer type 1 gene/protein (BRCA1), which displays reduced or undetectable expression in the majoriy of high-grade ductal carcinomas (Rakha et al., 2008).

Another potential tumour suppressor protein linked to a range of different cancer types is the Sprouty-2 protein (Spry2), which has been characterised as a negative modulator of the mitogen-activated protein kinase/extracellular signal-regulated kinase (MAPK/ERK) signalling pathway (Kawazoe and Taniguchi, 2019). Dysregulation of this signalling pathway has been shown to lead to excess cellular proliferation, differentiation, migration, and tumourigenesis (Dhillon et al., 2007). Indeed, reduced Spry2 expression has been implicated in many cancer types including lung adenocarcinoma (Walsh and Lazzara, 2013), hepatocarcinoma (Wang et al., 2012), prostate cancer (Gao et al., 2019), and colon cancer (Feng et al., 2011). It has also been suggested that Spry2 might be useful in predicting chemotheraputic side-effects, such as the post-treatment (carbotaxol) development of ascites, which correlates with a decreased expression of Spry2 in epithelial ovarian cancer patients (Masoumi-Moghaddam et al., 2015a).

To understand how dysregulation of tumour suppressor proteins like Spry2 contribute to disease, it is critical to investigate the normal function of the protein during common cellular processes, such as cell growth. This includes investigating the various protein interactions and post-translational modifications (PTMs) that influence the localisation and function of the protein. Recent evidence, which could expand the understanding of Spry2, revealed a previously unknown interaction between Spry2 and the

acyltransferase, zDHHC17, which mediates the S-acylation of Spry2 (Lemonidis et al., 2017a). S-acylation is a post-translational form of lipidation involving the reversible covalent attachment of fatty acids on to cysteine residues *via* thioester linkages.

## 1.1 Protein lipidation

The post-translational modification (PTM) of proteins is a major occurrence in eukaryotic cells and involves chemical modification of amino acid side chains with a diverse array of modifying groups (Ramazi and Zahiri, 2021). Common and well-studied PTMs include phosphorylation, which involves the modification of serine, threonine, and tyrosine residues with phoshate derived from ATP, which regulates a broad range of cellular processes and pathways, most notably cell signalling (Lavoie et al., 2020). Another well-studied PTM is ubiquitination, the attachment of the small regulatory protein ubiquitin typically onto lysine residues of proteins (Song and Luo, 2019). Polyubquitin conjugation of proteins is typically involved in marking proteins for ubiquitn-dependent degredation. This is seen, for example, in mouse double minute 2 homolog (MDM2) mediated ubiquitination of the tumour supressor p53 (Moll and Petrenko, 2003). MDM2 is a RING-finger E3 ubquitin ligase that modulates p53 activity by targting the protein for 26S proteosomal degredation, thus limiting the growth suppressive function of this protein (Love et al., 2013).

Lipidation refers to a group of different modifications involving the attachment of lipid or lipid-like groups onto proteins. The modifying groups include fatty acids, isoprenoids, phospholipids, and sterols. Lipidation can have a variety of functions including increasing protein hydrophobicity, regulating protein traffiking, promoting membrane attachment, or impacting protein stability, and structure (Chamberlain and Shipston, 2015). For example, the attachemnt of the caprylic acid (octanoic, C8:O) onto the “hunger hormone” ghrelin is required for the gastric peptide hormone to bind and activate the ghrelin receptor; which subsequently results in the regulation of appetite and energy homeostasis (Wang et al., 2021b). Common lipid modifications include N-myristoylation, C-terminal prenylation, S-acylation, O-cholesterylation, and glycosylphosphatidylinositol (GPI) anchoring (Jiang et al., 2018, Kallemeijn et al., 2021).

First discovered in 1978 in fungi (*Rhodotorula toruloides*) (Kamiya et al., 1978), prenylation (also known as isoprenylation) is a ubiquitous form of lipidation involving the transfer of either 20-carbon geranylgeranyl isoprenoid or a 15-carbon farnesyl group onto cysteine residues of proteins (Wang and Casey, 2016). This process is mediated by a family of prenyltransferase enzymes - farnesyltransferase (FTase) and geranylgeranyl transferase (GGTase), which most commonly recognises a C-terminal consensus motif known as a CaaX box. Where C is a cysteine residue, a is generally an aliphatic/hydrophobic amino acid, and X is a specifc amino acid which governs which prenyltransferease can recognise the substrate and therefore determines which isoprenoid is attached to the protein. If X is alanine, glutamine, methionine, or serine, then the protein will be farnesylated; whereas, if X is a isoleucine, leucine, or phenylalanine residue it will be geranylgeranylated (Palsuledesai and Distefano, 2015). Alongside many other proteins, prenylation is a well-described modification of the Ras family of GTPases. The C-terminal end of HRAS contains the CaaX box (CVLS), which is recognised by FTase for the attachment of farnesyl chains. Farnesylation is important for membrane association and activation of RAS, and Tipifarnib, a potent and selective FTase inhibitor, reduces plasma membrane association and the levels of GTP-bound HRAS, thus reducing signaling through effector pathways (Odeniyide et al., 2022). Importantly, blocking prenylation is also known to reduce the activity of oncogenic RAS proteins, and there is interest in targeting this modifcation as a therapeutic strategy in RAS-driven cancers (Palsuledesai and Distefano, 2015). The C-terminal end of HRAS contains the CaaX box (CVLS), which is recognised by FTase for the attachment of farneysl chains.

N-myristoylation is another form of lipidation that involves the covalent irreversible attachment of myristic acid (C14:0) via amide bonds onto glycine resides of proteins. This process was first decsribed in 1982 (Aitken et al., 1982, Carr et al., 1982), and is predominantly a co-translational modification mediated by a family of N-myristoyltransferases (NMT1 and NMT2) (Wang et al., 2021a). Like prenylation, myristoylation occurs on a consensus motif, MGXXXS/T (where M is the initiating methionine and X is any amino acid) (Chamberlain and Shipston, 2015). As the myristate chain is added to the amine group of Gly-2, N-myristoylation requires the cleavage of the initaiting methionine residue (Giglione et al., 2004). It is interesting to note that N-myristoylation can also occur post-translationally, specifically following the caspase-mediated proteolytic cleavage of proteins during apoptosis where cryptic

myristoylation sequences can be exposed (Udenwobele et al., 2017, Martin et al., 2011). N-myristoylation has also been shown to regulate protein localisation, and this is seen for both co-translational and post-translational myristoylation, for example, in the case of the pro-apoptotic protein, BH3-interacting-domain death agonist (Bid). Following cleavage by caspase-8, a newly exposed glycine of c-terminal Bid (ctBid) is myristoylated, resulting in ctBid translocation to mitochondria to signal cell death (Martin et al., 2011). It was shown that preventing myristoylation of the glycine in ctBID (by replacement with an alanine) led to a 30% reduction in mitochondrial association and a 350% reduction in cytochrome-c activation efficacy compared to wild-type myristoylated ctBID (Martin et al., 2011, Zha et al., 2000, Udenwobele et al., 2017)

## 1.2 Protein S-acylation

One of the most prevalent forms of lipidation (and the focus of this thesis) is S-acylation, which is also sometimes referred to as palmitoylation (Chamberlain and Shipston, 2015). S-acylation involves the reversible attachment of long chain fatty acids onto protein substrates via a liable thioester bond to cysteine residues. The term palmitoylation is often used interchangeably with S-acylation, and this is historical based on early work that used $^{3}$H-palmitate to study S-acylation (palmitic acid – C16:0) (Forrester et al., 2011). However, subsequent studies have shown that S-acylated proteins can be modified by a variety of saturated and unsaturated fatty acyl chains, including myristic acid (C14:0), palmitoleic acid (C16:1), stearic acid (C18:0), oleic acid (C18:1), linoleic acid (C18:2), and arachidonic acid (C20:4) (Greaves et al., 2017, Chamberlain and Shipston, 2015). Since being discovered in 1979 using thin-layer and gas-liquid chromatography, S-acylation is becoming more widely studied and better understood, with an ever-increasing diversity of S-acylation substrates being elucidated. Indeed, proteomic analyses have suggested that at least 20% of the human proteome might be S-acylated (Schmidt and Schlesinger, 1979, Chamberlain and Shipston, 2015, Blanc et al., 2015, West et al., 2022, Blanc et al., 2019).

The principal effect of S-acylation is to increase the hydrophobicity of the modified protein, and this can impact membrane association, protein trafficking, stability, and protein interactions. Despite these range of effects of S-acylation on proteins, it is not possible to accurately predict the effect(s) that S-acylation will have on an individual protein; however, the modification of soluble proteins is normally followed by a change

in membrane association and localisation (Chamberlain and Shipston, 2015). For example, soluble steroid receptors that are usually localised to the nucleus of cells (e.g., oestrogen, progesterone, and androgen receptors) become associated with the plasma membrane when S-acylated at a single cysteine residue in the ligand binding domain of the receptor (Pedram et al., 2012, Chamberlain and Shipston, 2015).

## 1.3 The zDHHC family of enzymes

The process of protein S-acylation is mediated by a family of twenty-three mammalian "zDHHC" acyltransferase enzymes (Fukata et al., 2004) (Figure 1.1). Collectively, zDHHC enzymes mediate the S-acylation of over 10% of proteins in the mammalian proteome, covering at least 1,838 mammalian genes which encode an S-acylated protein (Sanders et al., 2015, Zhang and Hang, 2017). These enzymes, which were first discovered in 2002 in the yeast *Saccharomyces cerevisiae* (Lobo et al., 2002, Chamberlain and Shipston, 2015), are defined by the presence of a conserved 51-amino acid zinc finger cysteine-rich domain (CRD) containing an aspartic acid – histidine – histidine – cysteine (DHHC) tetra peptide motif, which is the catalytic site responsible for S-acylation activity (Lobo et al., 2002, Roth et al., 2002).

Protein S-acylation uses a co-enzyme A (CoA) derivative for the attachment of fatty acids to substrates. The main enzymatic process is theorised to occur through the catalytic triad of active site residues at the DHHC region (for zDHHC20, this is at Asp153, His154 and/or His155, and Cys156). The domain operates through a catalytic "ping-pong" reaction in which His154 is polarised by Asp153 and then extracts a proton from Cys156 creating a cysteine thiolate nucleophile, which in turn attacks the fatty acyl-CoA to form an "autoacylated" DHHC intermediate. The acyl chain is subsequently transferred to a cysteine residue of a protein substrate (Rana et al., 2018b). It is also worth noting that a small number of zDHHC enzymes have atypical catalytic motifs, including the DQHC motif in zDHHC13 (Malgapo and Linder, 2021) and the DHYC motif in yeast Akr1p (Mitchell et al., 2006). Furthermore, mutational analyses have found that a DHHR mutant of SwF1 retains activity (González Montoro et al., 2015) and a DAHC mutation in yeast ERF2-ERF4 undergoes autoacylation but is unable to transfer the acyl chain to substrates (Mitchell et al., 2010, Rana et al., 2018b).

All zDHHC enzymes are predicted to be polytopic integral membrane proteins that share some conserved topology (Figure 1.2). The highest percentage amino acid identity between zDHHC enzyme isoforms is in the catalytic DHHC-CRD that it is situated within the cytoplasm (Chamberlain and Shipston, 2015). Most zDHHC enzymes have four transmembrane domains (TMDs), however variations between zDHHC isoforms do exist: zDHHC4 and zDHHC24 have five TMDs, and zDHHC13, zDHHC17 and zDHHC23 have six TMDs (Malgapo and Linder, 2021). zDHHC13 and zDHHC17 are also notable due to the presence of an N-terminal cytosolic ankyrin repeat (AR) domain which has been shown to be important for enzyme-substrate recognition (Figure 1.2) (Lemonidis et al., 2015c).

Research from the Banerjee group in 2018 reported the first X-ray crystal structures of zDHHC enzymes (Rana et al., 2018a). Specifically, the team published the structures for human zDHHC20 and for zebrafish zDHHS15 (catalytically inactive). For zDHHC20, (365 aa), the N-terminus is cytoplasmic (aa 1-14) followed by four TMDs (TMD1 – aa 15-35; TMD2 – aa 54-74; TMD3 – aa 170-190; TMD4 – aa 208-231), with two lumenal loops (aa 36-53 & aa 191-207), a cytosolic loop (aa 75-169), and a C-terminal cytoplasmic tail (aa 232-365); with the DHHC-CRD present in the cytosolic loop and extending into TMD3 (aa 126-176). The four transmembrane helices of zDHHC20 were found to form a “tepee-like” topology in the membrane with the tip facing the extracellular/lumenal side of the membrane and the wider cavity structure being cytoplasmic. This open cavity structure allows for the insertion of acyl chains i.e., fatty acid acyl-CoA (Malgapo and Linder, 2021). The amino acid residues in the TMDs and spatial availability within the cavity have been shown to contribute to the acyl-CoA selectivity of the zDHHC enzymes.

The acyl chain preference of zDHHC20 was shown to be for shorter chain fatty acids (C14, C16), whereas the enzyme was not as well acylated by C18 chains. Analysis of the crystal structure identified that Tyr-181 in TMD3 formed a H-bond with Ser-29 in TMD1 that appeared to close the cavity at the lumenal side of the membrane. Indeed, replacement of Tyr-181 with a less bulky alanine residue resulted in an increased preference for stearoyl (C18)–CoA. They further showed that introduction of a bulkier phenylalanine in place of Ser-29 increased the preference of the enzyme for short-chain acyl-CoA (Rana et al., 2018a). These findings with zDHHC20 help inform the results of an earlier study from the Greaves and Chamberlain groups, which looked at the differences in fatty acid selectivity between the two related enzymes, zDHHC3

and zDHHC7 (Greaves et al., 2017). Specifically, zDHHC3 was shown to be significantly less able to incorporate longer C18:0 chains into substrate proteins than zDHHC7. Detailed mutagenic analysis and construction of chimeric proteins found that this difference in fatty acid selectivity was attributable to a single amino acid in TMD3. Replacement of a highly-conserved Ile-182 in zDHHC3 with a less bulky serine (present at the same position in zDHHC7), led to zDHHC3 having the same fatty acid selectivity profile as zDHHC7 and an increased ability to use longer chain fatty acids (Greaves et al., 2017). Interestingly, Ile-182 of zDHHC3 is present at the same position in TMD3 as Tyr-181 of zDHHC20.

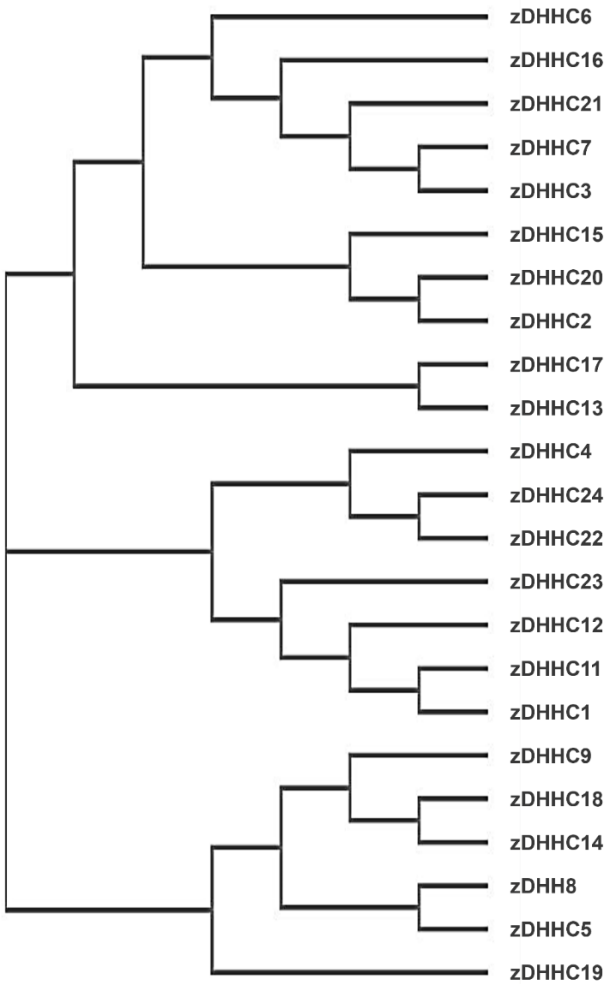


***Figure 1.1 Evolutionary relationship between zDHHC enzymes.*** *Phylogenetic cladogram tree of the 23 human zDHHC acyltransferases generated using the ClustalW2 package via the Simple Phylogeny tool from EMBL-EBI (Saitou and Nei, 1987, Madeira et al., 2022).*

The majority of zDHHC enzymes appear to localise to the endoplasmic reticulum (ER) and Golgi. However, it is important to note that the analysis of zDHHC localisation has been restricted to the use of epitope-tagged over-expressed enzymes. Furthermore, there are some conflicting reports on the localisation of certain isoforms that could relate to over-expression effects or cell type differences. In addition to ER and Golgi localisation, there are a small number of proteins that appear to associate with post-Golgi compartments including the plasma membrane and recycling endosomes - these include zDHHC2, zDHHC5 and zDHHC20 (Ohno et al., 2006, Lemonidis et al., 2015c, Greaves et al., 2011, Fernández-Hernando et al., 2006). Furthermore, zDHHC2 and zDHHC5 has been shown to cycle between the plasma membrane and recycling endosomes (Salaun et al., 2017, Greaves et al., 2011, Brigidi et al., 2015). Super-resolution microscopy explored the distribution of Golgi zDHHC enzymes in more detail and showed that most Golgi isoforms were localised to the *cis*-Golgi, with zDHHC9, 11 & 15 being *trans*-Golgi (Ernst et al., 2018). zDHHC17 has also been found to associate with both cytoplasmic vesicle membranes (Goytain et al., 2008) and presynaptic cell membranes (Stowers and Isacoff, 2007).

There is currently little information about specific mechanisms that mediate zDHHC localisation (Chamberlain and Shipston, 2015). However, zDHHC4 and zDHHC6 have been shown to contain lysine-based sorting signals within their C-terminal tails that restrict these enzymes to the ER (Gorleku et al., 2011). This study found that the ER targeting signals for these enzymes were a KXX motif for zDHHC4 and a KKXX motif for zDHHC6 (at the extreme C-termini of the enzymes). These sites were further confirmed as ER retention signals as their appendage onto the C-terminus of zDHHC3 redistributed this Golgi isoform to the ER (Gorleku et al., 2011). More recently, a transcriptional variant of zDHHC20 triggered by SARS-CoV-2 infection has been discovered that is N-terminally extended by 67 amino acids. Not only is this zDHHC20-long variant 37x more efficient at S-acylating the spike protein of SARS-CoV-2, but surprisingly it localises exclusively to the ER (as opposed to the plasma membrane for the canonical zDHHC20 isoform) (Mesquita et al., 2023). The team from the lab of Gisou van der Goot, were further able to show through protein truncation mutagenesis and confocal microscopy that a tetrapeptide PERW motif at the N-terminus of zDHHC20-long was responsible for its localisation to the ER (Mesquita et al., 2023).

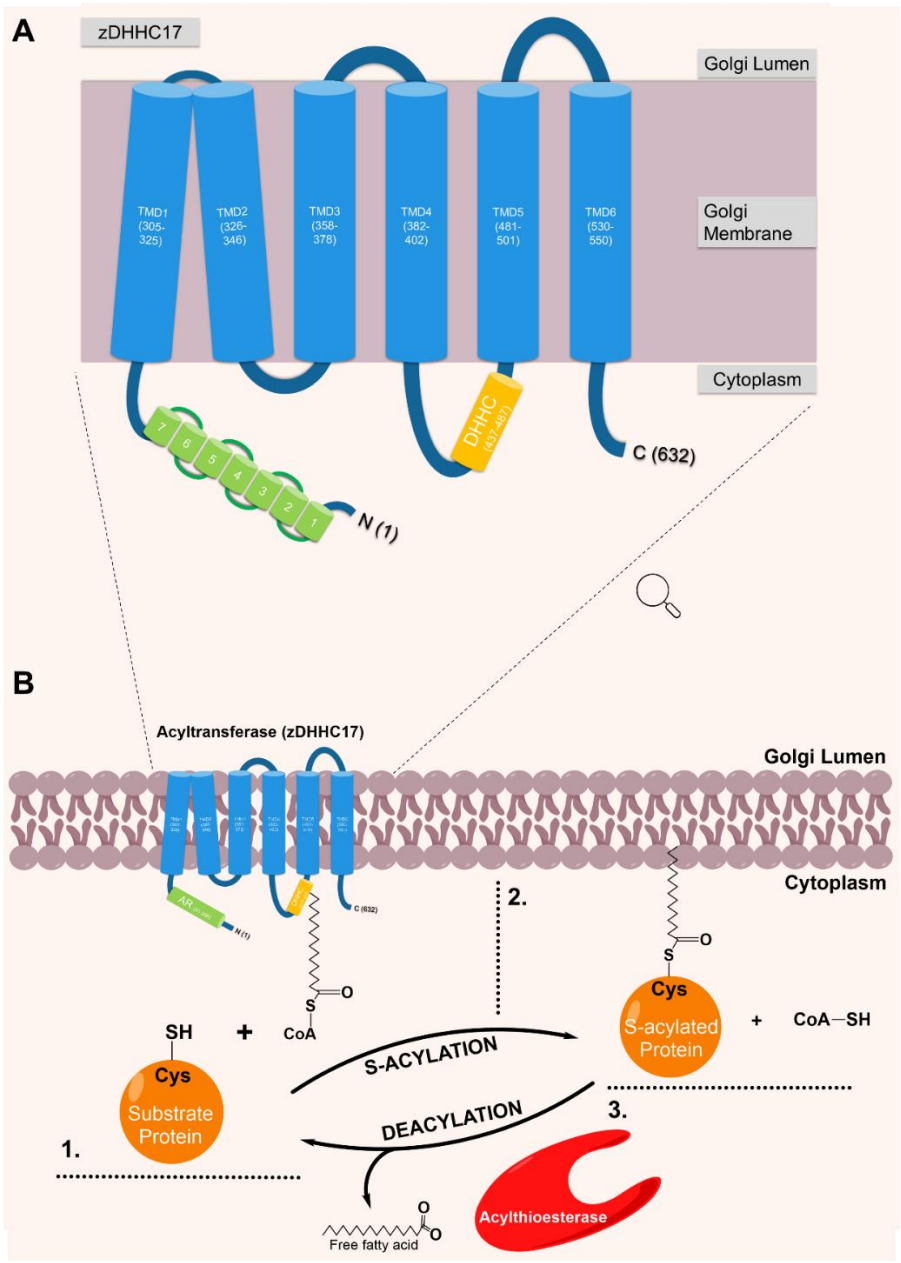


***Figure 1.2. Topology of zDHHC17 and the S-acylation of proteins.*** *(A)Schematic diagram of zDHHC17, displaying the topological placement of the ankyrin repeat, aa 51-286 (green); DHHC domain (orange), aa 437-487; and transmembrane domains (TMD) (blue): TMD1, aa 305-325; TMD2, aa 326-346; TMD3, aa 358-378; TMD4, aa 382-402; TMD5, aa 481-501; and TMD6, aa 530-550. (B) (1.) Reversible fatty acid attachment to substrate proteins through co-enzyme A (CoA) transfer of palmitate or other long-chain fatty acids presented by zDHHC enzymes. (2.) S-acylated protein association at the plasma membrane via fatty acid attachment/increased hydrophobicity. (3.) De-acylation of S-acylated proteins through acylthioesterase mediated detachment of long-chain fatty acids.*

## 1.4 zDHHC17

As highlighted above, zDHHC13 and zDHHC17 are unique in the zDHHC enzyme family as they contain an N-terminal ankyrin repeat domain that has been shown to be important for substrate selectivity (Lemonidis et al., 2015a). For zDHHC17 (632 aa – UniProt: Q8IUH5, ZDH17_HUMAN), the N-terminus is cytoplasmic (aa 1-304) and encompasses the ankyrin repeat (AR) domain (aa 51 - 286). This motif is comprised of seven ankyrin repeats each made up of 33 amino acids, which per repeat form two alpha helices separated by a loop. Following the large N-terminal cytoplasmic region are six TMDs (TMD1 - aa 305-325; TMD2 - aa 326-346; TMD3 - aa 358-378; TMD4 - aa 382-402; TMD5 - aa 481-501; TMD6 - aa 530-550), with two lumenal loops (aa 379-381 & aa 502-529), two cytosolic loops (aa 347-357 & aa 403-480), and a C-terminal cytoplasmic tail (aa 551-632); with the DHHC-CRD (aa 437-487) present in the cytosolic loop between TMD4 and TMD5 (figure 1.2 and figure 1.4).

zDHHC17 has also been shown to interact with a number of different proteins. For instance, the biomedical interaction repository database, BioGRID, curates a list of 295 proteins from studies with data showing that they interact with human zDHHC17 (Stark et al., 2006). The top BioGRID interactors of human zDHHC17 in Table 1.3, shows proteins from BioGRID that have three or greater points of evidence for interaction with zDHHC17. Alongside this, figure 1.3 shows the top interactions of zDHHC17 generated using the protein-protein association network website - STRING (v11) (Szklarczyk et al., 2019). For comparison, outputs generated in figure 1.3, are also highlighted in Table 1.3 From these results two of the highest scoring proteins are Huntingtin protein (HTT) and DnaJ (Hsp40) homolog, subfamily C, member 5 (DNAJC5), which were shown to bind to the ankyrin repeat domain of zDHHC17 (Lemonidis et al 2015). DNAJC5 is also known as Cysteine string protein α (CSPα), and the latter name will be used throughout the thesis.

| Table 1.3: Top BioGRID interactors of human zDHHC17 | | |
|---|---|---|
| **No.** | **Interactor** | **Description** |
| **1** | **HTT** | **Huntingtin** |
| **2** | **SPRY2** | **Sprouty homolog 2 (Drosophila)** |
| **3** | **DNAJC5 (CSP)** | **DnaJ (Hsp40) homolog, subfamily C, member 5** |
| **4** | **FAM135B** | **Family with sequence similarity 135, member B** |
| 5 | BSCL2 | Berardinelli-Seip congenital lipodystrophy 2 (seipin) |
| 6 | NRG1 | Neuregulin 1 |
| **7** | **TAF8** | **TAF8 RNA polymerase II, TATA box binding protein (TBP)-associated factor, 43kDa** |
| **8** | **SPRED1** | **Sprouty-related, EVH1 domain containing 1** |
| 9 | C3AR1 | Complement component 3a receptor 1 |
| **10** | **PLSCR4** | **Phospholipid scramblase 4** |
| **11** | **SPRED2** | **Sprouty-related, EVH1 domain containing 2** |
| 12 | LPAR1 | Lysophosphatidic acid receptor 1 |
| Interactors in **bold** were also outputs from the protein-protein association network website, STRING (v11) - figure 1.3 | | |

***Table 1.3. Top BioGRID interactors of human zDHHC17.*** *Table showing the top protein interactors of zDHHC17. Total number of protein interactors generated from the BioGRID biomedical interaction repository database = 295. Only proteins with three or greater points of high and/or low throughput physical evidence of interaction evidence are shown (Stark et al., 2006). Interactors in bold were also outputs from the protein-protein association network website, STRING (v11) - figure 1.3.*

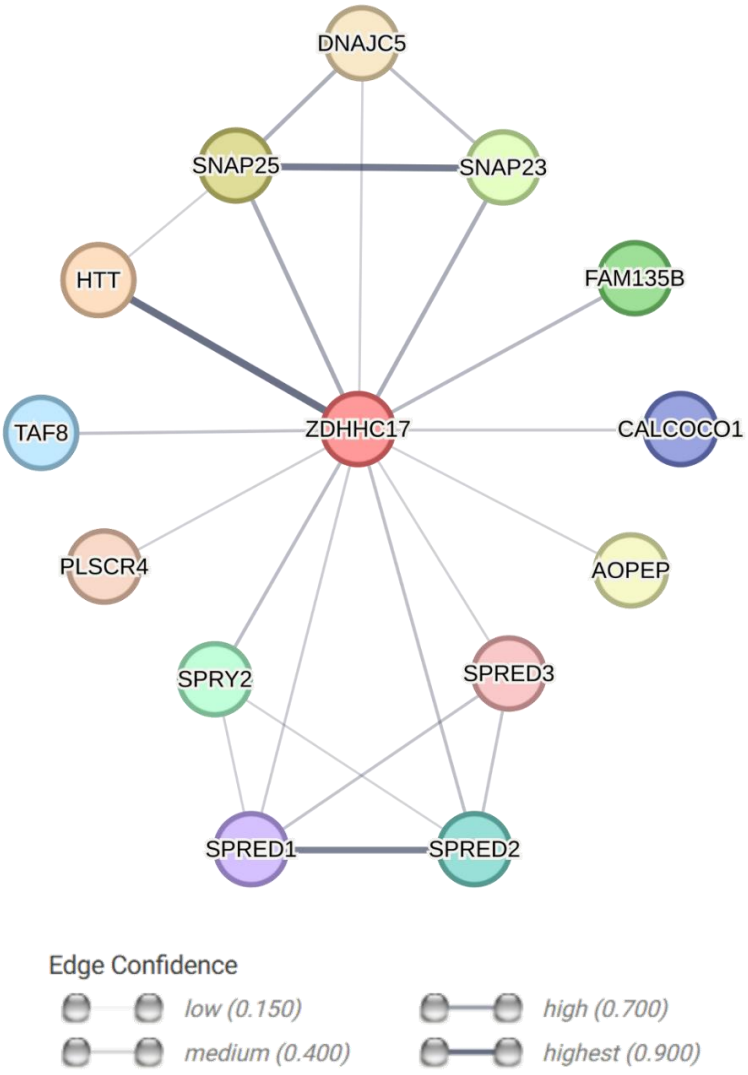


***Figure 1.3. Interactions of zDHHC17.*** *Interaction network for Homo Sapiens acyltransferase ZDHHC17 generated using the protein-protein association network website - STRING (v11) (Szklarczyk et al., 2019). Network nodes (circles) represent proteins splice isoforms or post-translational modifications are collapsed, i.e., each node represents all the proteins produced by a single, protein-coding gene locus. Edges (lines) represent shared physical complex. The edges indicate that the directly linked proteins are part of the same physical complex; commonly in large complexes this may not signify they are directly binding to each other. Line thickness indicates the strength of data support: low (0.150), medium (0.400), High (0.700), and highest (0.900). Data support includes experiments (experimental/biochemical data), databases (association in curated databases only), and textmining (co-mentioned in PubMed abstracts). Interactions with strength of data support > 0.300 are shown.*

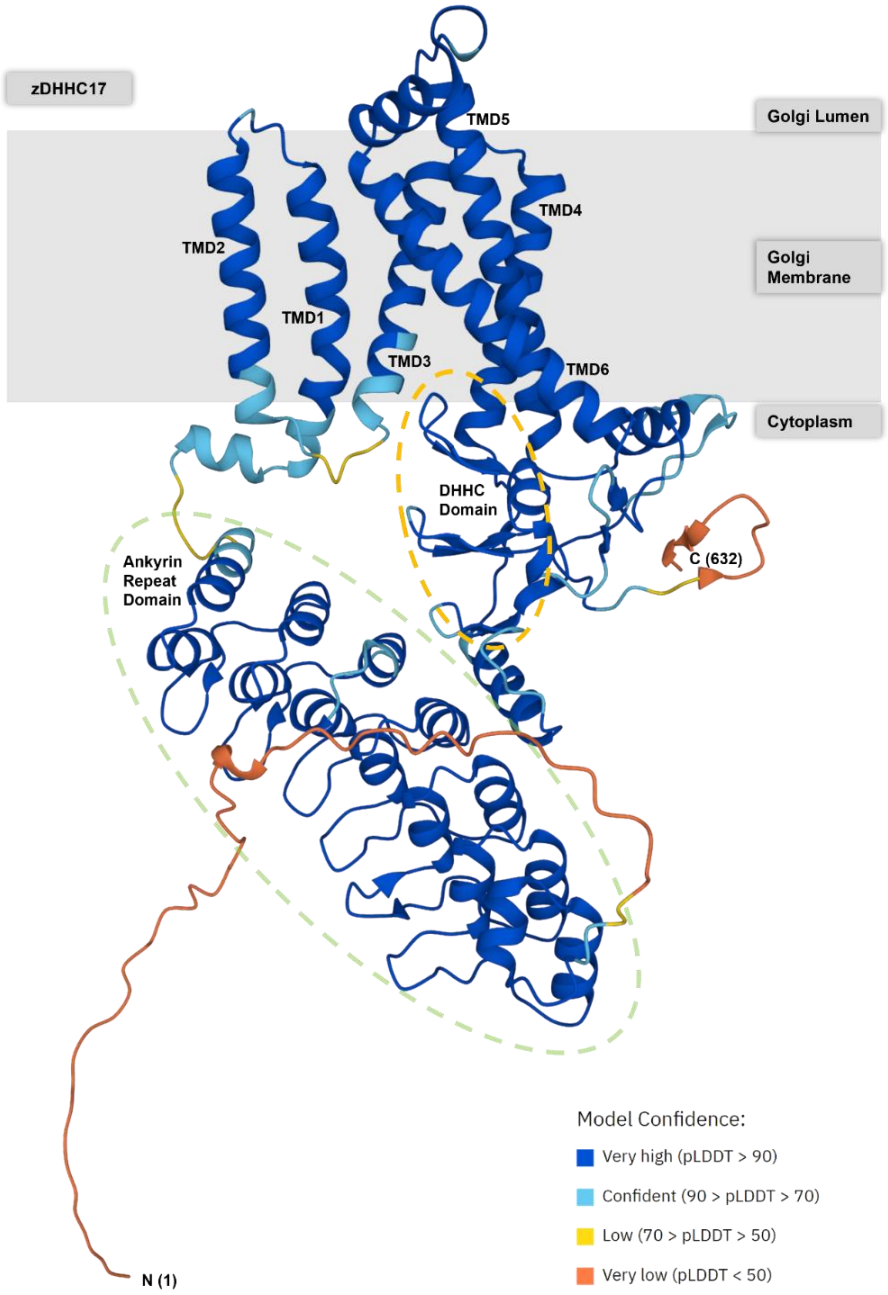


***Figure 1.4. Structure of zDHHC17.*** *AlphaFold structural prediction model of palmitoyltransferase zDHHC17 (Homo sapiens; UniProt: Q8IUH5 - ZDH17_HUMAN). Schematic indicating the approximate spatial location of the ankyrin repeat domain, the DHHC domain, transmembrane domains 1-6 (TMD), and the N/C terminal ends, relative to the Golgi membrane. AlphaFold produces a per-residue confidence score (pLDDT) between 0 and 100. Some regions below 50 pLDDT may be unstructured in isolation. AlphaFold protein structure database developed by DeepMind and European Molecular Biology Laboratory-European Bioinformatics Institute (EMBL-EBI) (Varadi et al., 2022, Jumper et al., 2021).*

## 1.5 Protein deacylation

S-acylation is a reversible modification and deacylation is mediated a variety of deacyltransferases which facilitate the hydrolysis of fatty acyl chains from protein substrates. Three classes of deacylation enzymes have been identified including: acyl-protein thioesterases (APTs), α/β hydrolase domain-containing proteins (ABHDs), and palmitoyl-protein thioesterases (PPTs) (Koster and Yoshii, 2019).

### Acyl-protein thioesterases (APT)

APT1 and APT2 (also known as LYPLA1 & 2) were identified in two separate studies in 1998 and 1999, respectively (Duncan and Gilman, 1998b, Toyoda et al., 1999). There is a 68% amino acid identity between these two proteins (UniProt alignment, percentage identity between LYPLA1_HUMAN (230 aa) & LYPLA2_HUMAN (231 aa)), however, they have been shown to be functionally active against different substrates (Chamberlain and Shipston, 2015, Greaves, 2021). For instance, APT1 is active against eNOS (Yeh et al., 1999), H/N-RAS (Duncan and Gilman, 1998a), β2-adrenergic receptors (Adachi et al., 2016), Gα subunits (Duncan and Gilman, 1998a), and BK potassium channels (Tian et al., 2012). Whereas APT2 is active against tumour necrosis factor receptor (TNFR) (Zingler et al., 2019), GAP-43 (Tomatis et al., 2010), zDHHC6 (Abrami et al., 2017), Scrib (Hernandez et al., 2017), melanocortin 1 receptor (Chen et al., 2019), and HRAS (Duncan and Gilman, 1998a).

APTs were shown to also be S-acylated, with this modification regulating the cellular localisation of these soluble enzymes (Vartak et al., 2014, Koster and Yoshii, 2019). APT1 is anchored to the Golgi by S-acylation, and deacylation releases the enzyme into the cytoplasm (Vartak et al., 2014). Deacylation is mediated either by APT1 “autodeacylation” or by APT2 (Vartak et al., 2014, Kong et al., 2013). APT2 is also reversibly S-acylated on Cys-2. An S-acylation-defecient mutant of APT2 (Cys2Ser) was shown to have weak membrane affinity and was more suceptiable to lysine ubiquitination/proteosomal degredation, and had a faster turnover rate than APT2 WT (Abrami et al., 2021). Overall, these results highlight the importance of S-acylation and deacylation as important regulatory steps for APT stabilisation, localisation, and function.

**Protein palmitoyl thioesterases (PPT)**

Prior to the discovery of APT1 and APT2, the first thioesterase discovered was PPT1 (palmitoyl protein thioesterase 1), and this enzyme was shown to be active towards HRAS (Camp and Hofmann, 1993). Four years later, a related enzyme PPT2 was identified and cloned by the same group (Soyombo and Hofmann, 1997). Unlike, APTs, PPT1 and PPT2 are targeted to lysosomes and late endosomes, where they are believed to play a role in the catalysis of deacylation in the lysosome during protein degradation (Chamberlain and Shipston, 2015, Verkruyse and Hofmann, 1996). PPT1 and PPT2 share 26% amino acid identity (UniProt alignment, percentage identity between PPT1_HUMAN (306 aa) & PPT2_HUMAN (302 aa)). Importantly however, a comparison between the crystal structures of PPT1 and PPT2 showed that PPT2 is actually structurally/conformationally constrained in its enzymatic activity. Specifically, although PPT2 can still remove thioester-linked fatty acyl groups, a significantly smaller/restricted binding groove within this enzyme means that it is unable to remove palmitate groups from “bulky” or branched heads of substrates (i.e. palmitoylated cysteine residues of proteins) (Calero et al., 2003, Soyombo and Hofmann, 1997). There is some controversy about the intracellular localisation of PPT1, with several groups studying the functions of the enzyme outside of lysosomes (Lehtovirta et al., 2001, Ahtiainen et al., 2003, Heinonen et al., 2000). It is still unclear how PPT1 can localise to both the lysosomes and cytoplasm, but functional studies have revealed cytosolic functions of the enzyme.

Analysis of knockout (KO) mouse models have revealed that PPT1 has an important function in the nervous system (Koster and Yoshii, 2019). For instance, PPT1 has been implicated in the inflammatory activation of astrocytes (Kielar et al., 2007), loss of GABAergic neurons (Bible et al., 2004), NMDA receptor dysregulation, immature dendritic spine morphology (Koster et al., 2019), and axonal connectivity deficits (Chu-LaGraff et al., 2010). The importance of these activities is reflected in the reduced lifespan of PPT1/PPT2 KO models by 10 months of age, there is a 100% mortality rate for PPT1 KOs and a 20% mortality rate for PPT2 KOs (Gupta et al., 2001, Swarbrick et al., 2020). In humans, mutations in the PPT1 gene cause infantile neuronal ceroid lipofuscinosis (INCL) (Gupta et al., 2001, Vesa et al., 1995). This lysosomal storage disorder has the characteristic feature of acculmulation of autofluorescent storage material (‘lipofuscin’) and subsequent neurodegeneration (a

topic which will be discussed later in the text), which leads to rapid and early death of affected infants (Won et al., 2018).

**α/β hydrolase domain proteins (ABHDs)**

APT enzymes are members of the metabolic serine hydrolase (mSH) superfamily family, which also include α/β hydrolase domain (ABHD) proteins. There are more than 50 different ABHD isoforms, which share common/conserved features. Notably ABHD proteins contain a cannonical α/β hydrolase fold made up of eight β-strands with an antiparralel β2 strand. The β-strands form a core β-sheet surrounded by α-helices and loops which connect the β-strands (See figure 1 of Lord, Thomas and Brown (2013)) (Bononi et al., 2021). The enzymes mediate their hydrolytic activity via a highly conserved catalytic triad comprised of a nucleophile residue (Ser, Cys, or Asp) in strand β5, an acidic residue (Glu or Asp) after strand β7, and a histidine residue after the last β8 strand. Most ABHDs also exhibit acyltransferase activity due to the conserved His-XXXX-Asp region (where X is any amino acid). Conversely making some ABHDs (such as ABHD5) both hydrolases and acyltransferases (Bononi et al., 2021, Lord et al., 2013)

ABHD17 proteins are of particular interest and are further subdivided into ABHD17A, ABHD17B, and ABHD17C (Remsberg et al., 2021). Like other deacylases identified so far ABHDs undergo dynamic S-acylation at their N-terminal end (Won et al., 2018; Zaballa and van der Goot, 2018). ABHD17 proteins share a highly conserved N-terminal cysteine-rich region containing 4-5 cysteine residues, which are now known to be S-acylated. This S-acylation appears to be important for the localisation of ABHD17, as an N-terminal truncation mutant of ABHD17 lacking the modified cysteines displayed reduced plasma membrane association compared to the WT protein in HeLa cells (Martin and Cravatt, 2009).

ABHD17 proteins share between 76-78% amino acid identity (UniProt alignment, percentage identity between AB17A_HUMAN (310 aa), AB17B_HUMAN (288 aa), and AB17C (329 aa)), and ABHD17 A/B/C have been shown to act on similar substrates. Specifically, the proteins have been shown to mediate the deacylation of MAP6 (Tortosa et al., 2017), PSD95, and N-RAS (Remsberg et al., 2021). In COS-7 cells the deacylation of N-RAS by ABHD17 was shown to redistribute the RAS protein away from the plasma membrane (as N-RAS is anchored to the membrane via S-

acylation) (Lin and Conibear, 2015, Remsberg et al., 2021). These observations have sparked interest in the potential of ABHD17 to have a tumour suppressor role via its effects on N-RAS localisation, as plasma membrane association is required to promote cell growth/signalling. Interestingly, the 2015 study by Lin and Conibear showed that ABHD17A was the most effective isoform at mediating the deacylation of N-RAS and PSD95. ABHD17A was found to localise to Rab5- and Rab11-positive endosomes, in addition to the plasma membrane (Lin and Conibear, 2015). The membrane localisation of ABHD17 is critical to allow it to deacylate its substrate proteins and an N-terminal truncation of ABHD17A lacking the S-acylated cysteine was unable to act on either PSD95 or N-RAS (Lin and Conibear, 2015). Overall, the findings from this study show that both an active α/β hydrolase catalytic domain and appropriate ABHD localisation are required for the deacylation of ABHD17 substrates.

## 1.6 Effects of S-acylation on substrate proteins

A large body of published research over the last few decades has highlighted a range of effects of S-acylation on modified proteins. The principal effect that S-acylation has on proteins is presumably an increase in hydrophobicity and subsequent increased association of the protein or specific proteins domains with membranes. This change in hydrophobicity and membrane association can subsequently alter protein interactions, localisation, stability, and trafficking (Chamberlain and Shipston, 2015).

### S-acylation of peripheral membrane proteins

One of the most prominent effects of S-acylation is to increase membrane association of soluble proteins (i.e., proteins that lack a transmembrane domain). Cytosolic proteins and/or intrinsically hydrophilic proteins are targeted to and anchored at the cytoplasmic face of the plasma membrane via the attachment of long-chain fatty acids. These proteins are often signalling molecules and indeed one of the most widely studied protein families that makes use of S-acylation for this purpose is the Ras family. Ras proteins are small GTPases which couple extracellular signals to intracellular effector pathways acting as molecular switches (switching between GTP and GDP binding modes) (Busquets-Hernández and Triola, 2021). Ras proteins have key functions in cell differentiation, proliferation, differentiation, and survival (Daniotti

et al., 2017), and indeed hyperactivating Ras mutations are a frequent cause of cancer (Murugan et al., 2019). It is thought that around 20% of cancer patients exhibit mutations in RAS, with the protein being among one of the most frequently altered oncogenes (Hobbs et al., 2016, Prior et al., 2020, Busquets-Hernández and Triola, 2021). In humans, three RAS genes encode for four Ras proteins: N-RAS, H-RAS, K-RAS4A, and K-RAS4B (K-RAS is encoded as two alternatively spliced isoforms) (Hobbs et al., 2016).

Peripheral membrane proteins that are S-acylated, such as Ras, often undergo “dual” lipid modification where the proteins are modified by both S-acylation, and also N-myristoylation or prenylation. For instance, both H-Ras and N-Ras undergo prenylation (farnesylation) due to the presence of a C-terminal CaaX box domain, and S-acylation of neighbouring cysteine residues in the C-terminus. Ras proteins first undergo farnesylation in the cytosol allowing transient association with cell membranes including the cytosolic face of the ER. Once at the ER, the C-terminal aaX motif is cleaved by the endopeptidase Rce1, and the exposed farnesylated cysteine residue is subsequently methylated by the isoprenylcysteine carboxyl methyltransferase, Icmt (Daniotti et al., 2017). In this state, Ras only has a weak membrane affinity and cycles on and off membranes. This membrane cycling allows Ras to “sample” cell membranes and when it interacts with the Golgi complex, it becomes S-acylated by resident zDHHC enzymes (likely by zDHHC9/GCP16). H-Ras is S-acylated at both Cys181 and Cys184, whereas N-Ras is S-acylated at Cys181 alone. This modification and increase in hydrophobicity results in stable membrane association of Ras and allows it to move into budding vesicles that deliver it to the plasma membrane by vesicle-mediated transport (Daniotti et al., 2017, Rocks et al., 2006). Once at the membrane, H-RAS and N-RAS have been observed to cycle between membrane-bound and soluble states in response to S-acylation and de-acylation, respectively (Rocks et al., 2010, Vartak et al., 2014) (Figure 1.2 B).

**S-acylation of transmembrane proteins**

Although transmembrane proteins are intrinsically attached to membranes, S-acylation can have profound effect on their stability, activity, structure, and topology (Chamberlain and Shipston, 2015). For instance, a recent study investigating showed that S-acylation of the plant receptor kinase flagellin sensing 2 (FLS2) protein, which is essential for immunity against bacterial pathogens, is required to stabilise co-

receptor interaction at the plasma membrane for effective signal transduction (Hurst et al., 2023). Specifically, FLS2 S-acylation stabilies the interaction between FLS2 and BRI1-associated receptor kinase 1 (BAK1) at the membrane. This interaction delays endocytosis of activated FLS2 complexes, thereby maintaining constitutive active signalling (Hurst et al., 2023). Although FLS2 is modified at a pair of cytosolic juxta-transmembrane domain cysteines (Cys-830 & Cys-831; where FLS2 TMD is V807-I827), these residues were dispensable for the observed effects of S-acylation. Instead, two additional downstream cysteine residues (Cys-1132 & Cys-1135) in the C-terminal end of the protein were also shown to be S-acylated and responsible for FLS2-BAK1 stabilisation.

In addition to modification at N- or C-terminal cysteines, S-acylation can also occur at other regions of transmembrane proteins. In particular, transmembrane proteins are often S-acylated in close proximity to the membrane interface, where the addition of a fatty acid chain may confer structural constraints to the TMD protein. For instance, the calcium-binding glycoprotein-interacting protein, calnexin is S-acylated on Cys-502 & Cys-503, which are just at the end of the TMD helix and at the membrane/cytosol interface. S-acylation of calnexin on these residues has been suggested to modify the orientation of the TMD and cytoplasmic tail, which in turn enhances the targeting of calnexin to ER ribosome-translocon complexes (as opposed to ER tubules) (Chamberlain and Shipston, 2015, Lakkaraju et al., 2012). This type of membrane proximal cysteine S-acylation was attributed to the activity of zDHHC6 which is localised to the ER (Lakkaraju et al., 2012). Indeed, a recent study suggested that zDHHC6 may play a broad role in the modification of ER proteins with cysteines positioned at the cytosol/membrane interface (Salaun et al., 2023).

TMD proteins can also be S-acylated at intracellular loops between the TMDs of multi-pass domains. For instance, the calcium-activated potassium channel subunit α-1 (also known as $K_{Ca}1.1$ or BK channel α-subunit) are voltage gated $K^+$ channels essential for the regulation of several key physiological processes including smooth muscle tone and neuronal excitability (Yang et al., 2015). Research from the Shipston group in 2010, showed that BK channels are S-acylated at Cys-53, 54, & 56, within a cytosolic linker region between the first TMD (termed S0) and the second TMD (termed S1) (Jeffries et al., 2010). Immunofluorescence analysis of mutants with substitutions in the S-acylation sites (C53/54/56A) revealed that this modification is important for cell surface expression. However, S-acylation at these sites did not

appear to have any effect on single channel conductance or the calcium/voltage sensitivity (Jeffries et al., 2010).

It was subsequently shown that S-acylation of the BK channel intracellular loop is mediated by zDHHC22 and zDHHC23, whereas deacylation is mediated by APT1 (Tian et al., 2012). Furthermore, whereas S-acylation is known to regulate BK channel cell surface expression (Jeffries et al., 2010), APT1 deacylation of BK channels was also suggested to be a critical checkpoint in the control/trafficking of the ion channel for cell surface expression. Both the C53/54/56A mutant (S-acylation deficient) and WT channel showed accumulation at the trans Golgi network and reduced plasma membrane association when co-expressed APT1 (Tian et al., 2012). Interestingly, an alternatively spliced variant of the BK channel known as the ZERO variant, which lacks the Stress-regulated exon (STREX) insert is also S-acylated but by a different set of zDHHC enzymes (zDHHCs 3, 5, 7, 9, and 17) (Tian et al., 2008, Tian et al., 2010).

**S-acylation in protein trafficking**

S-acylation can impact the trafficking of both soluble and transmembrane proteins, including the C-C chemokine receptor type 5 (CCR5), which is a cell surface class A G-protein coupled receptor (GPCR), that functions as a chemokine receptor on white blood cells during the human inflammatory response (Jansen and Beaumelle, 2022). CCR5 interacts with Gα, Gβ, and Gγ at the plasma membrane and can activate signalling through PI-3K, JAK/STAT, and PLCβ, which leads to the activation of downstream effector pathways such as ERK1/2, p38, and JNK (Jansen and Beaumelle, 2022). CCR5 has been a focus of particular interest mainly due in its role as a co-receptor for the host cell entry of human immunodeficiency virus (HIV) (Barmania and Pepper, 2013, Dragic et al., 1996, El-Zohairy et al., 2021). In addition, CCR5 has been implicated in disease states including cancer (Jiao et al., 2018, Jiao et al., 2021) and brain injury (i.e., stroke) (Joy et al., 2019).

CCR5 is S-acylated on Cys-321, Cys-323 and Cys-324 in the C-terminal tail of the protein (Blanpain et al., 2001, Kraft et al., 2001). The S-acylation of these residues is essential for efficient trafficking and secretion of CCR5, with zDHHC3, 7, and 15, being identified as candidate enzymes for mediating the S-acylation of CCR5 (Boncompain et al., 2019). The S-acylation of CCR5 is important for trafficking of the

protein as non-acylated mutants are retained at the Golgi. Furthermore, non-acylated CCR5 that reaches the plasma membrane is rapidly internalised and degraded. The reason for this is unclear although S-acylation appears to be important for the association of CCR5 with cholesterol in plasma membrane raft domains and also plays a role in clathrin- and caveolae-dependent endocytosis (Jansen and Beaumelle, 2022, Boncompain et al., 2019). The reduced membrane association of non-acylated CCR5 affects its ability to interact with HIV, and therefore reduces in HIV-1 entry and *de novo* virus production (Boncompain et al., 2019). This observation has led to interest in targeting S-acylation of CCR5 as an effective therapeutic approach in controlling viral entry and/or other disease processes.

Another example of a transmembrane protein that is regulated by S-acylation is lipoprotein-receptor-related protein 6 (LRP6). LRP6 has been described for its role in the Wnt signalling pathway and more importantly has been found to be required for the endocytosis of anthrax toxins into the cytoplasm (Abrami et al., 2008a). LRP6 undergoes S-acylation of juxta-transmembrane cysteine residues at the ER, and blocking this process through mutagenesis of target cysteines leads to ER retention, aggregation, and degradation (via lysine monoubiquitination) (Abrami et al., 2008b). It was suggested that the retention of LRP6 occurs due to hydrophobic mismatch of the long TMD (23 aa) of LRP6 with the thin ER membrane. Resulting in the exposure of hydrophobic regions of the TMD with charged phospholipid headgroups and subsequent aggregation of the protein. In this case, modelling analysis predicted that S-acylation of cysteines in proximity to the TMD promoted its tilting in the membrane to minimise hydrophobic mismatch, allowing for proper assembly and trafficking to the plasma membrane (Abrami et al., 2008b).

**S-acylation and protein targeting to lipid rafts**

In addition to targeting CCR5 to raft domains, S-acylation has been proposed to be a more general signal for protein targeting to cholesterol-rich raft subdomains (Kordyukova et al., 2019). Lipid rafts are liquid-ordered domains found with cell membranes that are thought to be highly dynamic assemblies of cholesterol, sphingolipids, and relevant proteins. The proteins that are targeted to raft domains include GPI-anchored proteins but also acylated proteins modified with saturated acyl chains (which have a high affinity for tightly-packed raft structures) (Sezgin et al., 2017). Lipid rafts have been suggested to be organising platforms for signalling

pathways and neurotransmitter release pathways by facilitating co-sequestration and a closer interaction of interacting proteins at the membrane (Sviridov et al., 2020). One group of proteins that are known to associate with raft domains is the SNARE protein family, which play important roles in membrane fusion pathways, including those pathways that mediate neurotransmitter secretion (Greaves et al., 2010a). The related SNARE proteins, SNAP25 and SNAP23, are known to be targeted to the plasma membrane due to the S-acylation of a central cysteine-rich domain. Furthermore, the extent of S-acylation of this domain was shown to be a key factor controlling their association with lipid raft domains (Salaün et al., 2005a, Salaün et al., 2005b).

The cysteine-rich domain (CRD) of SNAP25b contains four closely spaced Cys residues: C85, C88, C90, & C92; whereas the CRD of SNAP23 contains five cysteines: C79, C80, C83, C85, & C87 (Greaves et al., 2010a, Vogel and Roche, 1999). In PC12 cells, endogenous SNAP23 exhibited a 54% association with detergent-insoluble lipid rafts, whereas SNAP25 only showed a 20% raft association (Salaün et al., 2005b). This was an interesting observation considering that the proteins share 61% amino acid identity (UniProt alignment, percentage identity between SNP25_HUMAN (206 aa) & SNP23_HUMAN (211 aa)). Interestingly, single point mutation analysis of both proteins revealed that Cys-79 within SNAP23 and Phe-84 within SNAP25b are the critical residues which determine the level of lipid raft association (Cys-79 and Phe-84 are present at the same position in SNAP23 and SNAP25, respectively). Specifically, it was shown that replacement of Cys-79 in SNAP23 with a Phe residue (to mimic SNAP25b) decreased detergent-insoluble lipid raft association to a similar level as seen for SNAP25b. Conversely, substitution of Phe84 in SNAP25b with a Cys residue (to mimic the sequence of SNAP23) enhanced raft association to a similar level as seen for SNAP23 (Salaün et al., 2005b). Strikingly, the F84C mutant of SNAP25 was less active in exocytosis than SNAP23 WT and the C79F mutant of SNAP23 was more active than SNAP23 WT (Salaun et al, 2005). These results suggest that the level of raft association of SNAP25 and SNAP23 might be determined by their level of S-acylation and that there is an inverse relationship between raft association and functional activity in exocytosis.

## 1.7 Links between S-acylation and disease

### Cancer

There is growing evidence linking S-acylation to cancer, which is perhaps not surprising given that many cancer driving genes are modified by acylation (Yeste-Velasco et al., 2015, Ko and Dixon, 2018). As previously discussed, S-acylation is important in the signalling activity of small GTPases such as RAS (Busquets-Hernández and Triola, 2021). In humans, three RAS genes encode for four Ras proteins: N-RAS, H-RAS, K-RAS4A, and K-RAS4B (K-RAS is encoded as two alternatively spliced isoforms) (Hobbs et al., 2016). Around 20% of cancer patients exhibit mutations in RAS, with the protein being among the most frequently altered oncogenes, and the oncogenic mutations typically trap RAS in a GTP-locked active state, leading to enhanced signalling and cellular proliferation (Hobbs et al., 2016, Prior et al., 2020, Busquets-Hernández and Triola, 2021).

In addition, there is also evidence linking specific zDHHC enzymes to cancer, including zDHHC14. This enzyme is ER/Golgi localised and highly expressed in the brain and female tissues (endometrium and breast). zDHHC14 is also predicted to be the only zDHHC that contains a C-terminal Type-I PDZ binding domain (S/T-X-hydrophobic-COOH) (Ohno et al., 2006, Sanders et al., 2020, Gunawardana, 2016). Within axons, zDHHC14 has been shown to control the S-acylation and clustering of PSD-93 and the associated Kv1-family potassium channels (Sanders et al., 2020). There is also evidence showing that zDHHC14 is capable of S-acylating β2-adrenergic receptors, with potential influence on G-protein coupled receptor signalling (Adachi et al., 2016). However, zDHHC14 has also been shown to associated with the development of cancer and with suggested roles in apoptosis (Yeste-Velasco et al., 2014), cell differentiation (Yu et al., 2011), and cell migration and invasion (Oo et al., 2014)

Early evidence in 2011, found that zDHHC14 was activated through chromosomal translocation t(6;14)(q25;q32) (Yu et al., 2011). The breakpoint of this chromosomal translocation is on chromosome 14 which contains the B-cell lymphoma/leukaemia 11 B (BCL11B) gene, associated to acute biphenotypic leukaemia (Wang et al., 2020). Quantitative real time RT-PCR analysis showed that zDHHC14 was upregulated by 15-fold in leukemic samples compared to controls (Yu et al., 2011). Furthermore, the same study showed that zDHHC14 overexpression in differentiating K526 cells

(human immortalised myelogenous leukaemia cell line) resulted in approximately 30% decrease of CD61 expression (CD61 is a marker of megakaryocytic differentiation). This observation suggested that zDHHC14 could inhibit cellular differentiation, which is an important aspect considering that inhibition of differentiation is an early and critical step in leukemogenesis (Yu et al., 2011, Chen et al., 2022). Subsequent work using siRNA knockdown and overexpression in gastric cancer cell lines gave evidence for the involvement of zDHHC14 in cancer progression/invasion by mediating cell adhesion (Oo et al., 2014). Conversely, it should also be noted however that zDHHC14 has also been implicated as a tumour suppressor in testicular germ cell tumours (TGCT), where evidence from 2014 suggested that zDHHC14 is involved in apoptosis via influence over the classic caspase-dependent apoptotic pathway (Yeste-Velasco et al., 2014). This study showed that *ZDHHC14* was downregulated in TGCT and prostate cancer, and next generation sequencing identified three different single nucleotide mutations in the *ZDHHC14* gene linked to cancer. One was in TGCT (L215S) (SUSA cells) and two in prostate cancer cells (C181Y & A373Y) (LNCaP) (Yeste-Velasco et al., 2014). Interestingly both the L215 and C181Y mutations are within the DHHC domain of zDHHC14, whereas the A373Y is within the C-terminal cytoplasmic tail.

**X-linked intellectual disability (XLID)**

In addition to cancer, there are also several links between S-acylation and neurological disorders. The strongest link is between zDHHC9 and X-linked intellectual disability (XLID) as gene mutations in the *ZDHHC9* gene cause this condition. In addition, disruption of the *ZDHHC15* gene has also been shown to cause XLID but the evidence for involvement of this isoform in the condition is more limited (Mansouri et al., 2005, Raymond et al., 2007). As of 2022, 162 genes had been linked to 42 named XLID syndromes (where XLID occurs with sign and symptoms affecting other parts of the body) and 27 numbered nonsyndromic XLID families (where a condition is not associated with other signs and symptoms) (Schwartz et al., 2023). Mutations in *ZDHHC9* are relatively common with 2% of XLID patients reported to have loss of function mutations in this gene (Baker et al., 2015, Shimell et al., 2019). The substrate network of zDHHC9 is not clear although there has been interest in the role of this enzyme as an acyltransferase against RAS since the discovery that the yeast zDHHC9 homologue (ERF2) was active against yeast Ras2p (Raymond et al.,

2007, Busquets-Hernández and Triola, 2021, Lobo et al., 2002, Swarthout et al., 2005).

The naturally occurring variants in zDHHC9 include nucleotide changes that result in amino acid substitutions R148W and P150S; these residues reside within the catalytic DHHC-CRD of the enzyme. Purified zDHHC9 enzymes containing the R148W and P150S substitutions were shown to have an altered autoacylation status, thereby lowering enzymatic activity (Chamberlain and Shipston, 2015, Mitchell et al., 2014). A major breakthrough in understanding how loss-of-function zDHHC9 mutations might cause XLID was delivered by work from the Bamji group in 2019. They showed that knockout of zDHHC9 led to reduced dendritic growth, a feature that has been seen in other forms of ID (Shimell et al., 2019, Quach et al., 2021). Furthermore, their analysis suggested that the loss of dendrite growth was caused by a loss of S-acylation of N-Ras. Another interesting finding from this study was that zDHHC9 knock out mice exhibit increased seizure activity and network excitability (Shimell et al., 2019). This was linked to a decrease in the activity of inhibitory synapses because of decreased S-acylation of the small GTPase TC10. Interestingly, childhood epilepsy is a frequent feature seen in people with zDHHC9 mutations, and it will be interesting to explore if this is also linked to changes in TC10 and synapse development (Baker et al., 2015). The Bamji group also recently reported that zDHHC9 knock out led to an impairment of oligodendrocyte maturation and myelin formation (Hollman et al., 2023), which might explain changes in the volume of the corpus callosum (a white matter tract connecting the two brain hemispheres) seen in both people with zDHHC9 mutations and zDHHC9 knockout mice (Baker et al., 2015, Kouskou et al., 2018). Taken together the results of these studies suggest that XLID (and epilepsy) caused by zDHHC9 mutations may arise due to a loss of S-acylation of RAS and TC10 with downstream effects on dendrite growth, synapse development, and maturation of oligodendrocytes (Shimell et al., 2019, Hollman et al., 2023).

**Huntington's disease (HD)**

Huntington's disease (HD) is typically an inherited autosomal-dominant adult-onset neurodegenerative disorder caused by mutations in the Huntingtin gene (HTT). HD has a prevalence of 10.6-13.7 individuals per 100 000 in western populations, and is associated with cognitive decline, motor disturbances, and psychiatric symptoms (McColgan and Tabrizi, 2018). The *HTT* gene on chromosome 4 contains a CAG

(encoding glutamine) repeat sequence, which gets expanded in HD, producing a mutant protein with an expanded polyglutamine (polyQ) repeat sequence in the N-terminus (McColgan and Tabrizi, 2018). The polyQ region causes protein misfolding, abnormal trafficking, aggregation, toxicity, neuronal dysfunction, and cell death (Sutton et al., 2013). It has been challenging to understand how mutant HTT causes HD as the protein has been reported to interact with over 100 other proteins (Goehler et al., 2004).

The first connection between HD and S-acylation came from a study that reported that HTT is S-acylated on a single cysteine (Cys-214) by zDHHC17 and that this is important for the normal trafficking of HTT. The same study also showed that S-acylation was disrupted for mutant HTT (mHTT) (Yanai et al., 2006). These findings suggested that changes in mHTT S-acylation might contribute to the observed toxicity of the mutant protein. Surprisingly, a subsequent study also suggested that wild-type HTT, but not mHTT, enhances the S-acylation activity of zDHHC17 (Huang et al., 2011). Furthermore, the same study showed that mHTT also has a reduced interaction with zDHHC17 (Sutton et al., 2013). This observation suggested that decreased activity of zDHHC17 (due to loss of regulation by HTT) might also contribute to some of the features of HD. Indeed, zDHHC17 deficient mice were shown to develop neuropathological and behavioural features that were consistent with features seen in HD. These included defects in motor coordination, pre-pulse inhibition, and hippocampal-dependent spatial learning and memory (Sutton et al., 2013, Chamberlain and Shipston, 2015). The phenotype of the zDHHC17 mutant mice is consistent with the notion that a loss of mHTT regulation of zDHHC17 could contribute to some of the features of HD and this idea clearly warrants further investigation. Of interest, it is currently unclear how HTT binding to zDHHC17 might regulate enzyme activity, not least because the mechanism of HTT interaction with zDHHC17 was suggested to be similar to other substrate proteins such as SNAP25 (Lemonidis et al., 2015a, Huang et al., 2011, Sanders et al., 2014, Yang and Cynader, 2011).

**Neuronal ceroid lipofuscinosis**

Neuronal ceroid lipofuscinoses (NCL) are a group of inherited neurodegenerative disorders that characteristically exhibit an accumulation of autofluorescent “lipofuscin” in neurons and other cells of the body (Simonati and Williams, 2022). Fourteen

different genes have been genetically linked to human NCL, and depending upon the age of onset, NCLs are classed as early infantile, late infantile, juvenile, and adult (Henderson et al., 2016, Greaves et al., 2012). One of the best characterised forms of NCL is infantile NCL (INCL), which is caused by mutations in the lysosomal PPT1 enzyme, which mediates protein deacylation during degradation (Henderson et al., 2016). INCL is associated with rapid neurodegeneration and death at an early age (2-4 years old) and there is no known cure for this condition (Simonati and Williams, 2022). Interestingly, another link between S-acylation and NCL came with a group of studies that reported mutations in the DNAJC5 gene as a cause of adult-onset NCL (ANCL) (Henderson et al., 2016, Mole and Cotman, 2015).

DNAJC5 encodes cysteine string protein α (CSPα), which was first described in 1990 as a synaptic vesicle localised chaperone protein (Burgoyne and Morgan, 2015, Zinsmaier et al., 1990, Chamberlain and Shipston, 2015). The 198 aa protein regulates exocytosis by functioning as a co-chaperone for the SNARE protein SNAP25 (described above). CSPα contains a cysteine-rich motif consisting of 14 S-acylated cysteines within a 25 aa region (aa 112-137) (Burgoyne and Morgan, 2015). CSPα has been shown to interact with and be S-acylated by zDHHC17 (as well as zDHHC3, 7, & 15) (Greaves et al., 2012). ANCL is caused by mutations that substitute amino acids in the cysteine-rich domain, specifically L115R or ΔL116. Analysis of these mutant proteins showed that they undergo aggregation and that these aggregates are visible on SDS gels. Furthermore, the aggregates were shown to be dependent on S-acylation and perhaps formed due to changes in the S-acylation status of the mutant proteins (Greaves et al., 2009, Nosková et al., 2011, Benitez et al., 2011, Velinov et al., 2012, Cadieux-Dion et al., 2013, Diez-Ardanuy et al., 2017). Interestingly, a subsequent study identified a potential link between PPT1 and CSP in INCL and ANCL, respectively. Analysis of mutant human CSPα (L115R or ΔL116) cortex homogenates, revealed that PPT1 mRNA and protein levels showed a dramatic increase of approximately 90-fold (Henderson et al., 2016). It would be interesting to explore if this increase in PPT1 levels relates to an inability to deacylate mutant CSP during its degradation in lysosomes, which could lead to accumulation of acylated peptide aggregates as a possble cause of lysosomal dysfunction.

## 1.8 S-acylation of SARS-CoV-2

S-acylation is a highly conserved biological process that is not only limited to mammalian proteins and systems. S-acylation has also been described in plants (Hurst and Hemsley, 2015), protist, viruses, as well as a few bacterial proteins that are likely autoacylated (Sobocińska et al., 2017, Chamberlain and Shipston, 2015). Indeed, the first S-acylated protein to be identified was the glycoprotein of the vesicular stomatitis virus (Schmidt and Schlesinger, 1979). More recently there has been an unparalleled volume of research surrounding the severe acute respiratory syndrome coronavirus 2 (SARS-CoV-2), which has been responsible for a global pandemic and the development of the associated respiratory illness, coronavirus disease 2019 (COVID-19) (Markov et al., 2023). Where globally as of the 2$^{nd}$ of November 2023, there have been 771,679,618 confirmed cases of COVID-19, including 6,977,023 deaths, reported to the W.H.O (World Health Organisation, 2023).

SARS-CoV-2 is a positive-sense single-stranded RNA virus within the family of *Coronaviridae* that is contagious in humans (Chan *et al*., 2020; Machhi *et al.,* 2020). The genome of SARS-CoV-2 is arranged into 14 open reading frames (Orf) which encode 31 proteins, grouped into four structural: S (spike), M (membrane), envelope (E), N (nucleocapsid), 16 non-structural proteins, and 11 accessory proteins (figure 5.0, adapted from Redondo et al., (2021)). Although there have been a small number of studies investigating the S-acylation of the envelope protein (Sun et al., 2021), by far the most intensive research has focused on S-acylation of the spike protein. In order for SARS-CoV-2 to enter the host cell, the viral spike protein (which is a transmembrane glycoprotein) must interact with the host cell surface protein angiotensin-converting enzyme 2 (ACE2). Following this, the spike protein is cleaved by transmembrane serine protease 2 (TMPRSS2) which activates the viruses membrane-fusion capacity (or endocytosis). Viral genomic RNA (gRNA) is then released into the cytosol and hijacks host-cell machinery to initiate replication of the SARS-CoV-2 genome. Assembly of newly synthesised SARS-CoV-2 structural components takes place within an ER–Golgi intermediate compartment (ERGIC), which subsequently forms into an exocytotic vesicle enclosing a newly formed virion (Malone et al., 2022).

ERGIC assembly of the spike protein creates trimers which are present on the viral membrane. Each spike monomer is composed of two subunits: an extracellular S1 subunit (which binds ACE2) and a transmembrane S2 subunit with a cytosolic tail.

The S-acylation of viral proteins is known to be involved in virus assembly, membrane fusion, and infection (Wu et al., 2021). The spike protein has 10 cysteine residues within the first 20 amino acids of the cytosolic C-terminal tail, making it one of the most cysteine-rich proteins encoded by animal viruses (Mesquita et al., 2021, Sanders et al., 2021), and acyl-biotin exchange (ABE) assays in HEK-293T cells using Flag-tagged spike protein have shown that the viral protein is S-acylated at its cytosolic C-terminal end (Wu et al., 2021). Wu and colleagues further showed that the spike protein interacts with and is S-acylated by the zDHHC5-GOLGA7 complex. Furthermore, the same study revealed that altering spike S-acylation suppressed spike-mediated membrane fusion and the entry of SARS-CoV-2 pseudovirus into host cells. This was achieved using luciferase-expressing lentiviruses pseudotyped with either WT spike protein or a C-terminal truncated mutant lacking key cysteine residues. The entry of these pseudoviruses into ACE2-expressing HEK-293T was inferred via luciferase activity (Wu et al., 2021).

Other studies have also concluded that the cytoplasmic tail of SARS-CoV-2 spike protein is the determining factor for spike membrane trafficking, localisation, and enhancement of fusion events (Li et al., 2022b). The role of the C-terminus and S-acylation of spike in SARS-CoV-2 infection is likely to be a conserved feature of coronaviruses, as work on the precursor virus SARS-CoV also showed that S-acylation of its C-terminal domain was important for virus-induced cell-to-cell fusion (Petit et al., 2007). This 2007 study made use of African green monkey kidney (Vero) cell monolayers transfected with ACE2 receptor and flag-tagged spike protein, followed by immunohistochemical detection under live cell conditions to show the importance of S-acylation (Petit et al., 2007). Alignment of spike sequences from other human (SARS, MERS, OC43, 5HKU1, NL63 & 229E), and animal (BCoV, MHV-JHM, MHV2, IBV, TGEV, FIPV, RATG13) coronaviruses confirm the presence of a conserved C-terminal cytosolic cysteine-rich region.

In addition to zDHHC5-GOLGA7, other zDHHC enzymes have been reported to S-acylate spike including zDHHC2, 3, 4, 5, 8, 9, 11, 14, 16, 19, and 20, which were identified through ABE assays (Li et al., 2022a). In addition, an earlier study using click-chemistry based S-acylation assays identified zDHHC2, 3, 6, 11, 12, 20, 21, and 24, as being active against spike protein (Puthenveetil et al., 2021). A further study from 2022 identified zDHHC9 as an interactor and S-acylating enzyme of spike protein (Ramadan et al., 2022).

Added to this, a study from the lab of Gisou van der Goot, implicated zDHHC 8, 9 and 20 in S-acylation of the spike protein and subsequent enhancement of virus infectivity. These enzymes were identified by analysing the incorporation of $^{3}$H-palmitate on ectopically expressed spike proteins, in HeLa cells which were depleted of each zDHHC enzyme using siRNA. Unlike other studies discussed above, further analysis by Mesquita et al., suggested that the main S-acylation enzyme for the spike protein is zDHHC20, but that this is followed by further modification by zDHHC9 (Mesquita et al., 2021). Specifically, it was proposed that zDHHC20 is responsible for spike S-acylation at the ER, and that zDHHC9 subsequently S-acylates spike upon translocation to Golgi compartments. Interestingly, zDHHC20 (and zDHHC2, 8, & 15) was previously reported to S-acylate hemagglutinin A of influenza virus (Gadalla et al., 2020). Mesquita and colleagues (2022) were able to show using a metabolic $^{3}$H-palmitate pulse-and-chase approach that spike deacylation is mediated by APTs in spike transfected HeLa cells. However, similar experiments in Vero E6 cells (which are used as host cells for growing viruses), displayed no significant loss of palmitate from spike protein, inferring that spike deacylation might be absent or ineffective during SARS-CoV-2 Infection (Mesquita et al., 2021). Under these conditions, the deacylation of other cellular proteins was still detected, suggesting that at least some APTs are still active. It was suggested that the spike protein may be rapidly segregated from APTs during early Golgi virion formation and infection (which would not occur during simple HeLa cell transfection experiments) (Mesquita et al., 2021). As S-acylation of the spike protein is a critical feature for infectivity of SARS-CoV-2, this segregation from APTs may be critical for subsequent infection activity (Bader et al., 2022, Santopolo et al., 2021).

The same study by Mesquita and colleagues (2022) also investigated SARS-CoV-2 membrane lipid organisation using coarse-grained molecular dynamics simulations, and membranes comprised of: 50% dipalmitoylphosphatidylcholine, 30% dilinoleylphosphatidylcholine, and 20% cholesterol. This analysis suggested that S-acylation of the C-terminal end of the spike protein leads to the collapse of the cytoplasmic tails (in subunit 2), which then encourages acyl chains to position close to the spike protein transmembrane domain (in subunit 1), leading to a 9-fold increase in local acyl chain concentration and the formation of cholesterol/sphingolipid-rich raft-like domains (Mesquita et al., 2021, Vilmen et al., 2021). Indeed, spike protein was also detected in detergent-resistant membranes (DRMs) which have been used previously to suggest the association of proteins with cholesterol-rich lipid raft

domains. zDHHC20 siRNA (but not zDHHC9) knockouts led to reduced association of spike proteins to these DRM structures (Mesquita et al., 2021). Taken together, the studies into SARS-CoV-2 suggest that S-acylation of spike is involved in virus assembly, membrane fusion, and infection. Highlighting the S-acylation machinery as potential targets for the development of therapeutic drug treatments.

## 1.9 Specificity of zDHHC substrate interactions

Understanding how zDHHC enzymes recognise and interact with their substrates is an important step in the development of specific inhibitors or therapeutics. However, research into zDHHC-substrate specificity has proven to be a complex and nuanced area of investigation. Many zDHHC enzymes exhibit a varying degree of specificity for their substrates. For example, zDHHC3 and zDHHC7 have been reported to be high activity/low specificity enzymes, whereas zDHHC13 and zDHHC17 have been suggested to act as low activity/high specificity enzymes (Lemonidis et al., 2014). zDHHC enzymes with high S-acylation activity are thought to achieve this promiscuity by being able to transfer their acyl chains rapidly to any accessible and reactive cysteine in close proximity (Lemonidis et al., 2017b).

The mechanisms that define higher specificity interactions between zDHHC enzymes and specific substrates is currently not well-defined (Malgapo and Linder, 2021). In most reported cases these interactions are mediated by the presence/recognition of amino acid motifs or conserved regions present in the enzyme and substrate. For instance, aside from the DHHC domain, three additional short regions of homology between zDHHC enzymes which contain motifs/highly conserved residues have been reported. These are the DPG (Asp-Pro-Gly) motif (Mitchell et al., 2006), the TTxE (Thr-Thr-x-Glu) motif (Mitchell et al., 2006), and the PaCCT (palmitoyltransferase conserved C-terminal) motif (González Montoro et al., 2009). In all zDHHC enzymes, these three motifs are predicted to be cytosolic facing, with the DPG motif preceding the DHHC domain, and the TTxE and PaCCT motifs positioned within the C-terminal cytoplasmic end of the enzymes (Malgapo and Linder, 2021). Although these motifs have been suggested to structurally stabilise zDHHC enzymes, there is little currently known about their exact function (Malgapo and Linder, 2021).

In addition to these conserved domains, several zDHHC enzymes have also been reported to contain other domains that might contribute to substrate interactions.

zDHHC3, 5, 7, 8, 14, 16, 17, 20, and 21, have been shown to contain PSD-95/discs large/ZO-1 (PDZ) domains. These domains are common small structural folds of 80–90 aa consisting of 5-6 β-strands and 2-3 α-helicies (Malgapo and Linder, 2021, Elliot Murphy and Banerjee, 2022, Lee and Zheng, 2010). These PDZ domains are one of the largest classes of protein-protein interaction (PPI) domains in the human proteome, and since their discovery in the early 1990s, over 268 PDZ domains have been identified in 151 distinct human proteins (Christensen et al., 2019). PDZ binding domains are classified into three types based on the C-terminal motifs that they bind too: type I – S/T-X-Ψ-COOH, type II – Ψ-X-Ψ-COOH, and type III – D/E-X-Ψ-COOH, (where X is any amino acid and Ψ is any hydrophobic residue (Kalyoncu et al., 2010). zDHHC14 (SSV-COOH) contains a type I PDZ binding motif, whereas all other zDHHCs that contain PDZ binding motifs, they are type II, such as in zDHHC5 (ISV-COOH) and zDHHC8 (ISV-COOH). It should be noted that not all PDZ domains adhere strictly to these rules, and also that several PDZ proteins contain more than one PDZ domain such as glutamate receptor-interacting protein (GRIP) which has seven PDZ domains (Lee and Zheng, 2010, Kalyoncu et al., 2010).

PDZ domains are often found in signalling proteins (i.e., PSD93 and PSD95) and typically recognise PDZ binding domains present in the extreme C-termini of target proteins (i.e., in zDHHC enzymes). PDZ domains often facilitate the anchoring of receptor proteins in the membrane to cytoskeletal components, helping to stabilise and organise signalling complexes at cellular membranes (Christensen et al., 2019, Lee and Zheng, 2010). Of the zDHHC enzymes which contain a PDZ domain at the C-terminal end, zDHHC5, 8, and 14, have been the most well studied. In 2012, it was shown that the C-terminal ends of zDHHC5 and zDHHC8 bind to (via yeast two-hybrid screen) and S-acylate (via acyl-biotinyl exchange (ABE) assay) GRIP1b via PDZ domain/motif binding (Thomas et al., 2012). Both zDHHC5 and zDHHC8 are important for neuronal regulation (Thomas et al., 2012, Collura et al., 2020), and their S-acylation of GRIP1b was shown to target this substrate protein to dendritic endosomes, allowing GRIP1b to link these endosomes to microtubule motors. The zDHHC/S-acylation-mediated localisation of GRIP1b places the protein in a favourable position to mediate activity-dependent AMPA receptor trafficking and recycling (Thomas et al., 2012). AMPA receptors are ionotropic glutamate receptors that play a major role in excitatory neurotransmission, and defects in AMPA receptors can lead to excitotoxicity, impaired neurotransmission, and neuronal/axonal degradation (Moretto and Passafaro, 2018, Zanetti et al., 2021). Given this role of

zDHHC5 and zDHHC8, it is perhaps not surprising that both enzymes are highly expressed in neurons and are associated to neuropsychiatric conditions with a pathology of errant neuroexcitatory activity such as bipolar disorder, schizophrenia, and epilepsy (Shimell et al., 2021, Mukai et al., 2004, Yang et al., 2018, Thomas et al., 2012).

zDHHC14 interacts with and S-acylates PSD93 (also known as DLG2), which is a membrane-associated guanylate kinase that also contains a type I PDZ domain (through which it interacts with zDHHC14) (Sanders et al., 2020). PSD93 is a key postsynaptic multimeric scaffold protein that forms complexes with and promotes the clustering of receptors, ion channels, and associated synaptic signalling proteins. Thereby generating postsynaptic signalling networks and controlling synaptic transmission (Guo et al., 2012). The 2020 study by Sanders et al., explored the role of zDHHC14 in the clustering of PSD93 and also the associated type-I voltage-gated potassium (Kv1) channels at the axon initial segment. They showed that the loss of zDHHC14 or the impairment of PSD93 S-acylation disrupted the targeting of Kv1 to axon initial segments. This effect on Kv1 targeting is predicted to adversely affect voltage-gated channel activity and/or impair action potential repolarisation, which may present phenotypically as a number of neurological conditions with their basis in neuronal hyperexcitability (i.e., epilepsy) (Sanders et al., 2020). For example, the impairment of KV1 channels has been shown to lead to motor disorders such as episodic ataxia type 1, which is a neurological disorder involving myokymia and episodic ataxia (Browne et al., 1994, Imbrici et al., 2006)

Alternative mechanisms of zDHHC-substrate specificity have also been described. For example, although zDHHC5 interacts with GRIP1b through PDZ domains, this enzyme has been shown to also have an alternative mode of recognition for the substrate cardiac Na-K ATPase (Na-pump) accessory sub-unit, Phospholemman (PLM). PLM (also known as FXYD1) is one of seven small membrane proteins within the FXYD family of ion transport regulators, which all share a highly conserved N-terminal domain beginning with an FXYD amino acid motif (Jin et al., 2021). PLM (and other FXYD proteins) has been shown to colocalise/interact with and regulate Na-pumps in cardiac myocytes (Cheung et al., 2010). The dysregulation of Na-pump proteins has been linked to a wide variety of disorders including hypomagnesemia, seizures, oncogenesis, and various cardiopathies (Biondo et al., 2021, Gagnon and Delpire, 2020). Na-pumps have been shown to be regulated by a balance of PLM

phosphorylation which activates the Na-Pump and PLM S-acylation which inhibits the Na-pump (Howie et al., 2018, Plain et al., 2020). Using truncation mutant analysis of zDHHC5 it was shown that the intracellular C-terminal region of zDHHC5 (between N218 and T334) was required for the interaction with PLM (PLM binding site was between S37 and R72) (Howie et al., 2014). As previously mentioned, the C-terminal end zDHHC5 contains two conserved C-terminal motifs (TTxE and PaCCT) and a PDZ binding domain, however these were not implicated as being responsible for PLM interaction. Instead, an amphipathic helix of zDHHC5 was identified that binds to the Na-Pump α-subunit, and not to PLM directly (Plain et al., 2020). A model was thereby proposed in which zDHHC5 is able to S-acylate PLM via an indirect recruitment of the substrate through binding to the Na-pump α subunit. Thus a complex formed between the C-terminal region of zDHHC5 and the Na-pump, would place PLM in a favourable position to access the catalytic DHHC domain, where it can then be S-acylated (Plain et al., 2020, Malgapo and Linder, 2021).

In addition to the aforementioned examples of zDHHC-substrate specificities, zDHHC17 and zDHHC13 are two other zDHHC enzymes that operate as high-specificity enzymes (Chamberlain and Shipston, 2015). As previously mentioned, zDHHC13 and zDHHC17 are distinct among the zDHHC family as they contain an N-terminal ankyrin (Ank) repeat domain. This Ank domain has been shown to be important for the substrate recognition of HTT (Singaraja et al., 2002), SNAP25b, and CSPα (Lemonidis et al., 2014). However, although zDHHC13 is an interactor it should be noted that zDHHC13 was not found to be catalytically active towards these substrates, likely due to the presence of a non-conforming DQHC motif, instead of the typical DHHC motif (Lemonidis et al., 2014). Further analyses of the interaction of these substrates with zDHHC17 identified a hexapeptide consensus motif (VIAP)(VIT)XXQP that interacts with ANK17 (Lemonidis et al., 2015a). The sequences of the hexapeptide motif in the substrates discussed above are: HTT (IITEQP), SNAP25b (VVASQP), and CSPα (PIVIQP). This consensus sequence was termed as the “zDHHC ankyrin-repeat binding motif” (zDABM) and it is required to be present in a cytosolic unstructured region of the protein to allow binding to ANK17 (Lemonidis et al., 2015a).

The identification of the zDABM was furthered in 2017 by the Banerjee group who were able to generate a high-resolution crystal structure of ANK17 in complex with a SNAP25b peptide fragment containing the zDABM (aa 111-GVVASQPARV-120;

zDABM is underlined) (Verardi et al., 2017). This study further showed that residues N100 and W130 within ANK17 were critical for zDABM binding. This interaction was proposed to be established via the aromatic ring of W130 forming key contacts with the critical proline residue, P117 within the zDABM of SNAP25b. Together with N100 in ANK17 forming hydrogen bonds with V113 in the zDABM of SNAP25b (Verardi et al., 2017). Additionally, E89 and D122 in ANK17 establishes hydrogen bonds with Q116 in the SNAP25b peptide, and Y67 of ANK17 interacts with V112 in SNAP25b via van der Waals interactions (Verardi et al., 2017).

Building on the specificity of this new recognition site, subsequent research by Lemonidis and colleagues predicted and validated zDABM sequences from 90 different proteins that could bind to zDHHC17/13 (Lemonidis et al., 2017a). They were able to achieve this by using peptide-array screening to examine the binding of the AR of zDHHC17 to potential zDABMs present in different proteins. From the proteins identified to contain a zDABM, the entire family of Sprouty proteins (Spry1-4) and two of the three Sprouty-related SPRED proteins (SPRED1/2) were identified (SPRED3 does not contain a zDABM) (Figure 1.5). Although there were many potential substrates of zDHHC17/13 identified in this screen, Spry/SPRED proteins were considered worthy of further investigation as a “bioplex” interactome study identified that endogenous Spry2 and zDHHC17 form a complex in cells (Huttlin et al., 2015). The proteins are of additional interest due to the presence of a highly conserved C-terminal cysteine rich Sprouty (SPR) domain (which for Spry2 contains 26 cysteines). Furthermore, Spry/SPRED proteins have been linked to various cancers and have tumour suppressor activity (Masoumi-Moghaddam et al., 2014b). In general, there is little known about the S-acylation of such cysteine-rich proteins, however Spry2 has now been shown to interact with and be S-acylated by zDHHC17 (Masoumi-Moghaddam et al., 2014b, Locatelli et al., 2020).

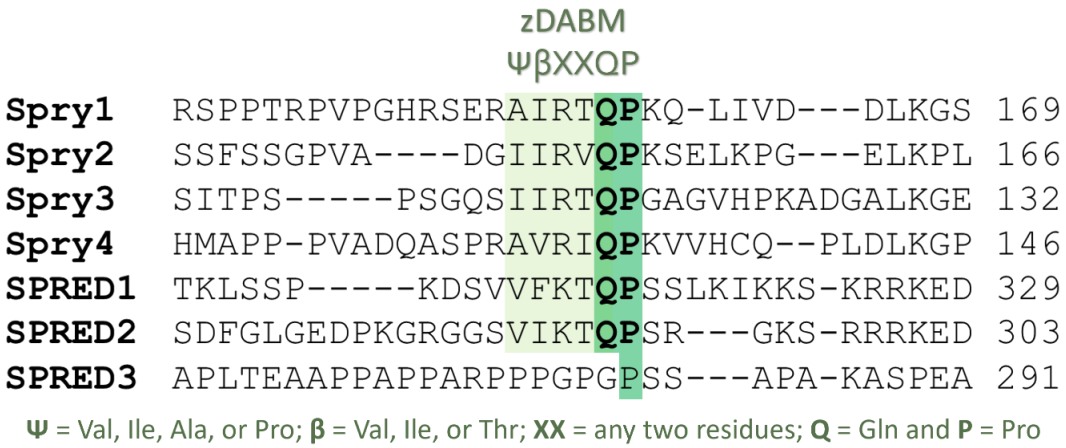


***Figure 1.5. Alignment of zDABM within Spry & SPRED proteins.*** *Protein sequence alignment of hSpry1, hSpry2, hSpry3, hSpry4, hSPRED1, hSPRED2, and hSPRED3. Generated using the align tool from UniProt (Consortium, 2022). The zDHHC ankyrin-repeat binding motif (zDABM) regions of the proteins are highlighted in light green, with the critical QP dipeptide emboldened and highlighted in dark green. SPRED3 does not contain a zDABM, but an aligned proline is still highlighted for visual reference. zDABM = ΨβXXQP, where Ψ = Val, Ile, Ala, or Pro; β = Val, Ile, or Thr; XX = any two residues; Q = Gln, and P = Pro).*

## 1.10 The Sprouty/SPRED family of proteins

Sprouty proteins were originally discovered as antagonists of the *Drosophila* branchless (Bnl)/fibroblast growth factor (FGF) signalling pathway which promotes *Drosophila* tracheal branching pattern formation (Sutherland et al., 1996, Hacohen et al., 1998). In the absence of Sprouty to inhibit this pathway, the seminal 1998 study reported an excessive occurrence of tracheal secondary ectopic branches 'sprouting' from primary apical stalks: hence the designated protein name (Hacohen et al., 1998). At that time, Hacohen and colleagues (1998) were also able to identify through an expressed sequence tag database (dbEST) three human homologues of *Drosophila* Sprouty protein: h-Sprouty1 (Spry1), h-Sprouty2 (Spry2), and h-Sprouty (Spry3). A fourth homologue, h-Sprouty4 (Spry4) was identified in subsequent studies, first in mice (de Maximy et al., 1999) and then in human (Leeksma et al., 2002). This protein family was further expanded through the discovery of Sprouty-related, EVH1 domain containing proteins (SPREDs) for which there are three homologues: h-SPRED1 and h-SPRED2 were isolated from an osteoclast complementary DNA library using a yeast two-hybrid system (Wakioka et al., 2001), and h-SPRED3 was cloned by the same authors two years later (Kato et al., 2003).

### SPR domain

Sprouty proteins are between 288-319 aa in length, whereas SPRED proteins are between 410-444 aa long. The defining feature of all Spry/SPRED proteins is the highly conserved Sprouty (SPR) domain, which can also be described as a unique cysteine-rich domain (CRD) (figure 1.6), which in Spry2 is 114 aa in length and contains 26 cysteine residues. The SPR region is predicted to be made up of parallel alpha helices which flank a central disordered region (figure 1.7) and it has been shown to be important for the hetero/homodimerisation of Spry/SPRED proteins (King et al., 2005) and also for localisation. These proteins are most commonly associated to the plasma membrane, often translocating to lipid raft domains and caveolae (Lorenzo and McCormick, 2020). S-acylation of Spry2 has been shown to be important to anchor the proteins to the membrane (Impagnatiello et al., 2001, Locatelli et al., 2020, Lorenzo and McCormick, 2020). S-acylation of SPRED1 is also thought to be important for the localisation of this protein as removal of the SPR domain led to mis-localisation. Interestingly, addition of a CaaX motif from KRAS4B (CIIM -

farnesylated) onto the SPRED1 mutant lacking the SPR domain was not only able to recover plasma membrane association but also restored the ability of SPRED1 to reduce EGF-induced Ras activation and inhibit ERK activation, thus highlighting the primary role of S-acylation as a membrane anchor for SPRED1 (Stowe et al., 2012).

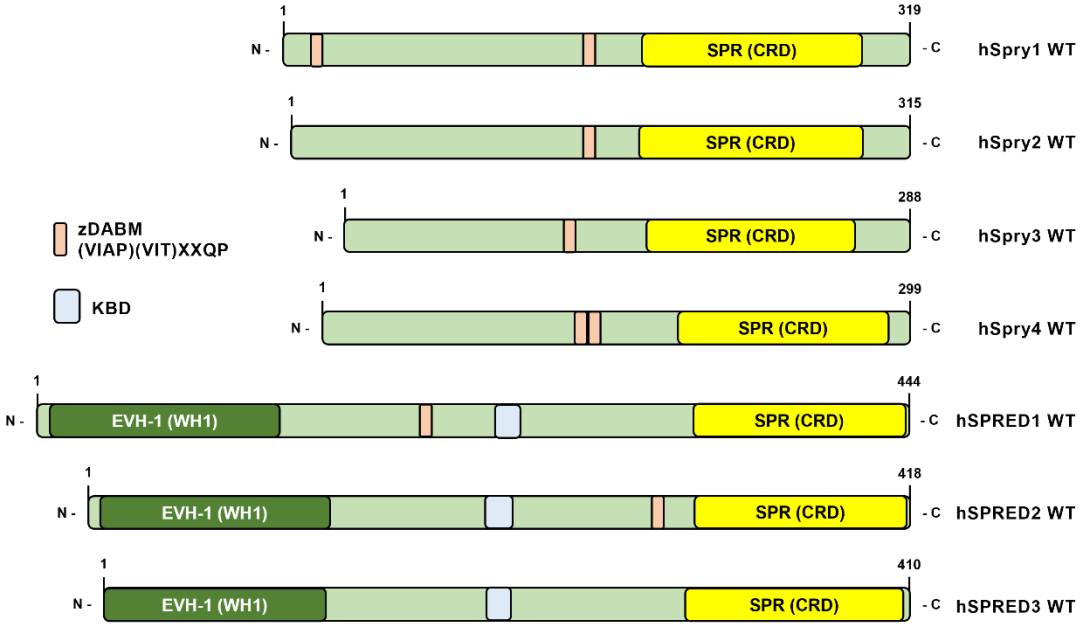


***Figure 1.6. Schematic diagram of the domain structure of Spry and SPRED protein.*** *(A) Schematic representation of hSpry1 (319 aa), hSpry2 (315 aa), hSpry3 (288 aa), hSpry4 (299 aa), hSPRED1 (444 aa), hSPRED2 (418 aa), and hSPRED3 (410 aa) (light green). Schematic representations are aligned at their C-terminal end. EVH1; Ena/VASP (enabled/vasodilator-stimulated phosphoprotein) homology 1 domain - also known as, WH1; WASP (Wiskott-Aldrich syndrome protein) homology 1 domain (dark green). zDABM; zDHHC ankyrin binding motif – (VIAP)(VIT)XXQP (orange). KBD; c-Kit kinase binding domain (light blue). SPR; Sprouty domain - also designated as, CRD; cysteine-rich domain (yellow).*

**Sprouty proteins**

Sprouty proteins (Spry) are key negative regulators of the MAPK/ERK signalling pathway (Masoumi-Moghaddam et al., 2014b), and have been implicated in a variety of embryonic, developmental, and physiological processes including the development of the lungs (Hashimoto et al., 2012), eyes (Shin et al., 2015), limbs (Wang and Beck, 2014), and brain/nervous system (Hausott and Klimaschewski, 2019). There is also a large body of evidence that describes the errant expression of Sprouty proteins within cancer (Kawazoe and Taniguchi, 2019), where they have been implicated in many different cancer types including: lung cancer (non-small-cell lung adenocarcinoma) (Tennis et al., 2010), prostate cancer (Patel et al., 2013a), breast cancer (He et al., 2016), and liver cancer (hepatocellular carcinoma) (Sirivatanauksorn et al., 2012).

The prevalence of changes in Spry proteins in cancer often makes them important prognostic biomarkers of disease. For instance, epithelial ovarian cancer (EOC) is one of the most common causes of female gynaecological cancer mortality, with most patients unable to be diagnosed until late presentation of advanced disease and widespread abdominal metastasis (Arora et al., 2023). A review from 2023 of US populations, estimated that in 2020 there were ~ 21,750 new ovarian cancer cases, with the estimated number of deaths at 13,940. These figures comprised 1.2% of all cancer cases and there was also a 5-year relative survival rate of only 48.6% (Arora et al., 2023). A study from 2015 showed that Spry1 is significantly downregulated in EOC tissues (Masoumi-Moghaddam et al., 2015b). This observation added to previous research from the same group which had shown that Spry1 was able to inhibit ERK activation and that there was an inverse correlation between Spry1 expression and EOC cell proliferation, migration, invasion, and survival (Masoumi-Moghaddam et al., 2014a). Together this data provides evidence to support Spry1 (and Spry proteins in general) as independent biomarkers of EOC prognosis or therapeutic assessment.

Although commonly associated with cancer, as previously mentioned, Spry proteins also have a key role in organogenesis and development. For example, one study which utilised Spry1$^{-/-}$; Spry2$^{-/-}$ double KO mice implicated these proteins in the normal development of mouse external genitalia (Ching et al., 2014). A previous study using transgenic Spry2 mice also provided evidence for the role of Spry2 in the indirect regulation of male sex organogenesis (Chi et al., 2006). Interestingly, both studies suggested that there was abnormal FGF regulation by the Spry proteins,

leading to uncharacteristic organogenesis. As a further example, analysis of genomic DNA from the peripheral-blood samples of congenital hypogonadotropic hypogonadism (CHH) patients identified the *Spry4* gene (but not *Spry2*) as being mutated in CHH individuals (Miraoui et al., 2013). CHH is characterised by absent or incomplete sexual maturation by the age of 18 years due to gonadotropin-releasing hormone (GnRH) deficiency and/or resistance (with no other abnormalities of the hypothalamic-pituitary axis) (Young et al., 2019). In the 2013 study, a range of Spry4 mutations were identified in individuals: S214Y, V16I, T100M, D105N, K177R, S241T, V281M, V304I, and interestingly C209Y (Miraoui et al., 2013). C209 is within the SPR domain of Spry4 and a mutation at this residue could in theory affect S-acylation, although this would need to be investigated experimentally. In fact, each of the described Spry4 variants have different phenotypic outcomes, all of which present with partial or absent puberty but there is variation between those presenting with/without hearing loss, dental abnormalities, low bone mass. The C209Y individuals present with none of these additional features, whereas S241 individuals present with dental abnormalities and low bone mass (Miraoui et al., 2013).

**SPRED proteins**

SPRED proteins, like Spry proteins, are also involved in suppressing/regulating growth factor mediated ERK activation and the development of cancer. This role of SPRED proteins is thought to be achieved through interaction with RAS and neurofibromin (NF1) to suppress the phosphorylation and activation of Raf (also having a role in the modulation of the small GTPases Rap1 and Rho) (Kawazoe and Taniguchi, 2019). SPRED proteins have been implicated in a variety of cancers including leukaemia (Pasmant et al., 2015), osteosarcoma (Miyoshi et al., 2004), prostate cancer (Kachroo et al., 2013), melanoma (Ablain et al., 2018), carcinoma/adenocarcinoma (Sharma et al., 2016), and more. A study from 2020, utilised The Genotype Tissue Expression (GTEX) Project to show mRNA expression profiling for SPRED proteins (Lorenzo and McCormick, 2020). The study found that although SPRED1/2 were widely expressed across human tissues, SPRED3 expression was limited to the brain, breast, and pituitary gland. Structurally, SPRED proteins also contain a C-terminal SPR domain (similar to Spry proteins), however, these SPREDs are also made up of an N-terminal EVH1 (Enabled/VASP homology-1) domain, and a central c-Kit-binding domain (KBD) (Lorenzo and McCormick, 2020).

The EVH1 domain primarily functions as an interaction unit that links signalling proteins via binding to proline-rich sequences, with many EVH1 containing proteins also being involved in actin binding and polymerisation (Peterson and Volkman, 2009). However, the most well-described interactor of the SPRED EVH1 domain is NF1, which does not contain a proline motif (Peterson and Volkman, 2009). NF1 is a tumour suppressor protein acting as a GTPase-activating protein that negatively regulates the MAPK pathway activity by promoting Ras GTP hydrolysis. Mutations in SPRED1 have been linked to a complex multisystem disorder known as neurofibromatosis 1 (also known as von Recklinghausen syndrome), with many clinical characteristics including: multiple café-au-lait macules, neurofibromas, optic gliomas, chronic pain, learning disabilities, anxiety, attention deficit, and psychological disorders (Spurlock et al., 2009, Lehtonen et al., 2013, Peltonen et al., 2017, Radtke et al., 2023).

The KBD of SPRED proteins is ~50 aa in length and has been implicated in the binding of the proto-oncogene receptor tyrosine kinase, c-Kit. First described in 1987, c-Kit is found on hematopoietic stem cells and typically respond to stem cell factor (Yarden et al., 1987, Sheikh et al., 2022). In mice, SPRED2 was found to negatively regulate c-Kit, and to inhibit MAPK and thereby regulate haematopoiesis in the aorta-gonad-mesonephros (Gong et al., 2020, Lorenzo and McCormick, 2020). For other cancer types, such as malignant melanoma, in ~80% of tumours the driver oncogenes are mutant BRAF, RAS and KIT (Pipek et al., 2023). Interestingly, 37% of mucosal melanomas examined in a 2018 study also showed a loss of SPRED1. Among those cases of SPRED1 loss, 30% also exhibited c-KIT alterations (Ablain et al., 2018). It should also be noted that most cases of melanoma which also showed a loss of SPRED1 in the 2018 study were triple wild-type melanomas (i.e., those where BRAF, NRAS and NF1 are not mutant). BRAF, NRAS, and NF1 all play a role in the regulation of the MAPK signalling pathway, and mutation of these proteins is the highest oncogenic factor within melanoma tumours (Pipek et al., 2023, Gupta et al., 2020). Altogether this wider association points to SPRED inactivation and/or disrupted SPRED1/2-c-KIT interactions in the promotion of MAPK signalling and oncogenesis (Ablain et al., 2018).

The SPRED-3 protein (UniProtKB - Q2MJR0, SPRE3_HUMAN) is comprised of 410 aa residues with a molecular weight of 42.670 kDa. Similar to all other members of the Spry/SPRED family SPRED3 contains a SPR domain (aa 296 – 407). SPRED3

also contains an N-terminal EVH1/WH1 domain (1-113) and an unfunctional KBD region (aa 195 – 244) (Kato et al., 2003). Other notable regions include two polar regions at aa 117 – 158 & 172-193, as well as a proline rich region at aa 260-283 (Figure 1.6 & 1.7). Similar to Spry/SPRED proteins, SPRED3 is thought to be a peripheral plasma membrane associated protein (Butland et al., 2014, Kato et al., 2003, Lorenzo and McCormick, 2020). Less is currently known about SPRED3 (compared to other Spry/SPREDs), and overall SPRED3 is an outlier in terms of interactions and efficacy. For instance, SPRED3 shares a low homology in the KBD (< 20% with SPRED1), and also contains a Gly-240 residue in place of a critical Ala-247 residue that is required for c-Kit binding and indeed SPRED3 is unable to bind to or be phosphorylated by c-Kit (Lorenzo and McCormick, 2020). Added to this, although SPRED3 can also inhibit ERK, its inhibitory effect is less than that of SPRED1 and SPRED2; a suspected consequence of SPRED3 lacking a KBD (Lorenzo and McCormick, 2020). Furthermore, unlike the other Spry/SPRED proteins which were identified to contain a consensus zDABM sequence related to zDHHC17 binding, SPRED3 does not contain a zDABM (Lemonidis et al., 2017). Despite this, in the year previous to the identification of the zDABM, SPRED3 (and SPRED2) was actually shown to interact with and be S-acylated by zDHHC17 (Butland et al., 2014).

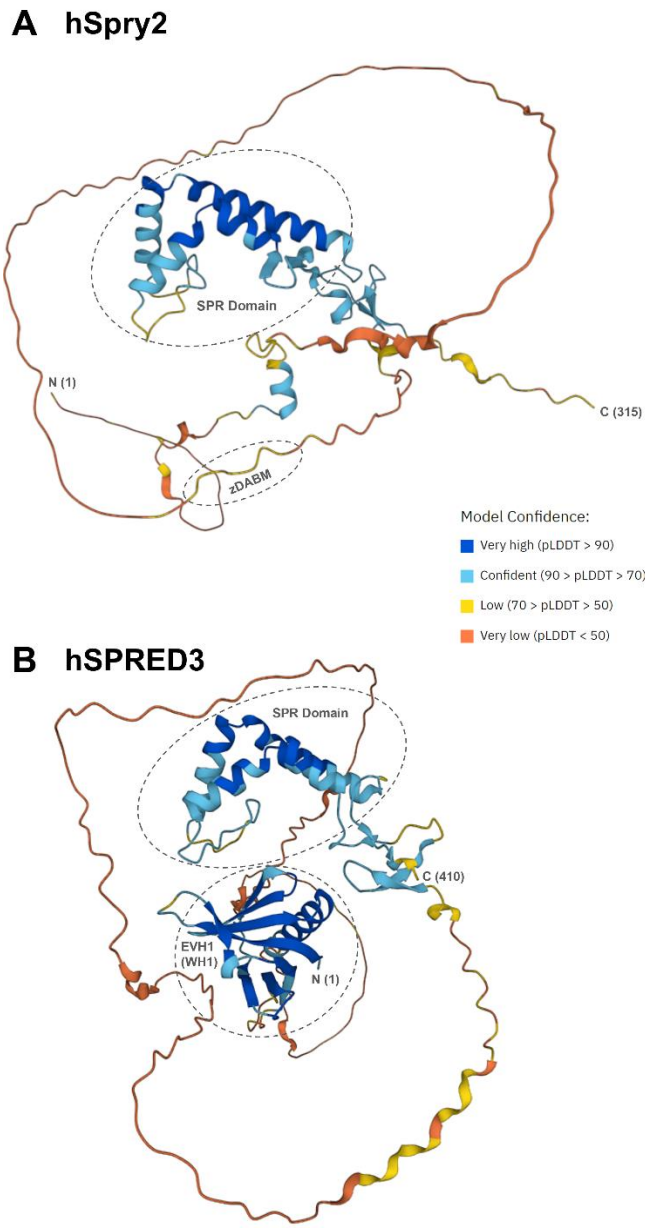


***Figure 1.7. AlphaFold structural prediction of Spry and SPRED structure.*** *(A) AlphaFold structural prediction model of Spry2 (Homo sapiens; UniProt: O43597 - SPY2_HUMAN). Schematic indicating the approximate spatial location of the SPR domain, the zDABM, and the N/C terminal ends. (B) AlphaFold structural prediction model of SPRED3 (Homo sapiens; UniProt: Q2MJR0 - SPRE3_HUMAN). Schematic indicating the approximate spatial location of the SPR domain, the EVH1 (WH1) domain, and the N/C terminal ends. AlphaFold produces a per-residue confidence score (pLDDT) between 0-100. Some regions < 50 pLDDT may be unstructured in isolation. AlphaFold protein structure database developed by DeepMind and European Molecular Biology Laboratory-European Bioinformatics Institute (EMBL-EBI) (Varadi et al., 2022, Jumper et al., 2021).*

## 1.11 The Sprouty-2 protein

The Sprouty-2 protein (Spry2) (UniProtKB - O43597, SPY2_HUMAN) is comprised of 315 aa residues with a molecular weight of 34.68835 kDa. Like all other members of the Spry family, Spry2 contains a SPR domain (aa 177-291) which also encompasses the CRD domain (aa 178-301) (figure 1.6 and 1.7). There are also other notable regions including a phosphorylated tyrosine (Y55), a poly-serine region (aa 125-131) and a cryptic proline region (aa 304-309). Unfortunately, only a short region of the Spry2 structure (aa 36-61) has so far been resolved through x-ray crystallography, which comes from a structure of the c-CBL tyrosine kinase binding domain (TKBD) with a phosphorylated Y55 Spry2 peptide. However, through advancements in the AlphaFold AI based protein structural prediction database, full-length structure for Spry/SPRED proteins have been predicted (figure 1.7). Spry2 is a soluble cytosolic protein that has been reported to localise to different intracellular structures such as the plasma membrane (Locatelli et al., 2020), caveolae (Impagnatiello et al., 2001), as well as microtubules and membrane ruffles (Lim et al., 2002, Lim et al., 2000).

### Interactions of Sprouty-2 protein

The nuanced nature of Spry2 regulation is reflected in the numerous interactions that it has been reported to engage in (Figure 1.8). Like other Spry/SPRED proteins, Spry2 has been identified as a negative regulator of multiple growth factor pathways including fibroblast growth factor (FGF), epidermal growth factor (EGF), and nerve growth factor (NGF). However, it should be mentioned that there is also evidence for Spry2 as a positive regulator of EGF signalling in mammalian cells (Wong et al., 2002). Spry2 can indirectly promote RTK signalling by sequestering the casitas B-linage lymphoma protein (CBL). CBL is an E3-ubiquitin-protein ligase capable of ubiquitinating receptor tyrosine kinases (RTK), resulting in their degradation and reduced growth factor signalling. Spry2 interacts with CBL through a phosphorylated tyrosine (Y55), leading to the degradation of Spry2 and attenuation of RTK ubiquitination/degradation (Wong et al., 2002). Other proteins such as protein phosphatase 2A (PP2A) have been suggested to compete with CBL for binding to Y55 in Spry2. This competitive binding would inhibit Spry2-CBL binding, promoting Spry2 stability but in turn increasing CBL-mediated EGFR ubiquitination (Masoumi-Moghaddam et al., 2014b). The Intersectin 1 (ITSN1) scaffold protein can also disrupt

the Spry2-CBL interaction and thereby promote EGFR degradation (Okur et al., 2012). ITSN1 has also previously been shown to bind other S-acylated proteins such as SNAP25 (Okamoto et al., 1999). ITSN1 binds Spry2 via its SH3 consensus sequence at the C-terminal end proline-rich region – VPTVP (aa 303-307) (Okur et al., 2012).

This proline-rich region is also the site at which Spry2 can bind the growth factor receptor-bound protein 2 (Grb2) (Lao et al., 2007a). Grb2 binds to the phosphorylated kinase domain of RTKs to facilitate the activation of the Son of Sevenless protein (SOS) and subsequently RAS activation at the top of the MAPK pathway. The canonical action of Spry2 to sequester Grb2 prevents SOS binding and in turn prevents the propagation of MAPK signalling (Degirmenci et al., 2020). This sequestering action is observed in other Spry proteins too, such as Spry4 which has been suggested to supress MAPK by binding to Raf1 - downstream of Spry2 action (Sasaki et al., 2013). Multiple/simultaneous binding interactions have also been reported, such as in the case of a suspected tripartite complex relating to the MET-hepatocyte growth factor signalling pathway. methyltransferase-like protein 13 (METTL13) was shown to co-immunoprecipitate with the Grb2-associated binding protein 1 (GAB1) and Spry2. It was suggested that METTL13 can supress deafness associated with mutations in GAB1; with Spry2 being differentially regulated between affected people and those in which the GAB1 mutations are non-penetrant (Yousaf et al., 2018).

Cell stimulation has been shown to result in the phosphorylation of specific sites in Spry2 (in addition to Y55). This includes the poly-serine region of Spry2 (aa 124-130), the function of which is not well understood. Evidence published in 2006 showed that the stability of Spry2 can be extended by the mitogen-activated kinase-interacting kinase 1 (MnK1) mediated phosphorylation of S112/121 within this serine-rich domain of Spry2 (DaSilva et al., 2006). This same poly-serine region has also been implicated in ubiquitin regulation, separate to that of Spry2 Y55. Specifically, the E3 ubiquitin-protein ligase, neural precursor cell expressed developmentally down-regulated protein 4 (Nedd4) has been shown to bind to S112/121 and ubiquitinate Spry2 leading to its degradation (Edwin et al., 2010). In addition to this, recently published work has given evidence for one mechanism of Spry2 intracellular stabilisation via phosphorylation of S112 by protein kinase D (PKD) (Martínez et al., 2023).

Taking all this information into account a sequential mechanism could be proposed whereby upon FGF stimulation, Src phosphorylates Y55 of Spry2 to allow PP2A binding. Once bound, PP2A can dephosphorylate S112 to expose the cryptic C-terminal proline site. This then allows the binding/sequestering of Grb2 to block Ras activation. This process is then modulated in a delicate balance through re-phosphorylation to prevent conformational change by MnK1, or through Spry2 degradation by CBL and Nedd4 at the phosphorylation sites Y55 and S112, respectively (figure 1.8). Aside from these regulatory interactions, a key regulatory mechanism of Spry2 action is also likely to be the plasma membrane translocation of the protein due to the highly conserved SPR/CRD domain (Yigzaw et al., 2001, Lim et al., 2002).

**Growth factor mediated Spry2 translocation**

The seminal study that reported the discovery of Spry proteins in 1998, also reported that Spry proteins can associate with the plasma membrane through co-localisation with the transmembrane protein, NOTCH (Hacohen et al., 1998), leading to subsequent interest in how this contributes to functional regulation of Spry2 and growth factor signalling (Yigzaw et al., 2001, Edwin et al., 2009). However, the precise mechanism of translocation/trafficking of Spry2 is unclear.

Spry2 is a cytosolic protein which has been shown using immunofluorescence analysis to translocate to the plasma membrane on growth factor stimulation (Lim et al., 2000). The researchers were able to show in both COS-1 monkey kidney cells and HEK-293T cells that following EGF stimulation, Spry2 translocated to membrane ruffles. The team was also able to identify the minimal region of Spry2 required for plasma membrane translocation as aa 178-282 (Lim et al., 2000). This minimal region is within the SPR domain (177-291) and the CRD (178-301). It is worth noting that in this same study (Lim et al., 2000), the researchers also suggested that in unstimulated COS-1 cells, Spry2 co-localises with microtubules before translocating to the membrane ruffles upon EGF stimulation.

Following on from their 2000 study, the Lim group suggested that Spry2 translocated to the plasma membrane upon growth factor stimulation, targeting the protein to phosphatidylinositol 4,5-bisphosphate (PIP2) (Lim et al., 2002). Furthermore, they identified a translocation-defective point mutant of hSpry2 (R252D) and showed by

immunoblotting of p-ERK in PC12 cells (rat pheochromocytoma), that this R252D mutant failed to inhibit MAPK phosphorylation. If the mechanism proposed by Lim and colleagues is indeed correct, S-acylation of Spry2 may function to increase the overall hydrophobicity of Spry2 to facilitate appropriate translocation. Indeed, this idea is supported by the findings of Locatelli *et al.,* (2020), which show that the S-acylation-defective C265A/C268A mutant of Spry2 exhibits reduced association with the plasma membrane in PC12 cells (Locatelli et al., 2020).

In addition to the reports suggesting a role for PIP2 in targeting Spry2 to the plasma membrane, other researchers have suggested that both Spry1 and Spry2 associate with caveolin-1 (cav-1) in perinuclear and vesicular structures and at the plasma membrane of endothelial cells (Impagnatiello et al., 2001). Impagnatiello and colleagues also suggested a relationship between S-acylation and cav-1 association and that Spry proteins associate with lipid rafts or caveolae during translocation. Again, this is an interesting theory, as evidence given by the experiments in this study and those by Locatelli, show occurrences of Spry2 localising to the plasma membrane during confocal imaging of PC12 cells. All of this together in the wider context that lipid raft/caveolae/plasma membrane targeting is a well-known feature of protein S-acylation (Sezgin et al., 2017, Salaün et al., 2005b, Chamberlain and Shipston, 2015).

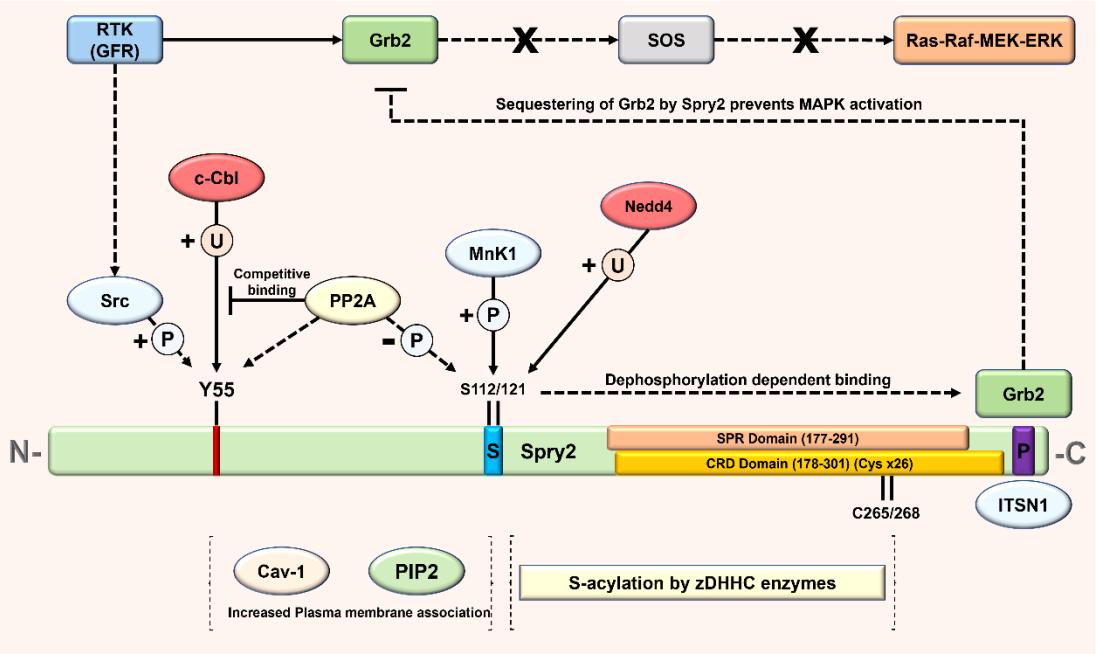


***Figure 1.8. Spry2 structure and interactions.*** Schematic diagram outlining key features and domains: Y55, tyrosine 55 (red); S, serine-rich region (blue); SPR, Sprouty-related domain (pink); CRD, cysteine-rich domain (yellow); P, proline-binding region (purple). *(Dashed line pathway)* Receptor tyrosine kinase/growth factor receptor (RTK/GFR) stimulated phosphorylation (P) of Y55 by of Src kinases allows protein phosphatase 2A (PP2A) binding. Once bound, PP2A dephosphorylation of S112 exposes Spry2 proline binding region for the sequestering of Grb2, therefore preventing Grb2 binding to son of sevenless (SOS) protein and blocking subsequent signalling. *(Solid line pathways)* The process is modulated through the re-phosphorylation of serine residues by mitogen-activated protein kinase interacting kinase 1 (MnK1). Spry2 is also ubiquitinated (U) for degradation by casitas B-linage lymphoma protein (CBL) at Y55 and by neural precursor cell expressed developmentally down-regulated protein 4 (Nedd4) at S112. Intersectin 1 (ITSN1) interacts with the proline-rich region. Caveolin-1 (Cav-1), phosphatidylinositol 4,5-bisphosphate (PIP2) and zDHHC enzymes have all shown interactions with for increased hydrophobicity and plasma membrane association.

## 1.12 Growth factor signalling

There is a wide variety of known growth factors, which include epidermal (EGF), fibroblast, (FGF) and nerve growth factors (NGF); each having its own corresponding growth factor receptor (GFR). Growth factors cause agonistic or antagonistic action upon cellular division, differentiation, growth, and proliferation; and are known to be involved in oncogenic processes, thus making them a key therapeutic target. (Normanno et al., 2006, Tiash and Chowdhury, 2015, Sasaki et al., 2013). EGF and NGF were two of the first growth factors to be discovered in 1960 and 1962, respectively, whereas FGF was discovered in 1978 (Levi-Montalcini and Booker, 1960, Cohen, 1962, Gospodarowicz et al., 1978, Schlessinger, 2014).

RTKs are a major class of cell receptor that respond to several extracellular ligands, such as growth factors. The discovery and classification of RTKs has been developing since the 1960s, with a total of 58 RTKs, comprised of twenty overall subfamilies with similar yet distinct forms (Lemmon and Schlessinger, 2010, Schlessinger, 2014). RTK signalling begins with extracellular ligand binding to facilitate RTK dimerisation and in turn auto-phosphorylation of the cytoplasmic protein tyrosine kinase region. This phosphorylation allows the propagation of signalling cascades including the PI3K-AKT, JAK/STAT, and MAPK cascade, for which Spry2 is a signalling antagonist (Du and Lovly, 2018).

The MAPK pathway (mitogen-activated protein kinases pathway; also known as the MAPK/ERK pathway or the Ras-Raf-MEK-ERK pathway) has been identified in mammals to have three distinct groups of MAPK modules including ERK, JNK, and P38 kinase; all of which have further subset modes e.g., ERK1 & ERK2, or JNK1, JNK2, & JNK3 (Dhillon et al., 2007). MAPK signalling is comprised of a three-teir system of phosphorylating kinases: a MAPK kinase kinase (MAP3K), a MAPK kinase (MAP2K), and a MAPK (Kim and Choi, 2010). Upon RTK activation, dimerisation, and autophosphorylation, the exposed C-terminal end of the receptor facilitates the binding of GRB2 via Src homology 2 (SH2) domains. The SH3 domains on the N-terminal region of GRB2 subsequently allows the binding of SOS, which is a guanine exchange factor for the GTP loading of the membrane bound small-GTPase, Ras. The activated membrane bound Ras-GTP can either act as a dimer or a nanocluster to recruit, bind and activate RAF or RAF/MEK heterodimers at the plasma membrane (the MAPK3 step in the cascade). The activated RAF/MEK proteins can then assemble as transient tetramers which facilitate RAF activation through back to back

dimerisation. The MEK proteins can then dock to the RAF dimers to form face-to-face dimers which are turned on by RAF. The activated MEK (which is the MAP2K) can then phosphorylate ERK1/2 (which is a MAPK) and propagate and generate further signalling for cell growth and transcription factors such as c-myc and c-fos (figure 1.9) (Degirmenci et al., 2020).

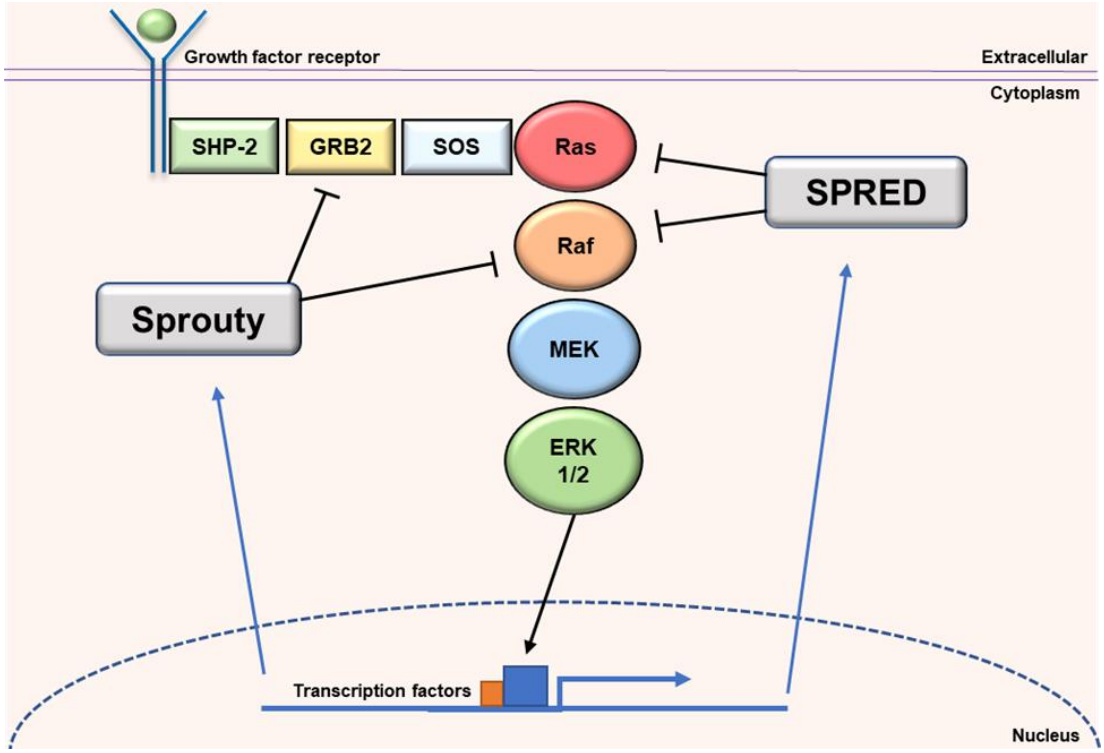


***Figure 1.9. General action of Sprouty/SPRED proteins on the MAPK pathway.*** *Schematic diagram of Spry/SPRED action on the MAPK pathway. Extracellular activation of growth factor receptors leading to downstream activation of: Src homology-2 domain-containing protein tyrosine phosphatase-2 (SHP-2); growth factor receptor-bound protein 2 (GRB2); son of sevenless protein (SOS); rat sarcoma GTPase (RAS); rapidly accelerated fibrosarcoma kinase (RAF); mitogen-activated protein kinase kinase (MEK); extracellular signal-related kinase (ERK); and subsequent transcription factors.*

## 1.13 Summary

S-acylation is a form of lipidation typically involving the attachment of fatty acid chains onto cysteine residues of proteins. S-acylation is mediated by a family of zDHHC acyltransferase enzymes, where dysfunction of either the PTM or enzyme has been linked to the progression of many diseases. zDHHC17 is unique among zDHHC isoforms, primarily due to the presence of an N-terminal AR domain which has been shown to be involved in substrate recruitment/recognition. Spry/SPRED proteins were recently identified as substrates of zDHHC17 due to the presence of a zDABM. Spry/SPRED proteins share a highly conserved SPR/CRD domain which has been shown to both be S-acylated and functionally important. Spry/SPRED proteins are important regulators of the MAPK growth factor pathway and dysregulation of this pathway is known to lead to oncogenesis. Recent work identified S-acylation as important for the stability and plasma membrane targeting of Spry2, however the role of S-acylation in Spry2 function has not been explored. Furthermore, the recognition of Spry/SPRED proteins by zDHHC enzymes needs further study to determine if canonical modes of recognition exist, or if there are other modes of enzyme-substrate interaction, or indeed if there are differences between Spry and SPRED isoforms.

## 1.14 Aim and hypothesis

It is still largely unclear how S-acylation affects Spry/SPRED proteins, but the dynamic changes in Spry/SPRED localisation upon growth factor stimulation (Kawazoe and Taniguchi, 2019), the presence of an extensive SPR/CRD, and the identification of zDHHC17 as a new binding partner/acylating enzyme (Lemonidis et al., 2017), makes the study of these proteins an exciting direction for further investigation. Spry2 presents itself as the most interesting candidate for investigation as recent work has shown that S-acylation of Spry2 by zDHHC17 is important for both the localisation and stability of the protein substrate (Locatelli et al., 2020). More specifically the 2020 study showed that the turnover of Spry2 was reduced when the protein was S-acylated by zDHHC17 and that Spry2 was unable to effectively localise to the plasma membrane when S-acylation is impaired. This study was also able to identify that the S-acylation of Spry2 by zDHHC17 is dependent on two specific cysteine residues (C265/268) within the SPR and/or three surrounding residues (N211/D214/K223) also within the SPR domain (Locatelli et al., 2020). Together these findings point to the

importance of Spry2 S-acylation, especially as this PTM is widely implicated in both protein stability and cellular localisation (Chamberlain and Shipston, 2015).

Subsequent work from the doctoral thesis of Dr Carolina Locatelli showed that although Spry2 contains a consensus zDABM, the protein does not show a significant loss in S-acylation when this region is mutated (Locatelli, 2021). Furthermore, mutation of the zDABM binding pocket in zDHHC17 (N100A/W130A; identified by Verardi *et al.*, (2017)) also had no effect on Spry2 S-acylation by zDHHC17 (Locatelli, 2021). This retention of S-acylation when the zDABM-ANK17 interaction is disrupted is currently unique to Spry2, whereas SNAP25 is completely dependent on its zDABM and residues N100/W130 in zDHHC17 for S-acylation (Greaves et al., 2010b, Lemonidis et al., 2015b). SPRED3 on the other hand, does not contain a zDABM motif, but surprisingly is still able to bind and be S-acylated by zDHHC17 (Butland et al., 2014). Current findings suggest that Spry/SPRED proteins contain an alternative zDHHC17 interaction site that is coupled to S-acylation (and/or other functions).

Therefore, the overarching hypothesis is that S-acylation is a critical feature that influences the trafficking, stability, and function of Spry/SPRED proteins in their regulation of growth factor signalling pathways. It is proposed that Spry/SPRED proteins contain a novel mechanism of recognition by zDHHC17 that is coupled to S-acylation and/or function and that is independent of the known zDABM interaction. Further to this, it is hypothesised that as SPRED3 does not contain a zDABM, that this protein would rely on an alternative and conserved interaction site for S-acylation by zDHHC17. The overall aim of this study is to investigate the interactions of Spry/SPRED proteins with zDHHC17, to further elucidate how these substrates are recognised and subsequently S-acylated, and to compare this to the known substrate-enzyme recognition mechanism already established for SNAP25-zDHHC17 involving zDABM sequences. Specifically, this thesis will:

I. Progress knowledge of Spry/SPRED protein S-acylation by zDHHC17 and develop an improved understanding of the mechanism of interaction that is linked to the efficient S-acylation of these proteins.

II. Explore the functional relevance of Spry2 and zDHHC17 S-acylation/interaction.

III. Examine the role of Spry2/SPRED proteins in regulating the stability of the Orf3d protein from the SARS-CoV-2 virus.

# CHAPTER 2

# MATERIALS AND METHODS

# Chapter 2 – Materials and methods

## 2.1 Cell culture

Human embryonic kidney 293T cells (HEK-293T, ATCC #CRL3216™, England, UK) were maintained in T75 $cm^2$ flasks (Corning®, Sigma-Aldrich Company Ltd., Dorset, UK) with Dulbecco's Modified Eagle Medium (DMEM) + GlutaMAX™ media (Gibco, LifeTechnologies™ Ltd., Paisley, UK) supplemented with 10 % foetal bovine serum (Gibco, LifeTechnologies™ Ltd., Paisley, UK). Cells were maintained in a humidified atmosphere of 37°C/5% $CO_2$ in a Thermo BB15 incubator (Thermo Fisher Scientific, Leicestershire, UK). For cell passage, after 7-days in culture, HEK-293T cells were briefly washed with 10 mL of warm phosphate-buffered saline (PBS) and dissociated from the flask for 3 minutes using 2.5 mL TrypLE express reagent (Gibco, LifeTechnologies™ Ltd., Paisley, UK). The flask was gently tapped to detach all adhered cells and 7.5 mL of fresh media was added to inactivate the TrypLE. Cells were collected into a 15 mL falcon tube and pelleted by centrifugation (Heraeus Multifuge 3 S-R) at 150 x g for 3 minutes. HEK-293T cells were resuspended in 10 mL of media and seeded into a new T75 $cm^2$ flask at a dilution of 1:20 with a final volume of 10 mL. For experiments, HEK-293T cells (between passage 20-50) were diluted to 1:50 with DMEM media and 0.5 mL of cell suspension was seeded on poly-D-lysine coated 24 well plates (Corning®, Sigma-Aldrich Company Ltd., Dorset, UK).

Rat pheochromocytoma cells (PC12, ATCC #CRL-1721™, England, UK) were maintained in T75 $cm^2$ flasks (Corning®, Sigma-Aldrich Company Ltd., Dorset, UK) with advanced RPMI (Roswell Park Memorial Institute) 1640 reduced-serum medium (Gibco, LifeTechnologies™ Ltd., Paisley, UK) supplemented with 10% horse serum (Gibco, LifeTechnologies™ Ltd., Paisley, UK), 5% foetal bovine Serum (Gibco, LifeTechnologies™ Ltd., Paisley, UK) and 1% L-glutamine (Gibco, LifeTechnologies™ Ltd., Paisley, UK). Cells were maintained at a humidified atmosphere of 37°C/5% $CO_2$ in a Thermo BB15 incubator (Thermo Fisher Scientific, Leicestershire, UK). For cell passage, PC12 cells were grown in suspension for 7-day intervals, collected into 15 mL falcon tubes and pelleted by centrifugation (Heraeus Multifuge 3 S-R) at 150 x g for 3 minutes. Pelleted cells were dissociated by incubating for 4 minutes in TrypLE express reagent (Gibco, LifeTechnologies™ Ltd., Paisley, UK). The dissociation reaction was inactivated by adding RPMI media at a 2:1 ratio (8 mL), followed by

centrifugation at 150 x g for 3 minutes. Cells were thoroughly resuspended in 10 mL RPMI media and seeded in a new T75 $cm^2$ flask at a dilution of 1:5 in growth medium (final volume of 12 mL per flask). For experiments, PC12 cells (between passage 20-50) were diluted to 1:50 with RPMI media and cells were seeded on poly-D-lysine coated 24 well plates (1 mL per well: Corning®, Sigma-Aldrich Company Ltd., Dorset, UK). For immunofluorescence and confocal microscopy experiments, cells were diluted to 1:100 with RPMI; and 1 mL of cells were seeded on poly-D-lysine coverslips (Corning® Sigma-Aldrich Company Ltd., Dorset, UK) in non-coated 24 well plates (Starlab, Blakelands, UK).

For growth factor experiments: 48 hours after seeding, cells were serum starved in serum-free media for 4-hours, followed by a 10-minute stimulation with either 0.5 ml serum-containing media 50 ng/mL of either epidermal growth factor (EGF; 321-EG/CF) or fibroblast growth factor basic (FGF; 3339-FB/CF) – (all growth factors used were recombinant rat isoforms purchased from R&D Biosystems, MN, USA). After stimulation, cells were washed in PBS and lysed on ice in 100 µL of 1x sample buffer containing 25 mM dithiothreitol (DTT; BPS72-5, Fisher, UK), phosphatase inhibitor cocktail 3 (1:100; P0044-1, Sigma, UK), and protease inhibitor cocktail (1:100; P8340-5, Sigma, UK). Samples were heated to 95ºC for 10 minutes before either further use or storage at -20ºC.

## 2.2 Plasmids

All zDHHC enzymes (mouse) cloned in pEF-BOS-HA vectors were provided by Professor Masaki Fukata (Fukata et al., 2004). Two truncated mutant forms of zDHHC17 WT (aa 11-632), ΔAnk (aa 287-632), and ΔC (aa 11-569) mutants were previously cloned through Gateway® Technology (Invitrogen Ltd., Paisley, UK) by Dr. Kimon Lemonidis (University of Strathclyde; Lemonidis et al., 2014). zDHHC17 mutant plasmids encoding for W130A (critical for zDABM interaction), C467A (DHHA, catalytically inactive), or C467S (DHHS, catalytically inactive) were previously synthesised within the Chamberlain lab via site-directed mutagenesis using the zDHHC17 pEF-BOS-HA plasmid from Professor Masaki Fukata as a DNA template.

Murine WT and mutant constructs of Spry2 (WT & P154A), SPRED1 (WT & P316A), and SPRED2 (WT & P284A) were previously cloned into pEGFP-C2 vectors through Gateway® Technology (Invitrogen Ltd., Paisley, UK) generated by Dr. Kimon Lemonidis (University of Strathclyde). Other Spry2 mutants cloned into pEGFP-C2 that were used (Spry2 N211/D214/K223A (NDK) and Spry2 C265/268A (DM)) were previously obtained through site-direct mutagenesis PCR by Dr. Carolina Locatelli (University of Strathclyde) and Irina Lousa (University of Porto), respectively. Spry2 was also previously subcloned into mCherry-C2-GW vector using the Gateway® Technology system (Invitrogen Ltd., Paisley, UK). The validity of the final clones was confirmed (GATC service by Eurofins Genomics, Wolverhampton, UK).

SPRED1 Chimeric mutants (mouse): SPRED1 with No-EVH1 domain (encoding aa 124-442 of mouse SPRED1) was subcloned (as described in sections 2.4-2.7) into pEGFP-C2 from mSPRED1 WT. SPRED1 with Spry2 end C291-315 (encoding aa 1-442 of SPRED1 + aa 291-315 of Spry2 added to SPRED1s C-terminal end), and SPRED1 with Spry2 middle region K155-176 (encoding aa 1-316 and 334-442 of SPRED1, with aa 317-333 of SPRED1 replaced with aa 155-176 of Spry2), were cloned into pcDNA3.1(+)-N-eGFP vectors (N-terminal tagged) by GenScript (GenScript Biotech (UK) Ltd, Oxford, UK).

Spry2 N-terminal truncated mutants (mouse): Spry2 100-315 (encoding aa 100-315 of Spry2), Spry2 120-315 (encoding aa 120-315 of Spry2), Spry2 140-315 (encoding aa 140-315 of Spry2), and Spry2 155-315 (encoding aa 155-315 of Spry2) were cloned into pcDNA3.1(+)-N-eGFP vectors (N-terminal tagged) by GenScript (GenScript Biotech (UK) Ltd, Oxford, UK).

Human WT and/or mutant constructs of Spry1 (NM_001258038), Spry2 (NM_005842), Spry3 (NM_001304990), Spry4 (NM_001127496) and SPRED3 (NM_005842) (listed below) were cloned into pcDNA3.1(+)-N-eGFP by GenScript (GenScript Biotech (UK) Ltd, Oxford, UK).

Spry2 alanine mutations (human): (1) hSpry2 WT with specific residues (L43, I46, P154, Y176, T298, V299 & C300A) mutated to alanine in different combinations. Constructs were cloned into pcDNA3.1(+)-N-eGFP by GenScript (GenScript Biotech (UK) Ltd, Oxford, UK).

- hSpry2 alanine mutant constructs:
  (2) P154A, (3) Y176A, (4) T298/V299/C300A, (5) L43/I46A, (6) P154/Y176A,
  (7) P154/T298/V299/C300A, (8) Y176/T298/V299/C300A,
  (9) P154/Y176A/T298/V299/C300A, (10) L43/I46/P154A, (11) L43/I46/Y176A,
  (12) L43/I46/P154/Y176A, (13) L43/I46/T298/V299/C300A,
  (14) L43/I46/P154/T298/V299/C300A, (15) L43/I46/Y176/T298/V299/C300A,
  (16) L43/I46/P154/Y176/T298/V299/C300A.

SPRED3 truncation mutants (human): SPRED3 1-113 (encoding amino acids 1-113 of human SPRED3), SPRED3 1-194 (encoding amino acids 1-194 of human SPRED3), SPRED3 1-244 (encoding amino acids 1-244 of human SPRED3), SPRED3 1-295 (encoding amino acids 1-295 of human SPRED3) and SPRED3 296-410 (encoding amino acids 296-410 of human SPRED3). Cloned into pcDNA3.1(+)-N-eGFP by GenScript (GenScript Biotech (UK) Ltd, Oxford, UK).

SPRED3 alanine scanning mutants (human): alanine scanning mutagenesis of residues in the SPR domain, where each mutant construct had a sequential sets of 10 aa substituted by alanine (excluding cysteine residues). These were named SPRED3 SPR mutants 1-10: 1. aa 296-307, 2. aa 308-318, 3. aa 319-328, 4. aa 329-340, 5. aa 341-351, 6. aa 352-363, 7. aa 364-373, 8. aa 374-386, 9. aa 387-399, 10. aa 400-410). Another set of mutants had the alanine substitutions in sequential sets of 20 aa (excluding cysteine residues). These were named SPRED3 SPR mutants A-E: A. aa 296-318, B. aa 319-340, C. aa 341-363, D. aa 364-386, E. aa 387-410). Cloned into pcDNA3.1(+)-N-eGFP by GenScript (GenScript Biotech (UK) Ltd, Oxford, UK).

SPRED3 Cysteine mutants (human): cysteine residues within the SPR domain of SPRED3 were replaced by alanine in groups of three residues at a time SPRED3. SPR cysteine mutants were cloned into pcDNA3.1(+)-N-eGFP by GenScript (GenScript Biotech (UK) Ltd, Oxford, UK).:

- Cys M1 (C297A/C300A/C315A); Cys M2 (C331A/C334A/C342A); Cys M3 (C354A/C356A/379A); Cys M4 (C381A/C382A/C389A); Cys M5 (C396A/C398A/C401A).

SNAP25b constructs (rat) were previously cloned into pEGFP-C2 vector (Greaves and Chamberlain, 2006; Greaves et al., 2009).

WT SARS-CoV-2-Orf3d construct tagged with N-terminal Strep-II were purchased from Addgene (Addgene, MA, USA) as pLXV-EF1alpha-2xStrep-SARS-CoV-2-orf3b-IRES-Puro plasmids (Plasmid #141384) (The Orf3b sequence in this plasmid has since been redesignated as Orf3d (Jungreis et al., 2021) – UniProtKB: P0DTG0 - ORF3D_SARS2).

WT SARS-CoV-2-Orf3d and WT SARS-CoV-2-Orf3d-2 tagged with C-terminal Myc-His were previously subcloned by PCR amplification into PCDNA3.1 Myc-His (C) (Clontech, Takara Bio Group), from pLXV-EF1alpha-2xStrep-SARS-CoV-2-orf3b-IRES-Puro by Dr. Christine Salaun (University of Strathclyde).

Cysteine mutant constructs (alanine substitutions) of Orf3d tagged with N-terminal Strep-II (M1 - C4/7/10/11A; M2 - C33/36/44A; M3 - C54/55A) were originally synthesised and purchased from GenScript (GenScript Biotech (UK) Ltd, Oxford, UK). These constructs were subsequently subcloned by PCR amplification into PCDNA3.1 (Clontech, Takara Bio Group) by Dr. Christine Salaun (University of Strathclyde).

The sequence of plasmid DNA was confirmed by sequencing performed by GATC Eurofins genetic sequencing service (GATC service by Eurofins Genomics, Wolverhampton, UK) or by sequencing performed by DNA Sequencing & Services (MRC I PPU, School of Life Sciences, University of Dundee, Scotland, www.dnaseq.co.uk) using Applied Biosystems Big-Dye Ver 3.1 chemistry on an Applied Biosystems model 3730 automated capillary DNA sequences.

## 2.3 Transfection of cells

PEI transfection of HEK-293T cells: HEK-293T cells were transfected 24 hours after seeding using polyethyleneimine (PEI; Alfa Aesar, 43896. Stock solution at 1 mg/ml in water, pH 7, sterile filtered, aliquoted in 1 ml and stored at -20) at a ratio of 2 µL PEI : 1 µg total plasmid DNA. For example, in co-transfections involving two plasmids, 0.4 µg of plasmid encoding the substrate protein and 0.6 µg of plasmid encoding the zDHHC enzyme were used. Both plasmid and PEI were diluted in a final volume of 50 µL serum-free DMEM + GlutaMAX™, vortexed, and incubated at room temperature for 20 minutes before 50 µL was added to each well of a 24-well plate. Cells were used 24 hours post-transfection.

Lipofectamine transfection of HEK-293T cells: HEK-293T cells were transfected 24 hours after seeding using Lipofectamine® 2000 reagent (2209775, Invitrogen Ltd., Paisley, UK) at a ratio of 2 µL Lipofectamine : 1 µg total plasmid DNA. Lipofectamine was used for transfections in the Orf3d Cys mutant experiment, which involved three plasmids; so, 0.33 µg of each plasmid was added to 50 µL of serum-free DMEM + GlutaMAX™. Lipofectamine was mixed separately and incubated for 5 minutes in 50 µL of serum-free DMEM + GlutaMAX™. After 5 minutes, the Lipofectamine mixture was added to the plasmid mixture, gently inverted, and incubated at room for 20 minutes before 100 µL was added to each well of a 24-well plate. Cells were used 24 hours post-transfection.

Lipofectamine transfection of PC12 cells: PC12 cells were transfected upon seeding using Lipofectamine® 2000 reagent (2209775, Invitrogen Ltd., Paisley, UK) at a ratio of 2 µL Lipofectamine : 1 µg total plasmid DNA. For example, for co-transfections, 0.4 µg of plasmid encoding substrate protein and 0.6 µg of plasmid encoding zDHHC enzyme was added to 50 µL of serum-free RPMI media. Lipofectamine was mixed separately and incubated for 5 minutes in 50 µL of serum-free DMEM + GlutaMAX™. After 5 minutes, the Lipofectamine mixture was added to the plasmid mixture, gently inverted, and incubated at room for 20 minutes before 100 µL was added to each well of a 24-well plate. Cells were used 24 hours post-transfection. For confocal microscopy experiments, 0.2 µg per plasmid DNA was used. Cells were adhered to the poly-D-lysine-coated coverslips in each well of a 24-well plate. Cells were used 48 hours after transfection.

## 2.4 Primer design

For sub-cloning into the multiple cloning site (MCS) of pEGFP-C2, primers were designed using the online software Primer3Plus (https://primer3plus.com/cgi-bin/dev/primer3plus.cgi) and with the addition of appropriate restriction sites. Primers were manufactured by Merck and resuspended in $_dH_2O$ for a stock concentration of 100 µM as per the supplied datasheet. Resuspended primers were stored at -20°C.

**Table 2.1. SPRED1 with No-EVH1 domain chimeric mutant (encoding aa 124-442 of mSPRED1)**

| Primer name | Digestion site | Sequence (5' – 3') |
|---|---|---|
| S124 SPRED1_FOR | EcoR1 (GAATTC) | gggGAATTCtctctagggtgcccagcg |
| S124 SPRED1_REV | BamH1 (GGATCC). | GggGGATCCtcacccagcagccttatgtt |

## 2.5 Polymerase chain reaction (PCR)

Using the desired primers, the region of interest was amplified by PCR using a 96-well thermal cycler (Life Tech, App Biosciences 2720). PCR reaction mixes contained 2 µL of 10 µM forward/reverse primers with 1.5 µL of 50 ng/µL plasmid DNA (pEGFP-C2 plasmid encoding full-length Spry2 WT), 1 µL of 2 mM dNTPs, 5 µL of 10X Pfu buffer (M774A, Promega, WI, USA), and 1 µL Pfu DNA polymerase (M776A, Promega, WI, USA); made up to a final volume of 50 µL with $_dH_2O$. Samples underwent PCR cycling with an initial denaturation step at 95°C for 2 min, followed by 35 cycles of: denaturation at 95°C for 1 min; annealing at 54°C for 0.5 min; elongation at 72°C for 2 min per kb DNA template. These cycles were followed by a final 5-min incubation at 72°C, before holding at 4°C until use. Successful PCR amplification was confirmed by gel electrophoresis (See 2.6) using 5 µL of PCR product, together with 2 µL 10 x digestion dye (green) made up to 20 µL in $_dH_2O$.

## 2.6 Agarose gel electrophoresis

PCR products or DNA Fragments were separated, identified, confirmed and/or purified by agarose gel electrophoresis. In principle, an electric current is applied to a buffer-submerged agarose gel with DNA-containing samples loaded into lanes in the gel. Due to the intrinsically negative phosphate backbone of DNA and its uniform mass/charge ratio, this results in the migration of DNA fragments toward the positively charged anode through agarose matrix at variable speeds due to size (i.e., DNA of smaller size migrates faster, and DNA of larger size migrates slower). 1 % (w/v) agarose (Bioline, UK) in 1X TAE buffer [stock 50X: 2M Tris base (Fisher, UK, T6066), 50 mM EDTA (Sigma, UK, E5134), glacial acetic acid (VWR Chemicals, UK) to pH 8] was used to make gels, supplemented with SYBR® Safe DNA gel stain (P/N S33102, Invitrogen, UK) at a dilution 1:10,000. Gels were immersed in 1X TAE buffer and samples were prepared by adding loading buffer (Fisher BioReagents$^{TM}$, Belgium) at a dilution ratio of 1:5. Samples were run at 130 V for 30 min (PowerPacTM Basic, BioRad, USA) alongside a 1 kb DNA ladder (G571A, Promega, WI, USA) as a marker of DNA size. After electrophoresis, the DNA samples were visualized under UV light by an Ingenius-Syngene Bio UV illuminator and associated camera (Synoptics Syngene Gelvue, GVM30).

## 2.7 Sub-cloning of plasmids

### *Digestion*

Products were digested for 1 h at 37ºC using 45 µL insert (PCR product), 1.5 µL EcoR1 digestion enzyme (FD0274, Thermo Scientific), 1.5 µL BamH1 digestion enzyme (FD0054, Thermo Scientific), 6 µL 10x fast digestion green buffer (LT-02241, Thermo Scientific), made up to 60 µL with $_dH_2O$. The desired plasmid vector backbone (pEGFP-C2) used for sub-cloning was digested using the same restriction enzymes, using 1 µL of 1 µg/µL backbone, 1 µL EcoR1 digestion enzyme, 1 µL BamH1 digestion enzyme, 2 µL 10x digestion buffer, made up to 20 µL with $_dH_2O$.

### *Purification*

Digested DNA products were resolved using agarose gel electrophoresis (130 V for 45 min). DNA bands were visualised by UV illumination (Stratagene transilluminator 4000), excised from the gel using a clean scalpel and placed into 1.5 mL Eppendorf tubes. The DNA was purified from the gel slice by using the Invitrogen PureLink® quick gel extraction kit as per manufactures instructions (K220001, Thermofisher Scientific). 500 µL of gel solubilisation buffer (L3) was added to the tubes containing the DNA slices and placed into a 50°C heat block (Fisher Scientific, FB15101, dry bath) until gel dissolution. The dissolved gels containing the DNA were loaded onto quick gel extraction columns and centrifuged at 12,000 x g for 1 min. After discarding the flow-through, 500 µL of wash buffer (W1) was added and two centrifugations, at maximum speed (corresponding to 16 x 000 g) for 1.5 min were performed. For DNA recovery, 30 µL of $_{d}H_2O$ was added followed by centrifugation at max speed for 1 min. Eluted DNA was stored either at 4°C short-term or at -20°C long-term.

### *Ligation*

Purified DNA was ligated into the desired digested plasmid overnight using 10 µL insert DNA, 2 µL backbone plasmid DNA, 1 µL T4 Ligase enzyme (M180A, Promega, WI, USA), and 1.4 µL 10x ligation buffer (C126B, Promega, WI, USA). Ligated products were transformed into bacterial cells and cultured for the amplification of DNA (See 2.9). Ligated plasmid constructs were confirmed by digestion and agarose gel electrophoresis. Successfully ligated constructs were further transformed into bacterial cells and cultured for the greater amplification of DNA (See 2.9).

## 2.8 Preparation of competent TOP10 *Escherichia. coli* cells

A 100 µL aliquot of competent TOP10 *E. Coli* cells was thawed on ice for 10 minutes. 200 µL of sterile Luria Broth (LB) [1 % Tryptone (LP0043, Oxoid, UK), 1 % NaCl (S/3160/60, Fisher, UK), and 0.5% yeast extract (LP0021, Oxoid, UK)] was added, and incubated in a shaking incubator (200 rpm) at 37°C for 45 minutes. Bacteria were spread on LB agar plates (without antibiotic; Sterillin, Thermo Scientific) (10 mL LB

broth with 1.5 % agar powder (LP001, Oxoid, UK) and incubated overnight at 37ºC. A single colony was then picked and used to inoculate 2 mL of LB (no antibiotics), which was then incubated in a shaking incubator (250 rpm). 1 mL of this culture was used to inoculate 100 mL of LB and was further incubated at 37ºC for ~2 - 3 hours until OD600 reached a reached a value of 0.2-0.7 (POLARstar Omega, BMG Labtech). Once achieved, the culture was chilled on ice for 15 minutes before being aliquoted into two 50 mL tubes and pelleted by centrifugation at 3,300 x g for 10 minutes at 4°C. The supernatant was discarded, and each bacterial pellet was resuspended in 10 mL of ice-cold sterile 0.1 M $CaCl_2$. Cells were incubated on ice for a further 30 minutes before being centrifuged at 3,300 x g for 10 min at 4°C. After discarding the supernatant, each pellet was resuspended in 3 mL of ice-cold sterile 0.1 M $CaCl_2$ containing 15% glycerol. The obtained 6 mL of bacteria was snap-frozen into 100 µL aliquots and stored at -80 °C for 3 to 6 months.

## 2.9 Transformation of bacterial cells and culture for the amplification of plasmid DNA

Plasmid constructs (or completed ligation reactions) were added to a 1.5 mL Eppendorf tube containing competent Top 10 *E. coli* cells and thawed on ice for 20 min. For ligation reactions, 10 µL was added to 100 µL of bacterial cells, and for plasmid transformations 0.2 µg was added to 35 µL of bacterial cells. Following incubation on ice, the transformation mixes underwent heat shock at 42 ºC for 1 min and were then returned to ice for 2 min. 100 µL of sterile LB broth was then added to the transformation tubes before being incubated in a shaking incubator (200 rpm) at 37ºC for 1 hour. The transformation mixes were then spread on agar plates (Sterillin, Thermo Scientific, UK) [10 mL LB broth with 1.5 % agar powder (LP001, Oxoid, UK) containing either 30 µg/ml Kanamycin (K4000-5G, Sigma-Aldrich, UK); or 100 µg/ml Ampicillin (A9518-25G, Sigma-Aldrich, UK)], and incubated overnight at 37ºC. The following day, single colonies were carefully picked using a sterile pipette tip and grown overnight at 37ºC (200 rpm) in either 3 mL LB broth/antibiotic for minipreps or 150 mL LB broth/antibiotic for midipreps. The bacterial culture was used as per the protocol in either the NucleoBond Xtra plasmid purification Miniprep (K210011, Invitrogen, ThermoScientfic, UK) or Midiprep kit (19081001, Machery-Nagel, Germany). DNA concentration was measured using a NanoDrop 2000/2000c

spectrophotometer (Thermo Fisher Scientific, UK). The sequence of plasmid DNA was confirmed by sequencing performed by GATC Eurofins genetic sequencing service (GATC service by Eurofins Genomics, Wolverhampton, UK) or by sequencing performed by DNA Sequencing & Services (MRC I PPU, School of Life Sciences, University of Dundee, Scotland, www.dnaseq.co.uk) using Applied Biosystems Big-Dye Ver 3.1 chemistry on an Applied Biosystems model 3730 automated capillary DNA sequences.

## 2.10 Analysis of protein expression

Expression of protein after DNA transfection was analysed by immunoblotting (see 2.19). 24 hours post-transfection, cells were washed once in PBS and lysed in 100 µL of 1X SDS sample buffer (0.4 % bromophenol blue, 200 mM Tris pH 6.8, 40 % glycerol, 8 % SDS) with 25 mM DTT. Lysates were scraped from wells, transferred to Eppendorf tubes and the samples were heated to 95ºC before being resolved through SDS-PAGE and examined by Western Blotting (see 2.19).

## 2.11 Fatty acid azide labelling and click chemistry

### Click-AK800 dye

Twenty-four hours post-transfection, (HEK-293T) cell media was aspirated and the cells were metabolically labelled by incubating the cells for 4 hours at 37°C in 300 µL per well of warm serum-free medium containing 1 mg/mL fatty acid free bovine serum albumin (A7030-100G, Sigma, UK) and 100 µM palmitic acid azide (C16-azide_DMSO Stock 50 mM, 500X) (synthesised by Professor Nicholas Tomkinson, University of Strathclyde). After 4 hours, cells were washed once with 500 µL of room temperature PBS and lysed on ice by adding 100 µL lysis buffer (50 mM Tris pH 8, 0.5% SDS) containing protease inhibitor cocktail, 1:100 (P8340-5, Sigma, UK) to each well. 80 µL of click chemistry reaction mix (2 mM $CuSO_4$, 0.2 mM TBTA and 2.5 µM alkyne dye) was then added to each lysate followed by 20 µL of 40 mM ascorbic acid (A15613, Alfa Aesar, UK). Samples were incubated for 1 hour with end-over-end rotation at room temperature. 67 µL of 4X SDS sample buffer (0.4 % bromophenol blue, 200 mM Tris pH 6.8, 40 % glycerol, 8 % SDS) was added together with DTT to

a final concentration of 25 mM. Samples were then heated to 95 ºC for 5 minutes before analysis by SDS-PAGE.

The alkyne reporter molecule “clicks” with the azide group of the palmitic acid azide in the labelling mix, causing palmitoylated proteins to fluoresce in the IR800 channel visualised by immunoblotting analysis.

**Click-PEGylation**

An alternative method which was utilised involved an alkyne-conjugated 5 kDa monomethoxy polyethylene glycol (mPEG; mPEG5K alkyne, Aldrich, JKA3177) reporter instead of the AK800 dye. For PEG-S-acylation experiments, twenty-four hours post-transfection, cell media was aspirated and the cells were metabolically labelled by incubating the cells for 4 hours at 37°C in 300 µL per well of warm serum-free medium containing 1 mg/mL bovine serum albumin (fatty acid-free) (A7030-100G, Sigma, UK) and either 100 µM of “cold” palmitic acid used as a negative control (one well per sample), or 100 µM of palmitic acid azide (two wells per sample) (both in DMSO Stock 50 mM, 500X). After 4 hours, cells were washed once with 500 µL room temperature PBS and lysed on ice by adding 100 µL lysis buffer (50 mM Tris pH 8, 0.5% SDS) containing protease inhibitor cocktail, 1:100 (P8340-5, Sigma, UK) to each well. 80 µL of click chemistry reaction mix (2 mM $CuSO_4$, 0.2 mM TBTA and 200 µM alkyne-PEG reporter dissolved in DMSO) was then added to each lysate followed by 20 µL of 40 mM ascorbic acid (A15613, Alfa Aesar, UK). Samples were incubated for 1 hour with end-over-end rotation at room temperature. 67 µL of 4X SDS sample buffer (0.4 % bromophenol blue, 200 mM Tris pH 6.8, 40 % glycerol, 8 % SDS) was added together with DTT to a final concentration of 25 mM. Samples were then heated to 95ºC for 5 minutes before analysis by SDS-PAGE.

The alkyne reporter molecule “clicks” with the azide group of the palmitic acid azide in the labelling mix, causing an increase in the protein molecular mass by 5 kDa. This results in a band shift which is visualized by immunoblotting analysis.

## 2.12 GFP-Trap® co-immunoprecipitation

Transfected HEK-293T cells were aspirated and washed in 500 µL PBS before being resuspended in 200 µL lysis buffer (PBS, 0.5 % Triton X-100 [Sigma, T8787] with added protease inhibitor cocktail, 1:100 [Sigma, P8340]). The cell lysis reaction was incubated on ice for 30 minutes with gentle inversion every 5 minutes. 300 µL of PBS was then added to each lysate to give a final Triton X-100 concentration of 0.2 % v/v. The diluted lysate was centrifuged at 14,000 x g for 5 min and the supernatant was collected. 45 µL of the supernatant was retained as an "input" sample, with the remaining supernatant being mixed with 10 µL of washed GFP Trap® agarose immunoprecipitation beads (gta-20, ChromoTek GmbH, Germany). The supernatant/agarose bead mixture was incubated for no less than 1 hour at 4ºC with end-over-end rotation.

After incubation, the agarose beads were pelleted by centrifugation at 3000 x g for 3 min and the supernatant was discarded. The beads were then washed twice in 1 mL PBS (by resuspension and centrifugation) and then resuspended in 50 µL of 2x sample buffer containing 100 mM DTT and heated for 10 minutes at 95ºC. The agarose beads were then pelleted by centrifugation at 3,000 x g for 3 minutes and the supernatant (containing immunoprecipitated proteins released from the beads) collected for subsequent analysis by SDS-PAGE and immunoblotting.

## 2.13 Click chemistry using immunoprecipitated proteins

For AK800-IR dye experiments, 48 hours post-transfection (PC12 cells) cell media was aspirated and the cells were metabolically labelled by incubating the cells for 4 hours at 37 °C in 300 µL per well of warm serum-free medium containing 1 mg/mL bovine serum albumin (fatty acid-free; A7030-100G, Sigma, UK) and 100 µM palmitic acid azide (C16-azide_DMSO Stock 50 mM, 500X) (synthesised by Professor Nicholas Tomkinson, University of Strathclyde). For mPEG S-acylation experiments, 24-hours post-transfection cell media was aspirated and the cells were metabolically labelled by incubating the cells for 4 hours at 37°C in 300 µL per well of warm serum-free medium containing 1 mg/mL bovine serum albumin (fatty acid-free; A7030-100G, Sigma, UK), and 100 µM of either palmitic acid-azide or palmitic acid (both in DMSO Stock 50 mM, 500X).

After 4 hours, cells were washed once with 500 µL room temperature PBS before being resuspended in 200 µL lysis buffer (PBS, 0.5 % Triton X-100 [Sigma, T8787] with added protease inhibitor cocktail, 1:100 [Sigma, P8340]). The cell lysis reaction was incubated on ice for 30 minutes with gentle inversion every 5 minutes. 300 µL of PBS was then added to each lysate to give a final Triton X-100 concentration of 0.2 % v/v. The diluted lysate was centrifuged at 14,000 x g for 5 min and the supernatant was collected. 45 µL of the supernatant was retained as an "input" sample, with the remaining supernatant being mixed with 10 µL of washed GFP Trap® agarose immunoprecipitation beads (gta-20, ChromoTek GmbH, Germany). The supernatant/agarose bead mixture was incubated for no less than 1 hour at 4°C with end-over-end rotation.

After incubation, the agarose beads were pelleted by centrifugation at 3000 x g for 3 min and the supernatant was discarded. The beads were then washed twice in 1 mL PBS (by resuspension and centrifugation, 3000 x g for 3 min) and then resuspended in 100 µL of PBS containing 0.2 % Triton X-100. 80 µL of click chemistry reaction mix (2 mM $CuSO_4$, 0.2 mM TBTA and 2.5 µM alkyne dye or 200 µM alkyne-mPEG) was then added to each resuspended precipitate followed by 20 µL of 40 mM ascorbic acid (A15613, Alfa Aesar, UK). Samples were incubated for 1 hour with end-over-end rotation at room temperature. After incubation, the beads were washed in 1 mL of PBS containing 0.2 % Triton X-100 (by resuspension and centrifugation, 3000 x g for 3 min), before being resuspended in 50 µL of 2x sample buffer containing 100 mM DTT and heated for 10 minutes at 95°C. The agarose beads were then pelleted by centrifugation at 3,000 x g for 3 minutes and the supernatant (containing immunoprecipitated proteins released from the beads) collected for subsequent analysis by SDS-PAGE and immunoblotting.

### 2.14 Cycloheximide chase to examine protein turnover

Twenty-four hours post-transfection, cells were incubated with 50 µg/ml of cycloheximide (CHX; C-7698, Sigma, UK) for different time points between 0 - 8 hrs depending on the experiment. Cells at each time point were washed once in PBS and lysed in 100 µL of 1X SDS buffer (25 mM DTT). Lysates were scraped from wells, transferred to Eppendorf tubes and the samples were heated to 95 °C before being examined by Western Blotting (see 2.19). Expression of relevant proteins (e.g., HA-

zDHHC17 or Orf3d-Strep-II) was quantified at each time point relative to the corresponding total protein stain (see 2.18).

## 2.15 Stimulation of the MAPK pathway

Cells were transfected with either EGFP-tagged Spry2 WT, Spry2, DM, Spry2 NDK; or co-transfected with HA-tagged zDHHC17 or zDHHC7. Twenty-four hours post-transfection, cells were serum starved for four hours in serum-free media. Serum-free media was then removed and replaced with 0.5 mL of media containing 50 ng/mL of growth factor for a designated time (typically 10 minutes). Growth factors used were either fibroblast growth factor (FGF; recombinant human FGF basic 146 aa, 233-FB, R&D Systems, UK) or epidermal growth factor (EGF; recombinant human EGF, 236-EG, R&D Systems, UK). After this time period, the media was removed, and cells were washed in PBS and lysed in SDS sample buffer (25 mM DTT). Lysates were scraped from wells, transferred to Eppendorf tubes and the samples were heated to 95$^{o}$C before being analysed by Western Blotting using TBS-T (see 2.19)

## 2.16 Incubation of cells with salt compounds

24 hours post-transfection, cells were washed once in PBS and incubated for 4 hours in DMEM (+ serum) with the addition of 100 μM of salt, either: Sodium Chloride (NaCl) (S/3160/60; Fisher Scientific, UK), Magnesium Chloride ($ZnCl_2$) (M/0600/53; Fisher Scientific, UK), Zinc Chloride ($ZnCl_2$) (Z/0850/53; Fisher Scientific, UK), Sodium Sulphate ($Na_2O_4$) (7757-82-6; Fisher Scientific, UK), Magnesium Sulphate ($MgSO_4$) (M/1050/53); Fisher Scientific, UK), or Zinc Sulphate ($ZnSO_4$) (10299; AnalaR, BDH Chemicals Ltd, UK ). After which cells were lysed in 100 μL of 1X SDS buffer (with 25 mM DTT) and scraped from wells before being transferred to Eppendorf tubes. Samples were heated to 95$^{o}$C and resolved through SDS-PAGE and examined by Western Blotting (see 2.19).

## 2.17 Sodium dodecyl sulphate-polyacrylamide gel electrophoresis (SDS-PAGE)

Gels were cast using two different gel compositions: a resolving polyacrylamide gel (8-15% acrylamide) at the bottom [40% acrylamide (Alfa Aesar, MA, USA, J60868), 100 µL of 438 mM ammonium persulfate (APS, Sigma, UK, A3678), 10 µL of TEMED (Sigma, UK, T9281), and 5 mL of resolving buffer (30 mM (w/v) SDS (Fisher, UK, S/P530153), 4 mM EDTA (Sigma, UK, E5134), 750 mM Tris base (Fisher, UK, T6066), pH 8.9)]. A polyacrylamide stacking gel was then added on top spaced by a 1.0 mm comb [0.9 mL of 40% acrylamide (Alfa Aesar, MA, USA, J60868), 100 µL of 438 mM APS (Sigma, UK, A3678), 10 µL of TEMED (Sigma, UK, T9281), and 4 mL of stacking buffer (30 mM (w/v) SDS (Fisher, UK, S/P530153), 4 mM EDTA (Sigma, UK, E5134), 250 mM Tris base (Fisher, UK, T6066), pH 6.8 in $_{d}H_2 0$)]. Samples were loaded into gel lanes and underwent sodium dodecyl sulphate-polyacrylamide gel electrophoresis (SDS-PAGE) in SDS running buffer (250 mM Tris base (Fisher, UK, T6066), 2 M glycine (Fisher, UK, G/0800/60), and 152 mM SDS (Fisher, UK, S/P530153)), alongside a molecular weight marker (BP3601-500, EZ-Run™ pre-stained protein marker, Fisher BioReagents™, UK). Gels were typically run at 80 V for 20 min followed by 150 V for 60 min (based on a 10 % resolving polyacrylamide gel). After SDS-PAGE, protein transfer to nitrocellulose membranes (6 x 9 cm) was conducted using a Bio-Rad Trans-Blot® SD cell (Bio-Rad Laboratories, Inc, UK). For this, nitrocellulose sheets were positioned on top of gels and filter paper placed at either side (all components pre-soaked in transfer buffer) before being placed into the transfer cassette. Transfer was then performed at 120 mA overnight (~16 hours) in transfer buffer [480 mM Tris base (Fisher, UK, T6066), 390 mM glycine (Fisher, UK, G/0800/60), 9 mM SDS (Fisher, UK, S/P530153), and 20 % (v/v) Methanol (VWR Chemicals, UK)].

## 2.18 Total protein stain

Nitrocellulose membranes were removed from the transfer apparatus and all proteins were stained using the LI-COR REVERT™ Total protein stain kit (LI-COR Biosciences UK Ltd, Cambridge, UK). As per the manufacturer's protocol, the transferred membranes were briefly rinsed in $_{d}H_2O$ and then incubated with REVERT total protein

stain for 5 minutes, with gentle shaking. This was followed by two washes (30 seconds each) with wash solution (67% (v/v) glacial acetic acid, 30% methanol, in $_dH_2O$). Membranes were then scanned using the 700 nm channel of a LI-COR Odyssey 9120 IR Imager (LI-COR Biosciences UK Ltd, Cambridge, UK). After scanning, the stain was completely removed from the membrane by incubating with gentle shaking in REVERT reversal solution for no longer than 10 minutes. Membranes were then briefly rinsed in $_dH_2O$ before further use.

### 2.19 Immunoblotting (Western blotting)

For immunoblotting analysis, membranes were first blocked for 45 minutes in 5% (w/v) defatted milk diluted in PBS-T (PBS containing 0.1 % Tween-20 (P1379-1L, Sigma, UK)). Membranes were then washed three times using PBS-T (5 minutes per wash). Membranes were then incubated for 2 hours with the appropriate primary antibody (table 2.2) diluted in PBS-T. Membranes were again washed three times in PBS-T before being incubated for 1 hour with appropriate secondary antibodies (table 2.2). Membranes were washed for a final time using PBS-T, three times for 5 minutes each, before being scanned using the 700 nm and 800 nm channels using a LI-COR Odyssey 9120 IR Imager (LI-COR Biosciences UK Ltd, Cambridge, UK). All incubations were performed at room temperature.

| Table 2.2. Antibodies involved in the immunodetection of proteins | | | | | |
|---|---|---|---|---|---|
| **Antibody** | **Species** | **Clonality** | **Source** | **Cat. Code** | **Dilution** |
| **Primary antibodies** | | | | | |
| **GFP (JL8)** | Mouse | Monoclonal, IgG | Clontech, Takara | *632381* | 1 : 4,000 |
| **α-HA (3F10)** | Rat | Monoclonal, IgG | Roche | *11867423001* | 1 : 1,000 |
| **p-ERK (E-4)** | Mouse | Monoclonal, IgG | Santa Cruz | *SC-7383* | 1 : 200 |
| **ERK 1/2 (H-72)** | Rabbit | Polyclonal, IgG | Santa Cruz | *SC-292838* | 1 : 200 |
| **Strep-II (THE™ NWSHPQFEK)** | Mouse | Monoclonal, IgG1 | GenScript | *A01732* | 1 : 2,000 |
| **MYC (9E10)** | Mouse | Monoclonal, IgG | Sigma | *M5546* | 1: 1,000 |
| **Secondary antibodies** | | | | | |
| **IR DYE 680RD Donkey anti-mouse** | | IgG | Licor Inc, USA | *926-68072* | 1:20,000 |
| **IR DYE 800CW Donkey anti-mouse** | | IgG | Licor Inc, USA | *926-32212* | 1:20,000 |
| **IR DYE 680RD Goat anti-rat** | | IgG | Licor Inc, USA | *926-68076* | 1:20,000 |
| **IR DYE 800CW Goat anti-rat** | | IgG | Licor Inc, USA | *926-32219* | 1:20,000 |
| **IR DYE 680CW Donkey anti-rabbit** | | IgG | Licor Inc, USA | *926-68073* | 1:20,000 |

## 2.20 Confocal microscopy

For confocal microscopy experiments, PC12 cells were seeded on poly-D-lysine coated coverslips as described above (see 2.1) and used 48 hours post-transfection. The coverslips were washed twice with PBS and fixed in 300 µL 4 % (v/v) formaldehyde (#28902, Pierce™, Thermo Fisher Scientific, UK) for 30 minutes at room temperature. The coverslips/cells were then washed twice with PBS and once with $_dH_2O$ before being air dried for 1 hour at room temperature. Coverslips were mounted on microscope slides (7101, Sailing boat, China) using Mowiol® aqueous mounting reagent and cured overnight to harden before being transferred to 4°C until required. Cells were imaged using a TCS SP8 Leica microsystems confocal microscope (Leica, UK).

## 2.21 Bioinformatics

### *Plasmid design*

DNA sequences were obtained and/or confirmed using reference sequences from the National Centre for Biotechnology Information (NCBI) database (National Library of Medicine; National Institutes of Health; U.S. Department of Health and Human Services). (https://www.ncbi.nlm.nih.gov/). DNA sequences/plasmid constructs were visualised and designed using ApE, A Plasmid Editor (Davis, M. W., & Jorgensen, E. M. (2022)).

### *Multiple sequence alignment*

Alignments of multiple protein sequences were generated using the UniProt alignment tool (https://www.uniprot.org/align). Obtained images were subsequently annotated/edited in Microsoft PowerPoint.

### *AlphaFold and Google ColabFold*

3D protein structure predictions were obtained from the open-access AlphaFold Protein Structure Database developed by DeepMind and EMBL-EBI (Jumper et al.,

2021, Varadi et al., 2022). For protein structures not available on AlphaFold DB, amino acid sequences of interest were uploaded in text format and modelled using Google ColabFold AlphaFold2 (Phenix version) (Mirdita et al., bioRxiv, 2021, (https://github.com/sokrypton/ColabFold). Outputs were produced as PDB files and subsequently visualised using the RCSB Protein Data Bank 3D Mol* Viewer (Sehnal et al., 2021). Obtained images were subsequently annotated/edited in Microsoft PowerPoint.

***PSIPRED***

Predictions of protein secondary structures, amino acid property analysis, membrane topology schematics, and feature-based function predictions of cellular function and localisation were produced using the PSIPRED 4.0 feature. Amino acid sequences were uploaded in text format to the UCL bioinformatics group protein structure analysis workbench (http://bioinf.cs.ucl.ac.uk/psipred). Obtained images were subsequently annotated/edited in Microsoft PowerPoint.

***NetWheel***

To determine the arrangement of amino acids within predicted alpha helices of proteins, amino sequences were uploaded in text format to the online NetWheels tool (http://lbqp.unb.br/NetWheels/) to produce helical wheel projections. Obtained images were subsequently annotated/edited in Microsoft PowerPoint.

***Hydropathy plot***

To evaluate hydrophilicity and hydrophobicity of Orf3d along its amino acid sequence a hydropathy plot was generated using the ProtScale resource from the Swiss bioinformatics resource portal, ExPASy (Wilkins et al., 1999). Hydropathy plot based on the Kyte & Doolittle hydropathy scale (Kyte and Doolittle, 1982).

## 2.22 Data and statistical analysis

Densitometry and quantification of all immunoblots was carried out using Licor® Image Studio™ Lite software (LI-COR® Inc., USA). All figures were created using Microsoft PowerPoint software. Statistical analysis was conducted using GraphPad Prism 8.0 (San Diego, CA, USA). Data was analysed using either; one-way ANOVA or two-way ANOVA followed by Tukey's multiple comparison test; or an unpaired t-test (correcting for multiple comparisons using the Holm-Sidak method where appropriate). Mean values ± standard error of the mean (± SEM) was plotted, and the number of replicates was indicated in the figure legends. For significant results **** denotes $P < 0.0001$, *** $P < 0.001$, ** $P < 0.01$, * $P < 0.05$, and ns denotes non-significance. Image J software (National Institutes of Health, USA) was used to process confocal microscopy images and conduct co-localisation analysis.

# CHAPTER 3

# CHARACTERISATION AND FUNCTIONAL EFFECTS OF SPRY/SPRED PROTEINS

# Chapter 3 - Characterisation and functional effects of Spry/SPRED proteins

## Introduction

For zDHHC13/17, a novel substrate-binding motif recognised by the ankyrin repeat (AR) domain of the enzymes was previously identified (Lemonidis et al., 2015b). Using alanine scanning mutagenesis and bioinformatics, the study revealed that the AR of these two enzymes recognises a hexapeptide consensus motif - (VIAP)(VIT)XXQP (named the “zDHHC ankyrin binding motif” or “zDABM” for short). The zDABM of SNAP25 is critical for its interaction with and S-acylation by zDHHC17 (Greaves et al., 2010b; Lemonidis, Sanchez-Perez, and Chamberlain, 2015b). Subsequent research by Lemonidis and colleagues utilised peptide array analysis to further predict and validate zDHHC17-interacting zDABMs from 90 different proteins (Lemonidis et al., 2017a). The proteins identified to contain a zDABM included several members of the Spry and SPRED families, however SPRED3 lacks a zDABM. Spry/SPRED proteins were considered worthy of further investigation as a “bioplex” interactome study identified that endogenous Spry2 and zDHHC17 form a complex in cells, suggesting that the interaction is physiologically relevant (Huttlin et al., 2015). The proteins are of additional interest due to the presence of a highly conserved C-terminal cysteine-rich SPR domain. In general, there is little known about the S-acylation of such cysteine-rich proteins. Furthermore, Spry/SPRED proteins have been linked to various cancers in their role as negative regulators of the MAPK growth factor signalling pathway. Spry2, has now been shown to interact with and be S-acylated by zDHHC17 (Masoumi-Moghaddam et al., 2014b, Locatelli et al., 2020).

Subsequent analysis has identified specific cysteines in Spry2 that are modified by zDHHC17 - C265 and C268. In addition, an NDK motif (N211/D214/K223) is also required for S-acylation (Locatelli et al., 2020). The same study by Locatelli et al., (2020) further characterised the role of zDHHC17, by showing that the S-acylation mutants of Spry2 have decreased plasma membrane localisation and a reduction in protein stability. As mentioned above, SPRED3 does not contain a zDABM motif, but yet has been shown to bind and be S-acylated by zDHHC17 (Butland et al., 2014). This suggests that SPRED3 (and possibly other Spry/SPRED proteins) may have an alternative zDHHC17 interaction site that is coupled to S-acylation.

The aims of this chapter were to (i) examine the interaction and S-acylation of the full Spry and SPRED protein families with zDHHC17; (ii) to explore the possible role of S-acylation of Spry2 on its function in growth factor signalling.

# Results

## 3.1 S-acylation of endogenous Spry2 in PC12 cells

Variability in mRNA expression between cell types is well known, which includes variable expression of zDHHC enzymes and their substrates. Previous work in the Chamberlain lab has shown that zDHHC17 substrates, such as SNAP25 are effectively S-acylated in PC12 cells (rat pheochromocytoma cells) without co-expression of recombinant zDHHC17 (Greaves and Chamberlain, 2011). This is furthered in experiments by Dr. Carolina Locatelli which also show a strong S-acylation of Spry2 in PC12 cells without the need for co-expressed zDHHC17 (Locatelli et al., 2020). Initial investigation and optimisation of techniques for the S-acylation of Spry2 was conducted in these neuroendocrine cells. Two different types of click chemistry analyses (infrared dye or PEG-acylation) were used to determine the S-acylation status of Spry2. Both methods are based on copper(I)-catalysed azide-alkyne cycloaddition (CuAAC) click chemistry which allows for the specific conjugation between azide and alkyne molecules. In this case bio-incorporated palmitic acid synthesised to include an azide molecule conjugates to an alkyne molecule attached to either a near-infrared IR800 fluorescent dye or a polyethylene glycol molecule of 5 kDa (mPEG).

Figure 3.1 A shows the effective detection of immunopurified Spry2 using the IR800 fluorescent dye method. This method focuses on the overall S-acylation of the protein, where the intensity of the dye (AK800) corresponds to level of S-acylation. In immunopurified Spry2 samples there is a significant increase in EGFP-tagged Spry2 S-acylation when compared to that of the EGFP alone negative control (figure 3.1 B). Figure 3.1 C shows the effective detection of immunopurified Spry2 using the PEG-acylation method. Once palmitic acid-azide is incorporated via S-acylation, alkyne-mPEG5K (monomethoxy polyethylene glycol, 5 kDa) can conjugate, thereby increasing protein mass by approximately 5 kDa per fatty acid attachment. Whereas the IR800 dye method discussed above focuses more on overall S-acylation; this mPEG-acylation method focuses more precisely on the S-acylation of specific

cysteine residues (i.e., the more cysteine residues that are S-acylated, then the more bands that are visible on the immunoblot). In immunopurified Spry2 samples there is a reduction in non-acylated EGFP-tagged Spry2 at ~65 kDa, but an increase in S-acylated EGFP-tagged Spry2 at both 75 and 85 kDa (figure 3.1 C/D) when the samples are click with alkyne-mPEG5K. This indicates the presence of at least two cysteines that are specifically PEGylated.

Although both methods have their strengths, the IR800 dye method was taken forward to be used in this thesis, as Spry2 is known to have 26 cysteine residues. The PEGylation method of click chemistry analysis is not able to distinguish this potentially high number of modified cysteines or to give reliable quantification.

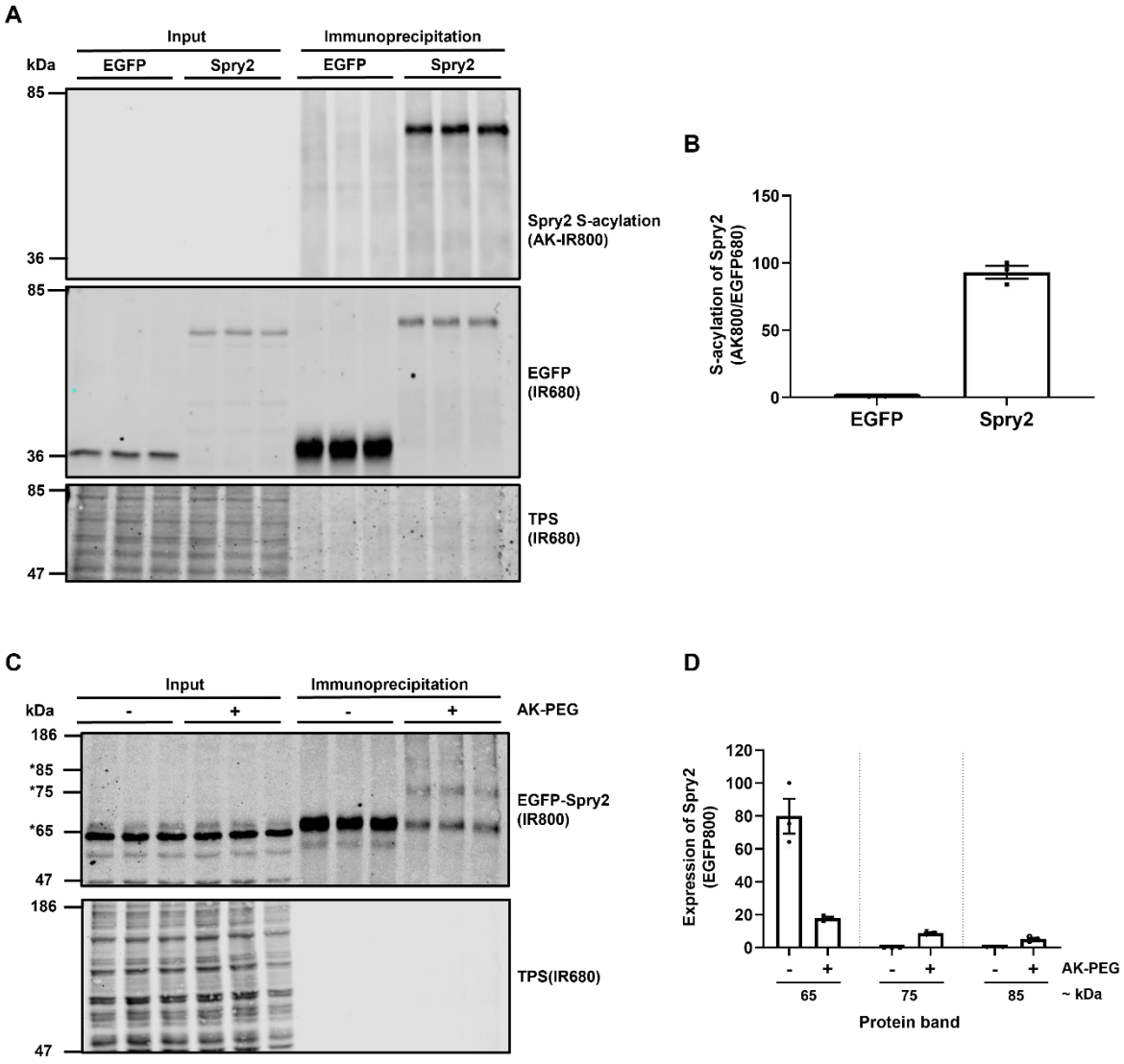

***Figure 3.1. Detection of Spry2 S-acylation in PC12 cells using click-chemistry coupled immunoprecipitation techniques.*** *(A) PC12 cells were transfected with plasmids encoding for EGFP-tagged Spry2 or EGFP alone as a control. Cells were incubated with 100 μM palmitic acid azide (C16:0-azide) for 4 h and subsequently incubated with agarose beads conjugated to an EGFP antibody overnight. Labelled and immunoprecipitated proteins were reacted with alkyne (AK) IRdye-800 nm. Representative images showing substrate S-acylation (top; AK-IR800) and substrate EGFP expression levels (middle; IR680) detected in input and co-immunoprecipitated samples on the same immunoblot. A total protein stain (TPS) is also shown (bottom panel; IR680). The positions of the molecular weight markers (kDa) are shown on the left side of all immunoblots. (B) Graph showing the mean intensity values of Spry2 and EGFP S-acylation relative to substrate expression (AK800/EGFP680), normalised to the highest value on the blot (n = 3, for a single experiment). Error bars represent ± SEM; each replicate is shown with filled circles. (C) PC12 cells were transfected with plasmids encoding for EGFP-tagged Spry2. Cells were incubated for 4 h with 100 μM of either palmitic acid-azide (+) or palmitic acid (-) as a control. Once incorporated via S-acylation, alkyne-PEG5K (monomethoxy polyethylene glycol, 5 kDa) conjugates through alkyne-azide click chemistry, thereby increasing protein mass by approximately 5 kDa per attachment. Representative images showing substrate S-acylation/PEGylation (top; EGFP800) detected by immunoblot. A total protein stain (TPS) is also shown (bottom panel; IR680). The positions of the molecular weight markers (kDa) and visible bands at ~65, ~75, and ~85 kDa (indicated by *) are shown on the left side of all immunoblots. (D) Graph showing the mean intensity values of Spry2 expression (IR800) at bands visible at ~65, ~75, and ~85 kDa, and normalised to the highest value on the blot (n = 3, for a single experiment). Error bars represent ± SEM; each replicate is shown with filled circles.*

## 3.2 All Spry proteins are effectively S-acylated by zDHHC17 in HEK-293T cells

Although endogenous Spry2 is S-acylated in PC12 cells, the transfection efficiency in this cell line is low and protein immunopurification is necessary for optimal visualisation/detection of S-acylation. Alongside this as PC12 are grown in suspension, other challenges arise such as reduced cell adhesion during serum starvation (required for click chemistry metabolic labelling), leading to excess cell loss

during washing and aspiration. As the prospective experiments required effective co-transfection of plasmid DNA, an alternative cell line was sought. Human embryonic kidney 293T cells (HEK-293T) have been previously used within the Chamberlain lab for analysis of S-acylation (Greaves et al., 2009, Locatelli et al., 2020) and are suitable for high transfection efficiency and protein expression (figure 3.2), as well as reliable growth and adhesion (Tan et al., 2021). Therefore, for experiments in this thesis, HEK-293T cells have been used, unless otherwise stated.

Spry2 has been shown in previous research to be effectively S-acylated (Locatelli et al., 2020). However, there has been less investigation into the S-acylation of Spry1, 3, & 4. Plasmids encoding EGFP-tagged Spry1, Spry2, Spry3, and Spry4 were transfected into HEK-293T cells together with a plasmid encoding HA-zDHHC17 or pEF-BOS-HA empty plasmid as a negative control. As can be seen in figure 3.2 B, all Spry proteins (1, 2, 3, & 4) can be S-acylated by zDHHC17. When S-acylation signals are normalised to the expression of the substrate signal (AK800/EGFP680) in figure 3.2 C, Spry3 has the highest level of S-acylation by zDHHC17 and Spry1 has the lowest signal. Spry2 and Spry4 were also highly S-acylated but less than that of Spry3 (figure 3.2 C). When S-acylation by zDHHC17 was expressed as a fold change above basal, Spry2 had the lowest mean fold change showing a 90% increase in S-acylation in the presence of zDHHC17 (figure 3.2 D). zDHHC17 still exhibited the greatest effect on Spry3 with a mean fold increase of nearly 300%. Spry1 and Spry4 fold change in S-acylation with zDHHC17 were 177% and 200%, respectively (figure 3.2 D).

The middle panels of figure 3.2 B (Spry-EGFP IR680) also indicates a differential band expression not only between Spry proteins, but also between samples with or without zDHHC17 co-expressed. This can be seen in the middle panel for Spry2 where a second upper band is more visible in co-expression with zDHHC17 than without (noting that the lower band is also much more well expressed). The upper band of Spry2 protein is generally reported to be a phosphorylated form of the protein (Lao et al., 2007b). For Spry1 and Spry3 there is also a clear lower to upper band shift in the presence of zDHHC17. However, for Spry4, although the expression of the protein is increased in the presence of zDHHC17, a band shift is harder to discern (figure 3.2 B).

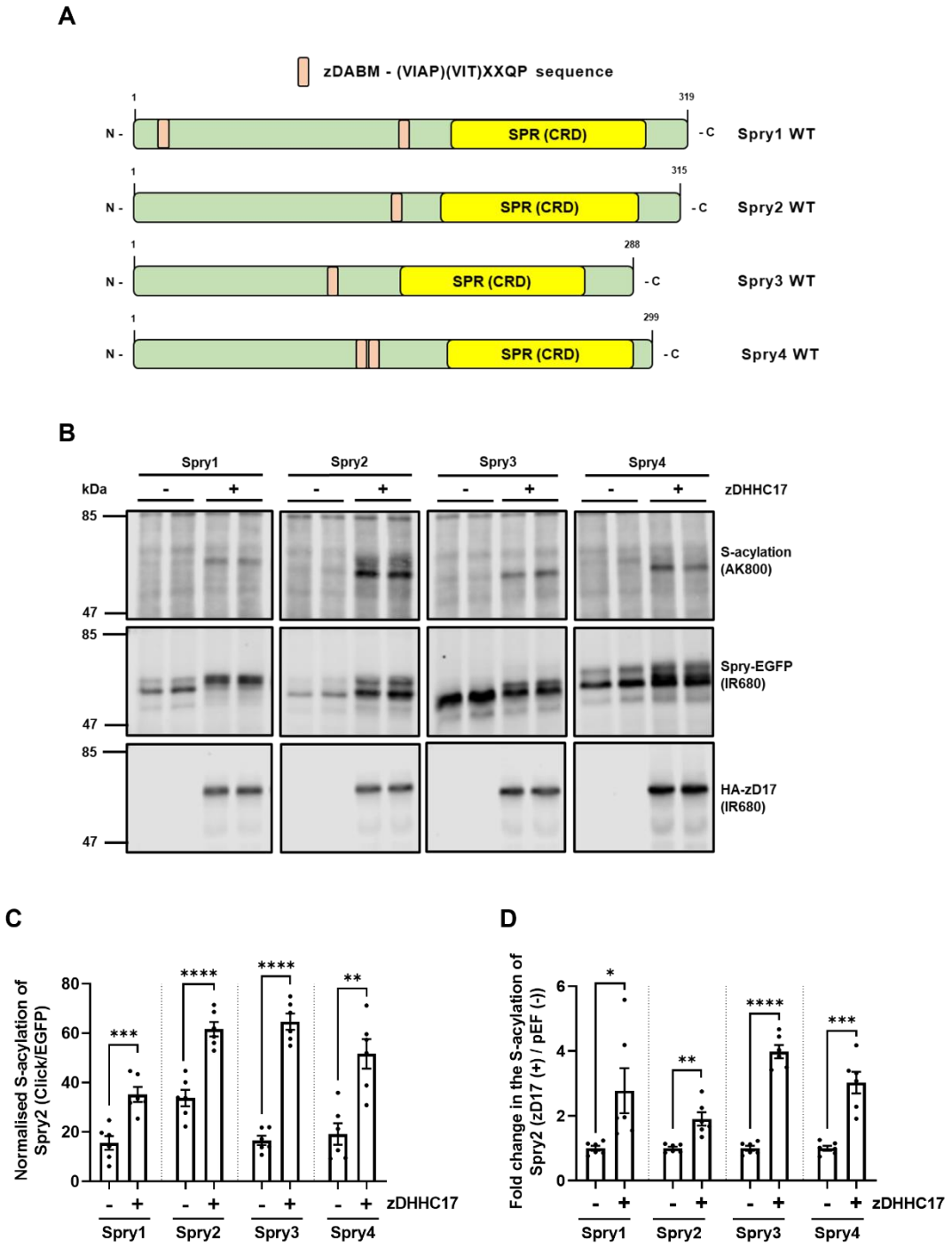


***Figure 3.2. All Spry proteins are S-acylated by HA-zDHHC17.*** *(A) Schematic diagram comparing Spry1, Spry2, Spry3, and Spry4 proteins. Regions conforming to canonical zDABM sites ((VIAP)(VIT)XXQP) are indicated; SPR, Sprouty domain also referred to as CRD (cysteine-rich domain). All constructs used have EGFP tags appended at the N terminus. (B) HEK-293T cells were transfected with plasmids encoding for EGFP-tagged Spry1, Spry2, Spry3, or Spry4, together with either pEF-*

*BOS-HA (as "-" in the figure) or HA-zDHHC17 (as "+" in the figure). Cells were incubated with 100 μM palmitic acid azide (C16:0-azide) for 4 h and labelled proteins reacted with alkyne (AK) IRdye-800 nm. Representative images showing Spry S-acylation (top; AK-IR800) and EGFP-tagged Spry levels (middle; IR680) detected on the same immunoblot. For zDHHC17, HA (bottom; IR680) was revealed for the same samples on a different immunoblot. The positions of the molecular weight markers (kDa) are shown on the left side of all immunoblots. (C) Graph showing the mean intensity values of Spry S-acylation relative to protein expression (AK800/EGFP680) and normalised to the highest value on each blot. (D) Graph showing the mean fold change between Spry S-acylation in the presence and absence of zDHHC17 (zDHHC17 (+) / pEF (-)). Error bars represent ± SEM; each replicate is shown with filled circles. Differences were analysed by unpaired t test (pEF v zDHHC17). **** denotes p < 0.0001, ***p < 0.001, **p < 0.01, *p < 0.05, (n = 6, for three independent experiments).*

### 3.3 SPRED1 and SPRED2 are not effectively S-acylated by zDHHC17

As previously discussed, Spry proteins share a high homology with another group of proteins known as Sprouty related EVH1 domain containing proteins, abbreviated as SPREDs. SPRED1 and SPRED2 contain a zDABM sequence making them interesting proteins to investigate in terms of S-acylation (Lemonidis et al., 2017a). SPRED1 has previously been reported to be S-acylated using click chemistry assays (Butland et al., 2014).

Co-transfections were therefore set up to examine if zDHHC17 was active against SPRED1 and SPRED2 in our assay systems (Spry2 was also included in these experiments as a control). In addition, the role of the zDABM sequences in the Spry/SPRED proteins was investigated by mutating the conserved proline in this motif to an alanine. In addition to zDHHC17, the highly active zDHHC7 isoform was also included as a positive control (Lemonidis et al., 2014, Locatelli et al., 2020). Plasmids encoding EGFP-tagged Spry2 WT, Spry2 P154A, SPRED1 WT, SPRED1 P316A, SPRED2 WT, and SPRED2 P284A were used. These were transfected into HEK-293T cells together with a plasmid encoding for HA-zDHHC17, HA-zDHHC7, or pEF-BOS-HA empty plasmid as a negative control. The transfected cells were incubated

with palmitic acid azide to label S-acylated proteins via conjugation to an alkyne-IR800 dye. Spry2 WT was found to be highly S-acylated by zDHHC7 and to a lower extent by zDHHC17 (figure 3.3 A). Interestingly, the proline mutant construct (P154A) was also effectively S-acylated by zDHHC17 (figure 3.3 A). Like Spry2, both SPRED1 and SPRED2 were S-acylated by zDHHC7, however neither the WT nor the proline mutant forms of these proteins were significantly S-acylated by zDHHC17 (figure 3.3 B and 3.3 C).

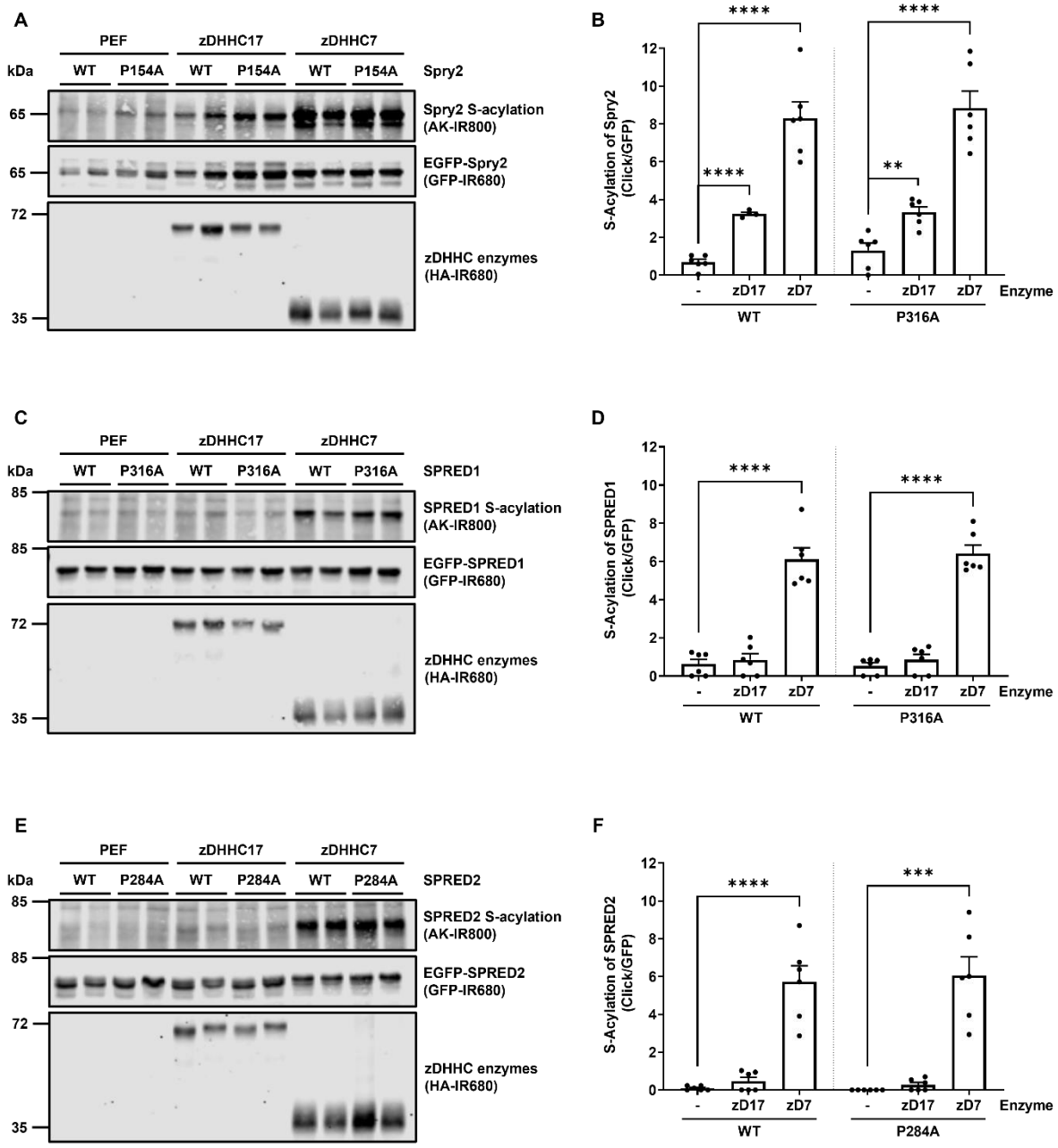

***Figure 3.3. S-acylation of WT and zDABM mutants of Spry2, SPRED1, and SPRED2 in HEK-293T cells.*** *HEK-293T cells were co-transfected with plasmids encoding for EGFP-tagged Spry2 WT, Spry2 P154A, SPRED1 WT, SPRED1 P316A, SPRED2 WT, and SPRED2 P284A, together with HA-tagged zDHHC17, zDHHC7, or pEF-BOS-HA negative control plasmid (as "-" in the figure). Cells were incubated with 100 μM palmitic acid azide (C16:0-azide) for 4 h and labelled proteins reacted with alkyne (AK) IRdye-800 nm. (A/C/E) Representative images showing Spry/SPRED S-acylation (top; AK-IR800) and EGFP-tagged Spry/SPRED levels (middle; IR680) detected on the same immunoblot. For zDHHC17/zDHHC7, HA (bottom; IR680) was revealed for the same samples on a different immunoblot. The positions of the molecular weight markers (kDa) are shown on the left side of all immunoblots. (B/D/F) Graphs showing the mean intensity values of Spry2/SPRED1/SPRED2 S-acylation relative to substrate expression (AK800/EGFP680) and normalised to the highest value on each blot. Error bars represent ± SEM; each replicate is shown with filled circles. Differences were analysed by unpaired t test (pEF v zDHHC17/zDHHC7). **** denotes p < 0.0001, ***p < 0.001, **p < 0.01 (n = 6, for three independent experiments). Data points less than < 0 were set to = 0. All samples showed a significant increase between the negative control (pEF-BOS) and zDHHC7, where P < 0.0001.*

### 3.4 SPRED3 is S-acylated by zDHHC17

SPRED3 is unique in the Spry/SPRED families as it lacks a typical zDABM sequence (Lemonidis et al., 2017a). However, a previous study reported that SPRED3 can be S-acylated by zDHHC17 (Butland et al., 2014). To examine if this result could be replicated under the conditions used in our S-acylation assays, HEK-293T cells were co-transfected with zDHHC17 and either Spry2 WT or SPRED3 WT and then incubated with C16:0-azide and processed for click chemistry detection of S-acylation (figure 3.4 A). As before, mean intensity values for the S-acylated band (IR800) of each substrate were normalised against the EGFP intensity for that protein (figure 3.4 B) or expressed as a fold increase above basal (figure 3.4 C).

As shown in Figure 3.4 B, both Spry2 and SPRED3 showed a significant increase in S-acylation when co-expressed with zDHHC17, compared with the basal for each sample. Spry2 exhibited a higher intensity in S-acylation than SPRED3. As the basal level of SPRED3 S-acylation was lower than Spry2, the fold increase in acylation by

zDHHC17 over basal was also calculated for both proteins. Figure 3.4 C shows that both Spry2 and SPRED3 exhibited a similar fold increase in mean intensity with zDHHC17, despite overall lower levels of fluorescence for SPRED3. The mean fold change for Spry2 in the presence of zDHHC17 was 4.594 ± 0.726 AU, and for SPRED3 was 3.485 ± 0.379 AU.

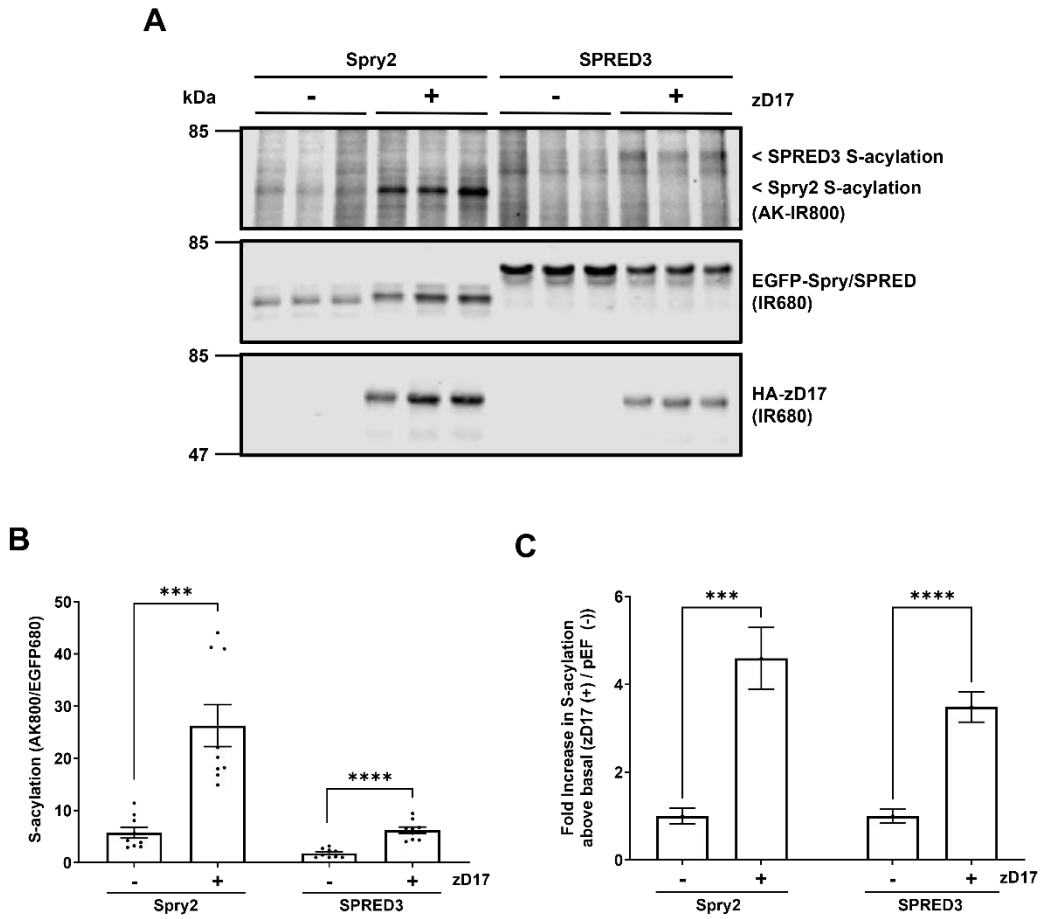


***Figure 3.4. S-acylation of SPRED3 and Spry2 by zDHHC17.*** *(A) HEK-293T cells were transfected with plasmids encoding for EGFP-tagged Spry2 WT or SPRED3 WT together with either pEF-BOS-HA (as "-" in the figure) or HA-zDHHC17 (as "+" in the figure). Cells were incubated with 100 µM palmitic acid azide (C16:0-azide) for 4 h and labelled proteins reacted with alkyne (AK) IRdye-800 nm. Representative images showing Spry/SPRED S-acylation (top; AK-IR800) and EGFP-tagged Spry/SPRED levels (middle; IR680) detected on the same immunoblot. For zDHHC17, HA (bottom; IR680) was revealed for the same samples on a different immunoblot. The positions of the molecular weight markers (kDa) are shown on the left side of all immunoblots.*

*B) Graph showing the mean intensity values of Spry/SPRED S-acylation relative to substrate expression (AK800/EGFP680) and normalised to the highest value on each blot. (C) Graph showing the mean fold change between Spry/SPRED S-acylation in the presence and absence of zDHHC17 (zDHHC17 (+) / pEF (-)). Error bars represent ± SEM; each replicate is shown with filled circles. Differences were analysed by unpaired t test (pEF v zDHHC17). **** denotes p < 0.0001, ***p < 0.001 (n = 9, for three independent experiments).*

### 3.5 AlphaFold prediction and testing of Spry2 interactions with the ankyrin repeat domain of zDHHC17

Understanding the structure of zDHHC enzyme-substrate complexes is important to predict and validate functional regions within these proteins. Complete crystal structures do not currently exist for either full-length zDHHC17 or Spry2. Structures are available for the ankyrin repeat of zDHHC17 (aa 51-288) in a complex with a SNAP25b peptide (Verardi et al., 2017), and for Spry2 aa 49-61 in a complex with the c-cbl-tkb domain of the E3 ubiquitin-protein ligase (Ng et al., 2008). However, recent developments in AlphaFold, an AI system developed by DeepMind and EMBL-EBI, now allow prediction of a protein's 3D structure from its amino acid sequence (https://alphafold.com/).

Although determined to be highly accurate, the AlphaFold database does not contain structures of protein-protein complexes. To overcome this, protein complex modelling software from Google Colab's AlphaFold-Multimer notebook (Evans et al., 2022) based on AlphaFold by DeepMind and EMBL-EBI (Jumper et al., 2021; Varadi et al., 2022) was used to explore the zDHHC17-Spry2 interaction. Initial AlphaFold modelling of Spry2 and the ankyrin repeat domain was conducted by Dr Kimon Lemonidis (University of Glasgow) and indicated the two proteins do interact (figure 3.5 A). Alongside residue P154A of Spry2, which is part of the zDABM of this protein (Lemonidis et al 2017), other predicted regions of interaction/interest in Spry2 were identified. These included amino acids L43/I46, Y176, and T298/V299/C300 (figure 3.5 B/C).

To investigate if these residues are important for interaction, mutant constructs of Spry2 containing one or more of these residues substituted with alanine were synthesised (figure 3.5 G). In this case, S-acylation of the mutant constructs by

zDHHC17 was used as a proxy for binding (mutants 2-6 are shown in figure 3.5 D; mutants 7-11 are presented in figure 3.5 E; and mutants 12-16 are shown in figure 3.5 F). When the Spry2 S-acylation was normalised to substrate expression, all mutant constructs showed equal or reduced acylation by zDHHC17 (figure 3.5 H). However, only mutant constructs 6 (P154/Y176A), 7 (P154/T298/V299/C300A), 12 (L43/I46/P154/Y176A), 13 (L43/I46/T298/V299/C300), 14 (L43/I46/P154/T298/V299/C300A), and 16 (L43/I46/P154/Y176/T298/V299/C300A) exhibited a significant reduction when compared to the WT (figure 3.5 H). Further analysis of this data showed that when normalised values of S-acylation were taken as a fold change compared to the wild-type, constructs: 6 (P154/Y176A), 7 (P154/T298/V299/C300A), 9 (P154/Y176/T298/V299/C300A, 14 (L43/I46/P154/T298/V299/C300A), and 16 (L43/I46/P154/Y176/T298/V299/C300A) showed a significant change in S-acylation (figure 3.5 I). Except for mutant construct 13 (L43/I46/T298/V299/C300), all other constructs that displayed significantly reduced S-acylation contained a P154A mutation in combination with any other mutation. The greatest reduction in S-acylation was observed for construct 16 which contained the most individual mutations.

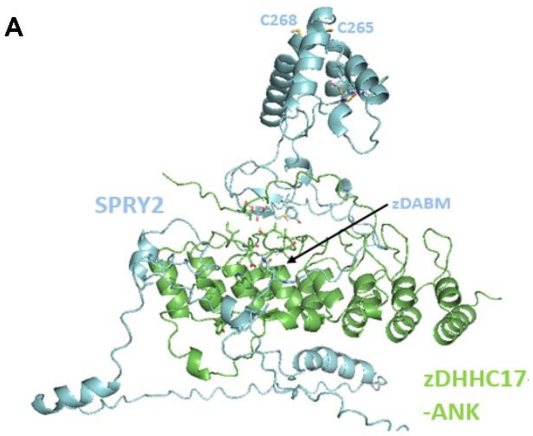


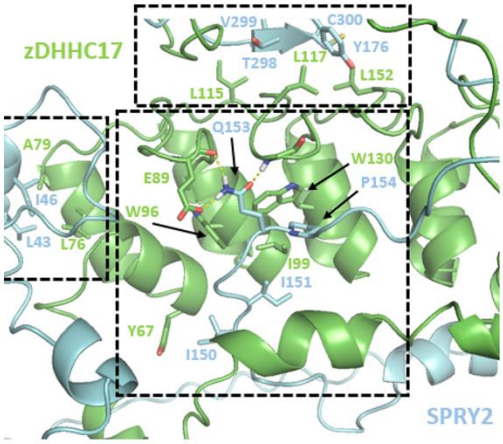


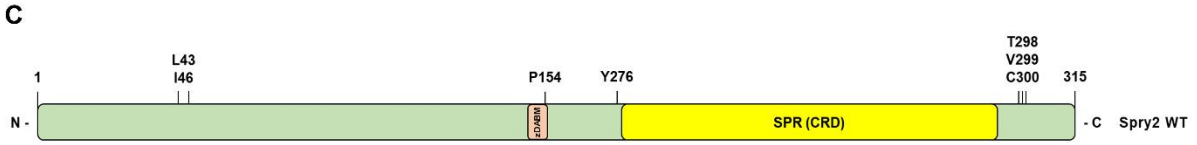


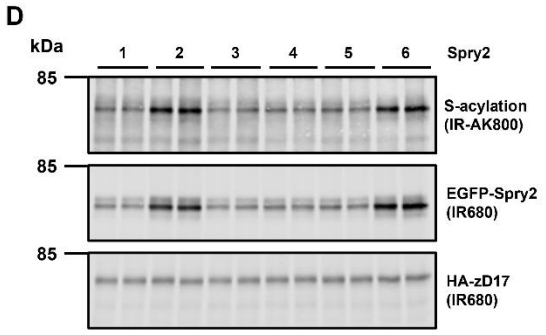


G

| hSpry2 mutant constructs | | | |
|---|---|---|---|
| 1 | WT | 9 | P154 / Y176A / T298 / V299 / C300A |
| 2 | P154A | 10 | L43 / I46 / P154A |
| 3 | Y176A | 11 | L43 / I46 / Y176A |
| 4 | T298 / V299 / C300A | 12 | L43 / I46 / P154 / Y176A |
| 5 | L43 / I46A | 13 | L43 / I46 / T298 / V299 / C300A |
| 6 | P154 / Y176A | 14 | L43 / I46 / P154 / T298 / V299 / C300A |
| 7 | P154 / T298 / V299 / C300A | 15 | L43 / I46 / Y176 / T298 / V299 / C300A |
| 8 | Y176 / T298 / V299 / C300A | 16 | L43 / I46 / P154 / Y176 / T298 / V299 / C300A |

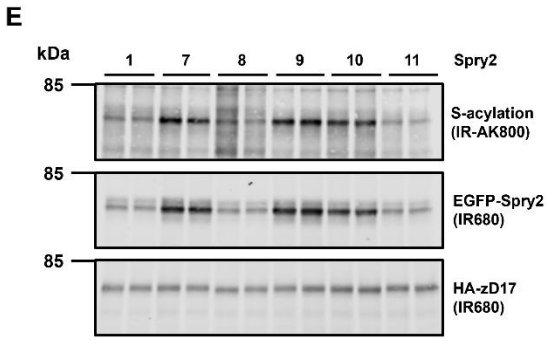


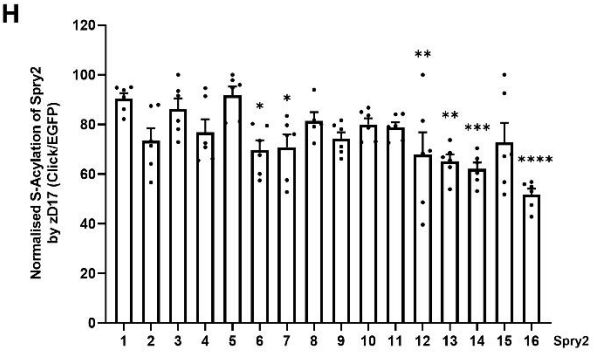


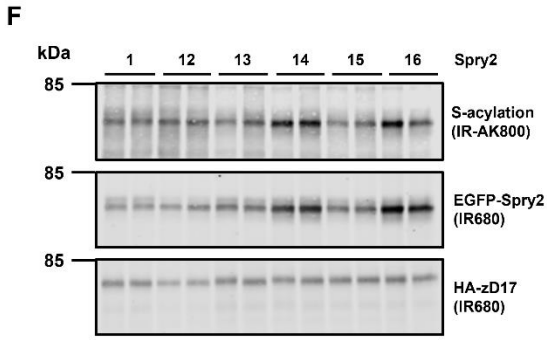


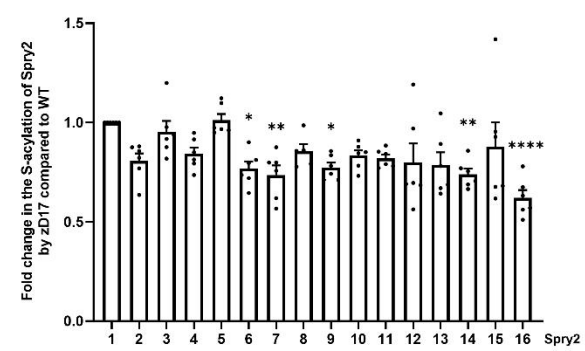

***Figure 3.5. S-acylation of Spry2 mutant constructs based on predictions from AlphaFold modelling of Spry2 interaction with the ankyrin repeat of zDHHC17.*** *(A) Protein structure predictions of protein Sprouty homolog 2 – UniProt: O43597 (SPY2_HUMAN) interacting with the ankyrin repeat of palmitoyltransferase zDHHC17, aa 51-286 – UniProt: Q8IUH5 (ZDH17_HUMAN). Protein complex prediction modelled using Google CoLab's AlphaFold-Multimer notebook (Evans et al., 2022) based on AlphaFold by DeepMind and EMBL-EBI (Jumper et al., 2021, Varadi et al., 2022). zDHHC17 protein chain is shown in green and Spry2 protein chain is shown in blue. (B) Enlarged image showing interactions Spry2 with the ankyrin repeat of zDHHC17. (C) Schematic diagram showing positions of residues mutated to alanine in hSpry2: L43, I46, P154, Y176, T298, V299, & C300A. Spry2 zDABM (IIRVQP) is indicated; SPR, Sprouty domain also referred to as CRD (Cysteine-rich domain). All constructs used have EGFP tags appended at the N terminus. (D) HEK-293T cells were co-transfected with plasmids encoding for either EGFP-tagged hSpry2 WT (1) or EGFP-tagged hSpry2 mutant constructs: 2 - P154A, 3 - Y176A, 4 - T298/V299/C300A, 5 - L43/I46A or 6 - P154/Y176A; alongside HA-zDHHC17. (E) HEK-293T cells were co-transfected with plasmids encoding for either EGFP-tagged hSpry2 WT (1) or EGFP-tagged hSpry2 mutant constructs: 7 - P154/T298/V299/C300A, 8 - Y176/T298/V299/C300A, 9 - P154/Y176A/T298/ V299/C300A, 10 - L43/I46/P154A, 11 - L43/I46/Y176A; alongside HA-zDHHC17. (F) HEK-293T cells were co-transfected with plasmids encoding for either EGFP-tagged hSpry2 WT (1) or EGFP-tagged hSpry2 mutant constructs: 12 - L43/I46/P154/Y176A, 13 - L43/I46/T298/V299/C300A, 14 - L43/I46/P154/T298/V299/C300A, 15 - L43/I46/ Y176/T298/V299/C300A, 16 - L43/I46/P154/Y176/T298/V299/C300A ; alongside HA-zDHHC17. Cells were incubated with 100 μM palmitic acid azide (C16:0-azide) for 4 h and labelled proteins reacted with alkyne (AK) IRdye-800 nm. Representative images showing Spry S-acylation (top; AK-IR800) and EGFP-tagged Spry levels (middle; IR680) detected on the same immunoblot. For zDHHC17, HA (bottom; IR680) was revealed for the same samples on a different immunoblot. The positions of the molecular weight markers (kDa) are shown on the left side of all immunoblots. (G) Table of human Spry2 mutant constructs. (H) Graph showing the mean intensity values of Spry S-acylation relative to substrate expression (AK800/EGFP680) and normalised to the highest value on each blot. (I) Graph showing the mean fold change between Spry2 mutant constructs and Spry2 WT (1). Error bars represent ± SEM; each replicate is shown with filled circles. Differences were analysed by ordinary one-way ANOVA with a Dunnett's multiple comparison test against WT Spry2. **** denotes $p < 0.0001$, ***$p < 0.001$, **$p < 0.01$, *$p < 0.05$, ($n = 6$, for three independent experiments).*

### 3.6 AlphaFold modelling predicts that full length zDHHC17 can interact with Spry2

Initial modelling of Spry2 and zDHHC17 shown in figure 3.5 was based on the ankyrin repeat domain. However, modelling of the full length Spry2-zDHHC17 complex was subsequently achieved (figure 3.6). Overall, the full-length model has differences to that of the Spry2-zDHHC17 Ank model (figure 3.5). Notably the previously investigated residues Y176 and T298/V299/C300 in the full-length Spry2-zDHHC17 model are no longer predicted to interact with any part of zDHHC17 (figure 3.5).

In agreement with the previous model (figure 3.5) and consistent with previously published X-ray crystallography data (Verardi et al., 2017), residue P154 and the wider zDABM region of Spry2 (IIRVQP) is predicted to interact within the ankyrin repeat domain of zDHHC17 (fig 3.6 C). Specifically, the zDABM region is predicted to interact with or be close to residues N100 and W130, which are the two major interacting residues identified to bind to the zDABM region of SNAP25 (Verardi et al., 2017). Another notable region protein of interest is the catalytic DHHC domain of zDHHC17. Cysteine residues C201 and C205 of Spry2 (which are within the SPR domain) are suggested in this model to interact and/or be spatial close to this catalytic domain (figure 3.6 B). However, it should be noted that published research has shown experimentally that alanine mutagenesis of C201/C205/C207 does not reduce the S-acylation of Spry2 by zDHHC17 (Locatelli et al., 2020).

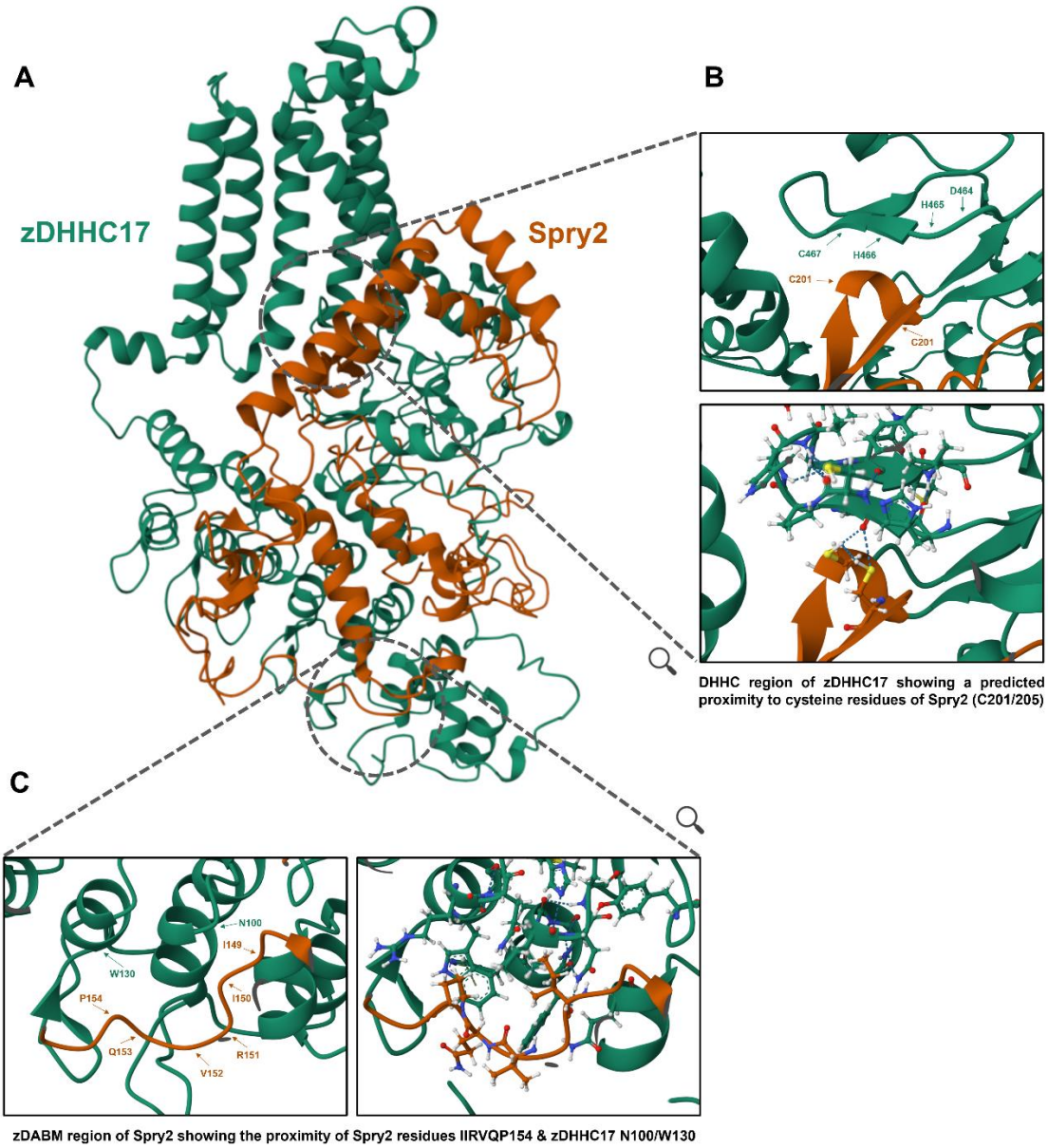


***Figure 5.6. AlphaFold modelling of full length Spry2-zDHHC17 interaction.*** *(A) Protein structure predictions of protein Sprouty homolog 2 – UniProt: O43597 (SPY2_HUMAN) interacting with palmitoyltransferase ZDHHC17 – UniProt: Q8IUH5 (ZDH17_HUMAN). Protein complex prediction modelled using Google Colab's AlphaFold-Multimer notebook (Evans et al., 2022) based on AlphaFold by DeepMind and EMBL-EBI (Jumper et al., 2021, Varadi et al., 2022). zDHHC17 protein chain is shown in green and Spry2 protein chain is shown in orange. (B) Enlarged image showing interactions of the DHHC region of zDHHC17, including interactions with cysteines C201/C205 of Spry2. (C) Enlarged image showing interactions of the zDABM region of Spry2 (IIVRQP-154), including proximity or interactions with residues N100 and W130 of zDHHC17.*

### 3.7 Chimeric constructs of Spry2 and SPRED1 were not S-acylated by zDHHC17

Results in figure 3.3 showed that SPRED1 and SPRED2 were not effectively S-acylated by zDHHC17. Despite the homology of SPRED1 to Spry2, there are notable differences which could potentially account for the observed differences in S-acylation efficiency by zDHHC17. Specifically: (i) SPRED1 contains an N-terminal EVH1 domain, (ii) The amino acid sequence between the zDABM and the CRD of SPRED1 is different to that of Spry2, and (iii) Spry2 contains an additional C-terminal region. To examine the impact of these sequence differences, three chimeric mutant constructs of SPRED1 were created to increase similarity with Spry2. These constructs included the removal of the N-terminal SPRED1 EVH1 domain (No EVH1), replacement of the amino acid sequence between the zDABM and CRD of SPRED1 with the corresponding region of Spry2 ((+) 155-176), and addition of the C-terminal sequence from Spry2 onto SPRED1 ((+) 291-315). These mutants are shown schematically in figure 3.7 A.

HEK-293T cells were co-transfected with either HA-zDHHC17, HA-zDHHC7 (positive control), or pEF-BOS-HA (negative control), together with either EGFP-tagged SPRED1 WT, or the chimeric constructs shown in figure 3.1 A. Cells were then incubated with C16:0-azide for 4 hours and cell lysates processed for click chemistry detection of S-acylation. Mean (± SEM) intensity values for the S-acylated band relative to the protein level (AK800/IR680) were then normalised to the respective negative control which was set at 1.00 AU. For zDHHC17, there was no significant difference in mean intensity values for SPRED1 WT or any chimeric SPRED1 mutants relative to the negative controls (Figure 3.7 B and C). In contrast, zDHHC7 co-expression, led to a significant increase in S-acylation for both wild-type and all mutant SPRED1 proteins (Figure 3.7 B and C).

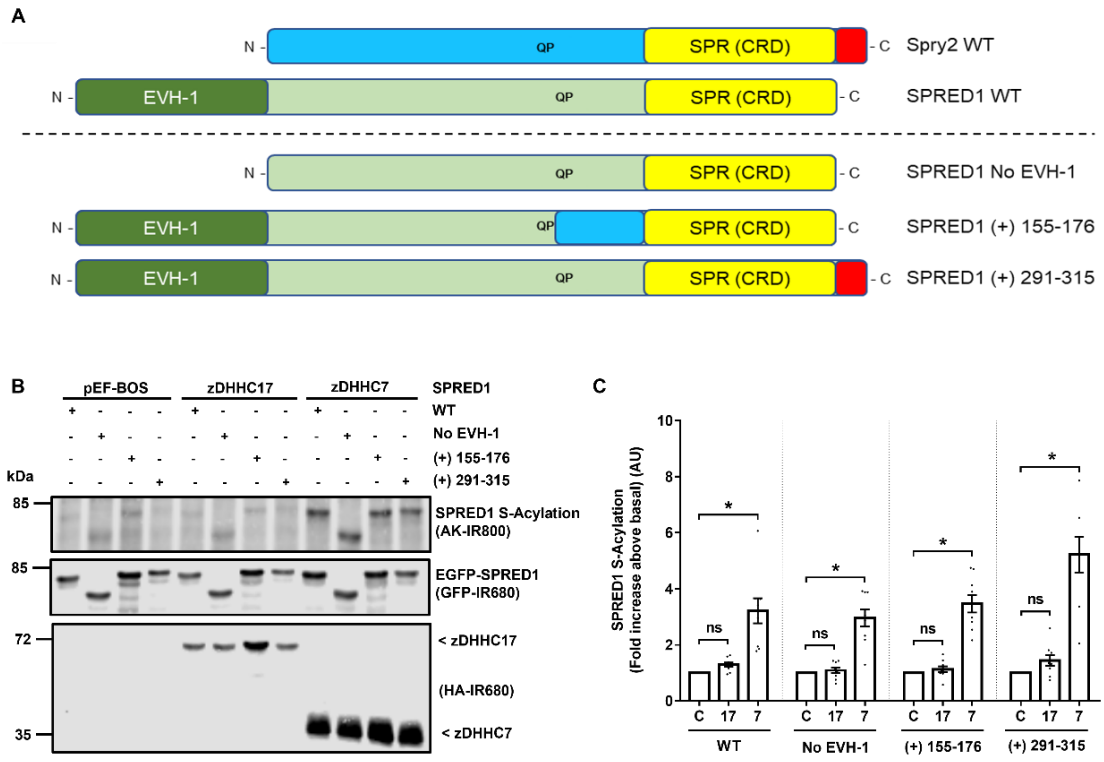


***Figure 3.7. S-acylation of SPRED1 chimeric mutants by zDHHC17 and zDHHC7.*** *(A) Schematic representation of the SPRED1-Spry2 chimeric mutant constructs. EVH1; Ena/VASP (Enabled/vasodilator-stimulated phosphoprotein) homology 1 domain - also known as, WH1; WASP (Wiskott-Aldrich syndrome protein) homology 1 domain. QP; amino acids Gln and Pro of the zDABM. SPR; Sprouty domain – also designated as, CRD; cysteine-rich domain. (B) HEK-293T cells were transfected with plasmids encoding EGFP-tagged SPRED1 WT, SPRED 1 No EVH1, SPRED1 (+) 155-176, and SPRED1 (+) 291-315, together with HA-zDHHC17, HA-zDHHC7 or pEF-BOS negative control plasmid (as "C" in the figure). Cells were incubated with 100 µM palmitic acid azide (C16:0-azide) for 4 h and labelled proteins reacted with alkyne (AK) IRdye-800 nm. Representative images showing SPRED1 S-acylation (top; AK-IR800) and EGFP-tagged SPRED1 levels (middle; IR680) detected on the same immunoblot. For zDHHC17/zDHHC7, HA (bottom; IR680) was revealed for the same samples on a different immunoblot. The positions of the molecular weight markers (kDa) are shown on the left side of all immunoblots. (C) Graph showing the mean fold change between SPRED1 S-acylation in the presence and absence of zDHHC17 or zDHHC7. Error bars represent ± SEM; each replicate is shown with filled circles. Statistical significance was analysed using a one-way ANOVA with a Tukey's multiple comparisons test, *p < 0.05, non-significant differences where P > 0.05, are denoted – ns. (n = 9, for three independent experiments).*

### 3.8 zDHHC17 can be co-immunoprecipitated by Spry1, 2, 3, 4, and SPRED3

Similar to zDHHC17, zDHHC3 and zDHHC7 are also localised to the Golgi apparatus and are able to S-acylate proteins (Lemonidis et al., 2014). However, zDHHC3 and zDHHC7 have been shown to have high activity for their substrates, such as SNAP25 or CSP; but typically have low specificity or weak protein-protein interaction for substrates. Whereas zDHHC17 has been shown to have less S-acylation activity but more specificity for substrates (Lemonidis et al., 2014). For instance, SNAP25 is dependent on its binding to zDHHC17, without which S-acylation cannot occur (Verardi et al., 2017, Butler et al., 2023). Knowing that SPRED3 and each of the Spry proteins (1, 2, 3, & 4) can be effectively S-acylated by zDHHC17 it was next prevalent to check how well they can bind/interact with the enzyme.

HEK-293T cells were co-transfected with either EGFP-tagged Spry1, Spry2, Spry3, Spry4, SPRED3, SNAP25 (positive control), or EGFP alone (negative control), alongside HA-zDHHC17 WT. Cell lysates were incubated for 1 hour with GFP-Trap® agarose immunoprecipitation beads, washed twice in PBS to remove unbound/excess lysate. Precipitates were eluted to release captured EGFP tagged proteins and any co-immunoprecipitated binding partners (i.e., zDHHC17). Eluted proteins were then resolved by SDS-PAGE and analysed by immunoblotting.

From figure 3.8 it can be seen that all transfected Spry/SPRED proteins were able to interact with and successfully co-immunoprecipitate zDHHC17 WT, above that of the EGFP negative control (figure 3.8 B). Spry1, 2, 3, and SNAP25 exhibited the highest mean levels of immunoprecipitated zDHHC17, with Spry4 and SPRED3 showing the lowest levels. When compared to Spry2 in an unpaired t-test, both Spry4 and SPRED3 had significantly lower levels of binding (figure 3.8 B). Spry1, Spry3, and SNAP25 binding was not significantly different to Spry2.

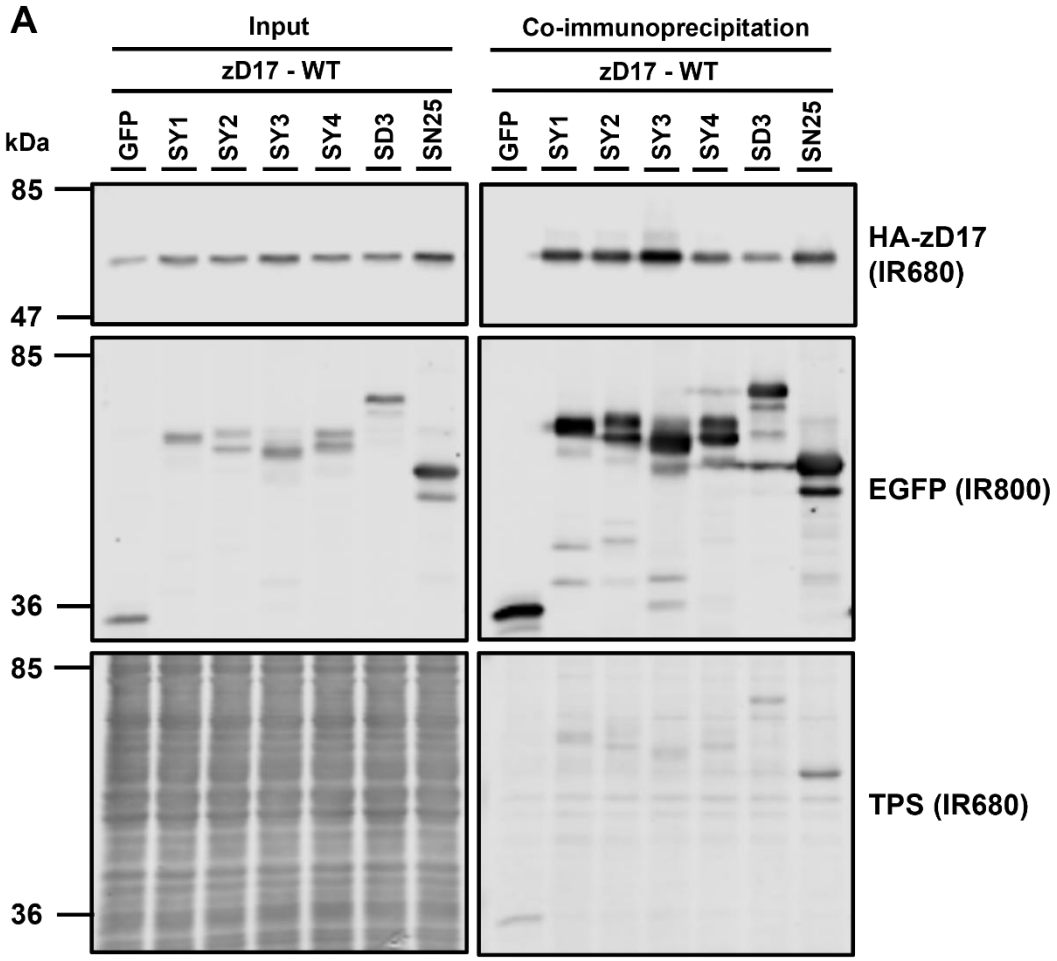
A
Input
Co-immunoprecipitation
zD17 - WT
zD17 - WT
kDa
GFP
SY1
SY2
SY3
SY4
SD3
SN25
85
47
85
36
85
36
HA-zD17
(IR680)
EGFP (IR800)
TPS (IR680)

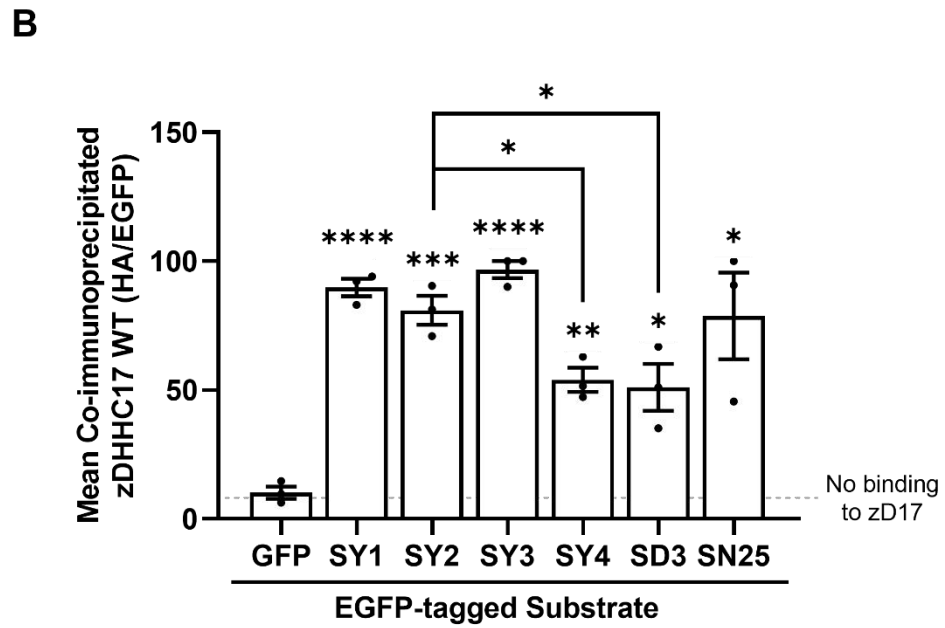
B
Mean Co-immunoprecipitated
zDHHC17 WT (HA/EGFP)
150
100
50
0
****
***
****
**
*
*
*
*
No binding
to zD17
GFP
SY1
SY2
SY3
SY4
SD3
SN25
EGFP-tagged Substrate

***Figure 3.8. Co-immunoprecipitation of zDHHC17 by Spry1, 2, 3, 4, and SPRED3.*** *(A) HEK-293T cells were co-transfected with HA-tagged zDHHC17 WT along with plasmids encoding for EGFP-tagged Spry1 WT, Spry2 WT, Spry3 WT, Spry4 WT, SPRED3 WT, SNAP25, or EGFP alone (as a negative control). Cell lysates were incubated with agarose beads conjugated to an EGFP antibody and co-immunoprecipitated proteins were analysed by immunoblotting. Representative images showing HA-tagged zDHHC17 (top; IR680) and EGFP-tagged substrate (middle; IR800) detected in input and co-immunoprecipitated samples on the same immunoblot. A total protein stain (TPS) is also shown (bottom panel; IR680). The positions of the molecular weight markers (kDa) are shown on the left side of all immunoblots. (B) Graph showing the mean value of co-immunoprecipitated zDHHC17 after normalisation to the highest value for each immunoblot. Error bars represent ± SEM; each replicate is shown with filled circles. Differences were analysed by unpaired t test between each substrate protein. **** denotes p < 0.0001, *** denotes p < 0.001, ** denotes p < 0.01, * denotes p < 0.05. n = 3, for three independent experiments. All values were significant above the EGFP controls.*

### 3.9 SPRED1 and SPRED2 can interact with zDHHC17, and the interaction is reduced but not ablated by zDABM mutations

The results from figures 3.2, 3.4, and 3.8, indicated that SPRED3 (and the Spry proteins) can effectively bind to and be S-acylated by zDHHC17. In contrast, SPRED1 and SPRED2 were not S-acylated by zDHHC17, even though both proteins do still contain a zDABM (Figure 3.3). To determine if the lack of S-acylation by zDHHC17 is due to an ability of SPRED1/2 to interact with zDHHC17, co-immunoprecipitation assays were performed (alongside Spry2 for comparison/control). In keeping with figure 3.3, plasmids encoding EGFP-tagged Spry2 WT, Spry2 P154A, SPRED1 WT, SPRED1 P316A, SPRED2 WT, SPRED2 P284A, or EGFP alone (negative control) were used, alongside HA-zDHHA17 (a catalytically inactive form of zDHHC17).

Figure 3.9 shows that the WT forms of SPRED1, SPRED2, and Spry2 can effectively co-immunoprecipitate zDHHC17. SPRED1 WT showed the highest intensity of zDHHC17 co-immunoprecipitation and SPRED2 WT had a similar interaction with zDHHC17 as that of Spry2 WT. In contrast, all proline mutant constructs exhibited an ~ 30-40% reduction in zDHHC17 co-immunoprecipitation when compared to their respective WT proteins. Although binding was reduced for all proline mutants, it was still significantly higher than the EGFP negative control.

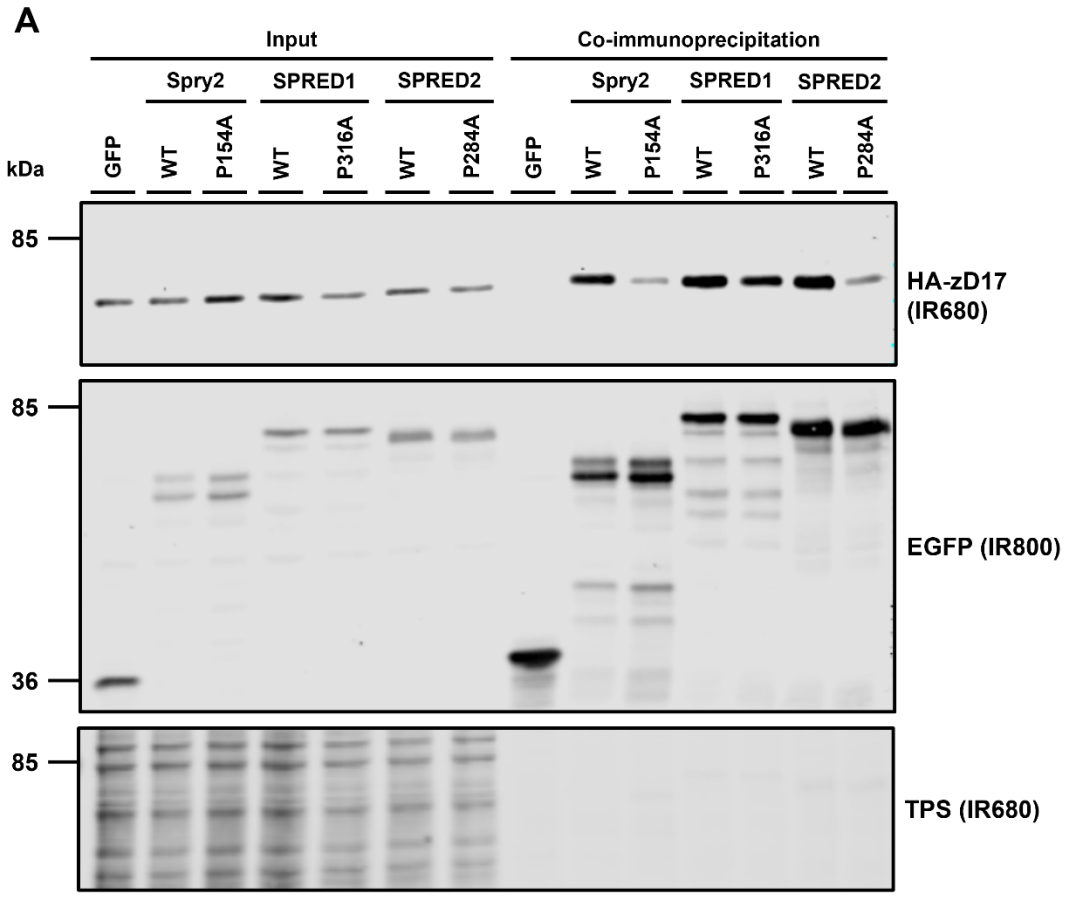
A
Input
Co-immunoprecipitation
Spry2
SPRED1
SPRED2
kDa
GFP
WT
P154A
P316A
P284A
85
36
HA-zD17 (IR680)
EGFP (IR800)
TPS (IR680)

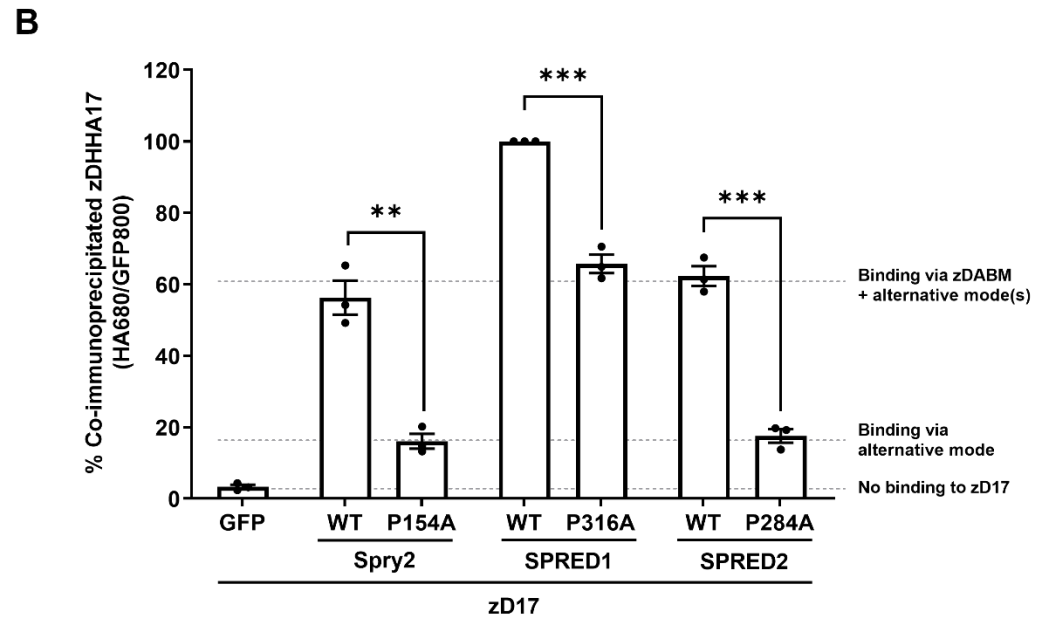
B
% Co-immunoprecipitated zDHHA17 (HA680/GFP800)
120
100
80
60
40
20
0
**
***
***
Binding via zDABM + alternative mode(s)
Binding via alternative mode
No binding to zD17
GFP
WT
P154A
WT
P316A
WT
P284A
Spry2
SPRED1
SPRED2
zD17

***Figure 3.9. Co-immunoprecipitation of zDHHC17 by SPRED1 and SPRED2.*** *(A) HEK-293T cells were co-transfected with HA-tagged zDHHA17 WT along with plasmids encoding for EGFP-tagged Spry2 WT, Spry2 P154A, SPRED1 WT, SPRED1 P316A, SPRED2 WT, SPRED2 P284A, or EGFP alone (negative control). Cell lysates were incubated with agarose beads conjugated to an EGFP antibody and co-immunoprecipitated proteins were analysed by immunoblotting. Representative images showing HA-tagged zDHHC17 (top; IR680) and EGFP-tagged substrate (middle; IR800) detected in input and co-immunoprecipitated samples on the same immunoblot. A total protein stain (TPS) is also shown (bottom panel; IR680). The positions of the molecular weight markers (kDa) are shown on the left side of all immunoblots. (B) Graph showing the mean value of co-immunoprecipitated zDHHC17 after normalisation to the highest value for each immunoblot. Error bars represent ± SEM; each replicate is shown with filled circles. Differences were analysed by unpaired t test between each substrate protein. *** denotes p < 0.001, ** denotes p < 0.01. n = 3, for three independent experiments. All values were significant above the EGFP controls.*

### 3.10 Time-course of FGF-stimulated ERK phosphorylation in the absence or presence of Spry2 over-expression

Having examined the S-acylation and binding of Spry and SPRED proteins to zDHHC17, the impact of S-acylation on protein function was examined, focusing on Spry2. The MAPK/ERK signalling pathway is a common therapeutic target for treating cancer progression (Kim and Choi, 2010). Spry and SPRED proteins are known regulators of the MAPK/ERK growth factor signalling pathway (Kawazoe and Taniguchi, 2019). In particular, Spry2 has been described as an antagonist of the fibroblast growth factor (FGF) signalling pathway (Hacohen et al., 1998). To test if Spry2 could inhibit this pathway in HEK-293T cells, a time course assay of FGF-stimulated activated/phosphorylated ERK expression was conducted. It was hoped that any effect of overexpressed Spry2 in this assay would allow the functional effects of Spry2 S-acylation to be examined though analysis of relevant cysteine mutants.

HEK-293T cells were transfected with EGFP-Spry2 or EGFP-alone, and serum starved before being subsequently treated with FGF for either 0, 2.5, 5, 10, 20, 40, or 80 minutes. Expression of phosphorylated ERK1/2 (p-ERK) was analysed relative to the expression of total ERK. The experiments shown in figure 3.10 reveal that the

phosphorylation of ERK1/2 increased from 2.5 minutes up to 20 minutes. After this time, the phosphorylation level of ERK1/2 decreased over time but at a slower and steadier rate than initial increase. When comparing the phosphorylation of ERK1/2 in the presence and absence of Spry2 overexpression, no significant difference was observed at any time point (Figure 3.10 C).

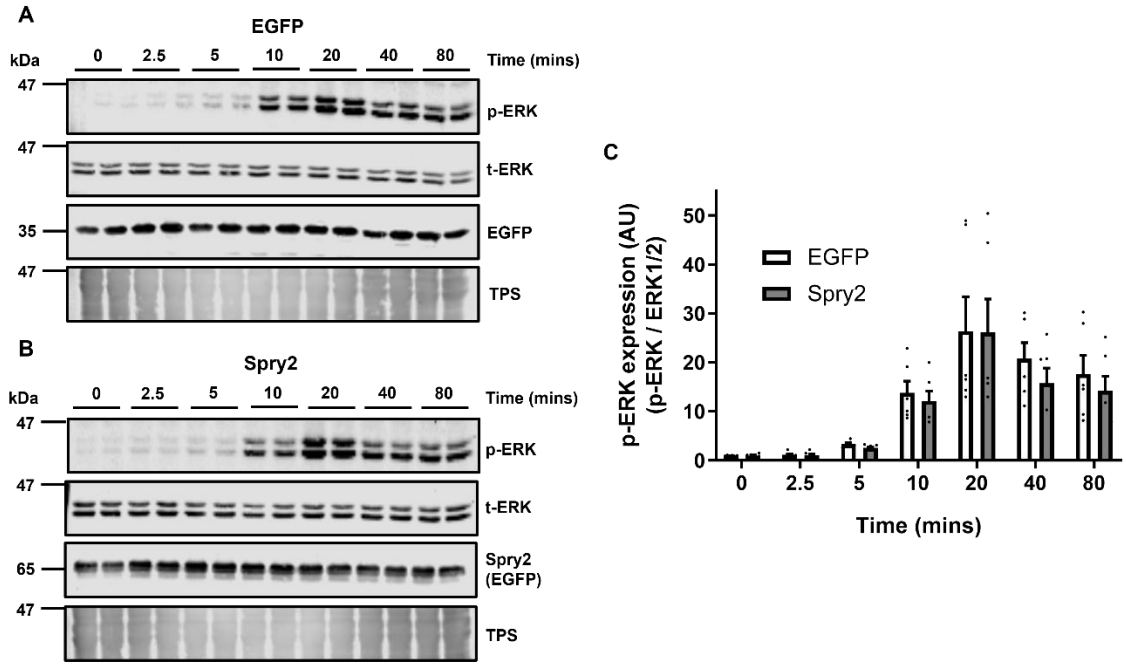


F***igure 3.10. FGF-stimulated time-course of p-ERK expression in the presence and absence of either EGFP or Spry2.*** *(A/B) Representative western blot showing the expression of FGF-stimulated p-ERK at time-points: 0, 2.5, 5, 10, 20, 40, and 80 minutes (first panel; IR800); with each sample's respective t-ERK expression shown (second panel; IR680). Expression/presence of either EGFP (A) or Spry2-EGFP (B) are also shown (third panel; IR800). The total protein stain (TPS) is shown for each representative blot (fourth panel; IR680). The position of molecular weight markers (kDa) is shown on the left of each panel. (C) Quantified data showing the mean (± SEM) of p-ERK (IR800) intensity value divided by the corresponding intensity value for t-ERK in each sample/lane (p-ERK/t-ERK). Statistical significance for p-ERK expression between EGFP and Spry2 at each time point, was analysed using multiple unpaired t-tests correcting for multiple comparisons using the Holm-Sidak method. n = 6, for three independent experiments. No significance was determined and as such is not indicated.*

### 3.11 Effects of Spry2 wild-type and S-acylation mutants on growth factor signalling

Previous research showed that S-acylation is essential for both plasma membrane targeting and stability of Spry2 (Locatelli et al, 2020). However, no evidence was presented regarding the effects of S-acylation on Spry2 function. The study by Locatelli et al. (2020) identified two S-acylation deficient mutants of Spry2: C265/268A (DM) and N211/D214/K223A (NDK). The DM mutant contains two alanine substitutions at cysteine residues that were shown to be modified by zDHHC17, whereas the NDK mutations disrupt S-acylation of Spry2 by both zDHHC17 and zDHHC7. In the following experiments, the NDK mutation was combined with mutation of the main zDHHC17 recognition site (P154A).

To investigate if S-acylation is critical for the action of Spry2 on the MAPK pathway, HEK-293T cells were transfected with either Spry2 WT, Spry2 DM, or Spry2 PNDK (combined NDK and P154A mutations) and subsequently stimulated with either EGF or FGF for 10 minutes. Activation of the MAPK pathway was monitored via the phosphorylation of ERK1/2 (p-ERK).

Figures 3.11 shows that cells transfected with either Spry2 WT, DM, or PNDK displayed a significant decrease in p-ERK expression in the absence of growth factor stimulation when compared to the unstimulated control. In contrast, cells transfected with the Spry2 constructs showed no significant difference in p-ERK compared to the control when activated with either EGF or FGF. When looking at the general effect of growth factors on p-ERK expression, all stimulated samples showed a significant increase when compared to unstimulated samples (significance not shown on graph).

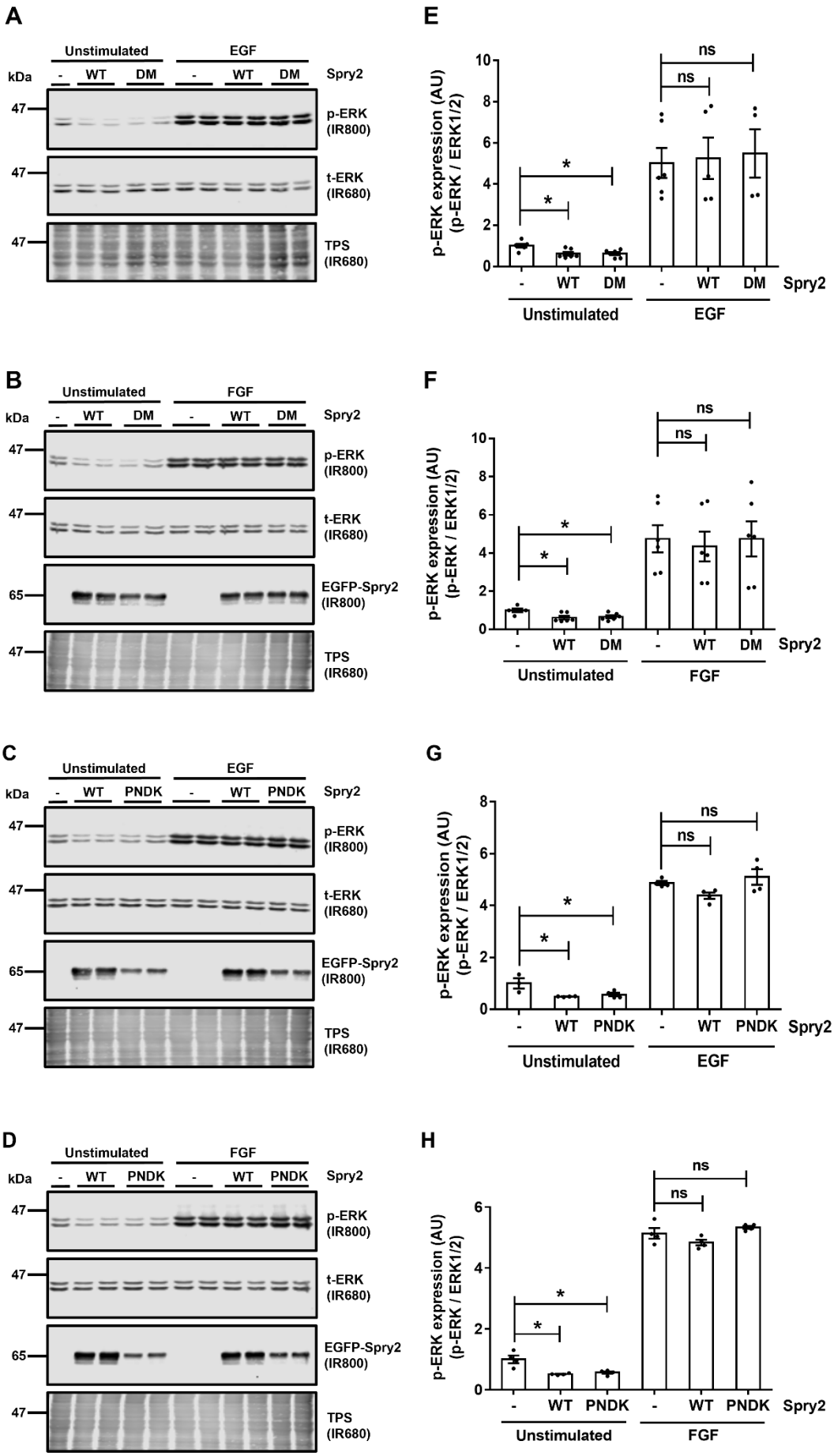
A
Unstimulated
EGF
kDa
-
WT
DM
-
WT
DM
Spry2
47
p-ERK
(IR800)
47
t-ERK
(IR680)
47
TPS
(IR680)
E
p-ERK expression (AU)
(p-ERK / ERK1/2)
10
8
6
4
2
0
*
*
ns
ns
-
WT
DM
-
WT
DM
Spry2
Unstimulated
EGF
B
Unstimulated
FGF
kDa
-
WT
DM
-
WT
DM
Spry2
47
p-ERK
(IR800)
47
t-ERK
(IR680)
65
EGFP-Spry2
(IR800)
47
TPS
(IR680)
F
p-ERK expression (AU)
(p-ERK / ERK1/2)
10
8
6
4
2
0
*
*
ns
ns
-
WT
DM
-
WT
DM
Spry2
Unstimulated
FGF
C
Unstimulated
EGF
kDa
-
WT
PNDK
-
WT
PNDK
Spry2
47
p-ERK
(IR800)
47
t-ERK
(IR680)
65
EGFP-Spry2
(IR800)
47
TPS
(IR680)
G
p-ERK expression (AU)
(p-ERK / ERK1/2)
8
6
4
2
0
*
*
ns
ns
-
WT
PNDK
-
WT
PNDK
Spry2
Unstimulated
EGF
D
Unstimulated
FGF
kDa
-
WT
PNDK
-
WT
PNDK
Spry2
47
p-ERK
(IR800)
47
t-ERK
(IR680)
65
EGFP-Spry2
(IR800)
47
TPS
(IR680)
H
p-ERK expression (AU)
(p-ERK / ERK1/2)
6
4
2
0
*
*
ns
ns
-
WT
PNDK
-
WT
PNDK
Spry2
Unstimulated
FGF

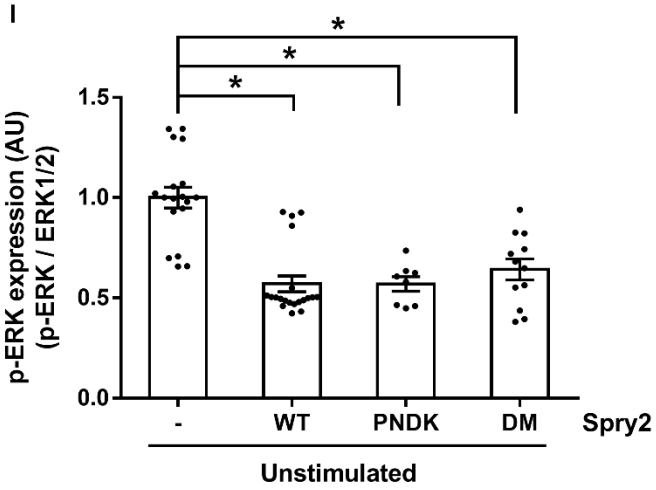


***Figure 3.11. FGF and EGF stimulated p-ERK expression in the presence and absence of Spry2 S-acylation deficient mutants.*** *(A-D) Representative western blots showing the expression of p-ERK in HEK-293T cells (first panel; IR800). After stimulation with EGF (A/C) or FGF (B/D); in the presence of either Spry2 WT (A-D), Spry2 DM (A/B) or Spry2 PNDK (C/D). For each sample the respective t-ERK signal is shown (second panel; IR680). Expression levels of EGFP-Spry2 are shown for each sample (third panel; IR800). The total protein stain (TPS) is shown for each representative blot (fourth panel; IR680). The position of molecular weight markers (kDa) is shown on the left of each panel. (E-I) Quantified data showing the mean (± SEM) of p-ERK (IR800) intensity value divided by the corresponding intensity value for t-ERK in each sample (p-ERK/t-ERK). (E) EGF/DM, n = 4-6 for three independent experiments; (F) FGF/DM, n = 6 for three independent experiments; (G) EGF/PNDK, n = 3-4 for two independent experiments; (H) FGF/PNDK, n = 4 for two independent experiments; (I) Unstimulated data from all experiments, over the three independent experiments, where n = 8-20, for control (-), WT, PNDK and DM, respectively. Statistical significance for a difference in p-ERK expression compared to control was analysed using a one-way ANOVA with a Tukey's multiple comparisons test; with unstimulated and stimulated groups tested independently. Significance where * denotes P < 0.05 and P > 0.05 is denoted as ns = non-significant.*

### 3.12 zDHHC17 and zDHHC7 do not significantly alter p-ERK expression

The results above showed that over-expression of Spry2 and mutants did not affect growth factor signalling. As an alternative approach to examining the possible role of S-acylation on growth factor signalling, the effects of zDHHC7/17 co-expression with Spry2 on FGF-stimulated p-ERK expression was investigated.

HEK-293T cells were co-transfected with either EGFP-tagged Spry2 or EGFP alone, alongside HA-tagged zDHHC17, zDHHC7, or pEF-BOS-HA as a control. Cells were serum starved and stimulated with FGF for 10 minutes, lysed and analysed by immunoblotting (figure 3.12). In contrast to the results in figure 3.11, the level of p-ERK1/2 in the presence of Spry2 over-expression was not significantly different from control. Furthermore, there was no significant difference in p-ERK between any of the unstimulated samples.

For samples stimulated with FGF, there was also no significant difference for any combination of conditions. When looking at the general effect of growth factors on p-ERK expression, all stimulated samples showed a significant increase when compared to unstimulated samples (significance not shown on graph).

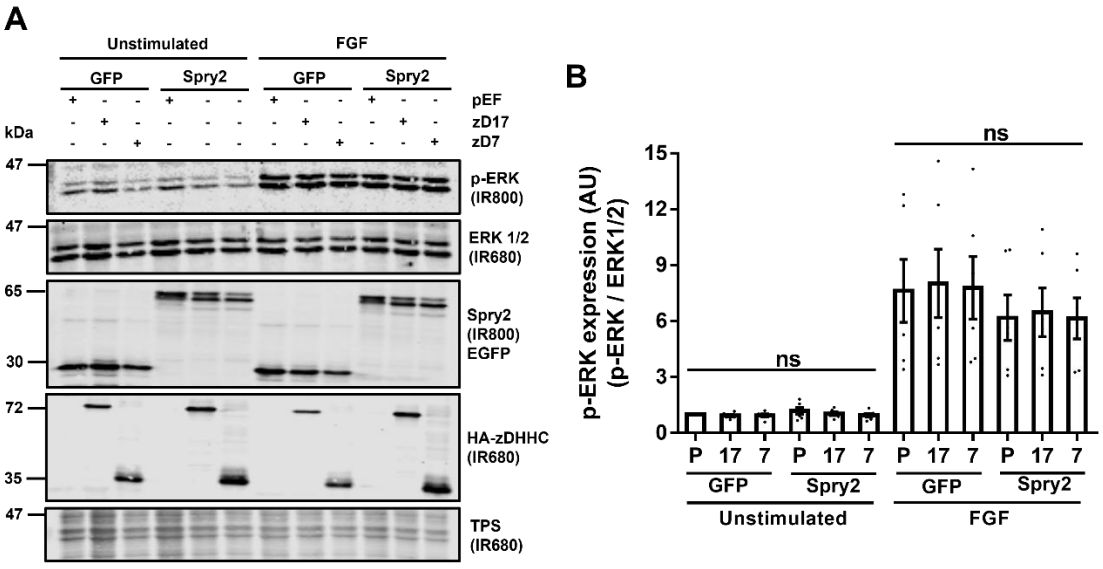


***Figure 3.12. FGF-stimulated p-ERK expression following over-expression of Spry2 with zDHHC17 or zDHHC7.*** *(A) Representative western blots showing the expression of p-ERK in HEK-293T cells with or without FGF stimulation (First panel; IR800). For each sample the respective total ERK1/2 signal is shown (Second panel;*

*IR680). Cells were either transfected with EGFP or EGFP-Spry2 WT (Third panel; IR800) together with either pEF-BOS-HA (negative control - P), zDHHC17, or zDHHC7 (Fourth panel; IR680). The total protein stain (TPS) is shown for each representative blot (fifth panel; IR680). The position of molecular weight markers (kDa) is shown on the left of each panel. (B) Quantified data showing the mean (± SEM) of p-ERK (IR800) intensity value divided by the corresponding intensity value for total ERK1/2 in each sample (p-ERK/ERK1/2). n = 6 from three independent experiments. Statistical significance for a difference in p-ERK expression compared to control (pEF) was analysed using a one-way ANOVA with a Tukey's multiple comparisons test, with unstimulated and stimulated groups tested independently. Non-significance where P > 0.05 is denoted as ns.*

### 3.13 Spry2 has a reciprocal stabilisation effect on zDHHC17

zDHHC17 was previously shown using cycloheximide chase assays to stabilise the expression of Spry2 (Locatelli et al., 2020). The clear effect exhibited upon Spry2 expression brought into question if this relationship was bi-directional. To explore if Spry2 also has an effect on zDHHC17 stability, HEK-293T cells were co-transfected with HA-tagged zDHHC17 and either EGFP-tagged Spry2 WT, Spry2 P154A, or EGFP (figure 3.13). The P154A mutation of Spry2 was used to establish if any effect on zDHHC17 expression was due to an interaction with the previously characterised zDABM motif of Spry2 (Lemonidis et al., 2015a). EGFP was used in this experiment as a control for basal zDHHC17 turnover. Transfected cells were treated with cycloheximide to block protein synthesis for up to 8 hours. Protein expression values at each hour of cycloheximide treatment were expressed relative to the respective 0-hour sample. After 8 hours treatment with cycloheximide, there was a significant difference in the expression of zDHHC17, when co-transfected with EGFP alone (figure 3.13 C), compared to Spry2 WT co-transfected cells (figure 3.13 A). For EGFP, the significant reduction in zDHHC17 expression was also observed in 4- and 6-hour samples (figure 3.13 D). The Spry2 P154A mutant (figure 3.13 B) did not show any significant effect/difference on zDHHC17 expression compared with WT Spry2. The quantified data is presented in figure 3.13 D.

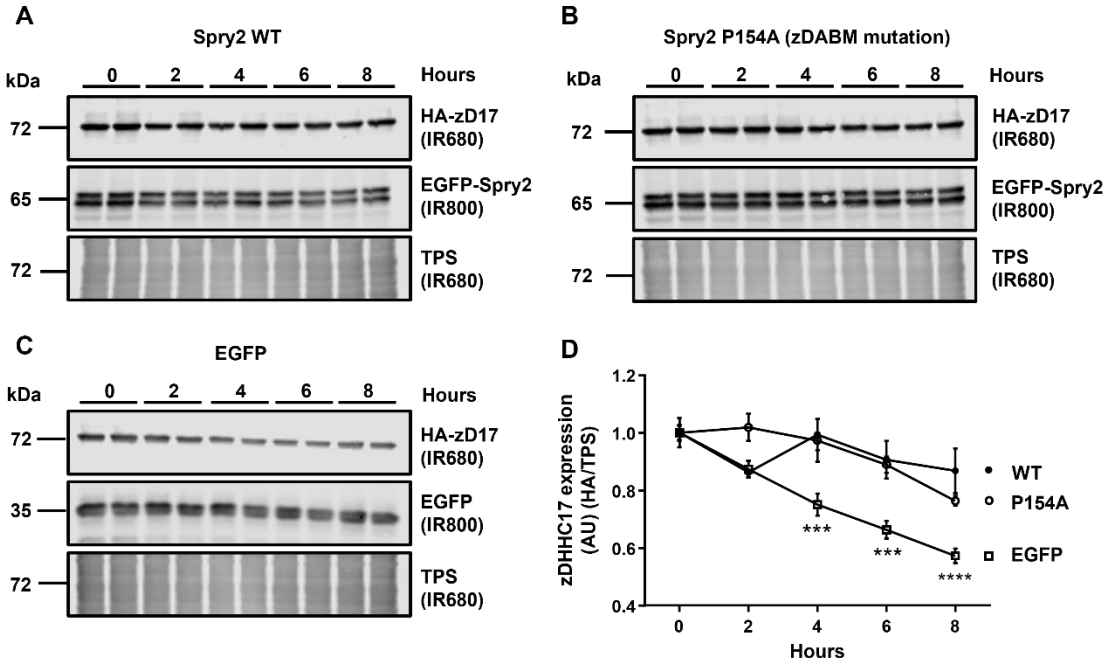


***Figure 3.13. Expression of zDHHC17 in the presence of Spry2 WT, Spry2 P154A, and EGFP.*** *(A-C) Western blot showing the expression of HA-zDHHC17 over 8 hours following addition of cycloheximide (top panel; IR680) when co-expressed with either Spry2 WT (A), Spry2 P154A (B), or EGFP (C) (middle panel; IR800). The total protein stain (TPS) is shown for each representative blot (bottom panel; IR680). The position of molecular weight markers (kDa) is shown on the left of each panel. (D) Quantified data showing the mean (± SEM) of zDHHC17-HA (IR680) intensity value divided by the corresponding intensity value of the TPS in each sample/lane (HA/TPS). Statistical significance was analysed using a two-way ANOVA with Tukey's multiple comparisons test. n = 6, for three independent experiments. Compared to zDHHC17 expression in the presence of Spry2 WT, a significant difference in zDHHC17 expression is denoted by *** P < 0.001 or **** P < 0.0001, on figure 3.13 D.*

### 3.14 The enhanced stabilisation of zDHHC17 is unique to Spry2 and is abrogated by the tripeptide NDK mutation

Spry and SPRED proteins have a highly conserved homology with Spry2 through the SPR domain and are known to possess similar physiological functions (Masoumi-Moghaddam et al., 2014b). Results from figure 3.13 in combination with previously published data (Locatelli et al., 2020), show that Spry2 WT and zDHHC17 have a reciprocal stabilisation effect on each other but it is unclear if this novel effect is specific to the Spry2 protein. As the greatest difference in zDHHC17 expression observed in figure 3.13 was at 8 hours, cycloheximide chase assays were conducted on other Spry/SPRED proteins comparing 0- and 8-hour time points.

In figure 3.14 A/B, HEK-293T cells were co-transfected with HA- tagged zDHHC17 and either EGFP-tagged Spry2 WT, Spry2 C265/268A (DM), P154/N211/D214/K223A (PNDK), SPRED1, SPRED2, SPRED3, or EGFP alone. In figure 3.14 C/D, HEK-293T cells were co-transfected with HA-tagged zDHHC17 and either EGFP-tagged Spry1 WT, Spry2 WT, Spry3 WT, Spry4 WT, or EGFP alone. EGFP alone was used in this experiment as a control for basal zDHHC17 turnover. 24-hours post-transfection, cells were treated with cycloheximide for either 0- or 8- hours, lysed and analysed by immunoblotting. In each independent experiment, values at 8-hours were expressed relative to the respective 0-hour sample. In figure 3.14 A/B, it can be seen that for all SPRED proteins there was a significant reduction in zDHHC17 expression with no significant difference to that of the EGFP control. This lack of effect on zDHHC17 expression was also seen for Spry1, Spry3, and Spry4 (figure 3.14 C/D). For all experiments in figure 3.14, and in agreement with figure 3.13, Spry2 WT showed a significant stabilisation of zDHHC17 expression compared with the EGFP control.

As Spry2 appears to play a specific role in zDHHC17 stabilisation, two other mutations of Spry2 (previously categorised by Carolina Locatelli) were also tested - Spry2 C265/268A (DM) and Spry2 N211A/D214A/K223A (NDK). Both of these mutations have previously been shown to have a detrimental effect on Spry2 S-acylation by zDHHC17 (Locatelli et al., 2020). For this experiment it should be noted that the Spry2 P154A/N211A/D214A/K223A (PNDK) mutant was used, but the P154A mutation was previously shown to have no effect on Spry2 stabilisation of zDHHC17 (Figure 3.13 B). The Spry2 DM showed no significant reduction in zDHHC17 expression when compared to Spry2 WT. However, when co-expressed with the Spry2 PNDK mutant there was a significant reduction in zDHHC17 expression following cycloheximide treatment, compared to zDHHC17 expressed with Spry2 WT (Figure 3.14 A/B). The PNDK mutation reduced zDHHC17 expression to a similar level as the EGFP control.

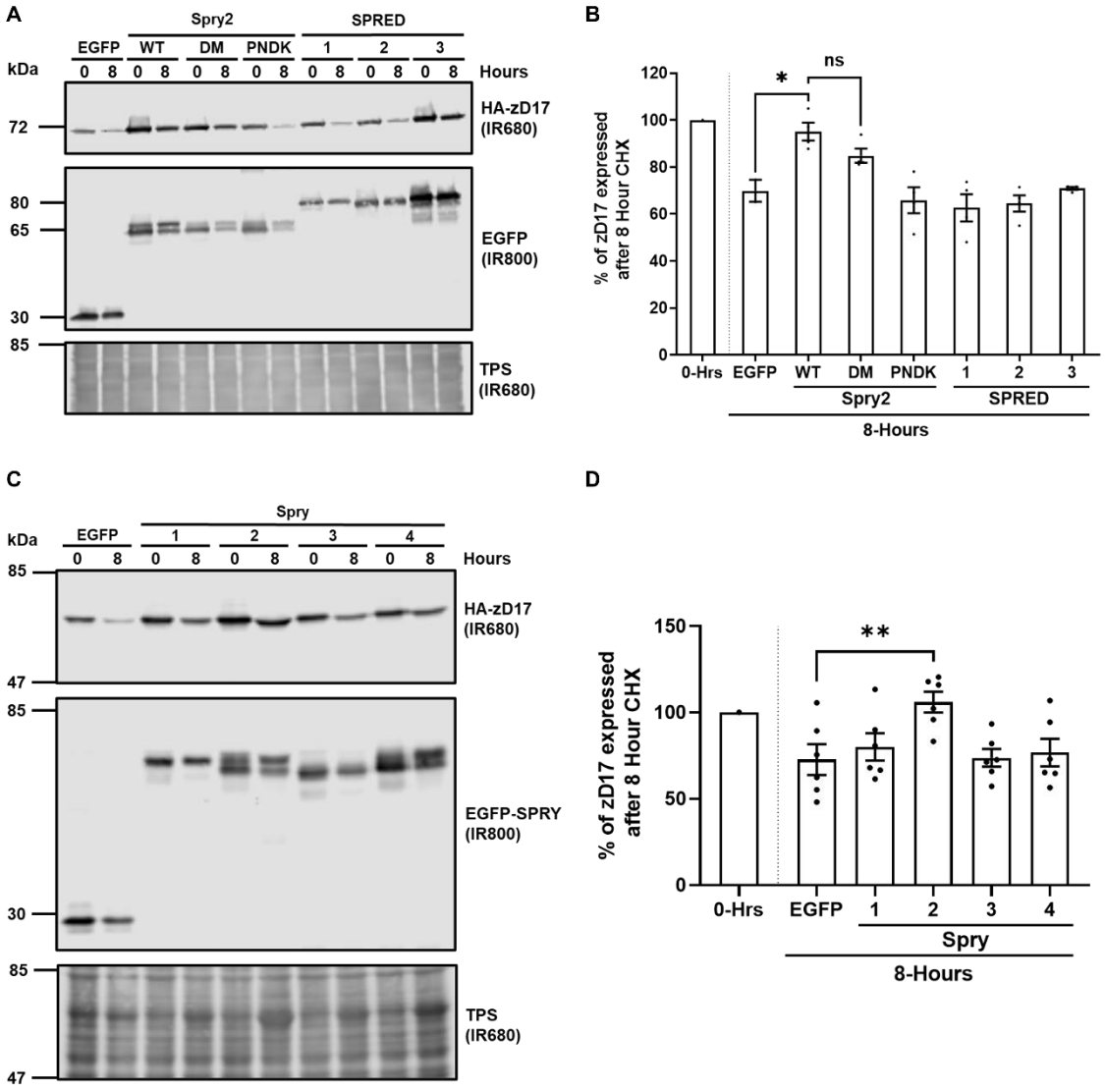


***Figure 3.14. Expression of zDHHC17 in the presence of Spry/SPRED proteins.*** *(A) Western blot showing the expression of HA-tagged zDHHC17 after 8 hours (top; IR680) with EGFP-tagged Spry2 WT, Spry2 C265/268A (DM), Spry2 P154A w/* N211A/D214A/K223A (*PNDK), SPRED1, SPRED2, SPRED2, or EGFP control (middle; IR800). The total protein stain (TPS) is shown for each representative blot (bottom; IR680). The position of molecular weight markers (kDa) is shown on the left of each panel. (B) Quantified data showing the mean (± SEM) of HA-zDHHC17 (IR680) intensity value divided by the corresponding intensity value of the TPS in each sample/lane (HA/TPS). Each condition was compared to EGFP or Spry2 WT at 8 hours cycloheximide treatment and statistical significance was analysed using an unpaired t-tests. n = 4, for two independent experiments. A significant difference in zDHHC17 expression is denoted by * for P < 0.05 and ns, denotes non-significant.*

*Error bars represent ± SEM; each replicate is shown with filled circles. (C) Western blot showing the expression of HA-tagged zDHHC17 after 8 hours cycloheximide treatment (top; IR680) with EGFP-tagged Spry1 WT, Spry2 WT, Spry3 WT, Spry4 WT, or EGFP control (middle; IR800). The total protein stain (TPS) is shown for each representative blot (bottom; IR680). The position of molecular weight markers (kDa) is shown on the left of each panel. (B) Quantified data showing the mean (± SEM) of HA-zDHHC17 (IR680) intensity value divided by the corresponding intensity value of the TPS in each sample/lane (HA/TPS). Each condition was compared to EGFP at 8 hours and statistical significance was analysed using an unpaired t-tests. n = 6, for three independent experiments. A significant difference in zDHHC17 expression is denoted by ** for P < 0.01. Error bars represent ± SEM; each replicate is shown with filled circles.*

### 3.15 Interactions between residues in the NDK region of Spry2

The stabilisation effect on zDHHC17 was shown in the figure above (figure 3.14) to be specific to Spry2 and was abrogated by the PNDK mutation. Although the SPR domain is highly conserved between Spry and SPRED proteins, bioinformatic analysis using the UniProt alignment tool reveals that residues N211/D214/K223 (NDK) within Spry2 are not fully conserved with other members of the Spry/SPRED family (figure 3.15 A). This information is furthered using the AlphaFold protein structure database and the RCSB PDB viewer for further analysis of Spry2 shown in figure 3.15, which reveals that residues Q210, D214 and K223 are predicted to interact (with N211 closely associated). This interaction occurs at a bend in the secondary structure of Spry2, bridging two alpha helices on either side of residues C265/268 (the cysteine residues shown to be functionally S-acylated by zDHHC17).

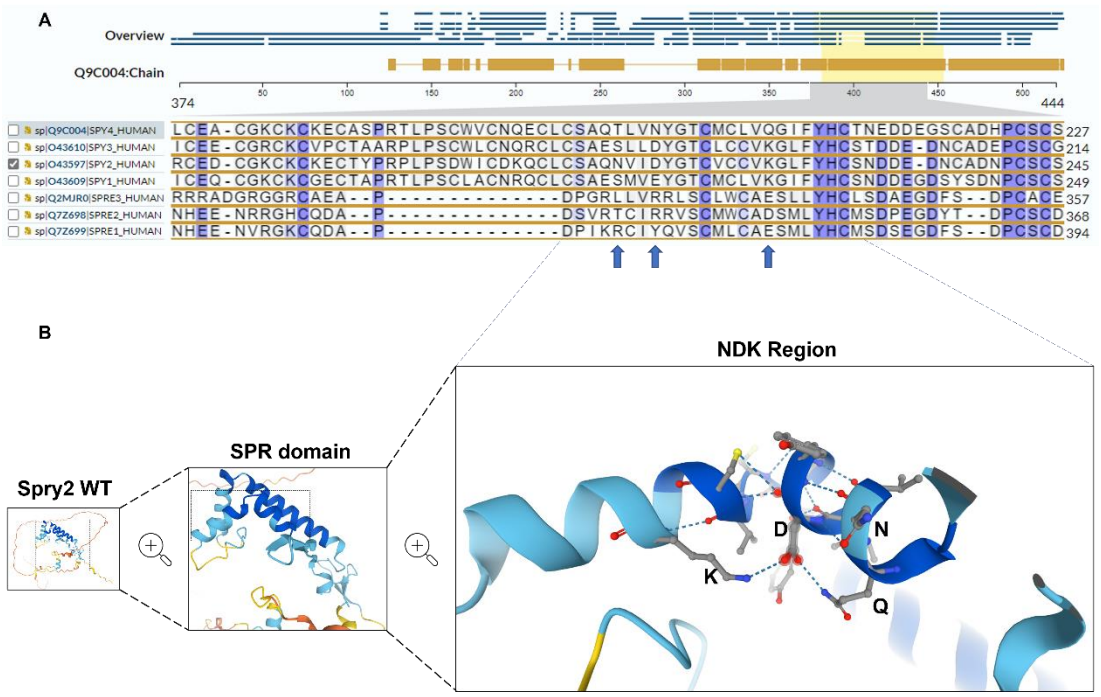


***Figure 3.15. Bioinformatic analysis of the NDK region of Spry2.*** *(A) Protein sequence alignment of Spry/SPRED proteins showing the region containing and surrounding residues N211/D214/K223 (NDK) of Spry2. Generated using the align tool from UniProt (Consortium, 2022). (B) Protein structure predictions of Sprouty-2 protein; O43597 (SPY2_HUMAN) from the AlphaFold protein structure Database developed by DeepMind and EMBL-EBI (Jumper et al., 2021, Varadi et al., 2022). Main chain is shown in blue with residues Q210, N211, D214, & K223 indicated.*

## Discussion

Understanding how proteins are expressed, modified, interact, and localise to regulate cell function is fundamental to developing novel ways to treat disease. S-acylation has been shown to be a critical PTM capable of influencing protein function and localisation (Chamberlain and Shipston, 2015, Locatelli et al., 2020). Spry/SPRED proteins are atypical compared to other characterised substrates of zDHHC17 as their S-acylation by this enzyme does not require zDABM sequences. Based on the current literature and the understanding of zDHHC enzymes and the S-acylation of proteins, the S-acylation of Spry2 was predicted to be essential for either its: interactions, stability, localisation, and/or regulation of signalling pathways. Understanding how Spry/SPRED proteins interact, why they are S-acylated and what effects this PTM has on function represents the first step in unlocking the potential targeting of Spry/SPRED S-acylation for the therapeutic treatment of dysregulation during oncogenesis.

### *Interactions and S-acylation of Spry and SPRED proteins with zDHHC17 WT*

The results within this chapter reveal a novel mechanism of interaction and S-acylation for Spry/SPRED proteins with zDHHC17. In contrast to previous analysis of SNAP25-zDHHC17 interaction and S-acylation (Lemonidis et al., 2015a, Greaves et al., 2009, Butler et al., 2023) the results of this chapter show that a simple zDABM interaction followed by substrate S-acylation model does not fit for Spry/SPRED proteins. All Spry proteins were shown to interact with and be S-acylated by zDHHC17. However, for the SPRED family, only SPRED3 was found to be a substrate of zDHHC17 despite this isoform lacking a zDABM motif. Interestingly, neither SPRED1 nor SPRED2 were modified by zDHHC17, despite these isoforms containing zDABMs. SPRED3 S-acylation by zDHHC17 was previously reported but interestingly the same study suggested that SPRED1 was modified by the same enzyme (Butland et al., 2014). However, this study found an 8-fold increase in SPRED3 S-acylation by zDHHC17 but only a 1.3-fold increase in SPRED1 S-acylation. Therefore, the results of this work and the work of Butland are broadly in agreement. Butland and colleagues purified the proteins used in their click chemistry S-acylation assays, and the added sensitivity of reducing background S-acylation may account for their effective detection of low levels of SPRED1 S-acylation.

To better understand why SPRED1 was a much poorer zDHHC17 substrate than Spry2, chimeric mutants were generated. However, none of the SPRED1 chimeric mutants investigated in figure 3.7 exhibited a significant gain in S-acylation by zDHHC17 when they were modified to increase the similarity with Spry2. The EVH1 domain is absent in Spry2 but makes up 26% of the amino acid sequence of SPRED1 (UniProtKB: Q7Z699). This sizable domain has its own interactions and very different secondary structure to the remainder of SPRED1 (Veltman and Insall, 2010). This led us to wonder if the EVH1 domain could have been obstructing or hindering SPRED1 binding and/or S-acylation. For the second construct (SPRED1 + 155-176), previous evidence has shown that the distance between the zDABM of SNAP25 and its S-acylated cysteines is important for modification by zDHHC17 (Salaun et al., 2020a). For SPRED1 this molecular spacer is both shorter and different in composition to that of Spry2 and so was substituted for the corresponding region of Spry2 (+ 155-176) – however this also had no significant effect on S-acylation by zDHHC17. The third mutant introduced a C-terminal sequence unique to Spry2 (+ 291-315), into SPRED3. This region of Spry2 has been shown to be functionally relevant and also contains a unique proline motif (VPTVP) involved in ITSN1 and GRB2 binding as part of the MAPK signalling pathway (Okur et al., 2012). The addition of this domain to SPRED1 also did not promote S-acylation by zDHHC17 (figure 3.7).

The development of AlphaFold protein structure prediction software developed by DeepMind and EMBL-EBI has been a major breakthrough in computational biology (Jumper et al., 2021; Varadi et al., 2022). Utilising Google Colab's AlphaFold-Multimer notebook (Evans et al., 2022), which is based on AlphaFold by DeepMind and EMBL-EBI (Jumper et al., 2021; Varadi et al., 2022), mutant constructs of Spry2 were able to be created and tested for interaction with the AR of zDHHC17. The results revealed that no single residue mutation on Spry2 was sufficient to completely reduce S-acylation by zDHHC17. The greatest fold change in S-acylation was observed for mutant construct 16 (L43/I46/P154/Y176/T298/V299/C300A) in figure 3.5 I, however this construct contained the most amino acid substitutions overall. Although significantly different to Spry2 WT, S-acylation of construct 16 was less than 40% different and did not show a complete loss of S-acylation. The compounding effect of multiple residue mutations (i.e., for construct 16 there are seven residue mutations), could adversely affect the overall structure of Spry2 and potentially account for observed loss of S-acylation by zDHHC17.

Alongside this information, results in figure 3.6 revealed that a full-length complex between zDHHC17 and Spry2 did not generate the same predicted interactions to that of Spry and zDHHC17-Ank. AlphaFold is a major resource for researchers in this field and in future years will only increase in accuracy. However, it is necessary to acknowledge that limitations to the resource do currently exist. The highest degree of accuracy in models exists for monomeric predictions such as those described in figure 3.15 but is far less reliable for multimer complexes. Also, due to factors such as low database homology or computational demands, AlphaFold modelling is less reliable for intrinsically disordered proteins, synthetic proteins, mutational analysis, proteins with multiple/variable conformations (i.e., translocated proteins), or protein influenced by co-factors or post-translational modifications (i.e., phosphorylation) (Bagdonas et al., 2021, EMBL-EBI, 2022)

*The inhibitory effect of Spry2 on p-ERK expression is unaffected by S-acylation-deficient mutations or by over-expression of zDHHC17/7*

In figure 3.11, the p-ERK expression in unstimulated samples was reduced by Spry2. This is consistent with all known information about Spry/SPRED proteins, as they have been shown to be regulators of the MAPK growth factor signalling pathway (Kawazoe and Taniguchi, 2019). However, neither of the S-acylation deficient mutants (DM and PNDK) identified by Locatelli *et al.,* (2020) showed any difference to wild-type Spry2 in this assay. Previous evidence has suggested that membrane translocation and phosphorylation of Spry2 are essential for its inhibitory action (Hanafusa et al., 2002), which is somewhat inconsistent with the results using the S-acylation-deficient mutants. In addition to this, other sources have discussed the necessity for S-acylation of the SPR domain of SPRED and Sprouty proteins for membrane localisation after growth factor stimulation (Bundschu et al., 2006, Lim et al., 2002). The S-acylation deficient mutants (NDK and DM) are described as defective in their S-acylation by zDHHC17 (Locatelli, 2021). The DM showed no change in S-acylation with zDHHC7 and there was a reduction in the S-acylation of the NDK mutant with zDHHC7, but not a complete loss (Locatelli et al., 2020). The greater specificity of these mutants to zDHHC17 may have no overall bearing on the action of Spry2 towards MAPK signalling, as Spry2 may be sufficiently S-acylated at a basal level to cause inhibition.

The results in figure 3.11. also showed that growth factor (EGF and FGF) enhanced p-ERK expression in HEK-293T cells, as expected. However, none of the Spry2 proteins (WT, DM, or PNDK) tested affected this growth factor stimulated increase in p-ERK expression (figure 3.11). Also, at no time point was there a significant change in p-ERK expression in the presence of Spry2 (figure 3.10). It is possible that the concentration of growth factors used in this study might overpower any minor effects of Spry2 expression and it would be interesting to undertake concentration dose response experiments of p-ERK expression in cells expressing Spry2 and the mutants.

Further developing the work in figure 3.11, the expression of p-ERK in the presence of both zDHHC17 and zDHHC7 was investigated (figure 3.12). It was hypothesised that if the general S-acylation of Spry2 is a key factor in the inhibitory effect of Spry2 on the MAPK pathway then the overexpression of zDHHC enzymes might increase p-ERK inhibition. However, for all samples tested there was no significant difference in p-ERK expression. This result suggests either that the original hypothesis is not correct or that the approach used is not sufficient to uncover functional effects of Spry2 S-acylation. In future work, it may prove useful to focus on the effects of Spry2 on other growth factor stimulated functions. Spry2 has been shown to be involved in process of cellular motility and protrusions, such as the proteins role in inducing membrane ruffling (Hanafusa et al., 2002). For instance, prolonged ERK signalling by nerve growth factor induces neurite outgrowth and cellular differentiation of neuroendocrine PC12 cells (Drubin et al., 1985). Spry2 has even been shown to inhibit both FGF and NGF stimulated neurite outgrowth in PC12 cells (Yim et al., 2015). Conversely in the same 2015 study, Spry2 was also shown to have a role in the stimulation of neurite outgrowth after EGF stimulation. Similar to experiments shown in 3.12, it would be important to investigate the role of S-acylation within this regulation of neurite outgrowth. These experiments could be undertaken either by inducing S-acylation through the stable transfection of zDHHC enzymes, analysis of S-acylation deficient mutants of Spry2, or if possible, the development of zDHHC17 and/or Spry2 knock-down/knock-in models of PC12 cells. This could be achieved by using either CRISPR Cas9 approaches or even by utilising si/shRNA knockdown techniques (Marvaldi et al., 2015).

*Spry2 protein has a specific and reciprocal stabilisation effect on zDHHC17 which is abrogated by the tripeptide NDK mutation*

Throughout this project, increased zDHHC17 expression in the presence of Spry2 after immunoblotting has been observed. In figure 3.13 A, it was confirmed through a cycloheximide chase assay that Spry2 WT can stabilise zDHHC17. It also observed in figure 3.13 B that the P154A mutation of Spry2 does not hinder zDHHC17 stabilisation. This result taken together with the result in figure 3.9, that the P154A mutation significantly reduces but does not ablate zDHHC17 binding, further indicates an alternative Spry2-zDHHC17 binding site/s coupled to S-acylation or stability. The S-acylation of proteins is known to increase stability (Linder and Deschenes, 2007). For example, in the case of the anthrax toxin receptor TEM8, S-acylation has been shown to restrict TEM8 in non-lipid raft domains, which sequesters the protein from undergoing Cbl mediate ubiquitination and degradation (Abrami et al., 2006). However, there have been no previous reports of substrate proteins stabilising zDHHC enzymes.

The effects of S-acylation deficient mutants (DM and PNDK) of Spry2, and other Spry and SPRED proteins on zDHHC17 stability was also investigated. An interesting aspect of this experiment is that none of the other Spry or SPRED proteins were able to effectively stabilise zDHHC17. For Spry2 mutants, the PNDK mutation significantly reduced zDHHC17 expression whereas the DM cysteine mutant was similar to WT Spry2. In previous experiments by Locatelli et al., (2020), it was shown that in the presence of zDHHC17, the NDK mutation of Spry2 was more rapidly degraded than Spry2 WT. This confirms part of the hypothesis that there is a dual/reciprocal stabilisation action between Spry2 and zDHHC17 as in the presence of each other, protein expression is enhanced and sustained. More specifically it is suggested that NDK region of Spry2 is critical for aspects of a novel Spry-zDHHC17 interaction and will be discussed further below.

The NDK region is comprised of residues N211/D214/K223 and is found within the first half of the SPR domain (amino acids 177-291). Monomeric protein structure prediction already reposited in the AlphaFold protein structure database (figure 3.15), predicted that the SPR domain is comprised of two acutely angled alpha helices linked by a disordered turn that cause them to run anti-parallel to each other (figure 3.15). The NDK region lies at the vertex of the first alpha helix, where D214 and K223 are predicted to interact. This region bridges across residues C265 and C268 which have

previously been shown to be S-acylated by zDHHC17 (Locatelli et al., 2020). Within the first alpha helix, 3 out of the 4 polar residues are the NDK residues with the fourth being Glutamine (Q210). All 4 of these residues very closely interact and appear at locations which could be considered structurally critical. One or all of the polar residues in this region may be structurally relevant to sustained SPR domain conformation and/or presentation of S-acylated cysteine residues 265/258 in Spry2.

Alternatively, the NDK region could play a more direct role in zDHHC17 binding/stabilisation. The two alpha helices and the inwardly presenting disordered turn create a space, which is surrounded largely by non-polar/hydrophobic residues but has “hot spots” of potentially critical polar regions such as leucine or tryptophan - this could be a prospective binding site for other proteins (Ma et al., 2003). Elsewhere in Spry2, the phosphorylation of Y55 has been shown to be functionally relevant for the inhibitory action of Spry2 on Grb2 in the MAPK pathway (Xu et al., 2018). The NDK region itself may directly contribute to this binding space and actually interact with zDHHC17, or the region could be crucial in supporting a nearby zDHHC17-Spry2 binding site. Given the reciprocal nature of this finding, the known complexity of action that Spry2 has on other proteins, and the specificity of the effect between zDHHC17 and Spry2, this stabilisation is suggested to be independent of the Spry2-zDHHC17 interaction which facilitates Spry2 S-acylation. However, it is pertinent to mention that without further investigation, the protein-protein stabilisation interaction may be still a secondary consequence of any Spry2 S-acylation interaction. Further to this, it is suggested that the Spry2 NDK mutation itself is not inherently a S-acylation deficient mutant but is a structurally destructive mutation that is either directly or indirectly disrupting both S-acylation and protein stabilisation.

A question of this chapter and of this interaction would be the physiological relevance/physiological need of having a reciprocal stabilisation effect. Spry proteins are known for being developmental proteins and have been implicated in regulating the MAPK/ERK pathway (Masoumi-Moghaddam et al., 2014b). As discussed above, they have also been shown to play a role in inhibiting neurite outgrowth in PC12 cells (Lao et al., 2006). zDHHC17 on the other hand has been implicated not only at the Golgi apparatus but also at the pre-synaptic cell membrane in trafficking of CSPα and SNAP25 (Stowers and Isacoff, 2007). An earlier study, has also suggested that zDHHC17 promotes axon outgrowth and that both neural stem cells (NSCs) and PC12 cells, exhibit limited neurite outgrowth and branching after the inhibition of

zDHHC17 (Shi et al., 2015). The same study even implicated zDHHC17 as an upstream factor of ERK1/2 signalling, also in PC12 cells. The rational in this study, is that zDHHC17 regulates the interaction between tropomyosin receptor kinase A (TrkA) and actin during neuronal and axon development (Shi et al., 2015). These two studies infer that both Spry2 and zDHHC17 have an action in the same processes but cause different/opposite outcomes. Both zDHHC17 and Spry in the same cell type have been implicated in neuronal growth, the MAPK/ERK pathway, cytoskeletal association, and membrane translocation for function. Seeing as zDHHC17 may promote ERK1/2 and neuronal development, and Spry2 may inhibit (or promote) these processes. A neuronal type of environment like that of the pre-synaptic membrane or cell types such as PC12 cells, may provide a more appropriate model when investigating any functional interaction and/or role between Spry2 and zDHHC17.

**Conclusions of chapter 3**

- Spry1, Spry2, Spry3, Spry4, and SPRED3 can effectively interact with and be S-acylated by zDHHC17 WT. Whereas although SPRED1/2 can interact, they are not efficiently S-acylated by zDHHC17. Also, the S-acylation of SPRED1 cannot be enhanced by increasing homology with that of Spry2.

- Spry2 contains a secondary binding site coupled to S-acylation and/or function, and the P154A mutant of Spry2 can interact with zDHHC17 at a reduced but still significant level.

- The P154A mutation does not affect the S-acylation of Spry2 by zDHHC17. Nor does the mutation affect the stabilisation of zDHHC, or the expression of p-ERK.

- AlphaFold modelling of Spry2-zDHHC17 is a valuable tool of reference to facilitate prediction and testing/validation of interactions, but it was shown to lack reliability in this study.

- Spry2 was shown to elicit an inhibitory effect upon p-ERK expression under unstimulated conditions with the S-acylation-deficient mutants displaying a similar effect. However, Spry2 had no effect on growth factor induced p-ERK activation. The co-expression of zDHHC17 and zDHHC7 also did not alter the expression of p-ERK.

- A unique interaction between Spry2 and zDHHC17 has a reciprocal stabilisation effect, which is abrogated by the tripeptide NDK mutation. The NDK region is suggested to be structurally critical to the SPR domain of Spry2.

# CHAPTER 4

# INTERACTIONS OF SPRY AND SPRED PROTEINS WITH ZDHHC17

# Chapter 4 - Interactions of Spry and SPRED proteins with zDHHC17

## Introduction

zDHHC17 has been previously implicated in the progression of disease states such as Huntington disease. Specifically, it was shown that decreased interaction between Huntington protein (HTT) and zDHHC17 resulted in impaired HTT trafficking, leading to subsequent aggregation, neuronal damage, and progression of Huntington's disease (Singaraja et al., 2002). Furthermore, zDHHC17 knockout mice exhibit developmental, memory, and synaptic changes, and display deficits in motor coordination, reduced body weight, and decreased prepulse inhibition (Singaraja et al., 2011, Milnerwood et al., 2013, Chamberlain and Shipston, 2015).

Compared to the other zDHHC enzymes, zDHHC17 (and zDHHC13) contain six TMDs (as opposed to the more typical four), and the enzyme also contains an N-terminal ankyrin repeat (AR) domain (aa 51 - 286). This motif is comprised of seven ankyrin repeats each made up of roughly 33 amino acids, which form two alpha helices separated by loops (Chamberlain and Shipston, 2015).

A novel zDHHC17 substrate-binding motif that is recognised by the AR domain of the enzyme was previously identified. This hexapeptide motif ((VIAP)(VIT)XXQP) was named the "zDHHC Ankyrin Binding Motif" or "zDABM" for short (Lemonidis et al., 2015b). Spry and SPRED proteins were subsequently identified to contain zDABMs that interact with the Ank domain of zDHHC17, however, interestingly, the SPRED3 isoform was reported to lack a zDABM (Lemonidis et al., 2017a). The interaction of the zDABM motif with zDHHC17 was further examined by Verardi et al. (2017), who reported that asparagine 100 (N100) and tryptophan 130 (W130) are the critical residues within the AR necessary for the interaction of ANK17 with zDABM sequences (Verardi et al., 2017). Alanine substitutions at these positions (N100A/W130A) block SNAP25 S-acylation by zDHHC17, and alanine substitution of Pro-117 within the zDABM of SNAP25 was shown to severely impair both binding to and S-acylation by zDHHC17 as previously reported by Greaves et, al,. (2009) and Lemonidis et, al. (2015).

Unlike SNAP25, current evidence indicates that the zDABM of Spry2 is not required for the efficient S-acylation of the protein (figure 3.3 A/B) and is also not the only site

of Spry2-zDHHC17 interaction (figure 3.9). The overall aim of this chapter is to further investigate the interaction between zDHHC17 and Spry/SPRED proteins, with the aim of identifying critical sites of interaction on both the enzyme and the substrate. It is hypothesised that because the zDABM of Spry2 is dispensable for S-acylation by zDHHC17, that Spry/SPRED proteins contain an alternative, novel, lower affinity, binding site coupled to S-acylation and/or function.

# Results

## 4.1 Spry proteins do not require interaction via the zDABM for effective S-acylation

Evidence given in figure 3.2 showed that zDHHC17 could effectively S-acylate Spry1, 2, 3, & 4. As discussed above, the critical residues within the AR domain of zDHHC17 for binding to zDABM substrates include N100 and W130. In the case of SNAP25, mutation of either residue is sufficient to abolish S-acylation and binding to zDHHC17 (Verardi et al., 2017). It was therefore important, as a first step to understanding the zDHHC17-Spry interaction, to test if these key residues within zDHHC17 are also important for the S-acylation of Spry proteins. Plasmids encoding for EGFP-tagged Spry1, Spry2, Spry3, or Spry4 were co-transfected into HEK-293T cells together with a plasmid encoding either HA-tagged zDHHC17 WT, zDHHC17 W130A, or pEF-BOS-HA empty plasmid. Cells were then incubated with C16:0-azide and processed for click chemistry detection of S-acylation (figure 4.1 A/B). As before, mean intensity values (± SEM) for the S-acylated band (AK800) of each substrate were normalised against the EGFP immunoreactive signal intensity for that protein (figure 4.1 C), and also expressed as a fold increase above basal (figure 4.1 D).

As seen in figure 3.2, all Spry proteins were significantly S-acylated by zDHHC17 WT. The Spry proteins were also significantly S-acylated by the zDHHC17 W130A mutant, and interestingly the level of S-acylation of Spry1, 2, & 3 with this mutant was significantly higher than that seen with WT zDHHC17 (figure 4.1 C). Spry2 and Spry3 also showed a significant fold-increase in S-acylation with W130A compared to WT zDHHC17, with Spry3 showing both the highest normalised and fold-change in S-acylation.

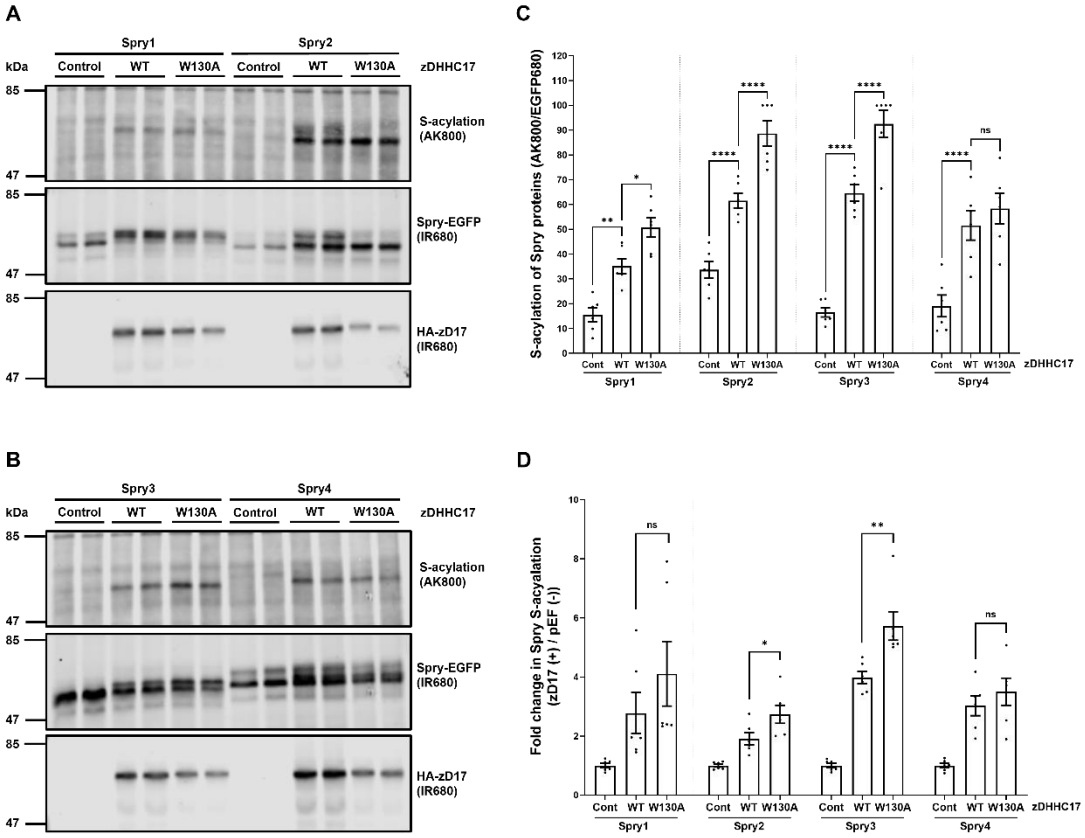


***Figure 4.1 S-acylation of Spry1, 2, 3, & 4 by zDHHC17 W130A.*** *(A) HEK-293T cells were transfected with plasmids encoding EGFP-tagged Spry1 WT or Spry2 WT together with either pEF-BOS-HA (as "-" in the figure), HA-zDHHC17, or zDHHC17 W130A. (B) HEK-293T cells were transfected with plasmids encoding EGFP-tagged Spry3 WT or Spry4 WT together with either pEF-BOS-HA (as "-" in the figure), HA-zDHHC17, or zDHHC17 W130A. Transfected cells were incubated with 100 μM palmitic acid azide (C16:0-azide) for 4 h and labelled proteins reacted with alkyne (AK) IRdye-800 nm. Representative images showing Spry S-acylation (top; AK-IR800) and EGFP-tagged Spry levels (middle; IR680) detected on the same immunoblot. For zDHHC17, HA (bottom; IR680) was revealed for the same samples on a different immunoblot. The positions of the molecular weight markers are shown on the left side of all immunoblots. Error bars represent ± SEM; each replicate is shown with filled circles. (C) Graph showing the mean intensity values of Spry S-acylation relative to protein expression (AK800/EGFP680) and normalised to the highest value on each blot. (D) Graph showing the mean fold change between Spry S-acylation in the presence and absence of zDHHC17 (zDHHC17 (+) / pEF (-)). Differences were analysed by unpaired t test (WT v W130A). **** denotes p < 0.0001, **p < 0.01, *p < 0.05, ns = non-significant (n = 6, for three independent experiments).*

## 4.2 Spry 1-4 and SPRED3 do not require zDABM binding for S-acylation and interact with zDHHC17 through an additional novel binding mode

The published evidence shows that the W130 residue of zDHHC17 is important for both S-acylation and interaction with SNAP25 (Verardi et al., 2017). In contrast, the results from figure 4.1 show that W130 is dispensable for the S-acylation of Spry proteins. Results from figure 3.8 showed that zDHHC17 WT can interact with Spry1-4, SPRED3, and also SNAP25. It was therefore of interest to understand how the W130A mutations in zDHHC17 affects binding to Spry and SPRED proteins. HEK-293T cells were co-transfected with either EGFP-tagged Spry1, Spry2, Spry3, Spry4, SPRED3, SNAP25 (positive control), or EGFP alone (negative control) together with either HA-tagged zDHHC17 WT or zDHHC17 W130A. Cell lysates were then incubated for 1 hour with GFP-Trap® agarose immunoprecipitation beads and washed twice in PBS to remove unbound/excess lysate. Bound proteins were then eluted, releasing the captured EGFP-tagged proteins and any co-immunoprecipitated binding partners (i.e., zDHHC17). The eluted proteins were resolved by SDS-PAGE and analysed by immunoblotting.

From figure 4.2, it can be seen that (as in figure 3.8) all transfected substrates (except EGFP) were able to interact with zDHHC17 WT. It can also be seen that the SNAP25 showed a complete loss of interaction with zDHHC17 W130A in agreement with published work (Verardi et al., 2017). Spry 1, 2, & 3 all showed a level of binding to zDHHC17 WT that was similar to SNAP25. However, when co-transfected with zDHHC17 W130 the level of interaction with Spry1, 2, & 3 was not abolished, and instead showed a reduction in zDHHC17 binding by ~ 40-60%. Furthermore, Spry4 and SPRED3 both showed equal binding to zDHHC17 WT and W130A. Interestingly all four Spry proteins and SPRED3 showed similar levels of interaction with zDHHC17 W130A.

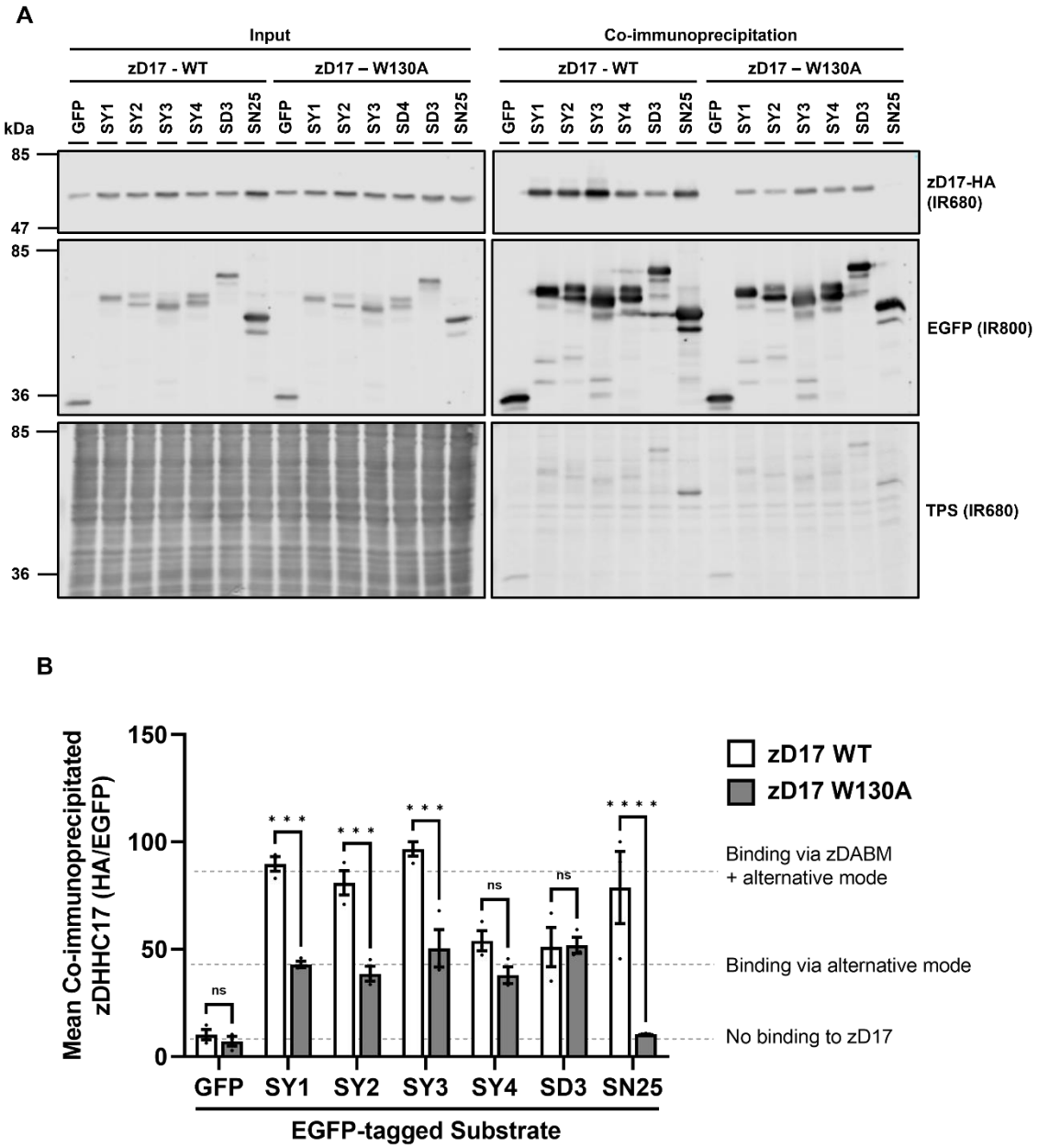


***Figure 4.2. Spry 1-4 and SPRED3 do not require a zDABM motif for interaction with zDHHC17.*** (A) HEK-293T cells were co-transfected with HA-tagged zDHHC17 WT or zDHHC17 W130A together with plasmids encoding for EGFP-tagged Spry1, Spry2, Spry3, Spry4, SPRED3, SNAP25, or EGFP. Cell lysates were incubated with agarose beads conjugated to an EGFP antibody and co-immunoprecipitated proteins were analysed by immunoblotting. Representative images showing HA-tagged zDHHC17 (top; IR680) and EGFP-tagged substrate (middle; IR800) detected in input and co-immunoprecipitated samples on the same immunoblot. A total protein stain (TPS) is also shown (bottom panel; IR680). The positions of the molecular weight

markers are shown on the left side of all immunoblots. (B) Graph showing the mean value of co-immunoprecipitated zDHHC17 after normalisation against the highest value for each immunoblot. Error bars represent ± SEM. Each replicate is shown with filled circles. Differences between zDHHC17 WT and zDHHC17 W130A were analysed by unpaired t test between each substrate protein. *** denotes $p < 0.0001$, *** denotes $p < 0.001$, and ns = non-significant. n = 3, for three independent experiments.

## 4.3 Spry2 truncation mutants containing the SPR domain but lacking the zDABM display reduced binding to zDHHC17 but effective S-acylation.

The results of figures 4.1 and 4.2 indicate that the S-acylation of Spry proteins by zDHHC17 does not require a zDABM interaction. As a next step, the regions of Spry2 that are required for S-acylation were investigated. To do this, a series of EGFP-tagged N-terminal truncation mutants of Spry2 (100–315, 120–315, 140–315 and 155–315 (previously synthesised by Dr Carolina Locatelli) (figure 4.3 A) were co-expressed with either HA-tagged zDHHC17 or pEF-BOS-HA in HEK-293T cells (figure 4.3 B). Click chemistry analysis of S-acylation showed that all four truncation mutants were S-acylated above basal by zDHHC17 (figure 4.3 B/C) including the 155 to 315 mutant that lacks the zDABM (at positions I149-P154).

These constructs were further utilised to study their interaction with zDHHC17 by co-immunoprecipitation. As described above (figure 4.2), HEK-293T cells were co-transfected with the EGFP-tagged truncated Spry2 constructs alongside HA-zDHHA17 WT, and immunoprecipitated using the GFP-Trap® agarose immunoprecipitation beads. For this experiment, a catalytically inactive mutant of zDHHC17 was used to prevent S-acylation-mediated changes in Spry2 expression. Figure 4.3 D shows that the Spry2 120-315 and 140-315 mutants co-immunoprecipitated zDHHC17 to a similar level to that of the full-length Spry2, with Spry2 100-315 showing the highest co-immunoprecipitation of zDHHC17. Interestingly, the 155 to 315 Spry2 mutant also captured zDHHC17 to a higher level than the EGFP negative control, but less than was captured by the other Spry2 proteins.

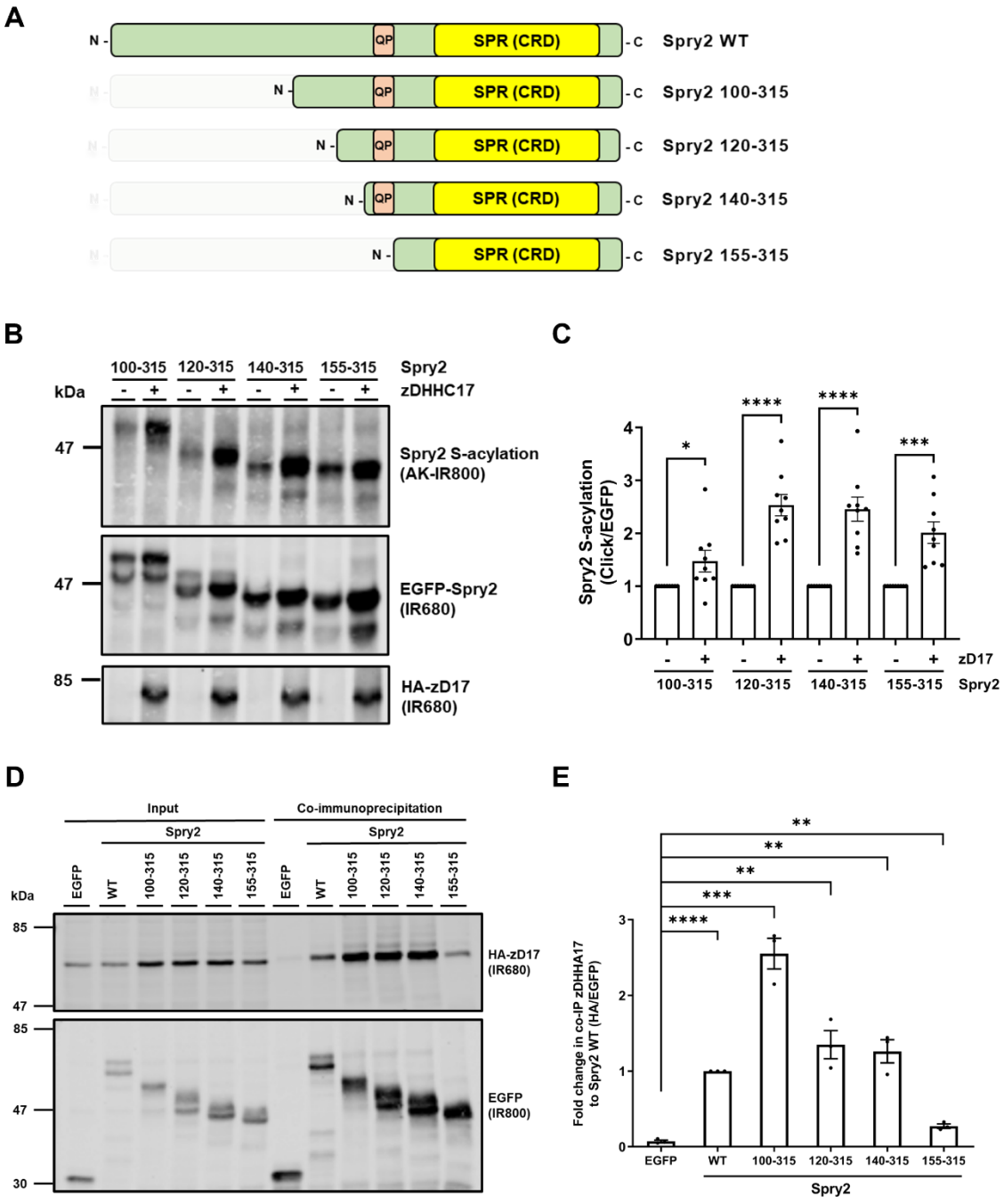


***Figure 4.3. Residues 155-315 of Spry2, which include the SPR domain, are sufficient for binding to, and S-acylation by zDHHC17.*** (A) Schematic of the Spry2 constructs employed in click chemistry and co-immunoprecipitation assays: Spry2 100 to 315, 120 to 315, 140 to 315, and 155 to 315 of the mouse sequence (UniprotKB - Q9QXV8). All constructs have EGFP tags appended at the N-terminus. Position of the zDABM containing proline-154 is denoted by "QP;" SPR denotes the Sprouty domain, which is also referred to as CRD (cysteine-rich domain). (B) HEK-293T cells

were transfected with plasmids encoding EGFP-tagged Spry2 100 to 315, Spry2 120 to 315, Spry2 140 to 315, or Spry2 155 to 315, together with either pEF-BOS-HA (referred to as "-" in the figure) or HA-zDHHC17 (referred to as "+" in the figure). Cells were incubated with 100 μM palmitic acid azide (C16:0-azide) for 4 h and labelled proteins reacted with alkyne (AK) IRdye-800 nm. EGFP- and HA-tagged proteins were labelled by immunoblotting using IRdye-680 secondary antibodies. Representative images showing Spry2 S-acylation (top; AK-IR800), Spry2 levels (middle; IR680), and zDHHC17 levels (bottom; IR680), detected on the same immunoblot. The positions of the molecular weight markers are shown on the left side of all immunoblots. (C) Graph showing mean Spry2 S-acylation levels after normalisation against the corresponding control samples (pEF-BOS-HA). Error bars represent ± SEM; each replicate is shown with filled circles. Differences were analysed by unpaired t test (**** denotes $p < 0.0001$, ***$p < 0.001$, *$p < 0.05$) (n = 9, for three independent experiments). (D) HEK-293T cells were co-transfected with HA-tagged zDHHA17 (a catalytically inert form of the enzyme) along with plasmids encoding for EGFP-tagged Spry2 100 to 315, Spry2 120 to 315, Spry2 140 to 315, and Spry2 155 to 315, or EGFP alone (as a control). Cell lysates were incubated with agarose beads conjugated to an EGFP antibody and co-immunoprecipitated proteins were analysed by immunoblotting. Representative images showing zDHHA17 (top; IR680) and Spry2 (bottom; IR800) levels in the input and immunoprecipitated samples detected on the same immunoblot. The positions of the molecular weight markers are shown on the left side of all immunoblots. (E) Graph showing the mean fold change in co-immunoprecipitated zDHHA17 levels after normalisation against Spry2 WT. Error bars represent ± SEM; each replicate is shown with filled circles. Differences were analysed by unpaired t test compared to the EGFP control (**** denotes $p < 0.0001$, ***$p < 0.001$, **$p < 0.01$, n = 3 from three independent experiments).

## 4.4 The 155-315 truncation of Spry2 co-localises in a similar manner to the WT

Previous evidence has shown that S-acylation deficient mutants of Spry2 (Spry2 C265A/C268A) exhibited a significant reduction in plasma membrane association (Locatelli et al., 2020). The results of figures 4.3 show that the Spry2 155-315 truncation mutant is still able to interact with and be effectively S-acylated by zDHHC17. As the 155-315 truncated mutant does not contain the zDABM but retains the entire SPR/CRD domain (figure 4.3 A), it was subsequently examined if the 155-315 mutant retains the same localisation as Spry2 WT.

As in the study by Locatelli et al (2020), PC12 cells were co-transfected with mCherry-tagged Spry2 WT together with either EGFP-tagged Spry2 WT, Spry2 C265A/268A, or Spry2 155-315. Using confocal fluorescent microscopy, the co-localisation of mCherry-Spry2 WT with each EGFP form of Spry2 was visualised (figure 4.4 A). Spry2 WT was used as a positive control and the C265A/C268A cysteine double mutant form of Spry2 (previously cloned by Carolina Locatelli) was used as a negative control (Locatelli et al., 2020). For all samples, a Pearson's coefficient was determined in relation to mCherry-Spry2 WT. $R_{total}$ values are given between +1 and -1, where a value towards +1 implies positive correlation, 0 implies no relationship and a value towards -1 implies negative correlation (Figure 4.4 B).

As expected, there was a significant reduction in co-localisation between Spry2 WT and Spry2 C265A/268A (figure 4.4 B). However, the 155-315 truncation form of Spry2 did not show any significant difference in co-localisation to that of Spry2 WT (figure 4.4 B). Consistent with the previously published data (Locatelli et al., 2020), the Spry2 C265A/C268A does not visually localise in a similar manner to that of the WT, i.e., reduced plasma membrane association of the mutant was visible.

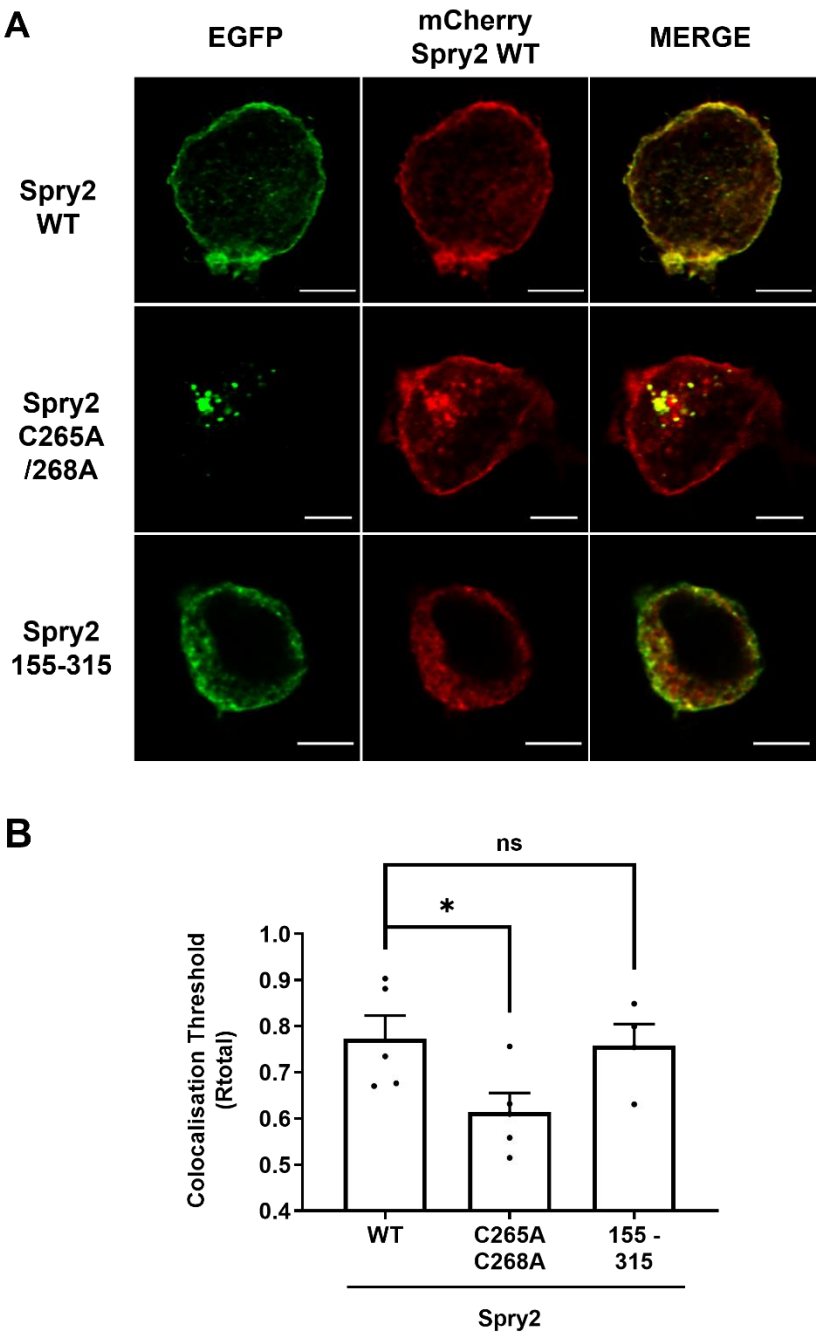


***Figure 4.4. Colocalisation of Spry2 WT, 155-315, and C265A/268A mutants in PC12 cells.*** *(A) Confocal imaging of PC12 cells co-transfected with plasmids constructs encoding for mCherry-Spry2 WT and either EGFP-tagged Spry2 WT, Spry2 155-315, or Spry2 C265A/C268A. Representative images are shown in the figure, scale bar = 5 µm. (B) Quantified data represents the Pearson's coefficient ($R_{total}$) of each sample showing the mean (± SEM) values of $R_{total}$. Statistical significance was analysed using an unpaired t-test compared to the WT. * Denotes P < 0.05 and ns denotes non-significance. n = 4/5.*

## 4.5 SPRED3 interaction with zDHHC17 involves the cysteine-rich SPR domain

Alignment of the Spry and SPRED proteins shows that SPRED3 is the only isoform that lacks a zDABM (figure 1.5). Despite this, SPRED3 has been shown to interact with zDHHC17 (figure 4.2) and is effectively S-acylated by zDHHC17 to a similar degree as Spry2 (figure 3.4). To further understand how zDHHC17 can recognise and S-acylate substrate proteins without zDABM interactions, SPRED3 was further analysed as it is proposed that this protein only has a single zDHHC17-binding site. Similar to experiments conducted in figure 4.3, to explore the features required for SPRED3 interaction with zDHHC17, a series of SPRED3 truncation mutant constructs were designed in which specific domains were removed (figure 4.5 A).

Consistent with results obtained for the Spry2 truncation mutant (155-315), the isolated SPR domain (amino acids 296–410) co-precipitated zDHHC17 (catalytically inert zDHHS mutant) albeit at reduced levels compared to WT SPRED3 (figure 4.5 B/C). A slight but significant binding of 1-244 and 1-295 SPRED3 truncation mutants to zDHHC17 was also detected in this assay, whereas SPRED3 constructs 1-113 and 1-194 showed no significant interaction with zDHHC17 (figure 4.5 B/C). In addition, although reduced compared to the WT, the SPR domain truncation mutant of SPRED3 (296-410) was efficiently S-acylated by zDHHC17 compared to the pEF-BOS-HA negative control in click chemistry assays (Figure 4.5 D/E).

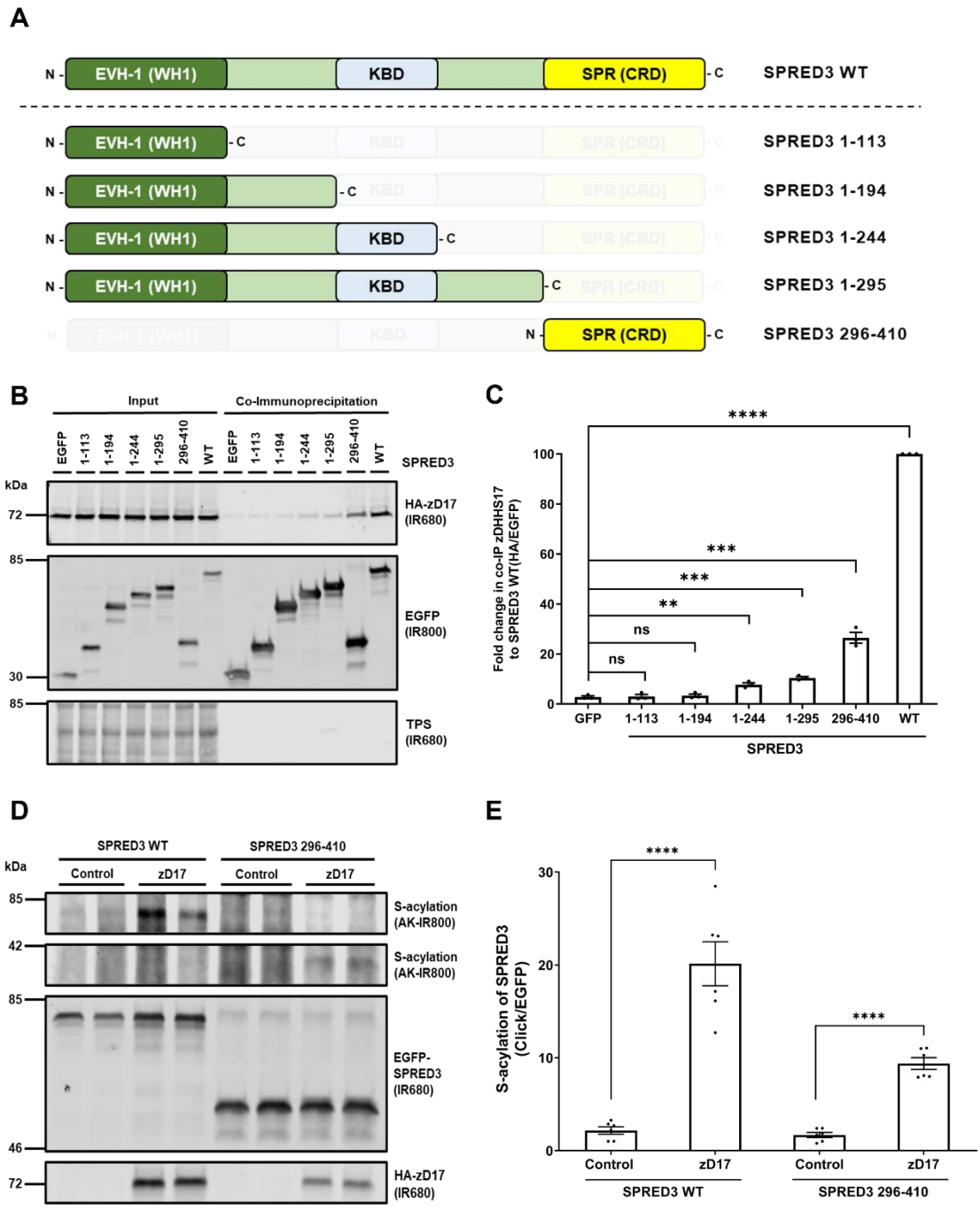


***Figure 4.5. The SPR domain of SPRED3 is sufficient for binding to, and S-acylation by* zDHHC17.** *(A)* Schematic representation of SPRED3 truncation mutant constructs used in click chemistry and coimmunoprecipitation assays: SPRED3 WT, 1-113, 1-94, 1-244, 1-295, and 296-410 (UniProt KB - Q2MJR0). EVH1, Ena/VASP (enabled/vasodilator-stimulated phosphoprotein) homology 1 domain, also known as WH1 for WASP (Wiskott–Aldrich syndrome protein) homology 1 domain; KBD, c-Kit kinase binding domain; SPR, Sprouty domain, which is also referred to as CRD

(cysteine-rich domain). All constructs used have EGFP tags appended at the N-terminus. (B) HEK-293T cells were co-transfected with HA-tagged zDHHS17 (a catalytically inert form of the enzyme) along with plasmids encoding for EGFP-tagged SPRED3 1-113, 1-194, 1-244, 1-295, 296-410, or EGFP alone. Cell lysates were incubated with agarose beads conjugated to an EGFP antibody and co-immunoprecipitated proteins were analysed by immunoblotting. Representative images showing zDHHS17 (top; IR680) and SPRED3 (middle; IR800) detected in input and immunoprecipitated samples on the same immunoblot. A total protein stain (TPS) is also shown (bottom panel; IR680). The positions of the molecular weight markers are shown on the left side of all immunoblots. (C) Graph showing the mean fold change in co-immunoprecipitated zDHHS17 after normalisation against the SPRED3 WT. Error bars represent ± SEM. Each replicate is shown with filled circles. Differences were analysed by unpaired t-test compared to the EGFP control. **** denotes $p < 0.0001$, ***$p < 0.001$, **$p < 0.01$, ns = non-significant (n = 3 for three independent experiments). (D) HEK-293T cells were transfected with plasmids encoding EGFP-tagged SPRED3 WT or SPRED3 296-410, together with either pEF-BOS-HA (referred to as “control” in the figure) or HA-zDHHC17. Cells were incubated with 100 μM palmitic acid azide (C16:0-azide) for 4 h and labelled proteins reacted with alkyne (AK) IRdye-800 nm. Representative images showing SPRED3 S-acylation (top; AK-IR800) and SPRED3 levels (middle; IR680) detected on the same immunoblot. For zDHHC17, HA (bottom; IR680) was revealed for the same samples on a different immunoblot. The positions of the molecular weight markers are shown on the left side of all immunoblots. (E) Graph showing mean SPRED3 S-acylation levels after normalisation against the corresponding control samples. Error bars represent ± SEM. Each replicate is shown with filled circles. Differences were analysed by unpaired t-test to the control for each substrate (**** denotes $p < 0.0001$, ***$p < 0.001$, **$p < 0.01$, n = 6 from three independent experiments).

## 4.6 SPRED3 binding to zDHHC17 does not require the Ank domain

As SPRED3 interaction with zDHHC17 involves the SPR domain of the substrate protein rather than a zDABM, it was next investigated if SPRED3 interacts with the ankyrin repeat of zDHHC17, as is reported for other substrates of zDHHC17 (Lemonidis et al., 2017a). To do this, HA-tagged zDHHC17 or a mutant lacking the ankyrin repeat domain (zDHHC17-ΔAnk; aa 287-632) (previously synthesised by Dr Kimon Lemonidis) were co-transfected with either EGFP-tagged SPRED3, Spry2, EGFP, or SNAP25 (shown to require an intact zDABM for S-acylation by zDHHC17 (Verardi et al., 2017). EGFP-tagged proteins were then captured on GFP-Trap® agarose IP beads and the co-immunoprecipitation of either HA-tagged zDHHC17 WT or the ΔAnk mutant was quantified.

As expected, SNAP25 was efficiently co-immunoprecipitated with zDHHC17 WT but failed to be captured by the ΔAnk mutant of zDHHC17. Spry2 interacted with both zDHHC17 WT and zDHHC17-ΔAnk albeit with reduced efficiency for the truncated mutant. SPRED3 displayed similar binding to zDHHC17-WT as Spry2 did to the zDHHC17-ΔAnk. However, SPRED3 showed an increased efficacy in co-immunoprecipitating the zDHHC17-ΔAnk, to a similar level as SNAP25 with zDHHC17 WT.

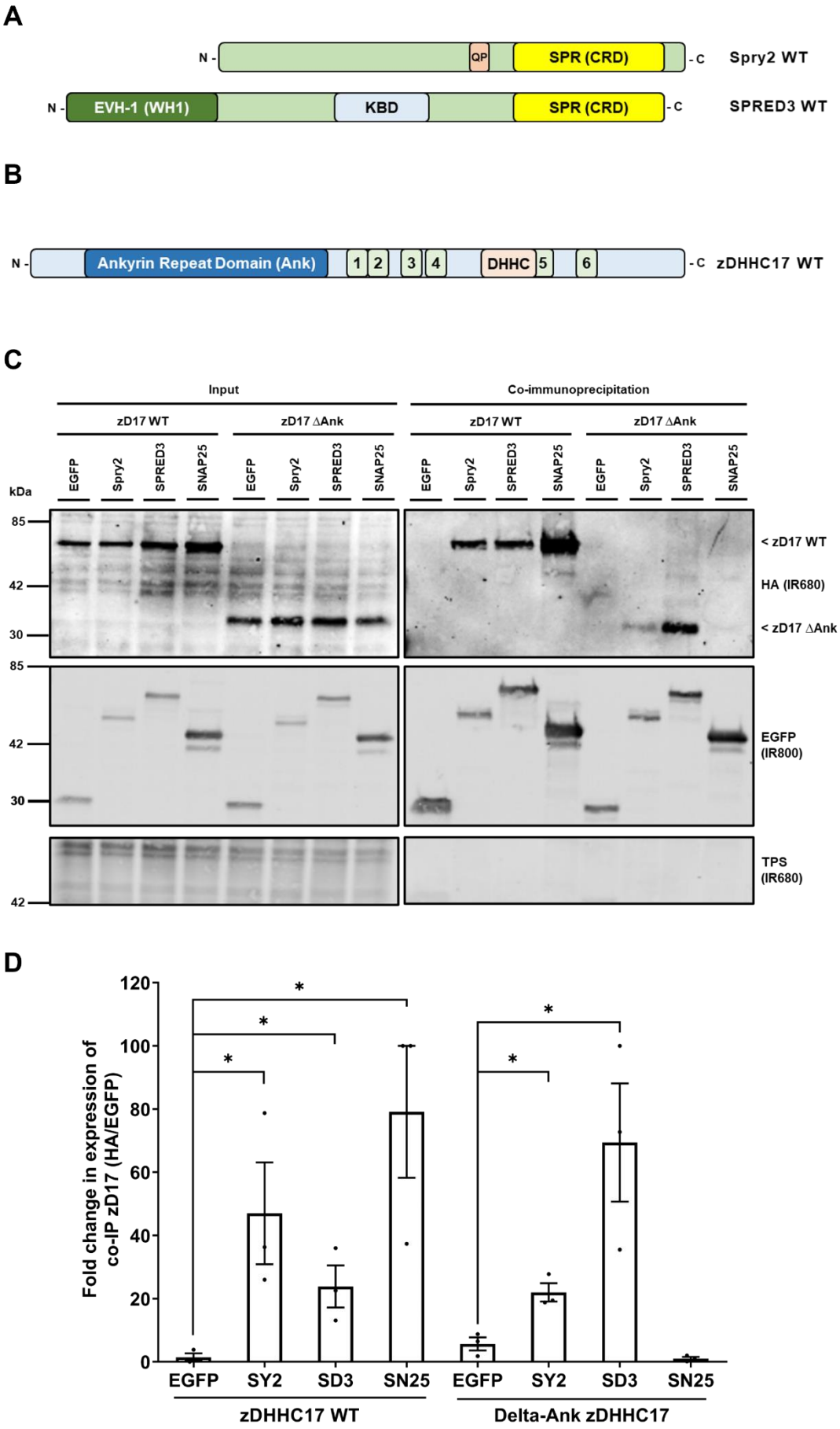
A
N -
QP
SPR (CRD)
- C
Spry2 WT
N -
EVH-1 (WH1)
KBD
SPR (CRD)
- C
SPRED3 WT
B
N -
Ankyrin Repeat Domain (Ank)
1
2
3
4
DHHC
5
6
- C
zDHHC17 WT
C
Input
Co-immunoprecipitation
zD17 WT
zD17 ΔAnk
zD17 WT
zD17 ΔAnk
EGFP
Spry2
SPRED3
SNAP25
kDa
85
42
30
< zD17 WT
HA (IR680)
< zD17 ΔAnk
EGFP
(IR800)
TPS
(IR680)
D
Fold change in expression of co-IP zD17 (HA/EGFP)
120
100
80
60
40
20
0
EGFP
SY2
SD3
SN25
zDHHC17 WT
Delta-Ank zDHHC17

***Figure 4.6. Spry2 and SPRED3 can both effectively bind zDHHC17 in the absence of the ankyrin repeat domain.*** (A) Schematic diagram comparing Spry2 and SPRED3 constructs. EVH1, Ena/VASP (enabled/vasodilator-stimulated phosphoprotein) homology 1 domain also known as WH1, WASP (Wiskott-Aldrich syndrome protein) homology one domain; KBD, c-Kit kinase binding domain; QP indicates the zDABM position; SPR, Sprouty domain also referred to as CRD (cysteine-rich domain). All constructs used have EGFP tags appended at the N-terminus. (B) Schematic diagram of zDHHC17 WT, ankyrin repeat domain (Ank), transmembrane domains (1–6), DHHC domain (DHHC). (C) HEK-293T cells were co-transfected with HA-tagged zDHHC17 WT or zDHHC17 ΔAnk together with plasmids encoding EGFP-tagged Spry2, SPRED3, SNAP25, or EGFP. Cell lysates were incubated with agarose beads conjugated to an EGFP antibody and co-immunoprecipitated proteins were analysed by immunoblotting. Representative images showing zDHHC17 (top; IR680) and EGFP-tagged proteins (middle; IR800) in the input and immunoprecipitated samples detected on the same immunoblot. A total protein stain (TPS) is also shown (bottom panel; IR680). The positions of the molecular weight markers are shown on the left side of all immunoblots. (D) Graph showing the fold change in co-immunoprecipitated zDHHC17 after normalisation. SY2 = Spry2, SD3 = SPRED3, SN25 = SNAP25. Error bars represent ± SEM. Each replicate is shown with filled circles. Differences were analysed by unpaired t-test compared to the EGFP control (* denotes $p < 0.05$, $n = 3$, from three independent experiments).

## 4.7 The SPR domain can bind to zDHHC17

The analysis in figure 4.6 suggests that the interaction of SPRED3 with zDHHC17 occurs outside of the Ank domain in the enzyme. The reduced but detectable binding of Spry2 to the ΔAnk mutant is also consistent with Spry2 having two binding sites, the major one being the zDABM interaction with the Ank domain and the second binding mode presumably being similar to the Ank domain–independent mode that occurs with SPRED3. To further test this hypothesis, zDHHC17 WT and zDHHC17 ΔAnk co-immunoprecipitation with the SPR domain truncation mutant of SPRED3 (296-41) was examined.

As in previous experiments, HEK-293T cells were co-transfected with HA-tagged zDHHC17 WT or zDHHC17 ΔAnk, alongside either EGFP-tagged SPRED3 WT, SPRED3 296-410, or EGFP (figure 4.7 A). As in figure 4.6, SPRED3 WT was able to co-immunoprecipitate both zDHHC17 WT and zDHHC17 ΔAnk. In addition, SPRED3 296-410, was also able to significantly precipitate both the WT and mutant enzyme (figure 4.7 B).

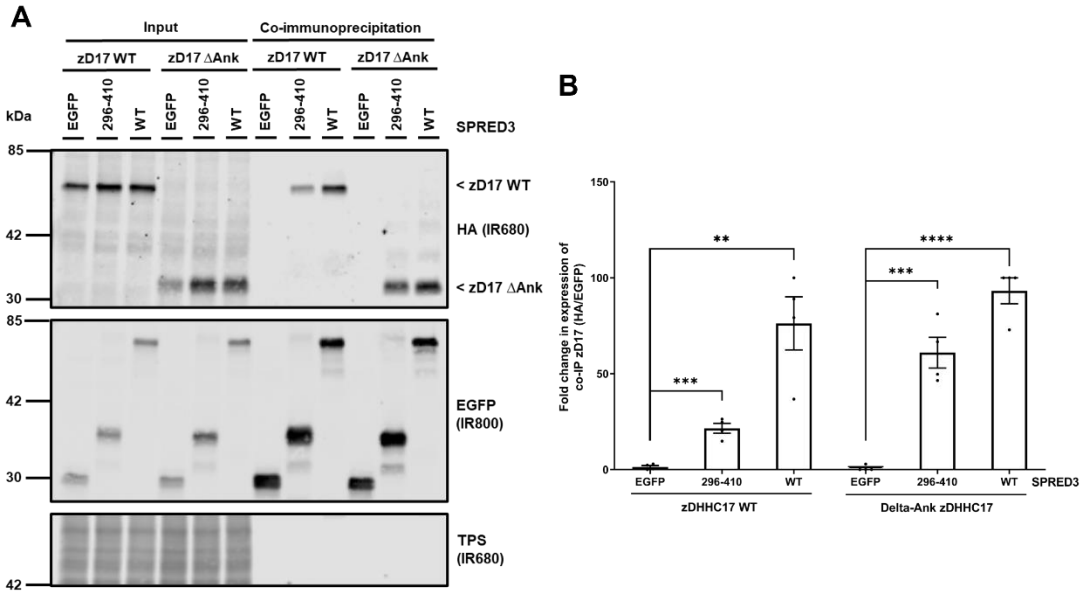


***Figure 4.7. The SPR domain of SPRED3 can bind a zDHHC17 mutant that lacks the ankyrin repeat domain.*** (A) HEK-293T cells were co-transfected with HA-tagged zDHHC17 WT or zDHHC17 ΔAnk together with plasmids encoding EGFP-tagged SPRED3 WT, SPRED3 296-410, or EGFP. Cell lysates were incubated with agarose beads conjugated to an EGFP antibody and co-immunoprecipitated proteins were analysed by immunoblotting. Representative images showing co-immunoprecipitated zDHHC17 (top; IR680) and SPRED3 levels (middle; IR800) detected on the same immunoblot. A total protein stain (TPS) is also shown (bottom panel; IR680). The positions of the molecular weight markers are shown on the left side of all immunoblots. (B) Graph showing the mean fold change in co-immunoprecipitated zDHHC17 after normalisation. Error bars represent ± SEM. Each replicate is shown with filled circles. Differences were analysed by unpaired t-test compared to the EGFP control (**** denotes $p < 0.0001$, ***$p < 0.001$, **$p < 0.01$, $n = 4$ from two independent experiments).

## 4.8 SPRED3 does not bind to the C-terminal end of zDHHC17, and also has a low affinity binding to zDHHC7

The current results suggest an interaction between the SPR domain of Spry/SPRED proteins and a region outside the ankyrin repeat domain of zDHHC17. To narrow down interaction sites, a zDHHC17 mutant lacking the cytosolic C-terminus was analysed. In addition to this, zDHHC7 was also included in the analysis to detect a possible interaction of SPRED3 with the conserved DHHC domain of zDHHC enzymes. zDHHC7 has been shown previously to substantially S-acylate Spry/SPRED proteins (figure 3.3).

HEK-293T cells were therefore co-transfected with either EGFP-SPRED3 or EGFP together with HA-tagged zDHHC17 WT, zDHHC17-ΔC (aa 11–569), or zDHHC7 WT. Cell lysates were incubated for 1 hour with GFP-Trap® agarose immunoprecipitation beads and washed twice in PBS to remove unbound/excess lysate. Precipitates were eluted to release captured EGFP-tagged proteins and any co-immunoprecipitated binding partners (i.e., zDHHC17/7). Eluted proteins were then resolved by SDS-PAGE and analysed by immunoblotting (figure 4.8 A). As in previous results in this chapter, SPRED3 was able to co-immunoprecipitate zDHHC17 WT. SPRED3 was also able to significantly interact with zDHHC17-ΔC (aa 11–569), to a greater degree than that of the zDHHC17 WT (figure 4.8 B). SPRED3 was also able to co-immunoprecipitate zDHHC7 but to a far lower degree than that of either zDHHC17 constructs.

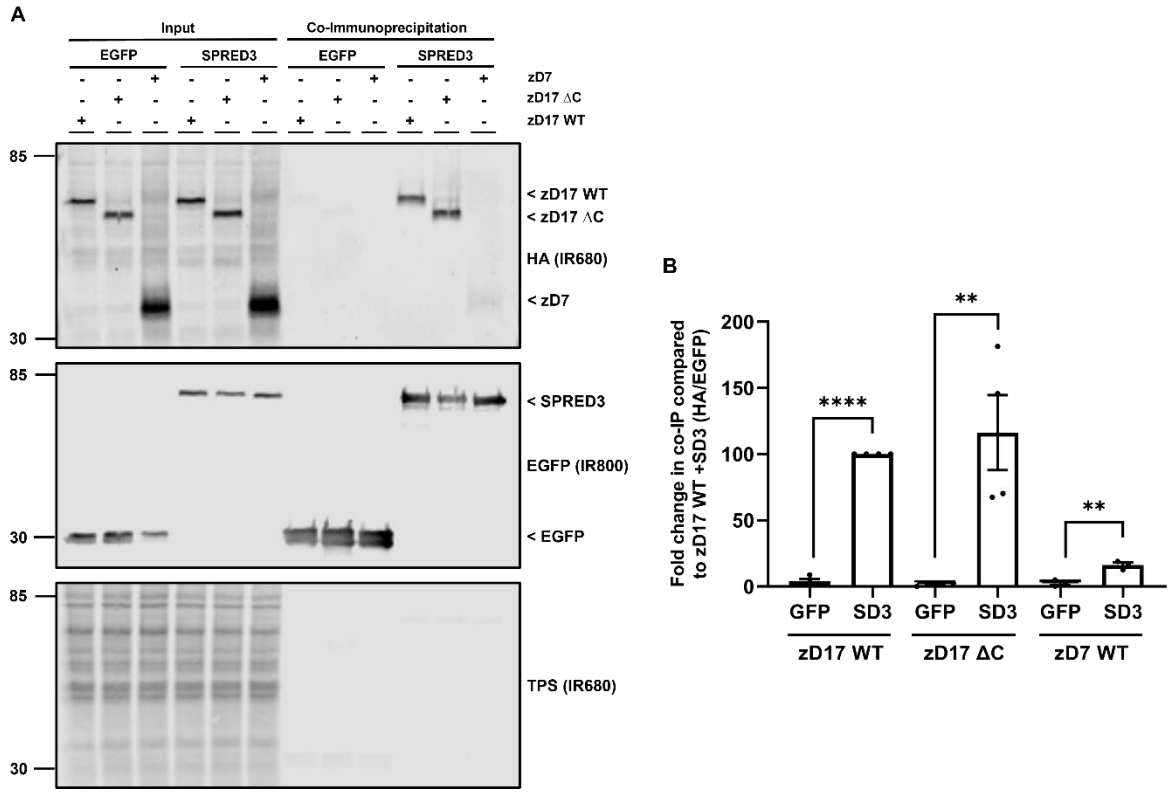


***Figure 4.8. SPRED3 can bind to a zDHHC17 mutant that lacks the C-terminus and displays stronger binding to zDHHC17 than zDHHC7.*** (A) HEK-293T cells were co-transfected with HA-tagged zDHHC17 WT or zDHHC17 ΔAnk (ankyrin repeat domain removed) together with plasmids encoding EGFP-tagged SPRED3 WT, SPRED3 296-410, or EGFP. Cell lysates were incubated with agarose beads conjugated to an EGFP antibody and co-immunoprecipitated proteins were analysed by immunoblotting. Representative images showing co-immunoprecipitated zDHHC17 (top; IR680) and SPRED3 levels (middle; IR800) detected on the same immunoblot. A total protein stain (TPS) is also shown (bottom panel; IR680). The positions of the molecular weight markers are shown on the left side of all immunoblots. (B) Graph showing the mean fold change in co-immunoprecipitated zDHHC17 after normalisation. Error bars represent ± SEM. Each replicate is shown with filled circles. Differences were analysed by unpaired t-test compared to the EGFP control (**** denotes $p < 0.0001$, ***$p < 0.001$, **$p < 0.01$, $n = 4$ from two independent experiments).

## 4.9 Alanine scanning mutagenesis of SPRED3 SPR domain

Taking the results of chapter 4 together so far, it is proposed that the alternative interaction between SPRED3 and zDHHC17 that is coupled to S-acylation likely occurs between the SPR domain of SPRED3 (aa 296-410), and a region between the end of the ankyrin repeat domain and the beginning of the C-terminal region of zDHHC17 (aa 287-569) (but likely not the DHHC domain due to minimal binding to zDHHC7). Therefore, the next step was to examine the SPR of SPRED3 in more detail to narrow down the interaction site.

EGFP-tagged SPRED3 alanine scanning mutants were generated covering the SPR domain but excluding cysteine residues (figure 4.9 A; appendix 1). The mutant constructs were either created in blocks of ten residues mutated to alanine (figure 4.9 B/C), or in blocks of twenty residues mutated to alanine (figure 4.9 D/E). SPRED3 constructs were co-transfected into HEK-293T cells with zDHHC17 WT, before being co-immunoprecipitated and analysed by immunoblotting (figure 4.9 B/D). None of the SPRED3 mutant constructs showed a significant reduction in co-immunoprecipitation of zDHHC17 (figure 4.9 C/E). Of all constructs tested, mutant 4 showed the greatest absolute reduction in zDHHC17 binding (although this was non-significant when compared to the WT). Conversely most mutant constructs actually led to a significant increase in co-immunoprecipitation of zDHHC17 WT. Constructs 3, 5, and 6 showed the greatest increase in figure 4.9 C, and mutant constructs C, D, and E showed the highest increase in figure 4.9 E.

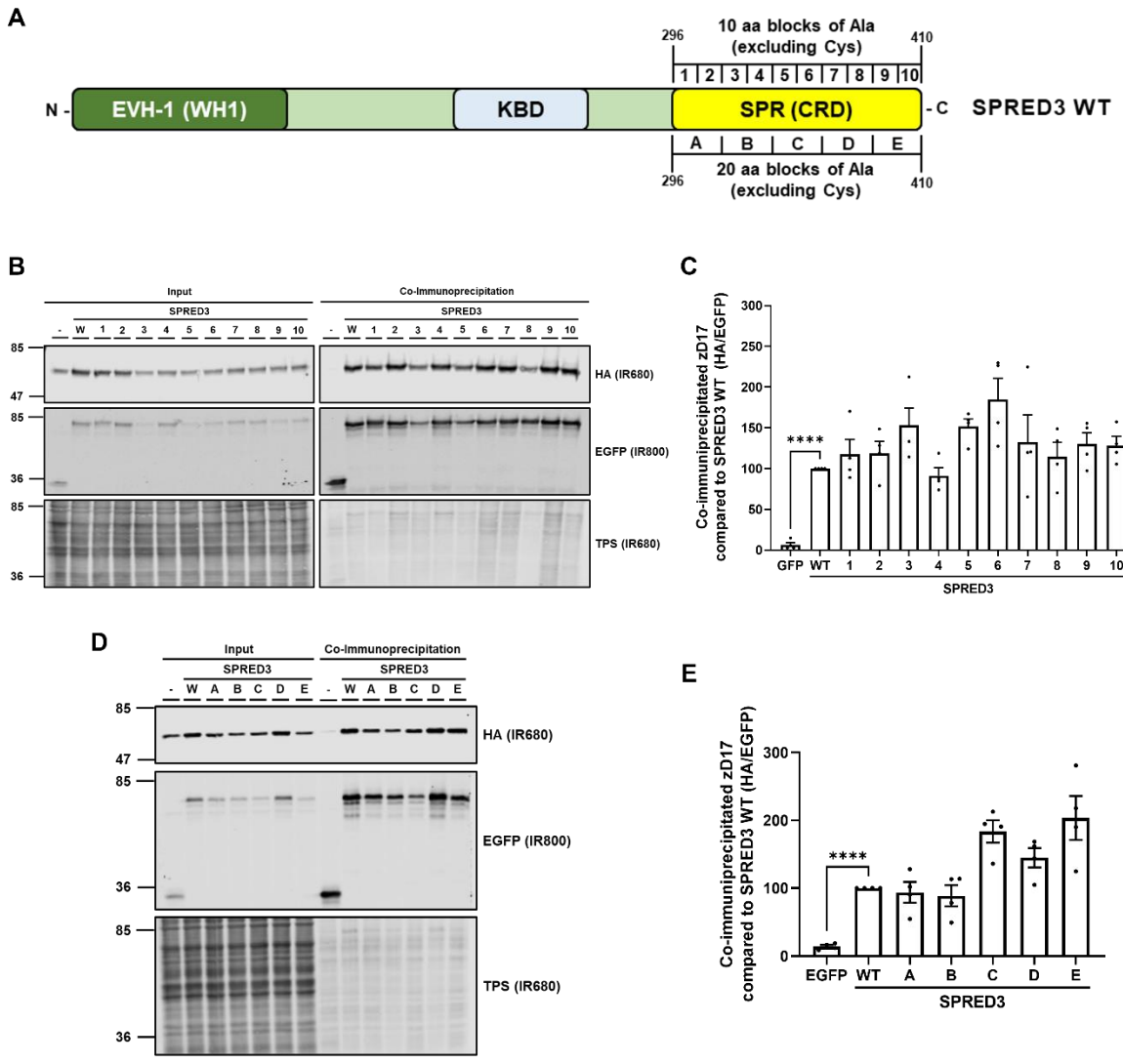


***Figure 4.9. Alanine mutagenesis of the SPR domain of SPRED3 does not perturb zDHHC17 binding.*** (A) Schematic representation of SPRED3 alanine scanning mutant constructs used in co-immunoprecipitations assays. The SPR domain was either mutated in ten aa blocks (mutants 1-10) or twenty aa blocks (mutants A-E) (UniProt KB - Q2MJR0). EVH1, Ena/VASP (enabled/vasodilator-stimulated phosphoprotein) homology 1 domain, also known as WH1 for WASP (Wiskott–Aldrich syndrome protein) homology 1 domain; KBD, c-Kit kinase binding domain; SPR, Sprouty domain, which is also referred to as CRD (cysteine-rich domain). All constructs used have EGFP tags appended at the N-terminus. (B) HEK-293T cells were co-transfected with HA-tagged zDHHC17 together with plasmids encoding EGFP-tagged SPRED3 WT or mutants with blocks of 10 residues mutated to alanine: 1. aa 296-297, 2. aa 298-318, 3. aa 319-328, 4. aa 329-340, 5. aa 341-351, 6. aa 352-363, 7. aa 364-373, 8. aa 374-386, 9. aa 387-399, 10. aa 400-410, or EGFP alone

(negative control). Cell lysates were incubated with agarose beads conjugated to an EGFP antibody and co-immunoprecipitated proteins were analysed by immunoblotting. Representative images showing zDHHC17 (top; IR680) and SPRED3 (middle; IR800) detected in input and co-immunoprecipitated samples on the same immunoblot. A total protein stain (TPS) is also shown (bottom panel; IR680). The positions of the molecular weight markers are shown on the left side of all immunoblots. (D) HEK-293T cells were co-transfected with HA-tagged zDHHC17 along with plasmids encoding EGFP-tagged SPRED3 WT or mutants with blocks of twenty residues mutated to alanine: A. aa 296-318, B. aa 319-340, C. aa 341-363, D. aa 364-386, E. aa 387-410, or EGFP alone (negative control). Cell lysates were incubated with agarose beads conjugated to an EGFP antibody and co-immunoprecipitated proteins were analysed by immunoblotting. Representative images showing zDHHC17 (top; IR680) and SPRED3 (middle; IR800) detected in input and co-immunoprecipitated samples on the same immunoblot. A total protein stain (TPS) is also shown (bottom panel; IR680). The positions of the molecular weight markers are shown on the left side of all immunoblots. (C/E) Graphs showing the mean fold change in co-immunoprecipitated zDHHC17 after normalisation against SPRED3 WT. Error bars represent ± SEM. Each replicate is shown with filled circles. Differences were analysed by unpaired t-test compared to SPRED3 WT (**** denotes $p < 0.0001$). No significant decrease was observed (except for EGFP control) and therefore is not indicated (n = 4, for three independent experiments).

### 4.10 Effects of SPRED3 cysteine mutations on zDHHC17 Binding

The alanine scanning mutagenesis conducted in figure 4.9 was unable to identify an alternative zDHHC17 interaction site in the SPR domain of SPRED3. One possibility is that the cysteine residues in this domain, which were not mutated in the constructs studied in figure 4.9, may play a role in zDHHC17 binding. To investigate this, triple cysteine to alanine mutant constructs of SPRED3 were generated (figure 4.10 A). These Cys mutants were: (1) SPRED3 C297A/C300A/C315A, (2) SPRED3 C331A/ C334A/C342A, (3) SPRED3 C354A/C356A/C379A, (4) SPRED3 C381A/C382A/ C389A, and (5) SPRED3 C396A/C398A/C401A. EGFP-tagged SPRED3 WT or Cys mutant constructs were co-transfected together with HA-tagged zDHHC17 WT before undergoing an immunoprecipitation assay (figure 4.10 B). Analysis of the data revealed that SPRED3 Cys mutant constructs 3 & 5 had a significant reduction in zDHHC17 binding compared with SPRED3 WT (figure 4.10 C).

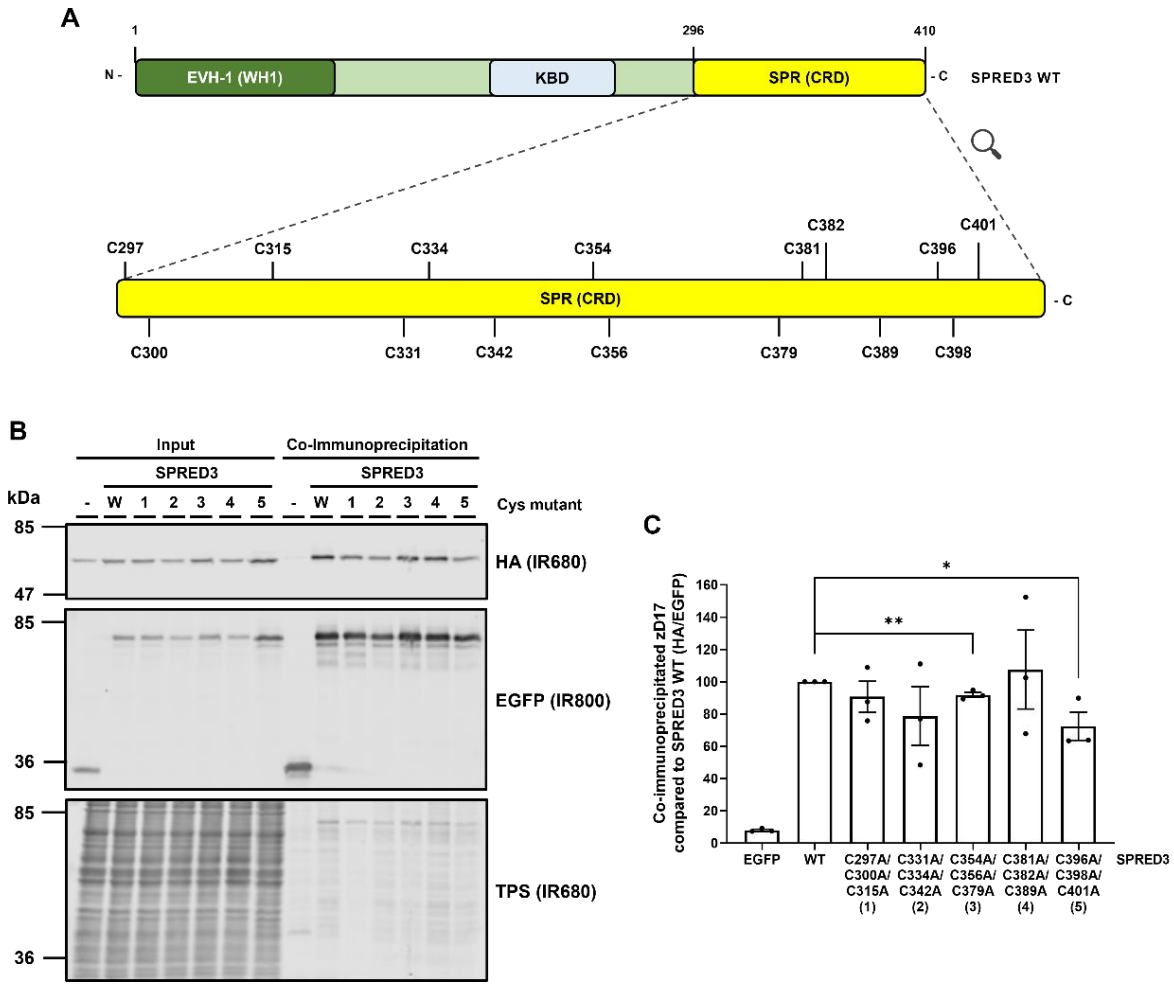


***Figure 4.10. Analysis of the binding of SPRED3 cysteine mutants to zDHHC17.*** (A) Schematic representation of cysteine residues within the SPR domain of SPRED3 (UniProt KB - Q2MJR0). EVH1, Ena/VASP (enabled/vasodilator-stimulated phosphoprotein) homology 1 domain, also known as WH1 for WASP (Wiskott–Aldrich syndrome protein) homology 1 domain; KBD, c-Kit kinase binding domain; SPR, Sprouty domain (aa 296-410), which is also referred to as CRD (cysteine-rich domain). All constructs used have EGFP tags appended at the N-terminus. (B) HEK-293T cells were co-transfected with HA-tagged zDHHC17 together with plasmids encoding for EGFP-tagged SPRED3 WT (as 'W' in the figure), EGFP alone (as '-' in the figure), or EGFP-tagged SPRED3 SPR domain cysteine mutant constructs, containing sequential cysteine to alanine mutations in groups of three: (1) SPRED3 C297A/C300A/C315A, (2) SPRED3 C331A/C334A/C342A, (3) SPRED3 C354A/ C356A/C379A, (4) SPRED3 C381A/C382A/C389A, and (5) SPRED3 C396A/ C398A/C401A. Cell lysates were incubated with agarose beads conjugated to an EGFP antibody and co-immunoprecipitated proteins were analysed by

immunoblotting. Representative images showing zDHHC17 (top; IR680) and SPRED3 (middle; IR800) detected in input and co-immunoprecipitated samples on the same immunoblot. A total protein stain (TPS) is also shown (bottom panel; IR680). The positions of the molecular weight markers are shown on the left side of all immunoblots. (C) Graph showing the mean fold change in co-immunoprecipitated zDHHC17 after normalisation against the SPRED3 WT. Error bars represent ± SEM. Each replicate is shown with filled circles. Differences were analysed by unpaired t-test compared to SPRED3 WT (* denotes $p < 0.05$) (EGFP control is significant, not shown on graph) (n = 3, for three independent experiments).

### 4.11 Effect of cysteine mutations on SPRED3 S-acylation

Previous work on the S-acylation of Spry2 identified that C265/C268 are the residues required for efficient S-acylation by zDHHC17 (Locatelli et al., 2020). S-acylation of the SPRED3 cysteine mutants in figure 4.10 was investigated next. HEK-293T cells were co-transfected with plasmids encoding HA-zDHHC17 or pEF-BOS-HA (empty vector as negative control) together with either EGFP-tagged SPRED3 WT, (1) SPRED3 C297A/C300A/C315A, (2) SPRED3 C331A/C334A/C342A, (3) SPRED3 C354A/C356A/C379A, (4) SPRED3 C381A/C382A/C389A, and (5) SPRED3 C396A/C398A/C401A. Cells were then incubated with C16:0-azide and processed for click chemistry detection of S-acylation (figure 4.11 A). As before, mean intensity values (± SEM) for the S-acylated band (AK800) of each substrate were normalised against the EGFP intensity for that protein (figure 4.11 B) or expressed as a fold increase above basal (figure 4.11 C).

The results show that all SPRED3 Cys mutant constructs with or without zDHHC17 exhibit an enhancement in basal S-acylation compared to the WT (figure 4.11 B). However only Cys mutant 2 displays a significant increase in S-acylation with zDHHC17 above its basal S-acylation (figure 4.11 B/C). Expressing the zDHHC17-mediated S-acylation as a fold change over basal in figure 4.11 C further emphasises the lack of any effect of zDHHC17 on SPRED3 mutants 3-5, in particular.

The immunoblot in figure 4.11 A also shows a visual difference in zDHHC17 expression levels with some of the SPRED3 mutants (figure 4.11 A bottom panel). Data quantification indeed revealed that zDHHC17 is significantly less well expressed when co-expressed with SPRED3 mutant constructs 2 and 5.

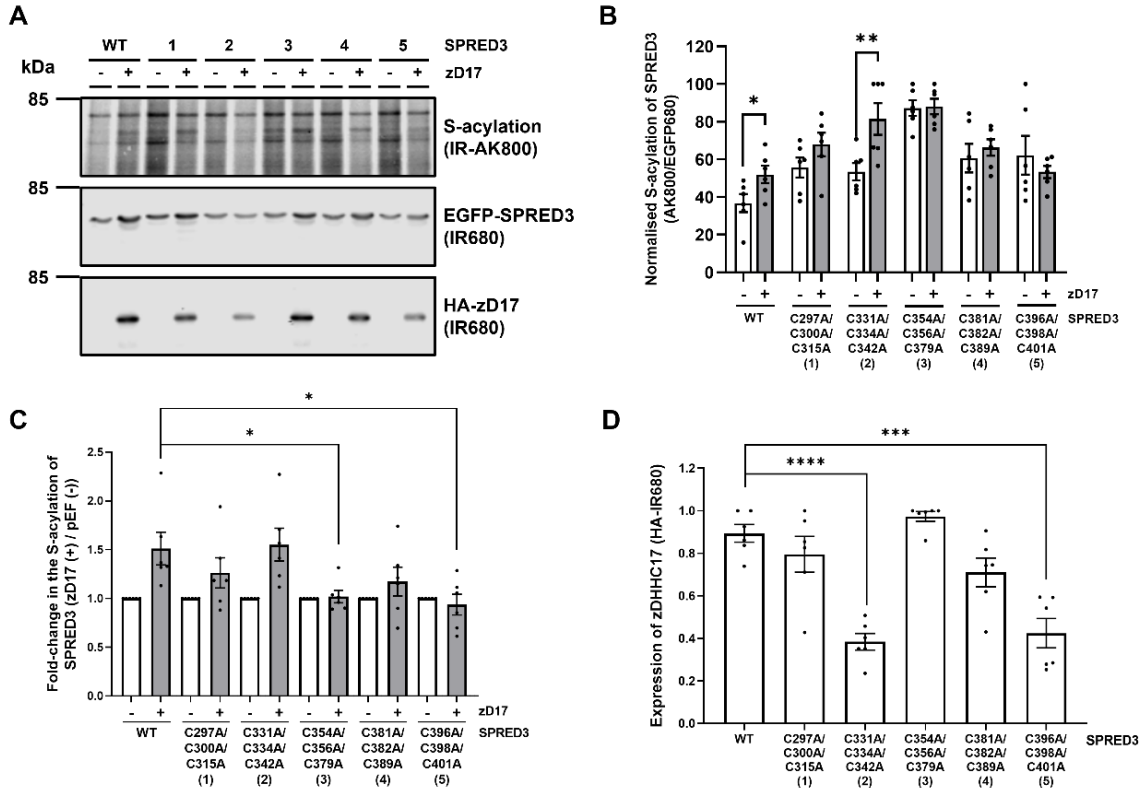


***Figure 4.11. S-acylation of SPRED3 mutants by zDHHC17 and effects of the mutants on zDHHC17 expression levels.*** (A) HEK-293T cells were transfected with plasmids encoding EGFP-tagged SPRED3 WT or SPRED3 SPR domain cysteine mutant constructs, containing sequential cysteine to alanine mutations in groups of three: (1) SPRED3 C297A/C300A/C315A, (2) SPRED3 C331A/C334A/C342A, (3) SPRED3 C354A/C356A/C379A, (4) SPRED3 C381A/C382A/C389A, and (5) SPRED3 C396A/C398A/C401A. These constructs were co-transfected with either pEF-BOS-HA (as "-" in the figure) or HA-zDHHC17. Cells were incubated with 100 μM palmitic acid azide (C16:0-azide) for 4 h and labelled proteins reacted with alkyne (AK) IRdye-800 nm. Representative images showing SPRED3 S-acylation (top; AK-IR800) and SPRED3 levels (middle; IR680) detected on the same immunoblot. For zDHHC17, HA (bottom; IR680) was revealed for the same samples on a different immunoblot. The positions of the molecular weight markers are shown on the left of all immunoblots. (B) Graph showing the mean intensity values of SPRED3 S-acylation relative to substrate expression (AK800/EGFP680) and normalised to the highest value on each blot. (C) Graph showing the mean fold change between SPRED3 S-acylation in the presence of zDHHC17 (zDHHC17 (+) / pEF (-)) compared to WT. (D) Graph showing the mean values of zDHHC17 expression (IR680). For all graphs, error bars represent ± SEM and each replicate is shown with filled circles. Differences were analysed by unpaired t-test compared to SPRED3 WT. **** denotes $p < 0.0001$, ***$p < 0.001$, **$p < 0.01$, *$p < 0.05$ (n = 6, for three independent experiments).

## Discussion

The results of this study uncover a striking difference in the mechanisms of recognition of different proteins by zDHHC17. In contrast to the analysis of SNAP25-zDHHC17 interactions, the findings in this chapter show that a simple zDABM interaction followed by substrate S-acylation model does not fit for all proteins. In fact, SNAP25, Spry, and SPRED proteins each show a different profile. For SNAP25, the zDABM interaction with zDHHC17 is coupled to and essential for S-acylation. For Spry2, the zDABM interaction with zDHHC17 occurs but is dispensable for S-acylation. Whereas for SPRED3, the substrate is S-acylated by zDHHC17 but lacks a zDABM sequence.

*Evidence for an alternative Spry/SPRED-zDHHC17 interaction site coupled to S-acylation*

The W130 residue in the Ank domain of zDHHC17 has been shown to be critical for the interaction with the zDABM of SNAP25 (Verardi et al., 2017). Evidence presented in figure 4.1 revealed the unexpected finding that mutation of this residue did not affect the S-acylation of Spry proteins, and in the case of Spry1, 2 and 3, S-acylation actually showed a significant increase with the W130A mutant compared with WT zDHHC17 (figure 4.2 C). Analysis of the interaction of Spry proteins with the W130A mutant revealed that although Spry1-3 binding was reduced compared to WT zDHHC17 it was still detectable (in contrast to SNAP25 binding which was completely ablated). For SPRED3, there was no loss of binding with the W130A mutant, consistent with the absence of a zDABM sequence in this protein. This data suggests for the first time that there is an alternative mode of binding use by some substrates of zDHHC17.

It should also be acknowledged that although Spry4 does contain a zDABM, it consistently exhibited reduced binding to both zDHHC17 WT and W130A. The reason for this is unclear but it is interesting to note that Spry4 contains two zDABM sites sequential to one another (128- AVRIQPKVVHCQP-140; UniProt: Q9C004 - SPY4_HUMAN). The presence of two zDABMs in close proximity like this could render both ineffective; however, currently this hypothesis is speculative and would require further investigation.

*Examining Spry/SPRED domains for alternative interaction sites*

With the knowledge that Spry2 does not require a zDABM for S-acylation (figure 4.1), it was important to explore other regions within the protein that could be important for its S-acylation. Truncation mutant experiments in figure 4.3 D/E showed that the Spry2 155 -315 mutant was still able to interact with zDHHC17. This truncation mutant also showed significant levels of S-acylation by zDHHC17 (figure 4.3 B/C), and the same localisation as Spry2 WT in PC12 cells (figure 4.4). Altogether, the data suggests that Spry2 may contain a second, lower affinity, zDHHC17-binding site downstream of the zDABM P154 residue. Incidentally, the 100 to 315 Spry2 mutant appeared to show elevated binding (figure 4.3 D/E) and lower S-acylation (figure 4.3 B/C) compared to the 120 to 315 and 140 to 315 mutants, and it is unclear whether these differences are meaningful or a consequence of different folding of these truncation mutants.

Results from figure 3.4 indicate that although SPRED3 has lower absolute levels of S-acylation by zDHHC17 compared to Spry2 (figure 3.4 B), the fold change above basal for Spry2 and SPRED3 is comparable. Additionally, the results of figure 4.2, show that both SPRED3 and Spry2 have comparative binding to zDHHC17 W130A. Collectively, these results are consistent with both SPRED3 and Spry2 containing an alternative zDHHC17 binding site that is coupled to their S-acylation. SPRED3 was selected for further investigation as the absence of a zDABM makes the analysis of binding to zDHHC17 simpler (i.e., because it has one rather than two binding modes).

Truncation mutants of SPRED3 were assessed for binding to zDHHC17 (figure 4.5). None of the C-terminal mutants lacking the SPR domain showed significant binding to zDHHC17 (figure 4.5 B/C). However, the N-terminal mutant comprised of amino acids 296-410 was able to effectively interact zDHHC17 (figure 4.5 B/C). In addition to this, the SPRED3 296-410 was also able to be S-acylated by zDHHC17 (figure 4.5 D/E). These data suggest that the novel binding site may be present in the SPR domain of SPRED3. This is consistent with the analysis of Spry2, which also suggested a binding site in the SPR domain between residues 155-315 (figure 4.3 & 4.4). For Spry2, the SPR domain is between amino acids 177-291, and for SPRED3 the SPR domain is between amino acids 296-407.

Another interesting finding in the previous chapter was that SPRED1/2 are not efficiently S-acylated by zDHHC17 despite containing a similar SPR domain as SPRED3. It will be interesting to explore the reasons why SPRED3 is a better substrate of zDHHC17 than SPRED1/2. Perhaps different cysteine configurations of

the SPR domains favour SPRED3 S-acylation over SPRED1/2 S-acylation. For instance it has been previously reported that S-acylation of SNAP25 by zDHHC17 critically depends on the length of the linker region between the binding site and the S-acylated cysteines (Salaun et al., 2020a).

*Alternative substrate interaction sites in zDHHC17*

The finding that Spry and SPRED proteins do not interact with zDHHC17 via a zDABM was unexpected and suggested that the Ank domain of this enzyme may also recognise a different motif/structural feature in Spry/SPRED. Surprisingly, in figure 4.6 it was found that the Ank domain of zDHHC17 is dispensable for binding to SPRED3 WT and that Spry2 also retains residual binding when the Ank domain is removed. Furthermore, figure 4.7 showed that the isolated SPR domain of SPRED3 (SPRED3 296-410; from figure 4.5) also interacts with zDHHC17 lacking the Ank domain. This, to our knowledge, is the first demonstration of Ank domain–independent interaction of zDHHC17 linked to substrate S-acylation. In addition, the C-terminus of zDHHC17 was also dispensable for SPRED3 binding (figure 4.8). Furthermore, the DHHC-CRD domain of zDHHC17 does not appear to be the second binding site for Spry/SPRED proteins, as this would predict a similar interaction of these substrates with other zDHHC enzymes (which was not observed for zDHHC7). Thus, the interaction may occur at cytosolic regions between TMDs 2 & 3; or alternatively, unique sequence elements in the DHHC-CRD of zDHHC17 may facilitate a specific interaction with this enzyme isoform. Further mutational analysis will be required to uncover the specific mechanism of interaction.

These further analyses could include chimeric mutant constructs containing domain swaps between zDHHC17 and zDHHC7. Although zDHHC enzymes are highly conserved in their DHHC-CRDs, there is actually only 50.98% homology between the DHHC domains of zDHHC17 and zDHHC7. Furthermore, the larger cytoplasmic regions between TMD loops 4 and 5 on zDHHC17 and the corresponding region between TMD loops 2 and 3 of zDHHC7, are only 39.47% identical to each other. With less than 20% identity in the cytoplasmic sequence before the DHHC domain (figure 4.12). Generating plasmid constructs which code for chimeric mutant zDHHC7/zDHHC17 domain swaps could therefore prove effective in clarifying, one way or another, the involvement of the DHHC-CRD region in Spry and SPRED binding.

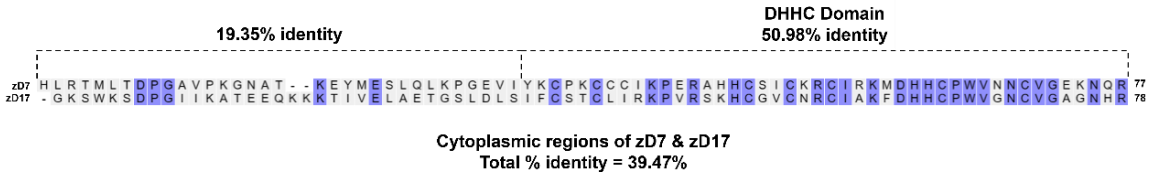


**Figure 4.12. Homology between the cytoplasmic/DHHC regions of zDHHC7 and zD*HHC*17.** *Protein sequence alignment and percentage identity between residues for the cytoplasmic/DHHC regions of zDHHC7 (aa 97-173) and zDHHC17 (aa 403-480). Generated using the outputs from the align tool from UniProt (Consortium, 2022).*

*Probing the SPR domain of SPRED3 for alternative interaction sites*

With the current evidence indicating that the SPR domain of Spry/SPRED proteins is the region which contains the alternative zDHHC17 interaction site, it was next important to analyse the residues within this region that mediate binding. However, alanine scanning mutagenesis of this domain was unable to conclusively discern a region of importance for the SPRED3-zDHHC17 interaction (figure 4.9). There was a slight significant decrease in SPRED3-zDHHC17 interaction with SPRED3 Cys mutant constructs 3 (C396A/C398A/C401A) and 5 (C381A/C382A/C389A). However, no other Cys mutant construct showed a significant reduction is zDHHC17 interaction. (figure 4.10 B/C). Potentially an alternative combination of Cys to Ala mutations in SPRED3 would be effective to disrupt zDHHC17 interaction.

These Cys mutant constructs were also tested for how well they could be S-acylated in figure 4.11. It was found that several of the cysteine mutants were not effectively S-acylated by zDHHC17. In addition, the expression of zDHHC17 was also examined and it was found that the expression of zDHHC17 was significantly lower in co-expression with SPRED3 Cys constructs 2 and 5. Overall, the results with cysteine mutants suggest that several of these cysteine are important for efficient S-acylation by zDHHC17 and also for the stabilisation of zDHHC17 mediated by SPRED3.

Why has the exact location of the alternative binding site in Spry and SPRED proteins been challenging to identify? Experiments in this thesis have been similar to work that identified the zDABM of zDHHC17 substrates (Lemonidis et al., 2015a). However, the zDABM is a linear hexapeptide motif (Lemonidis et al., 2015a), and one possibility is

that the alternative binding site within the SPR domain may not be linear and thus not readily apparent in alanine scanning mutagenesis experiments. For example, within the SPR domain there may be two or more regions of amino acids that are sequentially distant from one another but are spatially close due to the overall protein conformation. In this instance, alanine scanning mutagenesis may not prove an effective tool as only amino acids within a ten aa block are mutated.

The array of modifications that can occur on Spry/SPRED proteins also makes analysis of these proteins a little more complex. For example, in figure 4.1 A/B, the phosphorylated band pattern of the Spry proteins changes with and without the zDHHC enzyme. Without enzyme Spry1 presents as an unphosphorylated band (lower) and a phosphorylated band (higher); but in the presence of either zDHHC17 WT or W130A, the phosphorylated band is more prominent (figure 4.1 A). Spry2, has a differential pattern, where the upper phosphorylated band is only expressed in co-transfection with zDHHC17 WT, but not zDHHC17 W130A. The conformation of Spry2 has already been described under different circumstances and involves a delicate balance of interactions and post-translational modifications (figure 1.8). For instance, upon FGF stimulation, Y55 of Spry2 becomes phosphorylated which then allows PP2A binding (Lao et al., 2007b). Once bound, PP2A can dephosphorylate S112 of Spry2 to expose the cryptic C-terminal proline site – VPTVP (aa 303-307) (Lao et al., 2006). This SH3 consensus sequence region is able to bind the scaffold protein ITSN1, which can also disrupt the binding of Spry2 to CBL (a E3-ubiquitin-protein ligase) and thereby promote EGFR degradation (Okur et al., 2012). Interestingly, ITSN1 has also previously been shown to bind other S-acylated proteins such as SNAP25 (Okamoto et al., 1999).

What is the purpose of Spry2 (and other Spry proteins) possessing two zDHHC17 binding sites? One interesting possibility is that the zDABM-ANK17 interaction provides a means to regulate the timing of Spry2 S-acylation. For example, growth factor–dependent changes in Spry2 phosphorylation (or some other post-translational modification) might facilitate reorganisation of Spry2–zDHHC17 complexes, moving from a zDABM-dependent interaction to an alternative binding mode that facilitates Spry2 S-acylation, enhanced stability, and plasma membrane targeting (Locatelli et al., 2020). Conversely, the different binding modes of Spry2 might exert a regulatory effect on zDHHC17 and in so-doing contribute to the regulation of cellular S-acylation dynamics. Spry/SPRED proteins have been described to exist in multiple cellular

locations, such as the plasma membrane (Locatelli et al., 2020, Lim et al., 2002), membrane ruffles (Lim et al., 2000), actin cytoskeleton (Bundschu et al., 2006), cytoplasm (King et al., 2005), and even the nucleus (Walker and Land, 2018). It has also been shown that S-acylation is required for plasma membrane localisation, and also that it is specific cysteines responsible for this localisation/S-acylation (Locatelli et al., 2020). This brings into question whether the S-acylation of the specific cysteine residues within SPRED3 (and other Spry/SPRED proteins) is initially required for subsequent interaction with zDHHC17.

In figure 4.10, the immunoprecipitation experiments were conducted in co-expression with zDHHC17 WT, which is still catalytically active and capable of S-acylating SPRED3. Unlike figure 4.10, earlier binding experiments like those conducted in figures 4.3 & 4.5 utilised catalytically inert forms of zDHHC17 (either zDHHA or zDHHS). Therefore, it would be interesting to test if using a catalytically inert form of zDHHC17, in the co-immunoprecipitation of SPRED3 Cys mutant constructs (figure 4.10) would produce a similar result. Other proteins such as the zDHHC9 accessory protein, GCP16 (also known as GOLGA7) is a peripheral membrane protein that targets to Golgi membranes through the S-acylation of two specific cysteine residues (C69 and C72) (Ohta et al., 2003, Salaun et al., 2020b). The S-acylation of these two cysteine residues has also been shown to be important for the interaction of GCP16 to zDHHC9 (Mitchell et al., 2014, Salaun et al., 2020b).

Collectively, the results in this chapter provide evidence that Spry and SPRED proteins use a novel Ank domain-independent and zDABM-independent interaction mode for S-acylation by zDHHC17. Although, the exact regions of enzyme and substrate that mediate this interaction have not been identified, the results clearly support a role for the SPR domain of Spry/SPRED. Interesting questions that arise is whether other substrates of zDHHC17 also use alternative modes of binding to zDHHC17? Can multiple substrates bind at the same time to zDHHC17 through different interaction modes? Does the binding of proteins (such as Spry2) to the zDABM interaction site in zDHHC17 perturb or regulate the S-acylation of other substrates? It is clear that the substrate interactions of zDHHC17 are more complex than anticipated and involve a mixture of Ank domain-dependent and -independent mechanisms.

**Conclusions of chapter 4**

- A novel mode of zDHHC17-substrate binding that is linked to S-acylation has been identified.

- The presence of zDABM sequence(s) in zDHHC17 substrates does not imply their role in S-acylation.

- The novel mechanism of recognition/S-acylation for Spry & SPRED proteins is distinct from the mechanism of SNAP25 recognition/S-acylation by zDHHC17. Specifically, the zDABM sequence, which is the major interaction site for zDHHC17 was dispensable for S-acylation and binding.

- It is proposed that the SPR domain of Spry/SPRED proteins contains an additional uncharacterized zDHHC17 binding site that is coupled to S-acylation.

- It is also speculated that the CRD/DHHC domain of zDHHC17 is the site of interaction for substrates interacting via this novel mechanism.

# CHAPTER 5

# INVESTIGATION OF SPRY2 ACTION ON THE SARS-COV-2 ACCESSORY PROTEIN ORF3D

# Chapter 5 - Investigation of Spry2 action on the SARS-CoV-2 accessory protein Orf3d

## Introduction

Previously published data showed that zDHHC17 can stabilise Spry2 (Locatelli et al., 2020), with results in this thesis also showing that Spry2 can stabilise zDHHC17 (Chapter 3: figure 3.13 & 3.14). Unpublished work conducted by Dr. Christine Salaun within the Chamberlain lab identified that the expression of certain cysteine containing proteins of the SARS-CoV-2 virus could be significantly increased by co-expression of zDHHC7 (as well as by other distinct zDHHCs). Specifically, it was found that the accessory proteins Orf10 and Orf3d show enhanced S-acylation and higher expression levels when co-expressed with zDHHC7. Further analysis showed that Orf10 expression was only enhanced by the highly active and promiscuous enzymes, zDHHC3 and zDHHC7. By contrast, Orf3d expression could be enhanced by a wider set of enzymes including zDHHC2, 3, 7, 15, 17, and 5. Noting that zDHHC5 was only effective at increasing S-acylation of Orf3d when co-expressed with the accessory protein, GCP16 (Ko et al., 2019).

SARS-CoV-2 is a positive-sense single-stranded RNA virus (Chan et al., 2020, Machhi et al., 2020). The genome of SARS-CoV-2 is arranged into 14 open reading frames (Orfs) which encode 31 proteins, grouped into structural, non-structural, and accessory proteins (Figure 5.0) (Redondo et al., 2021). The recent pandemic has resulted in increased interest in how viral proteins are regulated, including by S-acylation. Work from the lab of Dr. Anirban Banerjee identified zDHHC mediated S-acylation of specific cysteines in the SARS-CoV-2 spike protein (Puthenveetil et al., 2021). In the same year, it was shown that the S-acylation of spike can enhance virus infectivity and also control membrane lipid organisation. The team from the lab of Gisou van der Goot were able to show that lipidation controls spike protein biogenesis and degradation, thereby driving the formation of lipid nanodomains in the early Golgi (Mesquita et al., 2021).

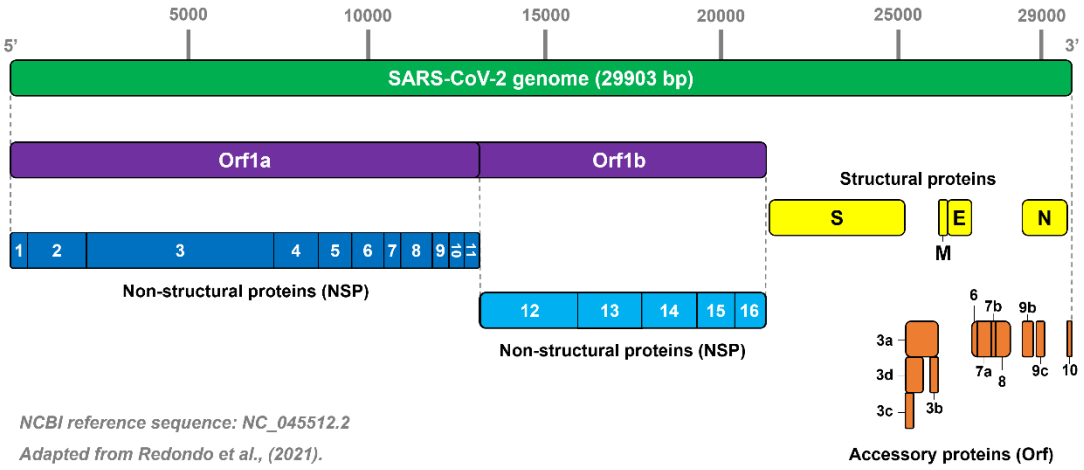


**Figure 5.0. Schematic representation of SARS-CoV-2 genome organisation.** *SARS-CoV-2 is a single-stranded positive-sense RNA molecule of approximately 29,900 nucleotides (NCBI reference sequence: NC_045512.2) arranged into 14 open reading frames encoding 31 proteins. Orf, open-reading frame; NSP, non-structural protein; S, spike protein; M, membrane protein; E, envelope protein; N, nucleocapsid protein. Figure is adapted from Redondo et al., (2021).*

Of the accessory proteins of SARS-CoV-2, Orf8 and Orf3d elicit the highest antibody response in COVID-19 patients and are proposed as potential serological markers of infection (Hachim et al., 2020). Orf3d is an overlapping gene region of Orf3a, where the same set of nucleotides can code for different proteins, due to intrinsic ATG (Met) start codons (UniProtKB - P0DTG0, ORF3D_SARS2). Orf3d consists of 57 amino acid (aa) residues, however due to a second start codon further upstream in this sequence, a shorter 33 aa isoform also exists named Orf3d-2. Current experimental evidence indicates the presence of both isoforms, but with a higher degree of certainty for Orf3d-2 (Nelson et al., 2020, Finkel et al., 2021). It is important to note that within the literature the initial designations for overlapping Orfs in the SARS-CoV-2 genome have been variably and confusingly referenced. In this case, research into Orf3d has also been published as Orf3b. In line with a published consensus article on SARS-CoV-2 nomenclature, the term Orf3d is to be used for the 57-codon gene (which is studied in this thesis). The term Orf3b is to be used for the 22-codon gene homologous to the 5' end of Orf3b in SARS-CoV (Jungreis et al., 2021).

Orf3d contains nine cysteine residues with the potential to be S-acylated (five cysteine residues within Orf3d-2). Little is currently known about the action or function of Orf3d (or indeed many of the Orfs), but some evidence has suggested at least one interaction with that of the mitochondrial protein, stomatin-like protein 2 (STOML2) (Gordon et al., 2020, Redondo et al., 2021). With regards to the current thesis, it is interesting to note that Spry4 has been identified as an interactor of Orf3d when analysed by immunoprecipitation coupled with mass spectrometry (St-Germain et al., 2020).

The aim of this chapter was to examine if the effects of Spry2 on zDHHC17 expression (see Chapter 3) have a subsequent impact on the S-acylation of Orf3d. Alongside this, the effects of Orf3d on Spry2 S-acylation will be examined to determine if this SARS-CoV-2 Orf accessory protein can lead to changes in the S-acylation of host cell proteins. These questions are of added relevance given the reported interaction of Spry4 (and therefore possibly also Spry2) with Orf3d (St-Germain et al., 2020).

# Results

## 5.1 Synergistic effect of Spry2 and zDHHC17 on the expression of Orf3d

As discussed in the previous chapters, zDHHC17 and Spry2 have a unique interaction that imparts a reciprocal stabilisation of both enzyme and substrate (chapter 3; figure 3.13). In figure 5.1, the expression of Orf3d was investigated as an indirect way to see if the stabilisation of zDHHC17 by Spry2 could also enhance enzyme activity towards a different substrate.

For this, Strep-II tagged Orf3d WT was co-expressed with HA-tagged zDHHC17, zDHHC7 or the inactive serine to alanine mutant of zDHHC17 (DHHS) together with either EGFP tagged-Spry2 WT, Spry2 N211A/D214A/K223A (NDK) (S-acylation deficient mutant), or EGFP alone (negative control for Spry2). Lysates were then prepared from transfected cells and Orf3d expression examined by immunoblotting. Mean band intensity of the upper Orf3d immunoreactive band was quantified as a fold difference relative to Orf3d expressed with zDHHC17, which was set at 1.0.

As can be seen from figure 5.1, zDHHC7 (lane 12) was the most effective enzyme at enhancing Orf3d expression and is used in these experiments as a positive control. In contrast, the effects of zDHHC17 on Orf3d where much lower than zDHHC7, but still significant (lane 2). Interestingly, Spry2 caused a substantial increase in Orf3d expression in the presence of zDHHC17 (compare lanes 2 and 6). The synergistic effect of Spry2 and zDHHC17 on Orf3d expression was dependent upon enzyme activity as it was not recapitulated with the catalytically inactive zDHHS17 mutant (lane 10). Furthermore, the effect was specific to WT Spry2 and was not seen with the Spry2 NDK mutant (S-acylation deficient) (lane 8). As Spry2 is known to stabilise zDHHC17 (chapter 3; figure 3.13), it was also investigated if doubling the concentration of the zDHHC17 plasmid (2x17) used for transfection could mimic the effects of zDHHC17/Spry2 co-transfection. However, there was no significant effect of increasing zDHHC17 levels without Spry2 (compare lanes 2 and 3). This data is consistent with the hypothesis that Spry2 enhances zDHHC17 activity towards Orf3d.

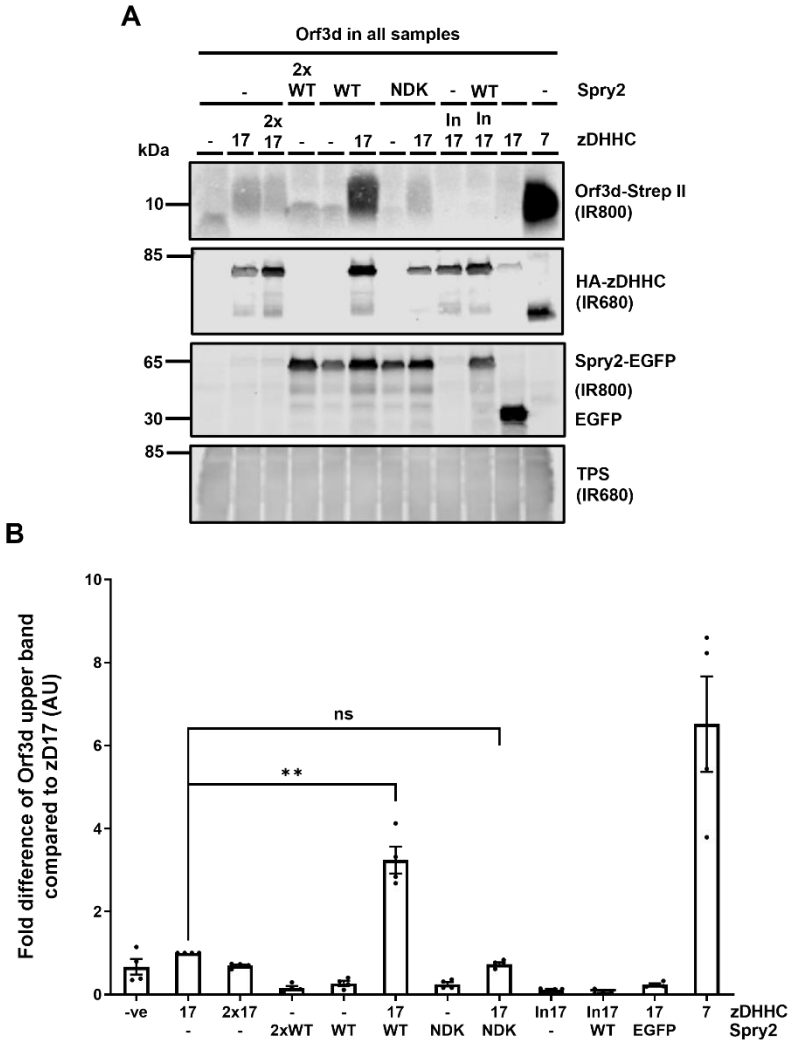


***Figure 5.1. Effect of zDHHC17 and Spry2 on the expression of Orf3d.*** *(A) HEK-293T cells were co-transfected with plasmids encoding for Strep-II tagged Orf3d WT, alongside HA-tagged zDHHC17 WT, zDHHS17 (In17) (as a negative control), or zDHHC7 (as a positive control), as well as EGFP-tagged Spry2 WT, Spry2* N211A/D214A/K223A (NDK), or EGFP-alone. R*epresentative images of the same immunoblots showing Strep-II tagged Orf3d (first panel; IR800), HA-tagged zDHHC/S enzyme (second panel; IR680), EGFP-tagged Spry2 (third panel; IR800), and a total protein stain (TPS) (fourth panel; IR680). The positions of the molecular weight markers (kDa) are shown on the left side of all immunoblots. (B) Graph showing the mean band intensity (± SEM) of Orf3d expression as a fold-difference to that of zDHHC17.* Error bars represent ± SEM. Each replicate is shown with filled circles. *Statistical significance was analysed using a one-way ANOVA with a Tukey's multiple comparisons test. ** denotes P < 0.01 and ns = non-significant (only select comparisons are illustrated), n = 4 for two independent experiments.*

### 5.2 Spry2 does not enhance the S-acylation of SNAP25 by zDHHC17

Other zDHHC enzymes such as zDHHC5 and zDHHC9, have been shown to require an activity modulating accessory protein, such as GCP16, for effective S-acylation activity (Ko et al., 2019, Nguyen et al., 2023). The results shown in figure 5.1 agreed with the hypothesis that Spry2 can enhance the action of zDHHC17, at least with respect to Orf3d. To investigate if this effect of Spry2 extends to other zDHHC17 substrates, a similar experiment was conducted using a well-characterised zDHHC17 substrate, SNAP25 (Lemonidis et al., 2014).

Figure 5.2 shows the S-acylation of SNAP25 by zDHHC17 in the presence of Spry2 using the PEG-acylation method. HEK-293T cells were co-transfected with plasmids encoding for mCherry-tagged (RFP) SNAP25, alongside EGFP-tagged Spry2 or EGFP alone (as a control), together with HA-tagged zDHHC17 or pEF-BOS-HA (as a control). Cells were incubated for 4 h with 100 μM of either palmitic acid-azide (+) or palmitic acid (-) as a control. Once palmitic acid-azide is incorporated on to the protein via S-acylation, alkyne-PEG5K (polyethylene glycol, 5 kDa) can be reacted with the azide group thereby increasing protein mass by approximately 5 kDa per attached fatty acid.

From the first panel of the representative immunoblot in figure 5.2, it can be seen that although zDHHC17 increased SNAP25 S-acylation, there was no further increase in SNAP25 S-acylation when Spry2 was also present (figure 5.2 B). Note that, as discussed in previous chapters, the expression of Spry2 is higher when co-expressed with zDHHC17. The S-acylation of Spry2 by zDHHC17 and the auto-acylation of the enzyme (which shows no change with or without Spry2) can also be observed in the second and third panels, respectively (figure 5.2 A). Together these results argue that Spry2 is not a general modulator of zDHHC17 enzymatic activity because it does not affect all substrates. This instead suggests that the effects of Spry2 are more specific to Orf3d. This experiment was only performed once with two replicates and so statistical analysis was not possible.

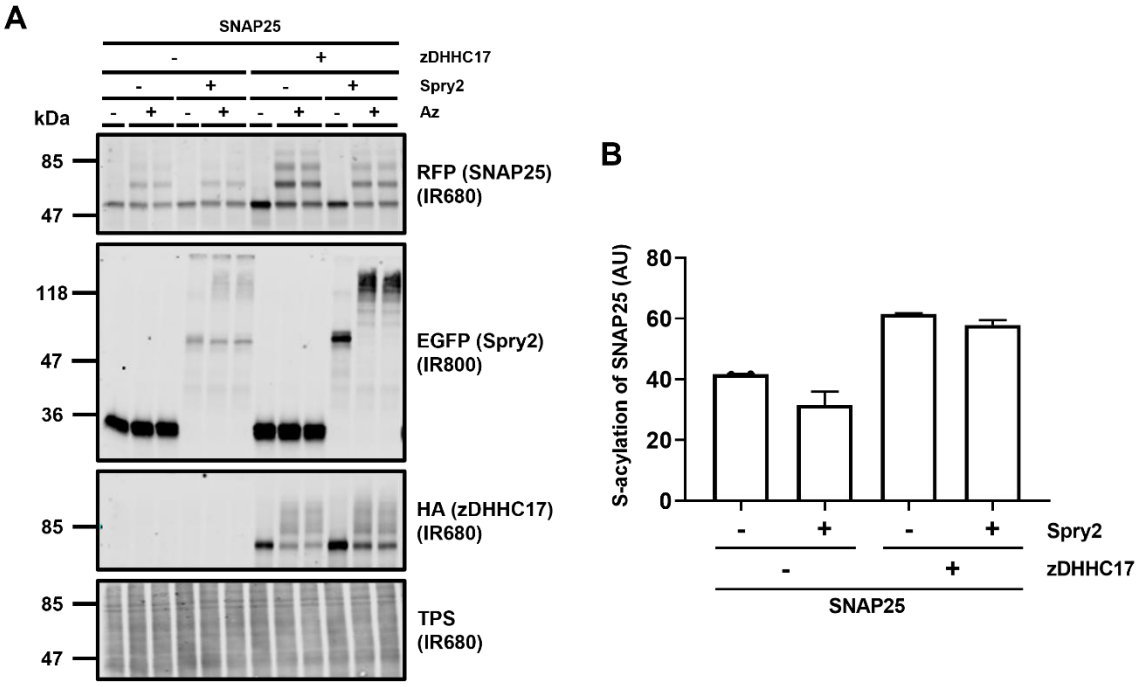


***Figure 5.2. S-acylation of SNAP25 by zDHHC17 in the presence of Spry2.*** *HEK-293T cells were co-transfected with plasmids encoding for mCherry-tagged SNAP25 alongside EGFP-tagged Spry2 or EGFP , and HA-tagged zDHHC17 or pEF-BOS-HA (as a control). Cells were incubated for 4 h with 100 μM of either palmitic acid-azide (+) or unconjugated palmitic acid (-). Once incorporated via S-acylation, alkyne-PEG5K (polyethylene glycol, 5 kDa) conjugates through alkyne-azide click chemistry, thereby increasing protein mass by approximately 5 kDa per fatty acid attachment.* R*epresentative images showing mCherry-tagged SNAP25 (first panel; IR680), EGFP-tagged Spry or EGFP (second panel; IR800), HA-tagged zDHHC17 (third panel; IR680), and a total protein stain (TPS) (fourth panel; IR680). The of the molecular weight markers (kDa) are shown on the left side of all immunoblots. n = 2 from one experiment.*

### 5.3 The effects of SPRED proteins and Spry2 mutants on Orf3d expression

Although the results of figure 5.1 indicated that Spry2 enhanced the effects of zDHHC17 on Orf3d expression, a similar effect was not seen for S-acylation of SNAP25. This initial data reveals a potential unique connection between Orf3d, zDHHC17 and Spry2. To further explore the interaction between the three proteins, additional constructs were tested for their efficacy in enhancing the zDHHC17-mediated increase in Orf3d expression. These constructs included Spry2 P154A, Spry2 C265/268A (DM) and Spry2 N211A/D214A/K223A (figure 5.3 A). In addition, the effects of SPRED1/2/3 proteins on Orf3d expression were also investigated, as other work in this thesis (chapter 3 & 4) has identified differences in the S-acylation of these proteins and their interactions with zDHHC17. To compare the effects of these proteins on Orf3d expression, similar experiments were undertaken to that shown in figure 5.1.

In figure 5.3 A/B, HEK-293T cells were transfected with plasmids encoding for Strep-II tagged Orf3d WT, as well as EGFP-tagged Spry2 WT, Spry2 C265/268A (DM), Spry2 P154A (P154A) or Spry2 N211A/D214A/K223A (NDK) with and without HA-tagged zDHHC17. HA-tagged zDHHC7 was also used with and without Spry2 as a positive control; these zDHHC7 samples are shown in representative immunoblots but not included in quantified graphs. The results of these experiments showed that the DM and P154A mutants were able to enhance Orf3d levels but to a lower extent than that of Spry2 WT. In contrast, the NDK mutant did not have any stabilisation effect on Spry2, a result which was also seen in figure 5.1 above. This experiment was only performed once, and so statistical comparisons are not shown in the figure. The data in figure 5.3 C/D show results from HEK-293T cells that were transfected with plasmids encoding for Strep-II tagged Orf3d WT, together with EGFP-tagged Spry2 WT, SPRED1 WT, SPRED2 WT or SPRED3 WT, and with or without HA-tagged zDHHC17. HA-tagged zDHHC7 was also used with and without Spry2 as a positive control; and is shown in representative immunoblots but not included in quantified graphs. Interestingly, the stabilisation of Orf3d was only seen with Spry2 and SPRED3 (co-expressed with zDHHC17), whereas SPRED1 and SPRED2 had no stabilising effect on the Orf3d protein. The level of increased Orf3d expression was not significantly different between cells transfected with Spry2 and SPRED3. The results of chapter 3 indicated that Spry2 and SPRED3 are effectively S-acylated by zDHHC17 (figure 3.4), whereas SPRED1 and SPRED2 are not (figure 3.3), suggesting that effective S-acylation of Spry/SPRED proteins could be a required for their effects on the zDHHC17-mediated increase in expression of Orf3d.

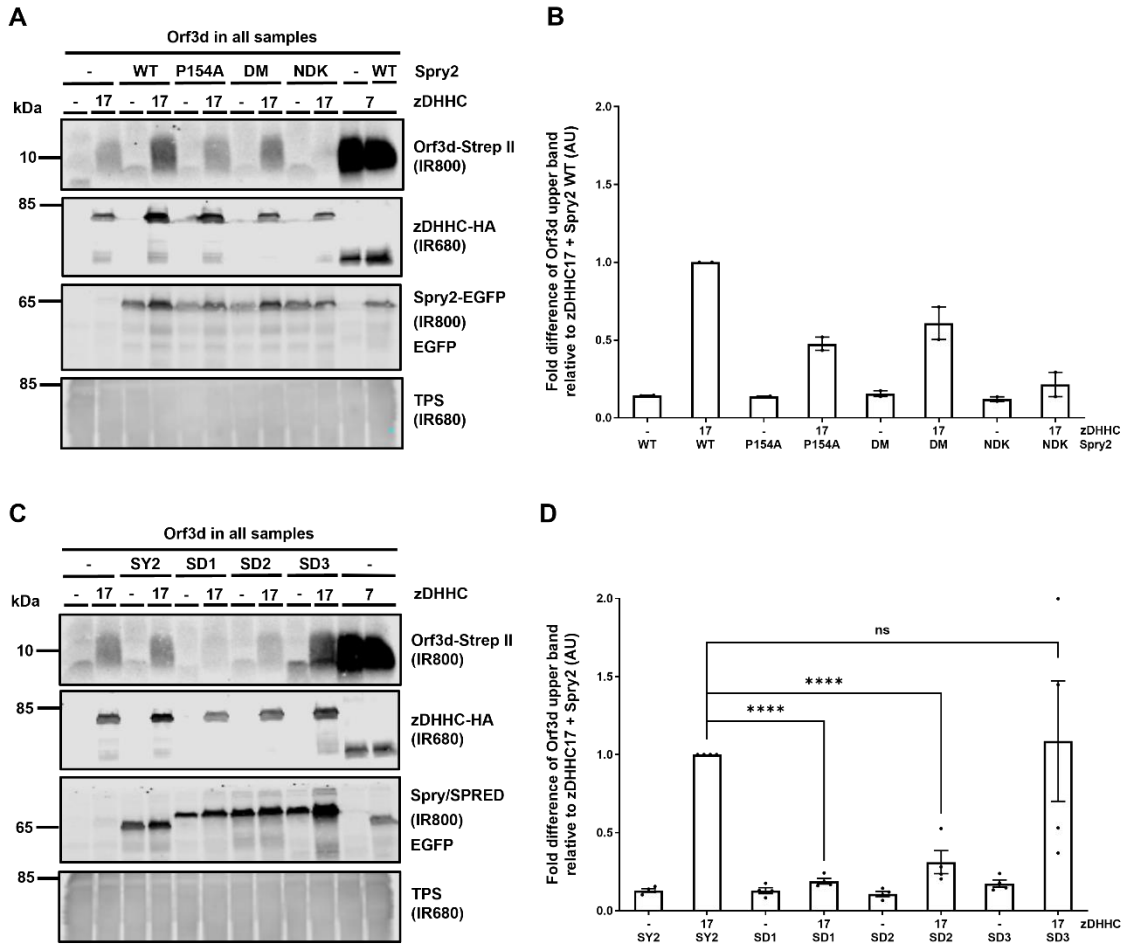


***Figure 5.3. Effect of Spry2 S-acylation deficient mutants and SPRED1/2/3 on the expression of Orf3d.*** *(A) HEK-293T cells were co-transfected plasmids encoding for with Strep-II tagged Orf3d WT, with HA-tagged zDHHC17 WT or zDHHC7 WT, and either EGFP-tagged Spry2 WT (SY2), Spry2 C265A/268A (DM), Spry2 P154A (P154A), or Spry2 N211A/D214A/K223A (NDK). Representative images of the same samples showing Strep-II tagged Orf3d (first panel; IR800), HA-tagged zDHHC17 or zDHHC7 (second panel; IR680), EGFP-tagged Spry/SPRED (third panel; IR800), and a total protein stain (TPS) (fourth panel; IR680). The positions of the molecular weight markers (kDa) are shown on the left side of all immunoblots. (B) Graph showing the mean band intensity (± SEM) of Orf3d as a fold-difference to that of with samples containing zDHHC17 + Spry2 WT. n = 2 from one experiment. (C) HEK-293T cells were co-transfected with plasmids encoding for Strep-II tagged Orf3d WT with HA-tagged zDHHC17 WT or zDHHC7 WT, and either EGFP-tagged Spry2 WT (SY2), SPRED1 (SD1), SPRED2 (SD2) or SPRED3 (SD3). Representative images of the same samples are shown for Strep-II tagged Orf3d (first panel; IR800), HA-tagged*

*zDHHC17 or zDHHC7 (second panel; IR680), EGFP-tagged Spry/SPRED (third panel; IR800), and a total protein stain (TPS) (fourth panel; IR680). The positions of the molecular weight markers (kDa) are shown on the left side of all immunoblots. (D) Graph showing the mean band intensity (± SEM) of Orf3d expression as a fold-difference to that of samples containing both zDHHC17 + Spry2 WT. Error bars represent ± SEM. Each replicate is shown with filled circles. Statistical significance was analysed using unpaired t-tests compared to zDHHC17 + Spry2 WT. **** denotes P < 0.0001 and ns = non-significant (only select comparisons are illustrated), n = 4 for two independent experiments.*

## 5.4 Several zDHHC enzyme isoforms are capable of enhancing Orf3d levels both with and without Spry2

In line with the overall focus of the thesis, the initial analysis in this chapter has been on zDHHC17. To extend on this initial analysis, a screen of all 23 zDHHC enzymes was conducted to identify which enzyme isoforms had an effect on the expression of Orf3d. HEK-293T cells were co-transfected with Strep-II tagged Orf3d WT together with HA-tagged zDHHC1-23 and either EGFP-tagged Spry2 WT or EGFP. Proteins were resolved by SDS-PAGE and examined by immunoblotting, with zDHHC7 as a comparative positive control on each immunoblot. All values are given as a fold-difference relative to the expression of Orf3d in the presence of zDHHC7. This experiment was conducted only once, and so no statistical analysis was possible.

Immunoblots are shown in figures 5.4 A-E, with quantified data shown in figures 5.4 F-J. The expression of either zDHHC 2, 3, 7, 15, or 17 was associated with the greatest increases in Orf3d expression. zDHHC 2, 3, and 15 showed high Orf3d expression without Spry2, whereas zDHHC17 showed lower levels of Orf3d expression without Spry2. For each of these enzymes, when Spry2 was also co-expressed there was a further increase in Orf3d expression. zDHHC7 showed the highest expression in Orf3d expression both with and without Spry2. No other zDHHC enzymes were able to effectively enhance Orf3d expression with or without Spry2. It should also be noted that Cherry-Spry2 used in this experiment was not well expressed explaining why it does not enhance the levels or Orf3d (panels D and I).

Although only performed once, this zDHHC screen has been undertaken by Dr. Christine Salaun with similar results (not shown).

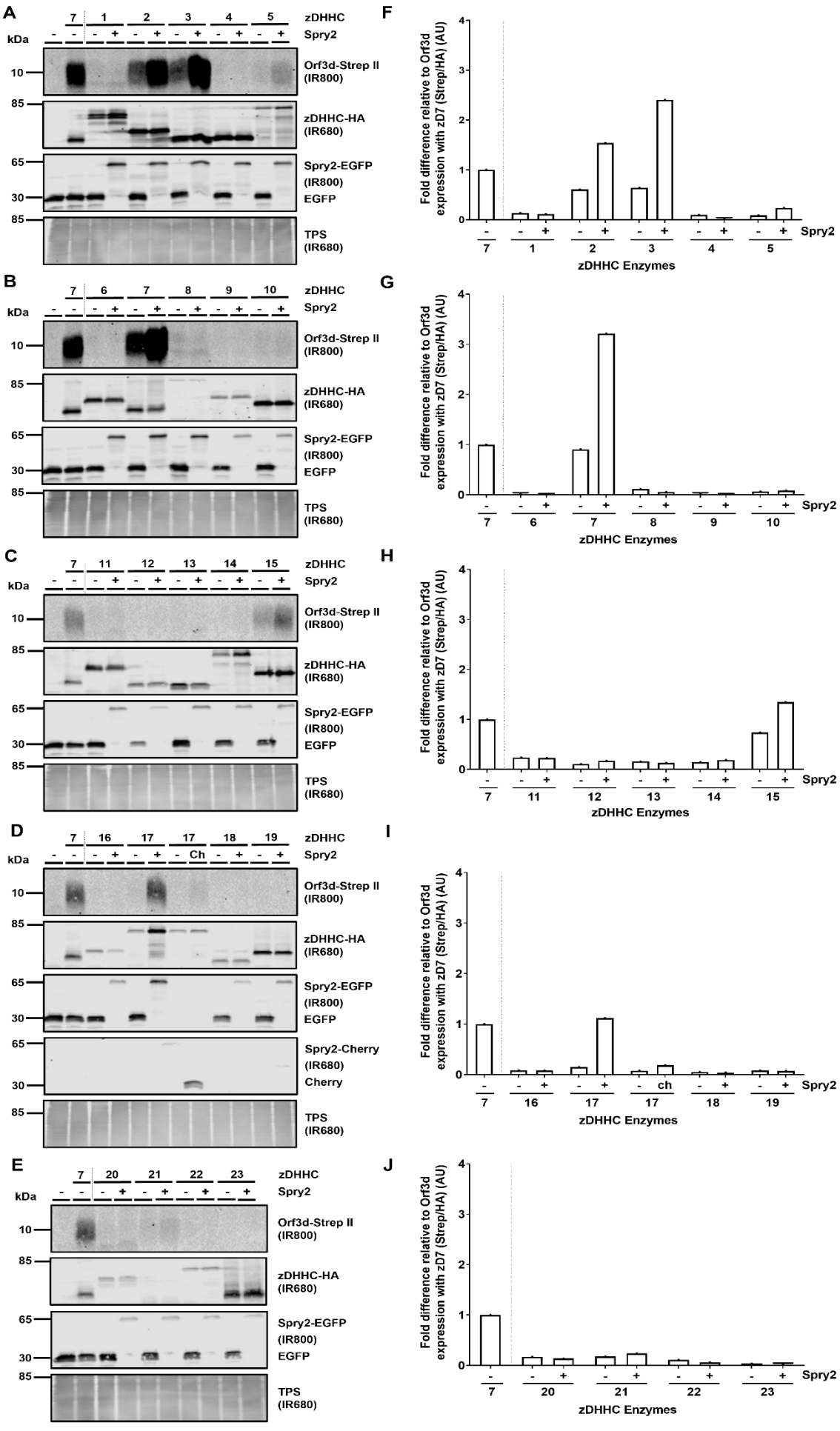
A
zDHHC
Spry2
kDa
Orf3d-Strep II (IR800)
zDHHC-HA (IR680)
Spry2-EGFP (IR800)
EGFP
TPS (IR680)
B
C
D
Spry2-Cherry (IR680)
Cherry
E
F
G
H
I
J
Fold difference relative to Orf3d expression with zD7 (Strep/HA) (AU)
zDHHC Enzymes

***Figure 5.4. Analysis of the effects of all 23 zDHHC enzymes on Orf3d expression with and without Spry2***

*(A-E) HEK-293T cells were transfected with plasmids encoding for Strep-II -tagged Orf3d WT together with EGFP-tagged Spry2 or EGFP (or Cherry-tagged Spry2, and the respective HA-tagged zDHHC enzymes – (A) zDHHC 1-5, (B) zDHHC 6-10, (C) zDHHC 11-15, (D) zDHHC 16-19, (E) zDHHC 20 – 23, (A-E). All immunoblots also included zDHHC7 (as a comparative control). Representative images showing Strep II-tagged Orf3d (first panel; IR800), HA-tagged zDHHC enzymes (second panel; IR680), EGFP-tagged Spry2 or EGFP alone (third panel; IR800), and a total protein stain (TPS) (bottom panel; IR680). Cherry-tagged Spry2 is also shown (panel D only, fourth panel; IR680). The positions of the molecular weight markers (kDa) are shown on the left side of all immunoblots. (F-J) Graphs showing the mean fold change in Orf3d expression with different zDHHC enzymes in the presence or absence of Spry2 – (F) zDHHC 1-5, (G) zDHHC 6-10, (H) zDHHC 11-15, (I) zDHHC 16-19, (J) zDHHC 20 – 23. The quantified data is normalised relative to the expression of Orf3d with zDHHC7. n = 1 for a single experiment.*

### 5.5 Spry2 does not influence the zDHHC enzymes mediated stability of Orf3d

Previously published data has shown that zDHHC17 can stabilise Spry2 (Locatelli et al., 2020), which is further expanded on in figures 3.13 and 3.14 of this thesis, which show that Spry2 can also stabilise zDHHC17. Added to this, the results of figure 5.4 revealed that the enhancement of Orf3d expression is unique to certain zDHHC enzymes, and also that the effect of Spry2 is seen with all of these enzymes. The initial hypothesis that we were investigating in this chapter was that effects of Spry2 on zDHHC17 expression might promote subsequent changes in Orf3d S-acylation. However, the results in this chapter so far suggest that this hypothesis may not be correct as Spry2 exerts effects when expressed together with any enzyme that can modify Orf3d. Therefore, an alternative hypothesis is that Spry2 may be preventing the degradation of Orf3d or changing the conformation of the protein to enhance its S-acylation.

To further investigate the effects of Spry2 on Orf3d degradation, cycloheximide chase assays were performed using the zDHHC enzymes identified in figure 5.4. For this, HEK-293T cells were transfected with plasmids encoding for Strep II tagged Orf3d WT, with or without EGFP-tagged Spry2, and in the presence of either HA- tagged zDHHC2 (figure 5.5 A), zDHHC3 (figure 5.5 B), zDHHC7, (figure 5.5 C), or zDHHC17 (figure 5.5 D). Cells were subsequently incubated with 50 µg/ml cycloheximide for either 0, 2.5, or 5 hours before lysates were resolved by SDS-PAGE and analysed by immunoblotting. In each independent experiment, Orf3d expression at each timepoint was quantified relative to the respective 0-hour sample.

For all zDHHC enzymes tested there was a greater than 60% loss of Orf3d expression after 5 hours. As can be seen from the quantified data (figure 5.5 E-H), Spry2 had no observable effects on Orf3d degradation at any time point or with any zDHHC enzyme. Therefore, although Spry2 expression increases the steady state levels of Orf3d, cycloheximide experiments suggest that this is not due to the inhibition of its degradation. Instead, it might be that Spry2 is enhancing S-acylation of Orf3d by altering its conformation to make it more accessible to zDHHC enzymes.

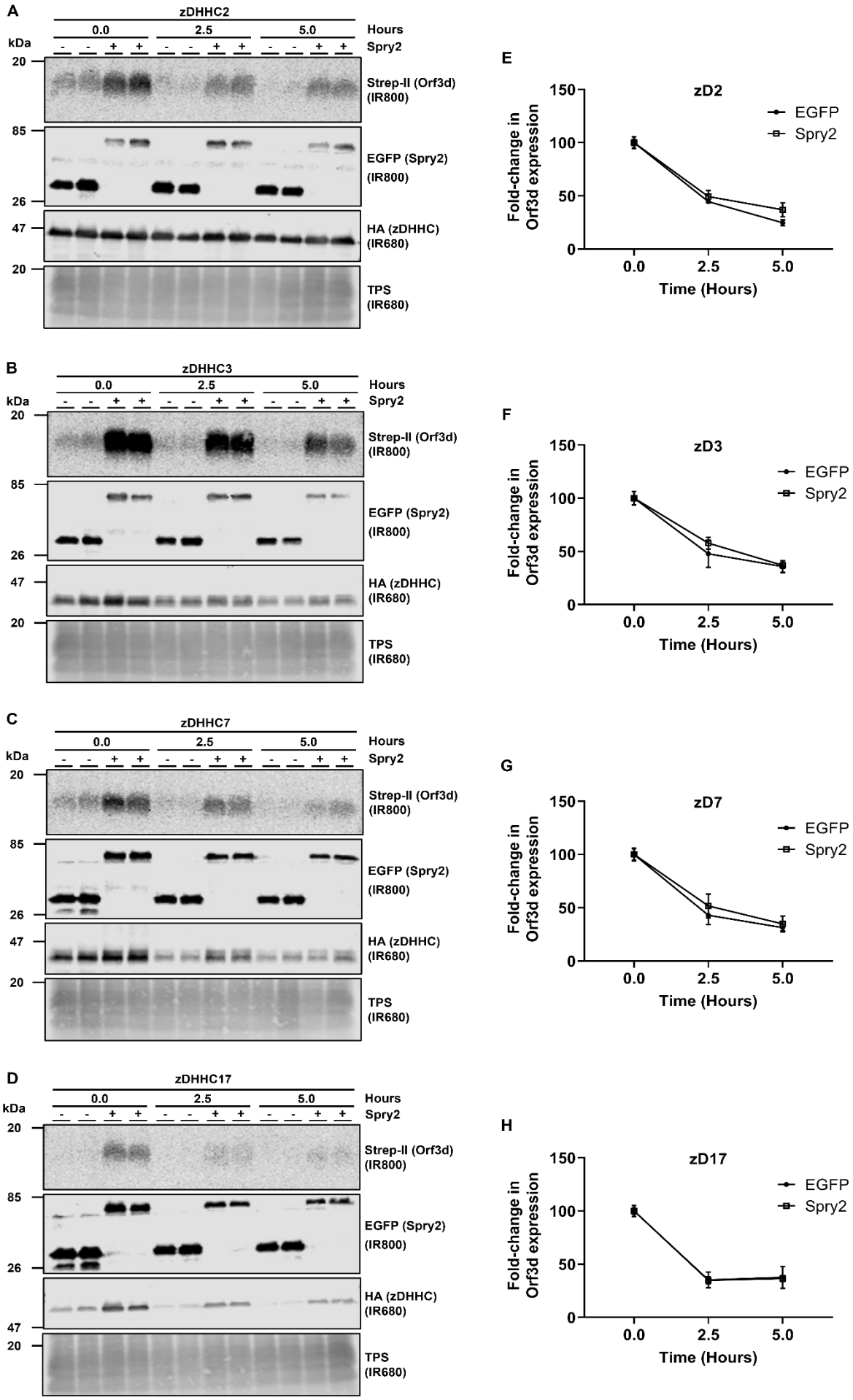
A
zDHHC2
0.0
2.5
5.0
Hours
kDa
Spry2
20
85
26
47
20
Strep-II (Orf3d)
(IR800)
EGFP (Spry2)
(IR800)
HA (zDHHC)
(IR680)
TPS
(IR680)
B
zDHHC3
C
zDHHC7
D
zDHHC17
E
zD2
F
zD3
G
zD7
H
zD17
Fold-change in
Orf3d expression
150
100
50
0
Time (Hours)
EGFP
Spry2

***Figure 5.5. Turnover of Orf3d in the presence of zDHHC 2, 3, 7, & 17, with and without Spry2.*** *(A-D) Western blots showing the expression of Orf3d in the presence of zDHHC enzymes, over 2.5- and 5-hours following addition of cycloheximide. HEK-293T cells were transfected with plasmids encoding for Strep-II-tagged Orf3d WT, together with EGFP-tagged Spry2 or EGFP, and HA-tagged zDHHC enzymes – (A) zDHHC2, (B) zDHHC3, (C) zDHHC7, (D) zDHHC17. Representative images showing Strep-II-tagged Orf3d (first panel; IR800), EGFP-tagged Spry2 or EGFP alone (second panel; IR800), HA-tagged zDHHC enzymes (third panel; IR680), and a total protein stain (TPS) (fourth panel; IR680). The positions of the molecular weight markers (kDa) are shown on the left side of all immunoblots. (E-H) Quantified data showing the reduction in Orf3d expression at different time points following addition of cycloheximide relative to time 0. (E) zDHHC2, (F) zDHHC3, (G) zDHHC7, (H) zDHHC17, in the presence/absence of Spry2. Orf3d (IR800) intensity values were divided by the corresponding intensity value of the TPS in each sample/lane (HA/TPS). Statistical significance was analysed using a two-way ANOVA with Sidak's multiple comparisons test. n = 5/6, for three independent experiments. Comparing the expression of Orf3d in the presence of Spry2 WT at each time point there was no significant difference at any time point.*

### 5.6 Bioinformatic analysis of Orf3d structure

Understanding the structural features of proteins is important to fully decipher their interactions with other proteins. For instance, Spry/SPRED proteins were identified through peptide array screening for potential zDHHC17 substrates based on the presence of a zDABM sequence (Lemonidis et al., 2017a). For Orf3d, little is currently known about its structure or function. Since Orf3d is a novel protein with no known homology to other annotated proteins, current bioinformatic/proteomic databases do not contain substantial and/or reliable reference data. For example, the UniProt database provides an “annotation score” based on a heuristic measure of annotation content for a UniProtKB entry or proteome. Bioinformatic entries for both Spry2 (SPY2_HUMAN) and zDHHC17 (ZDH17_HUMAN) score a rating of 5/5 for database content, whereas Orf3d (ORF3D_SARS2) only scores 1/5 (Consortium, 2022).

In figure 5.6.1, secondary structure predictions of Orf3d were generated using the UCL bioinformatics group PSIPRED Server workbench 4.0 (Jones, 1999, Buchan and Jones, 2019). This gave information about amino acid properties (figure 5.6.1 A) and predicted a secondary structure based on the properties of these residues (figure 5.6.1 B/C). For reference, the Orf3d-2 isoform initiates from the methionine at position 25. It can be seen from figure 5.6.1 B/C, that the N-terminal end of Orf3d has a propensity to be disordered, followed by downstream regions that contain multiple alpha helices separated by disordered regions. Other notable features in figure 5.6.1 A are a higher density of aromatic/cysteine residues at the N and C terminal ends (shown in blue), and a polar region between amino acids E14 to E24 (shown in red). It could also be inferred that the region between aa M25 to P50 has a higher concentration of small non-polar/hydrophobic residues (show in orange/green respectively).

Furthering the information in figure 5.6.2, AlphaFold monomeric protein structure predictions of both full length Orf3d (55 aa) and the truncated isoform Orf3d-2 (33 aa) were generated using Google ColabFold AlphaFold2 (Phenix version) (Mirdita et al., bioRxiv, 2021) based on AlphaFold by DeepMind and EMBL-EBI (Jumper et al., 2021; Varadi et al., 2022). It can be seen from figure 5.6.2, that in good agreement with the PSIPRED secondary structure prediction (figure 5.6.1), Orf3d is modelled to contain two alpha helices both separated and flanked by a disordered region. Orf3d-2 (which is 22 aa shorter at the N-terminus) is only modelled to contain the second distal alpha helix.

The information from both figures 5.6.1 and 5.6.2 both predict the presence of an alpha helix within both Orf3d and Orf3d-2. The residues within the AlphaFold-predicted helix of Orf3d (aa 30-47 aa) were further analysed by generating a helical wheel projection using the NetWheels online application (figure 5.6.3) (Mól, Castro and Fontes, 2018). The projection in figure 5.6.3 B revealed the presence of oppositely charged sides to the alpha helix, with one side being more polar and the other side predominantly non-polar. Also, the three cysteine residues within this helix are situated on the non-polar face of the helix.

The properties of Orf3d can be further analysed by analysing the hydrophobicity of the protein throughout the sequence. In figure 5.6.4, the Kyte & Doolittle Hydropathy scale (Kyte and Doolittle, 1982) was used to generate a hydropathy plot via the ProtScale resource from the Swiss Bioinformatics Resource Portal, ExPASy (Wilkins et al., 1999), where a hydropathy score of > 0 indicates hydrophobicity and a score of < 0 indicates hydrophilicity. In Orf3d, amino acids at positions 13 – 28 all gave a hydropathy score of < 0, with a minimum score of -2.711 at position 19. Amino acids at positions 29 – 53 gave a hydropathy score of > 0, with a maximum score of 2.756 at position 39.

To see if a featured-based function could be predicted for Orf3d, the FFPRED 3 feature (Cozzetto et al., 2016) from the UCL bioinformatics group PISPRED Server workbench 4.0 (Jones, 1999; Buchan and Jones, 2019) to assign Gene Ontology terms (Ashburner et al., 2000; Consortium et al., 2023) to eukaryotic protein chains was utilised. The outputs from the server, shown in figure 5.6.5, generated predictions for potential biological processes, molecular function, and a cellular component, which are given in figure 5.6.5. Although more predictions were generated only those with the highest degree of reliability and probability ( > 0.9) are shown. This included biological process predictions for Orf3d in the regulation of nitrogen compound metabolic processes, the regulation of RNA metabolic processes, and/or the regulation of gene expression. The output also included molecular function predictions which includes roles for Orf3d in zinc ion binding, ion transmembrane transporter activity, nucleic acid binding, and/or DNA binding. In addition, cellular component predictions were of Orf3d being associated with membranes, mitochondria, mitochondrial membranes, or as an integral component of membranes (figure 5.6.5).

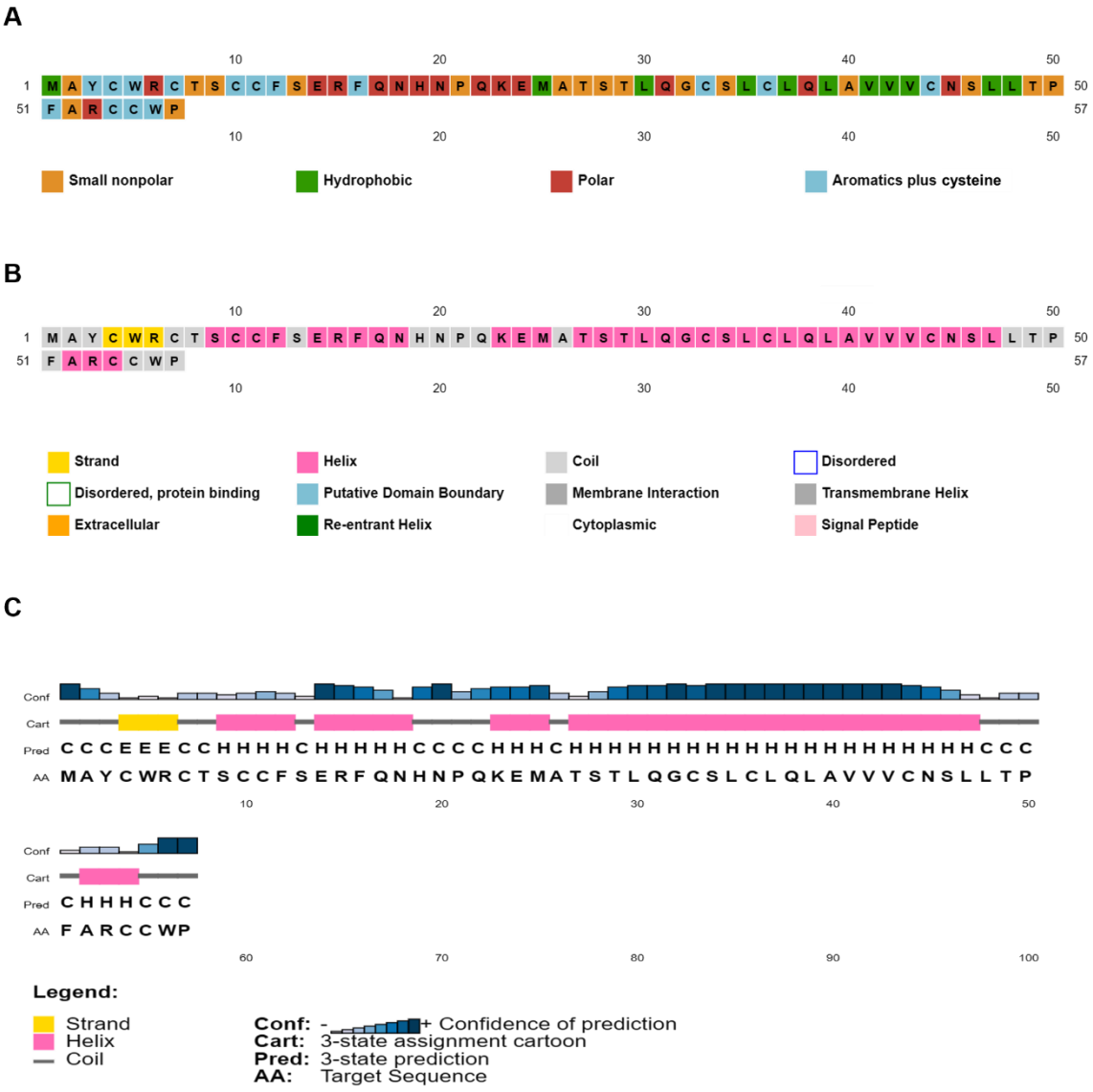


***Figure 5.6.1. Residue properties and secondary structure prediction of Orf3d.*** *Secondary structure prediction of Orf3d; UniProt: P0DTG0 (ORF3D_SARS2). Generated using the UCL bioinformatics group PISPRED Server workbench 4.0 (Jones, 1999, Buchan and Jones, 2019). (A) Sequence plot of Orf3d illustrating amino acid types and properties. (B) Sequence plot of Orf3d illustrating secondary structure prediction. (C) Cartoon schematic of Orf3d secondary structure prediction including confidence of prediction.*

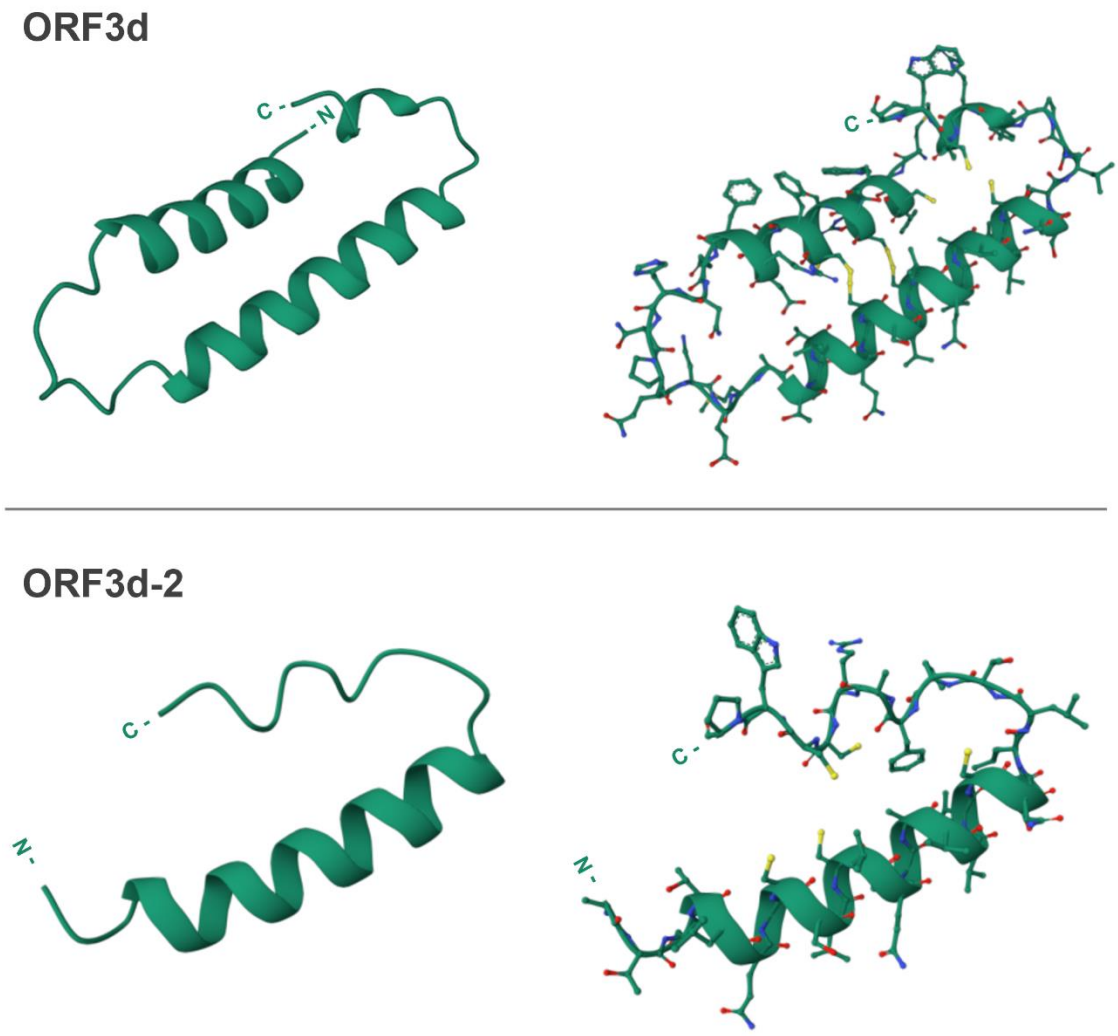


***Figure 5.6.2. AlphaFold predictions of the structure of Orf3d and Orf3d-2.*** *(A) AlphaFold protein structure prediction models of full length Orf3d (55 aa) and truncated isoform Orf3d-2 (33 aa), UniProt: P0DTG0 (ORF3D_SARS2 Monomeric prediction modelled using Google ColabFold AlphaFold2 (Phenix version) (Mirdita et al., bioRxiv, 2021) based on AlphaFold by DeepMind and EMBL-EBI (Jumper et al., 2021; Varadi et al., 2022). Orf3d/d-2 protein chain is shown in green with N- and C-terminal ends indicated.*

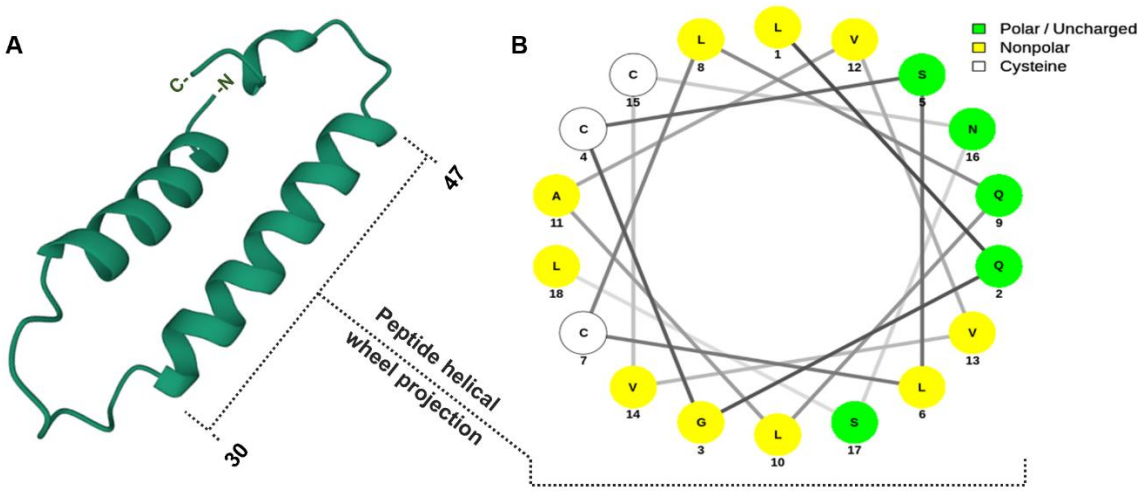


***Figure 5.6.3. NetWheels projections of the distal alpha-helix of Orf3d.*** *(A) AlphaFold protein structure prediction models of full length Orf3d (55 aa); UniProt: P0DTG0 (ORF3D_SARS2) (also shown in figure 5.7). Monomeric prediction modelled using Google ColabFold AlphaFold2 (Phenix version) (Mirdita et al., bioRxiv, 2021) based on AlphaFold by DeepMind and EMBL-EBI (Jumper et al., 2021; Varadi et al., 2022). Orf3d protein chain is shown in green with N- and C- terminal ends indicated. (B) Helical wheel projection of the predicted "distal" alpha helix of Orf3d (sequence 30-47 aa - LQGCSLCLQLAVVVCNSL) generated using the NetWheels online application (Mól et al., 2018). Cysteine residues C33, C36, and C45 are indicated in white, with non-polar residues in yellow, and polar residues in green.*

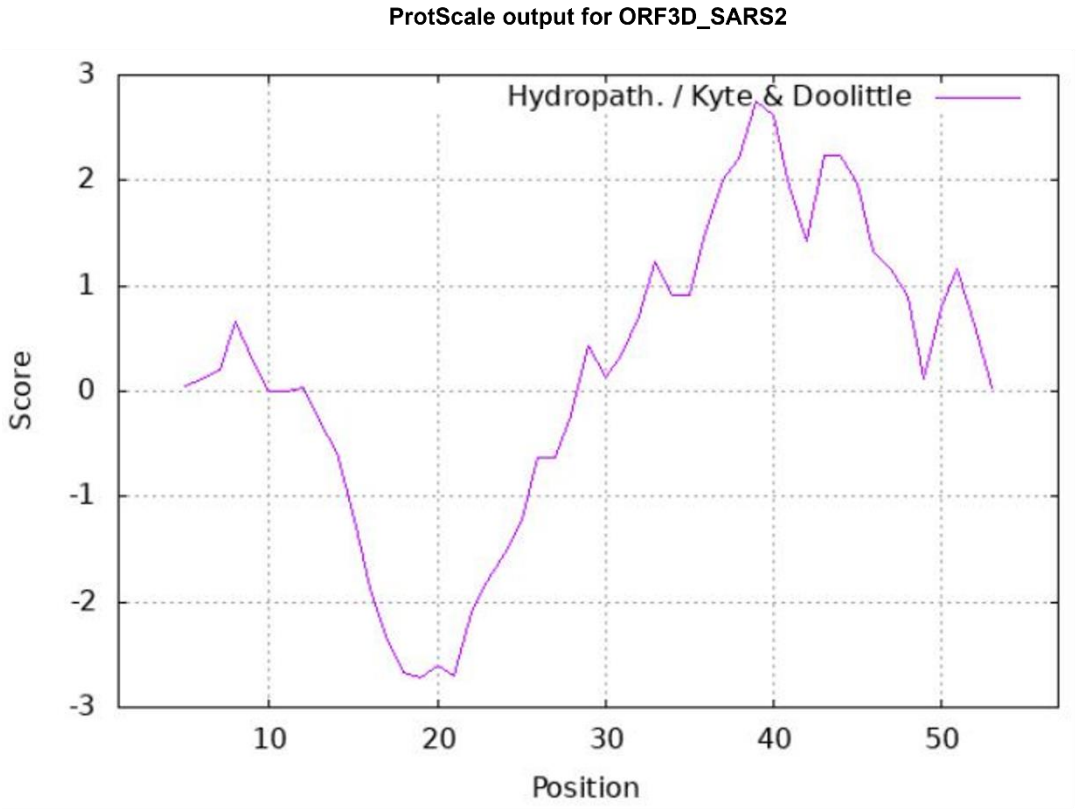


MAYCWRCTSCCFSERFQNHNPQKEMATSTLQGCSLCLQLAVVVCNSLLTPFARCCWP

Using the scale Hydropath. / Kyte & Doolittle, the individual score values for the 20 amino acids:

| | | | | | |
|---|---|---|---|---|---|
| Ala: 1.800 | Arg: -4.500 | Asn: -3.500 | Asp: -3.500 | Cys: 2.500 | Gln: -3.500 |
| Glu: -3.500 | Gly: -0.400 | His: -3.200 | Ile: 4.500 | Leu: 3.800 | Lys: -3.900 |
| Met: 1.900 | Phe: 2.800 | Pro: -1.600 | Ser: -0.800 | Thr: -0.700 | Trp: -0.900 |
| Tyr: -1.300 | Val: 4.200 : -3.500 : -3.500 : -0.490 | | | | |

***Figure 5.6.4. Kyte & Doolittle hydropathy plot of Orf3d.*** *Evaluation of the hydrophilicity and hydrophobicity of a Orf3d along its amino acid sequence using the Kyte & Doolittle hydropathy scale (Kyte and Doolittle, 1982). Hydropathy plot generated using the ProtScale resource from Swiss bioinformatics resource portal, ExPASy (Wilkins et al., 1999).*

| Feature-based function prediction - FFPred 3 | |
|---|---|
| **Name** | **Gene Ontology (GO) term** |
| **Biological process predictions** | |
| Regulation of metabolic process | GO:0019222 |
| Regulation of nitrogen compound metabolic process | GO:0051171 |
| Regulation of RNA metabolic process | GO:0051252 |
| Regulation of gene expression | GO:0010468 |
| **Molecular function predictions** | |
| Zinc ion binding | GO:0008270 |
| Ion transmembrane transporter activity | GO:0015075 |
| Nucleic acid binding | GO:0003676 |
| DNA binding | GO:0003677 |
| **Cellular componnent predicitons** | |
| Mitochondrial membrane | GO:0031966 |
| Membrane | GO:0016020 |
| Mitochondrion | GO:0005739 |
| Integral component of membrane | GO:0016021 |

***Figure 5.6.5. FFPred3 predictions of Orf3d function.*** *Prediction of Orf3d biological processes, molecular function, and cellular component using the FFPRED 3 feature (Cozzetto et al., 2016) from the UCL bioinformatics group PISPRED Server workbench 4.0 (Jones, 1999, Buchan and Jones, 2019) to assign Gene Ontology terms (Consortium et al., 2023, Ashburner et al., 2000) to eukaryotic protein chains. Functions generated above those that meet both a high support vector machine (SVM) reliability and a probability greater than 0.900.*

### 5.7 Spry2 can also enhance the expression levels of Orf3d-2

As previously discussed, two different isoforms of Orf3d might be expressed by SARS-CoV-2. Orf3d is made up of 57 amino acids, whereas Orf3d-2 initiates downstream at Met 25, making this isoform 33 amino acids in length. Current experimental evidence has even suggested that Orf3d-2 is more likely to be expressed than the longer isoform (Nelson et al., 2020; Finkel et al., 2021). Results in figure 5.6.2, indicate that Orf3d-2 retains the secondary structure of Orf3d despite being shorter in length. It was therefore of interest to compare the effects of zDHHC enzymes and Spry2 on Orf3d-2 and Orf3d expression.

HEK-293T cells were transfected with either C-terminally tagged Orf3d-Myc WT or Orf3d-2-Myc WT, together with either EGFP-tagged Spry2 or EGFP, and either zDHHC7 or pEF-BOS-HA. zDHHC7 was used in these experiments as previous results indicated that this enzyme promoted the greatest increase in expression of Orf3d (figure 5.4 B). To ensure that the previously presented results were due to zDHHC/Spry2 specific effects and not due to unexpected off target effects of the Strep-II plasmid (pLXV-EF1alpha-2xStrep-SARS-CoV-2-orf3b-IRES-Puro). A different plasmid vector (pcDNA3.1 Myc-His) was used in these experiments to express both Orf3d and Orf3d-2 with a C-terminal Myc-tag (and not an N-terminal Strep-II tag as before). Proteins were resolved by SDS-PAGE and analysed by Western blotting, and for quantification all mean intensity values were normalised to the highest value on each immunoblot.

The results of figure 5.7 reveal that expression of Orf3d-2 was enhanced by zDHHC7 to a similar level as seen for Orf3d. Both Orf3d and Orf3d-2 also exhibited a further increase in expression in the presence of both zDHHC7 and Spry2, with Orf3d-2 showing a greater increase in expression than Orf3d in these conditions. In contrast, neither Orf3d nor Orf3d-2 showed an increase in expression when co-transfected with Spry2 alone.

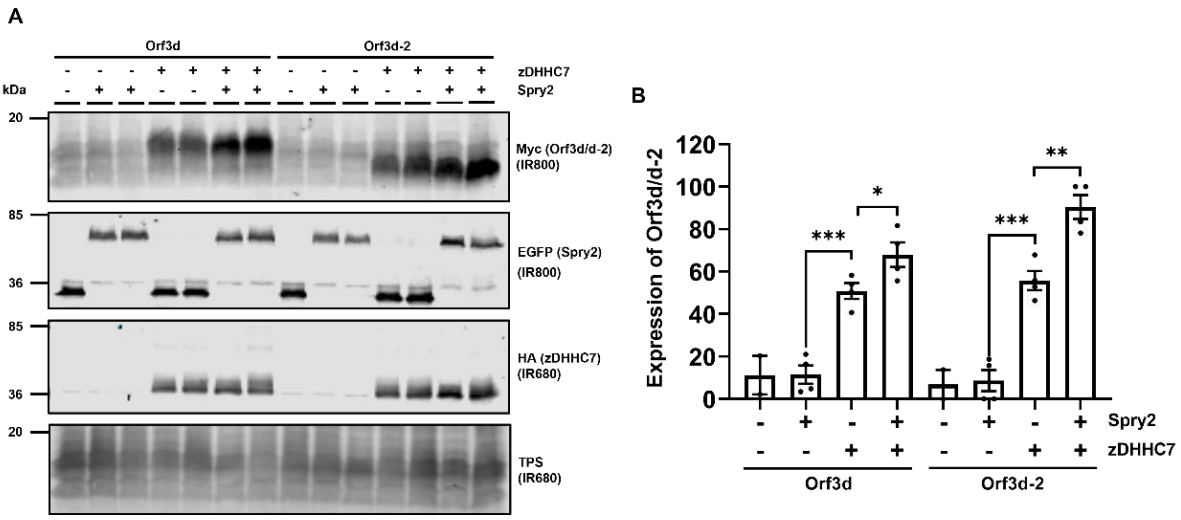


***Figure 5.7. Spry2 can also enhance the expression of Orf3d-2.*** *(A) HEK-293T cells were co-transfected with HA-tagged zDHHC7 WT or pEF-BOS-HA, together with plasmids encoding for C-terminal Myc-tagged Orf3d WT or Orf3d-2 WT, and either EGFP-tagged Spry2 or EGFP. Representative images of the same samples showing Myc-tagged Orf3d/d-2 (first panel; IR800), EGFP-tagged Spry2 or EGFP (second panel; IR800), HA-tagged zDHHC7 (third panel; IR680), and a total protein stain (TPS) (bottom panel; IR680). The positions of the molecular weight markers (kDa) are shown on the left side of all immunoblots. (B) Graph showing the expression of Orf3d and Orf3d-2 in the presence and absence of Spry2 and zDHHC7. Mean intensity values were normalised to the highest value on each immunoblot. Error bars represent ± SEM. Each replicate is shown with filled circles. All differences were analysed by unpaired t-test. *** denotes $p < 0.001$, ** denotes $p < 0.01$, * denotes $p < 0.05$. n = 4, for two independent experiments.*

### 5.8 Cysteine substitutions of Orf3d reveal residues critical for expression.

The results in this chapter have shown that expression of Orf3d is enhanced by zDHHC enzyme co-expression. To confirm that these changes in expression are linked to Orf3d S-acylation, cysteine to alanine substitution constructs of Orf3d were generated (figure 5.8 A).

HEK-293T cells were co-transfected with HA-tagged zDHHC7 WT along with plasmids encoding for Strep-II tagged Orf3d WT, Orf3d M1 (C4/7/10/11A), Orf3d M2 (C33/36/44A), or Orf3d M3 (C54/55A), as well as EGFP-tagged Spry2 or EGFP (figure 5.8). Lysates were resolved by SDS-PAGE and analysed by western blotting (figure 5.8 C), where all mean intensity values were normalised to the highest value on each immunoblot. A schematic representation of the three Orf3d Cys mutants (M1, M2, & M3) is shown in figure 5.8 A. The mutant constructs were generated in groups where: M1 has the initial four cysteines (C4/7/10/11A) contained within the first helix/strand region substituted, M2 has the next three cysteines (C33/36/44A) replaced, which would be in a second distal helix region, and M3 has final two cysteines at the C-terminal end of the protein (C54/55A) substituted (figure 3.8 B).

The results in figure 5.8 D show that both Orf3d M1 and M2 mutants are effectively stabilised by zDHHC7, with M1 showing a similar level of expression as the WT construct and M2 showing a greater level of expression. In addition, both of these mutants displayed a further significant increase in expression in the presence of Spry2. In contrast, the M3 mutant was expressed at very low levels when co-transfected with zDHHC7 and also showed no change with Spry2 (figure 3.8 D).

Interestingly, each of the different Orf3d mutant constructs exhibited a different molecular mass band on SDS gels, which might reflect changes in S-acylation (figure 3.8 C). Orf3d WT showed the highest molecular weight, M1 (four Cys mutated) showed the lowest molecular weight, with M2 (three Cys mutated), and M3 (two Cys mutated) exhibiting intermediate sizes (figure 3.8 C).

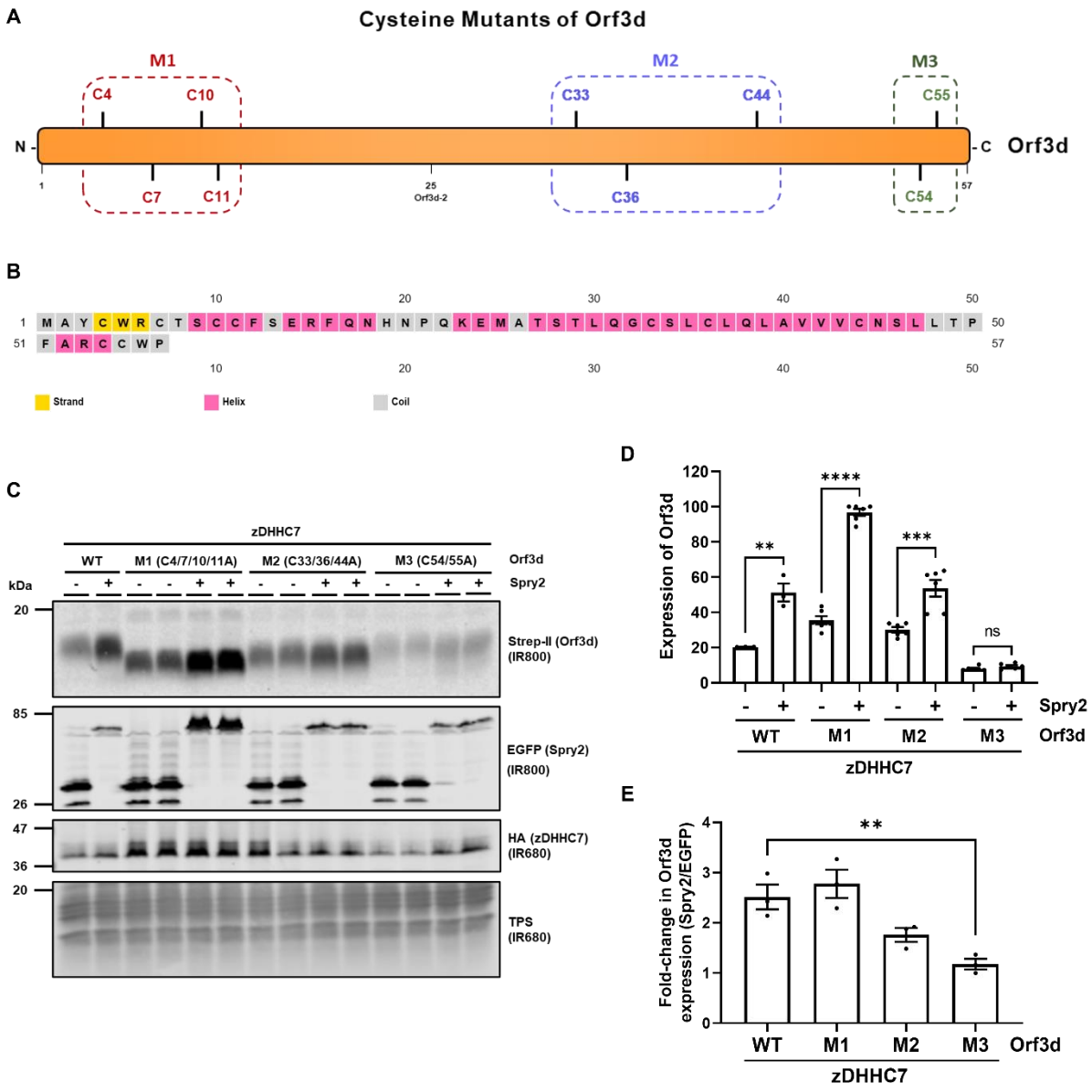


***Figure 5.8. Analysis of the effects of zDHHC7 and Spry2 on expression of Spry2 cysteine mutants.*** *(A) Schematic representation of cysteine residues within the Orf3d construct. Cysteine residues within each mutant construct are grouped and indicated in coloured boxes - Orf3d M1 (C4/7/10/11A) (red), Orf3d M2 (C33/36/44A) (blue), and Orf3d M3 (C54/55A) (green). (B) Secondary structure prediction of Orf3d (also show in figure 5.6.1 B) generated using the UCL bioinformatics group PISPRED Server workbench 4.0 (Jones, 1999, Buchan and Jones, 2019). (C) HEK-293T cells were co-transfected with HA-tagged zDHHC7 WT together with plasmids encoding for Strep-II tagged Orf3d WT, Orf3d M1 (C4/7/10/11A), Orf3d M2 (C33/36/44A), or Orf3d M3 (C54/55A), and either EGFP-tagged Spry2 or EGFP. Representative*

*images of the same samples showing Strep-II tagged Orf3d (first panel; IR800), EGFP-tagged Spry2 or EGFP (second panel; IR800), HA-tagged zDHHC7 (third panel; IR680), and a total protein stain (TPS) (fourth panel; IR680). The positions of the molecular weight markers (kDa) are shown on the left side of all immunoblots. (D) Graph showing expression of Orf3d in the presence of zDHHC7, with and without Spry2. (E) Graph showing the fold change in expression of Orf3d in the presence of zDHHC7, with and without Spry2 (Spry2 (+)/EGFP (-)).* Error bars represent ± SEM. Each replicate is shown with filled circles. All differences were analysed by unpaired t-test. **** denotes $p < 0.0001$, *** denotes $p < 0.001$, ** denotes $p < 0.01$. n = 6 (n = 3 for WT), for three independent experiments.

### 5.9 Zinc salts change the expression pattern of Orf3d

One of the highest scoring outputs of molecular function from figure 5.6.5 was the prediction that Orf3d would be able to bind zinc ions. Within proteins, $Zn^{2+}$ can bind amino acid ligands, most frequently to His, Glu, Asp, and Cys residues, to facilitate protein structure or catalytic activity (Auld, 2013). To determine if $Zn^{2+}$ might play a role in the relationship between Orf3d and zDHHC7, HEK-293T cells were co-transfected with Strep-II tagged Orf3d WT, along with plasmids encoding for either HA-tagged zDHHC7 WT or pEF-BOS-HA. Cells were incubated for 4 hours with 100 µM of salt, either: Sodium Chloride (NaCl), Magnesium Chloride ($MgCl_2$), Zinc Chloride ($ZnCl_2$), Sodium Sulphate ($Na_2SO_4$), Magnesium Sulphate ($MgSO_4$), or Zinc Sulphate ($ZnSO_4$). After incubation cells, lysates were resolved by SDS-PAGE and analysed by immunoblotting.

It can be seen from figure 5.9, that when co-expressed with zDHHC7 the expression of Orf3d visibly shifts to a lower molecular weight band after incubation with either of the zinc salts ($ZnCl_2$ or $ZnSO_4$). This band shift is not seen with any of the other conditions or controls, suggesting that Zn ions/salts may interfere with Orf3d S-acylation. In the samples without zDHHC enzyme it is also noticeable that the Orf3d is better expressed in the samples which contain zinc salts. Although this experiment provides some intriguing initial results, it will be important to understand why these changes are occurring in follow up experiments.

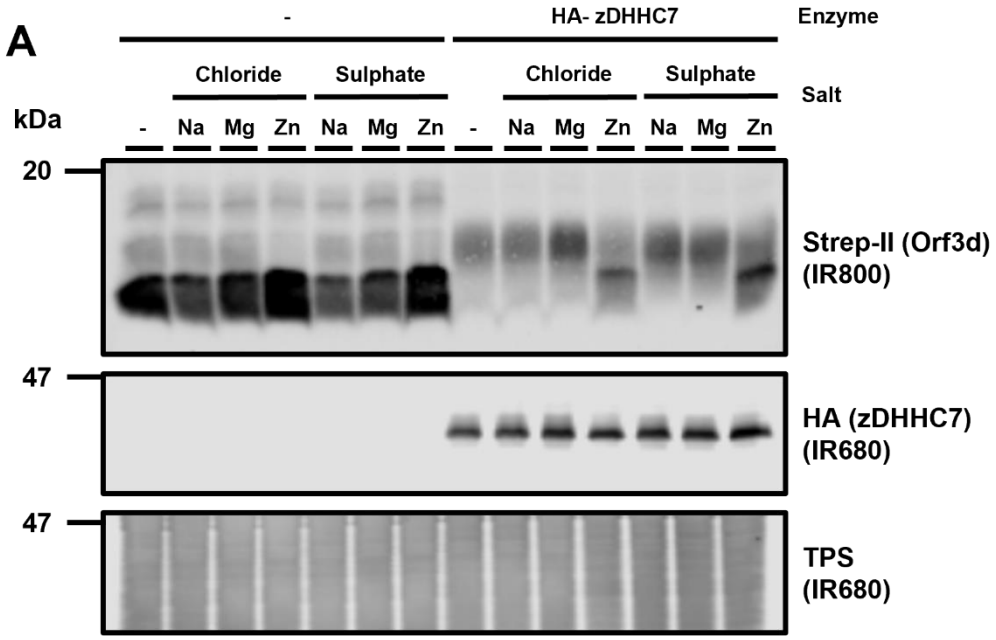


***5.9. Expression of Orf3d in the presence of different salts.*** *HEK-293T cells were co-transfected Strep-II tagged Orf3d WT, together with plasmids encoding for either HA-tagged zDHHC7 WT or pEF-BOS-HA. Cells were incubated for 4 hours with μM of salt, either: Sodium Chloride (NaCl), Magnesium Chloride ($ZnCl_2$), Zinc Chloride ($ZnCl_2$), Sodium Sulphate ($Na_2O_4$), Magnesium Sulphate ($MgSO_4$), or Zinc Sulphate ($ZnSO_4$). After incubation, cell lysates were resolved by SDS-PAGE and analysed by immunoblotting. Representative images of the same samples showing Strep-II tagged Orf3d (top panel; IR800), HA-tagged zDHHC7 (middle; IR680), and a total protein stain (TPS) (bottom panel; IR680). The positions of the molecular weight markers (kDa) are shown on the left side of all immunoblots (n=1).*

## Discussion

SARS-CoV-2 is part of the wider coronavirus family and has become a worldwide pandemic for infection in human and the causation of the respiratory illness COVID-19 (To et al., 2021). Currently, the most successful treatment for COVID-19 is to provide acquired immunity to SARS-CoV-2 via a series of vaccines (Ghazy et al., 2022). According to the World Health Organisation (W.H.O) as of the 24$^{th}$ of October 2023, a total of 13,534,457,273 vaccine doses have been administered. However, vaccine uptake across the globe has been varied due to a variety of economic, political, and social factors including vaccine hesitancy within the general population (Lazarus et al., 2023). Vaccines have been proven effective, especially in the attenuation of severe COVID-19 cases and the prevention of death caused by the virus (Yang et al., 2023). However, very few drugs have currently been developed and/or been found effective for the inhibition of SARS-CoV-2. There has been some success with antivirals such as Nirmatrelvir/Ritonavir (Paxlovid), which is a protease inhibitor developed by Pfizer to target the main protease ($M^{Pro}$) of SARS-CoV-2. Where compared to the placebo Paxlovid significantly reduced COVID-19 related hospitalisation or death from any cause by 88% (FDA, 2021, Lee et al., 2022).

Understanding the molecular mechanisms that underpin viral protein structure, function or interaction is crucial to discovering druggable targets and developing therapeutics. Typically, this has included targeting the structural proteins of SARS-CoV-2 (S (spike), E (envelope), M (membrane), and N (nucleocapsid) proteins) (Wu et al., 2020). However, analysis of other potential targets has included investigations into SAR-CoV accessory proteins, such as Orf7a which is characterised as a coronavirus virulence factor, along with the non-structural proteins (NSP), NSP1, and NSP3c (Wu et al., 2020). Orf7a has been shown to interfere with the host's innate immunity and assist coronavirus immune escape by preventing virion tethering (Taylor et al., 2015). Orf7a achieves this through inhibiting glycosylation of the antiviral protein Bone marrow stromal antigen 2 (BST-2; also known as Tetherin) (Wu et al., 2020, Taylor et al., 2015).

Of the accessory proteins, Orf8 and Orf3d elicit the highest antibody response in COVID-19 patients and are proposed as potential serological markers of infection (Hachim et al., 2020). However, the exact function of Orf3d is still to be determined. One study which investigated Orf3d (referred to in the study as Orf3b, 57 aa) using a dual luciferase reporter assay in 293FT cells gave evidence for Orf3d as a potent

interferon (IFN) antagonist (Lam et al., 2020). The same study also showed that 13 amino acids (1-MAYCWRCTSCCFS-13) of Orf3d alone are ineffective as an antagonist of IFNβ-luciferase. Targeting IFN pathways has been widely investigated in viral therapeutics, as IFNs (such as IFN-1) are innate anti-viral cytokines that act as one of the first-lines of defence in viral suppression (Kim and Shin, 2021). Therefore, if Orf3d has a role in reducing IFN this could help promote favourable conditions for SARS-CoV-2 infection and replication.

*Involvement of Spry and SPRED proteins in the zDHHC mediated expression of Orf3d*

The S-acylation of Orf3d by specific zDHHC enzymes such as zDHHC7 results in a dramatic increase in expression. Initial investigations by Dr. Christine Salaun identified that zDHHC17 was also able to enhance the expression of Orf3d. Enhanced levels of Orf3d provide an easy readout of the S-acylation activity, making the viral protein a good candidate as an indicator to investigate if Spry2 could modulate zDHHC17 activity, in addition to exploring the effects of Spry2 on Orf3d S-acylation more widely. In figure 5.1, increased expression of Orf3d occurred to a small degree with zDHHC17 but was dramatically enhanced when Spry2 was also present, thus revealing a potential co-operative interaction between Spry2 and zDHHC17. In line with data presented in chapter 3 suggesting that the S-acylation deficient N211/D214/K223A (NDK) mutant of Spry2 has a loss of function, this mutant was also found to abrogate the effect of Spry2 on Orf3d expression (figure 5.1).

The underlying properties of Spry2 that lead to an increase in Orf3d expression/S-acylation are not easy to determine. It could be Spry2 alters the conformation of Orf3d to make it more amenable to S-acylation, or that is a tertiary interaction between zDHHC17-Spry2-Orf3d that promotes enhanced S-acylation, or even that there is an indirect mechanism of influence of Spry2, e.g., through effects of Spry2 on cell signalling pathways or modulation of peripheral factors. It is clear that the effects of Spry2 are quite specific to Orf3d as similar effects were not seen on SNAP25 (Lemonidis et al., 2014). The results with SNAP25 further suggest that Spry2 is unlikely to be having the observed effects by modulating the enzymatic activity of zDHHC enzymes (via enhancing the expression of the enzyme).

Interestingly, whereas SPRED1 and SPRED2 did not show similar effects to Spry2 on Orf3d expression, SPRED3 did (figure 5.2 A/C). Throughout this thesis

comparisons between Spry2 and SPRED proteins have been made. Notably, it was shown that Spry2 and SPRED3 are S-acylated by zDHHC17, but SPRED1/2 are not (chapter 3, figure 3.3), and also that Spry2 can stabilise zDHHC17, but SPRED1/2/3 cannot (chapter 3, figure 3.14). Mutant forms of Spry2 were also tested in figures 5.2 B/D, and as discussed in figure 5.1, the NDK mutation removed the effect of Spry2 on Orf3d expression. Further work would need to be conducted to derive significant comparisons for both the P154A and C265/268A (DM) mutants of Spry2. However, initial results indicate that both mutations (P154A and DM) lower the expression of Orf3d but not to the same degree as the NDK mutation (figure 5.2 B).

*Influence of Spry2 on zDHHC-mediated expression of Orf3d*

Evidence given in figure 5.4 looking at all 23 zDHHC enzymes, indicates that five of the zDHHC enzymes, 2, 3, 7, 15, and 17, promote an increase in Orf3d expression. More importantly, only the enzymes which are effective at enhancing Orf3d expression show co-operativity with Spry2 (figure 5.4). Although this screen was only conducted once in this study, this is consistent with earlier data (without Spry2) from the lab. This result indicates that Spry2 action on Orf3d is not zDHHC17 specific, giving weight either to an Orf3d-Spry2 interaction being the defining factor, which is subsequently S-acylated by relevant zDHHC enzymes. Alternatively, Spry2 could have a more general action on a specific subset of zDHHC enzymes. In terms of homology between the enzymes within the screen, zDHHC2, 3, 7, & 15, are all four TMD multi-pass enzymes, whereas zDHHC17 is  a six TMD multi-pass enzyme with the inclusion of a cytosolic N-terminal ankyrin repeat domain (Chamberlain and Shipston, 2015).

Since both proteins (Orf3d & Spry2) are thought to be soluble, they could potentially be S-acylated by a variety of zDHHC enzymes. All five of the zDHHC enzymes have been identified as being localised to the Golgi apparatus (Ohno et al., 2006, Sharma et al., 2008). However, other Golgi enzymes (e.g. zDHHC1, 8, 9, 12, 13, 14, 18, 22, 23 (Ohno et al., 2006)) were not identified as active towards Orf3d in this assay (figure 5.4). zDHHC2 has also been identified at both recycling endosomes and the plasma membrane (PM) (Greaves et al., 2011, Salaun et al., 2017). zDHHC17 has also been shown to localise to both cytoplasmic vesicle membranes (Goytain et al., 2008) and presynaptic cell membranes (Stowers and Isacoff, 2007), and zDHHC2 and zDHHC15 have been identified at postsynaptic densities (Noritake et al., 2009, Shah

et al., 2019). It will be interesting to explore how the different localisations of these zDHHC enzymes impacts the subsequent intracellular localisation of Orf3d.

zDHHC2, 3, 7, & 17 each exhibited cooperativity with Spry2 in enhancing Orf3d expression. Previously published data has shown that zDHHC17 can stabilise Spry2 (Locatelli et al., 2020), which is furthered in this thesis (chapter 3; figures 3.13 & 3.14) by showing that Spry2 can also stabilise zDHHC17. In the absence of any zDHHC enzyme, Orf3d is very poorly expressed (figure 5.4). Cycloheximide based assays in figure 5.5 showed that Orf3d turnover was similar in the presence of all the active zDHHC enzymes and was unaffected by Spry2. This suggests that the enhanced expression of Orf3d by Spry2 is not due to a reduced turnover rate of Orf3d but instead might occur because more protein is being S-acylated preventing rapid degradation after synthesis.

*Structural and functional properties of Orf3d*

As not much is currently known about the function of Orf3d, this chapter also utilised bioinformatics to gather structural and functional insight into Orf3d. Orf3d is predicted to contain two major alpha helix regions (figure 5.6.1 & 5.6.2). The proximal predicted alpha helix (aa 3-16) within the first half of the protein chain is unique to Orf3d. This part of the protein contains four cysteines residues (C4/7/10/11), several aromatic residues (figure 5.6.1), and is predicted to be hydrophilic (figure 5.6.4). The two helices are connected by a disordered polar rich region (aa 17-26) (again, unique to Orf3d) (figure 5.6.1 & 5.6.2). However, the distal alpha helix (aa 27-46) within the second half of the protein is found in both isoforms, Orf3d and Orf3d-2 (figure 5.6.1). This region is hydrophobic (figure 5.6.4) and contains three cysteine residues (C33/36/44) (figure 5.6.1). Through the use of peptide wheel projections in figure 5.6.3, it can be seen that this distal helix is amphipathic with one side of the helix being rich in polar residues (5 residues), and the other containing non-polar and cysteine residues.

The structure of Orf3d shown in figure 5.6 was generated using AlphaFold. As discussed further in chapter 3, AlphaFold is a major resource for researchers in this field, however, it is necessary to acknowledge that limitations to the resource do currently exist (i.e., difficulty with intrinsically disordered proteins, modified proteins, or proteins that have multiple/variable conformations) (Bagdonas et al., 2021; EMBL-

EBI, 2022). For instance, in the full length model in figure 5.6.2, four cysteines are predicted to form disulfide bonds (C4/11 and C33/36), which would be unexpected for a protein in a cytosolic environment (Robinson and Bulleid, 2020). With that being said, research from 2020 reported an *in silico* structural prediction of Orf3d, which bears a striking resemblance to the AlphaFold model within this study (Robinson and Bulleid, 2020). Within this 2020 study, similar helical structures are predicted for the 57 aa protein with the main visual difference being a greater spatial difference between the two helices, which could be expected if the previously mentioned four cysteine residues are not actually in an interaction with one another. The other difference is that this study predicts three alpha helices instead of two which folds around to form a compact protein with ring-like structure (Lam et al., 2020). The 2020 study and this study agree on the presence of the second distal alpha helix within Orf3d-2, with the variation being that the 2020 study predicts the first proximal helix to be two separate helices separated by a flexible region instead of one continuous helix. In fact, the secondary structure prediction results of figure 5.6.1 B could be interpreted to support either possibility. In addition to the limitations of computer-based modelling as discussed, neither possibility can be discounted, however the exact conformation is likely closely approximated by both predictions. No general database structures of Orf3d currently exist and further structural data, such as X-ray crystallography structures would have to be available to have full certainty on any structure.

The shorter Orf3d-2 variant was also shown to be enhanced by zDHHC7 and Spry2. This shows that the increased expression (whether influenced by interaction, signalling, or S-acylation) depends on the 33 aa sequence found in Orf3d-2. This is further supported by figure 5.8, which shows that cysteine residues C54/55 positioned at the C-terminus of both Orf3d and Orf3d-2 are the critical residues responsible for the increased expression of the protein. Alongside the results in fig 5.8, the use of the catalytically inactive zDHHS17 mutant (In17) in figure 5.1 cements the role of S-acylation as a requirement for enhanced stabilisation/expression of Orf3d. In all figures of chapter 5, the expression of Orf3d presents as multiple bands which shift under different conditions. As discussed, this has been shown to be due to S-acylation of the protein causing an upwards band shift, confirmed by either the inactive zDHHC17 (In17) (figure 5.1) or more prominently the Orf3d cysteine mutants in figure 5.8 which showed a molecular weight decrease in the S-acylated band related to the number of cysteine residues substituted with alanine (figure 5.8 C). In the case of

cysteine-string protein (CSPα), S-acylation of the protein causes a noticeable band shift upwards in molecular mass (Greaves et al., 2012). In that particular study, the role of S-acylation in the band shift of CSPα was confirmed with the use of hydroxylamine to cleave thioester linkages between cysteine residues and palmitate chains. Similar hydroxylamine experiments could be conducted for Orf3d, or indeed the use of mPEG click chemistry like that in figure 5.2 would show the number of S-acylated cysteines on Orf3d based on the number of PEG-acylated band shifts.

S-acylation is known to increase membrane association of proteins, such as Ras, Src family kinases, and SNAP25 (Chamberlain and Shipston, 2015). The amphipathic nature and "one-sided" positioning of the cysteine residues within a helix in Orf3d could suggest it is a peripherally associated membrane protein, where it can stably associate to the membrane on one side (the side with modified cysteines), whilst presenting polar residues to the cytosol. Further investigation into the cellular localisation of Orf3d would be required, for instance through immunofluorescence confocal microscopy, or cellular fractionation, or a method similar to that which previously identified Spry4 as an interactor of Orf3d, namely, proximity-dependent biotin labelling (BioID) (St-Germain et al., 2020).

One of the highest outputs of molecular function from figure 5.6.5 was the prediction that Orf3d would be able to bind zinc ions. Indeed, the results of figure 5.10 indicated that zinc salts are able to interfere with the band shift of Orf3d to a higher molecular weight, suggesting that S-acylation is affected. Zinc is one of the most common metal ions to bind to viral proteins, playing important roles in virus survival and processes such as integration of viral DNA into specific sites or activation of transcription (Chaturvedi and Shrivastava, 2005). Conversely, zinc deficiency is linked to poor prognosis in COVID-19 patients and there is a history of zinc-based therapeutics as anti-viral treatments (Pormohammad et al., 2021, Panchariya et al., 2021). Other proteins such as the GLI1, GLI2 and GLI3 are known to also contain zinc finger domains (Park et al., 2000). These proteins are transcription factors which mediate the Sonic Hedgehog-patched signalling pathway, which like S-acylation is also involved in protein lipidation (Gu et al., 2021). GLI1-3 were found to activate transcription through a conserved transcription activation domain which is also found in herpes simplex virus, VP16 (Yoon et al., 1998, Chaturvedi and Shrivastava, 2005). Further to this zDHHC enzymes are so called as they contain zinc finger domains that coordinate $Zn^{2+}$ within their DHHC-CRD, which stabilises the enzyme structure

(Korycka et al., 2012). The zinc binding domain is comprised of Cys-Cys-His-Cys (CCHC), each interacting in a tetrahedral coordination with $Zn^{2+}$ ions. It has also been reported that cysteines involved in zinc coordination could be crucial for substrate S-acylation and/or interaction (Zmuda and Chamberlain, 2020).

As discussed above, an *In silico* study from 2020 predicted Orf3d to fold to form a compact ring like structure (Lam et al., 2020). The AlphaFold prediction models of this study show that the cysteine residues from each predicted alpha helix (C4/11 and C33/36) are situated inward towards each other. Proteins are able to tetrahedrally co-ordinate $Zn^{2+}$ ions to a pair of symmetry related Cys residues (Auld, 2013). For instance, a structural Zn coordination site occurs in the human endothelial nitric oxide synthase, eNOS (or NOS3), between a pair of cysteines (C96 and C101) on each eNOS dimer (Auld, 2013). eNOS has also been found to be attached to caveolae via N-myristylation (Gly2) and S-acylation of separate cysteine residues (C15/26), which is important for eNOS activity and membrane localisation (Oliveira-Paula et al., 2016). With the results of figure 5.9 indicating that increased zinc concentrations interfere with Orf3d S-acylation, many different theories could be postulated. It could be suggested that the high concentrations of zinc force the Cys residues between the alpha helices of Orf3d to tetrahedrally co-ordinate zinc resulting in an unfavourable substrate conformation, localisation, and/or cysteine presentation for zDHHC enzymes. Zinc concentration for Orf3d may also cause an equilibrium imbalance where Zinc competes for Cys availability, and therefore would impair its ability to be S-acylated. Alternatively high zinc ion concentration may interfere with the intrinsic $Zn^{2+}$ coordination of zDHHC structure resulting in impaired enzymatic activity. However, further analysis and the inclusion of robust controls would have to be conducted to attain more definitive conclusions about the effects of $Zn^{2+}$. Indeed, it would be important to ascertain that intracellular levels of $Zn^{2+}$ are increased under these conditions.

With all cysteine residues on the same side of the alpha helix, S-acylation could facilitate stable attachment of this helix in Orf3d within a membrane. The results in figure 5.7 show a critical importance for C54/55 S-acylation in Orf3d stability. Whereby the C-terminal end of the protein could be cytosolic and potentially S-acylated either for enhanced stability or an as yet unknown function and/or interaction. The results of figure 5.6.5 further suggested a role of Orf3d not only in the regulation of metabolic processes but also predicts association with mitochondria and/or

mitochondrial membranes (figure 5.6.5). As previously discussed little is currently known about the action or function of Orf3d (or indeed many of the Orfs), but some evidence has suggested at least one interaction with that of the mitochondrial protein STOML2 (Gordon et al., 2020, Redondo et al., 2021). The C-terminal cytosolic tail could be functional either to be S-acylated or to interact with other protein counterparts, such as mitochondrial proteins such as STOML2. However, although STOML2 has been shown as an interactor of Orf3d (Gordon et al., 2020), the protein is thought to be localised to the inner membrane of mitochondria (Hu et al., 2021).

**Conclusions of chapter 5**

- zDHHC2, 3, 7, 15, and 17, are able to enhance the expression of Orf3d. This expression is further enhanced in the presence of Spry2 (and SPRED3).

- Spry2 does not enhance the enzymatic activity of zDHHC17 when tested on SNAP25 S-acylation.

- The S-acylation of Spry2 is required for it to enhance Orf3d expression.

- Spry2 and zDHHC enzymes do not significantly affect the turnover of Orf3d.

- Orf3d-2 expression is also enhanced in the presence of zDHHC/Spry2.

- C-terminal cysteine residues C54 and C55 are critical for the action of both zDHHC7 and Spry2 on Orf3d.

The schematics shown in Figure 5.10 highlight possible mechanisms linking S-acylation and Spry to enhanced expression of Orf3d.

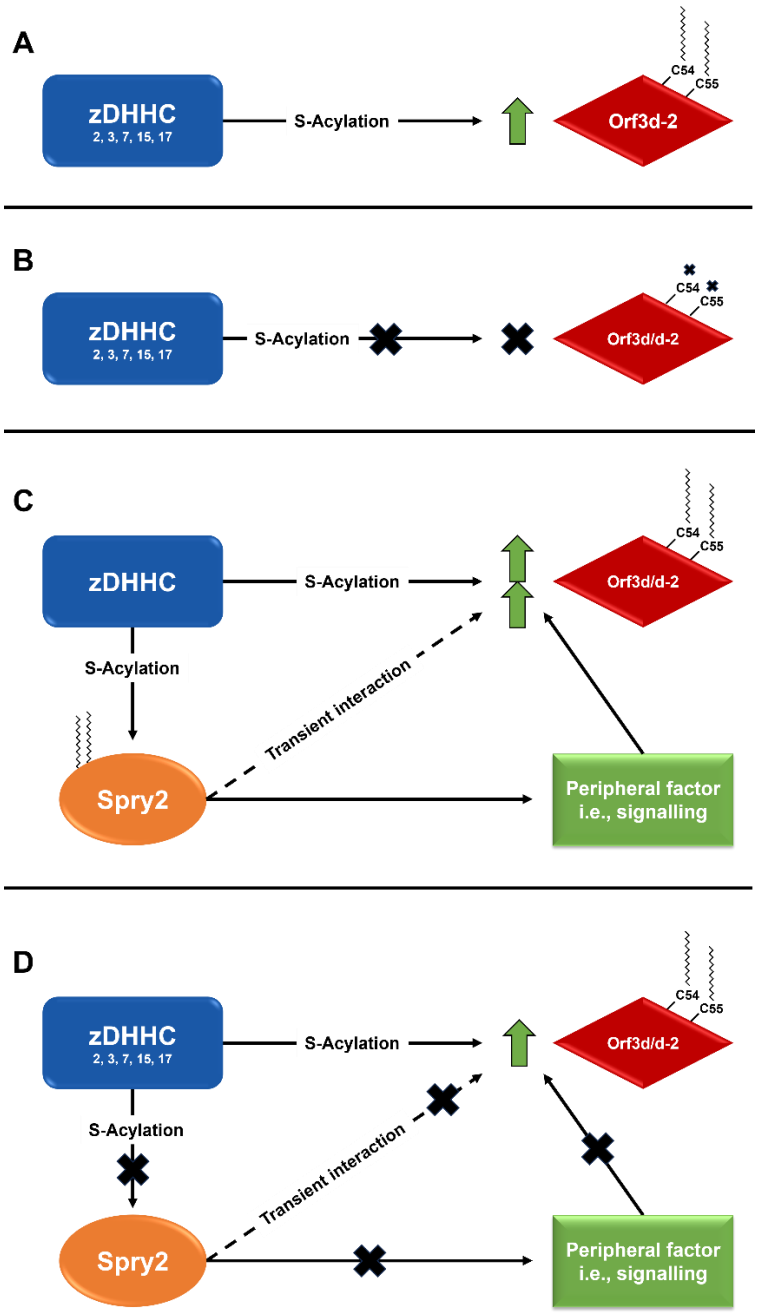


***Figure 5.10. Schematic diagram of models for enhanced Orf3d.*** *(A) zDHHC2, 3, 7, 15, and 17 are able to S-acylate Orf3d/d-2 to enhance expression. C54 and C55 of Orf3d/d-2 are critical for this enhanced expression. (B) If zDHHC mediated S-acylation is impaired, or if C54 and C55 are impaired, then Orf3d/d-2 is not well expressed. (C) The S-acylation of Spry2 is required for a further enhancement of zDHHC mediated expression of Orf3d/d-2. This may occur either through a transient interaction between Spry2 and Orf3d/d-2, or through a peripheral factor mediated by S-acylated Spry2. (D) If the S-acylation of Spry2 is impaired (i.e., S-acylation deficient mutants, or any part of a Spry2 mediated pathway) then zDHHC enzymes act alone to enhance Orf3d/d-2 expression as described in A.*

# CHAPTER 6

# GENERAL DISCUSSION

# Chapter 6 - General discussion

S-acylation is a multifaceted, post-translational modification vital to the properties and function of many proteins. S-acylation was first implicated in the action of Spry proteins over twenty years ago (Impagnatiello et al., 2001) and we now understand that this modification plays a key role in determining both the intracellular localisation and stability of Spry2 (Locatelli, 2021). The work presented in this thesis reports the first detailed analysis of the wider Spry/SPRED family of proteins and specifically their interaction with the zDHHC17 acyltransferase. Studies using zDHHC17 KO mice have uncovered an important role for this enzyme in brain function and possible links to pathology seen in Huntington's disease (Singaraja et al., 2011, Milnerwood et al., 2013, Sutton et al., 2013). A unique feature of zDHHC17 that coordinates its interaction with substrates such as HTT and SNAP25 is the N-terminal AR domain. It appears that many proteins, including HTT and SNAP25, use a disordered hexapeptide motif, known as zDABM, to interact with AR domain of zDHHC17 prior to S-acylation. Indeed, it was the presence of a zDABM sequence in Spry/SPRED proteins that ultimately led to them being identified as substrates of zDHHC17. It was proposed that interaction of zDHHC17 with the zDABM in Spry/SPRED proteins facilitated subsequent S-acylation of the downstream SPR/CRD domain which has an extensive number of cysteines. As Spry/SPRED proteins are important negative regulators of the MAPK growth factor pathway and because dysregulation of this pathway is known to lead to oncogenesis (Kawazoe and Taniguchi, 2019), it was important to develop a more refined understanding of the mechanisms and outcomes of Spry/SPRED S-acylation.

The schematics shown below in Figure 6.1 highlight the main conclusions of the thesis.

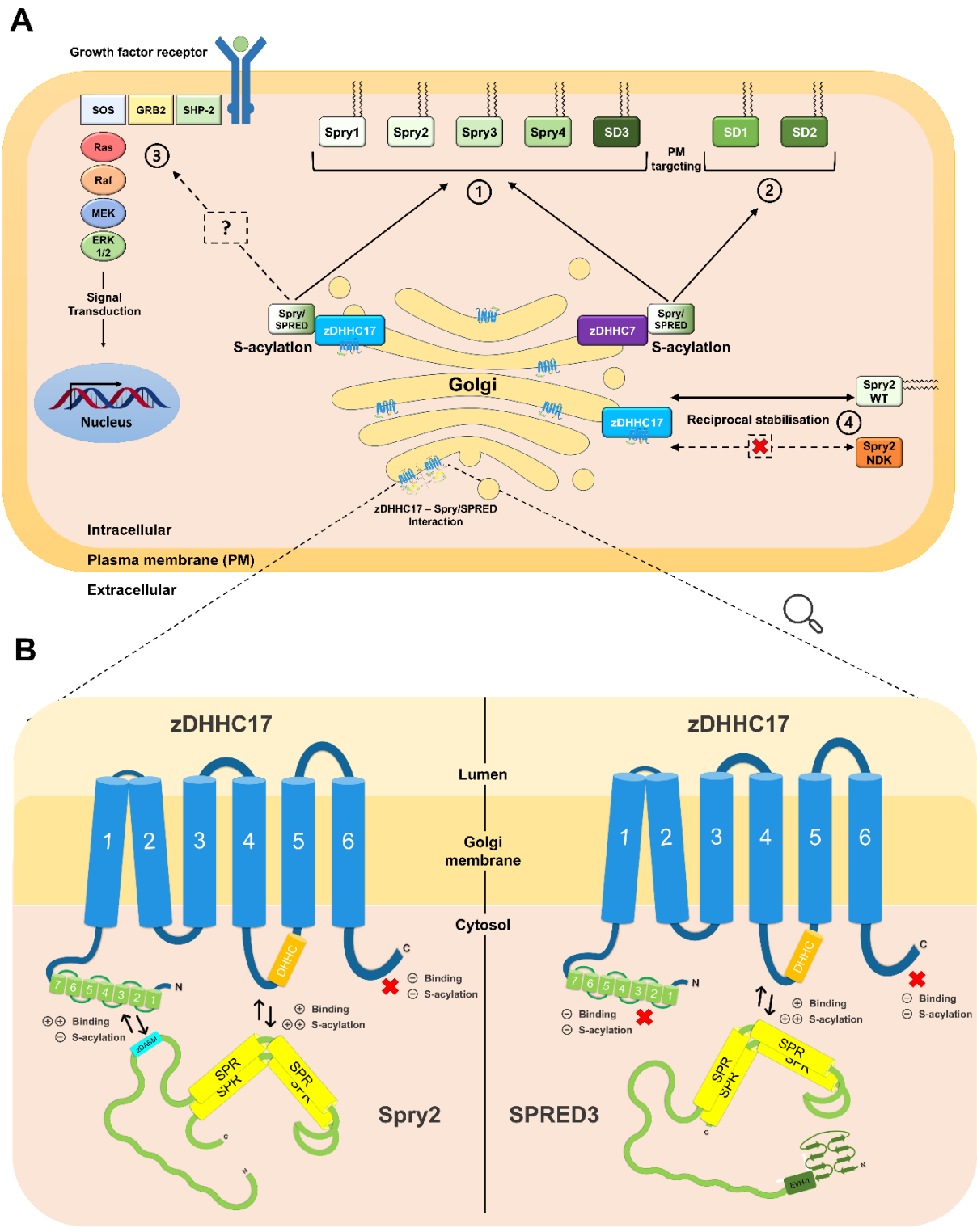
A
Growth factor receptor
SOS
GRB2
SHP-2
Ras
Raf
MEK
ERK 1/2
Signal Transduction
Nucleus
3
?
Spry1
Spry2
Spry3
Spry4
SD3
SD1
SD2
PM targeting
1
2
Spry/ SPRED
zDHHC17
S-acylation
zDHHC7
Spry/ SPRED
S-acylation
Golgi
zDHHC17
Reciprocal stabilisation
4
Spry2 WT
Spry2 NDK
zDHHC17 – Spry/SPRED Interaction
Intracellular
Plasma membrane (PM)
Extracellular
B
zDHHC17
Lumen
Golgi membrane
Cytosol
1 2 3 4 5 6
DHHC
Binding
S-acylation
Spry2
SPRED3
EVH1

***Figure 6.1. Main conclusions of the thesis represented in a schematic diagram**. (A) (1.) zDHHC17 can effectively S-acylate Spry1-4 as well as SPRED3 (SD3). The S-acylation of Spry2 has been shown to be crucial for the plasma membrane targeting of the protein. Furthermore, the SPR domain is sufficient for the S-acylation and localisation of Spry2. (2.) Although SPRED1 (SD1) and SPRED2 (SD2) were not found to be S-acylated by zDHHC17, other zDHHC enzymes such as the highly active zDHHC7 are able to S-acylate these proteins. (3.) The effect of S-acylation of Spry2 on the expression of ERK1/2 and growth factor signalling is not currently known. Extracellular activation of growth factor receptors leading to downstream activation of: Src homology-2 domain-containing protein tyrosine phosphatase-2 (SHP-2); growth factor receptor-bound protein 2 (GRB2); son of sevenless protein (SOS); rat sarcoma GTPase (RAS); rapidly accelerated fibrosarcoma kinase (RAF); mitogen-activated protein kinase kinase (MEK); extracellular signal-related kinase (ERK); and subsequent transcription factors. (4.) Spry2 exerts reciprocal stabilisation of zDHHC17 in a zDABM-independent manner. This reciprocal stabilisation is unique to Spry2 and is abolished by the NDK mutation of Spry2 (shown in orange).*

*(B) Interactions of Spry/SPRED proteins with zDHHC17. The Spry2 protein is able to strongly interact (++) with the ankyrin repeat domain of zDHHC17 via the zDABM; however, this interaction is dispensable for S-acylation (-). The SPR domain of Spry2 and SPRED3 can interact with zDHHC17 via a region between TMD1 and TMD6 which excludes both the ankyrin repeat domain and the C-terminal tail of zDHHC17. This as yet unspecified interaction is responsible for the S-acylation of Spry2/SPRED3 (++), despite being a weak interaction (-). The C-terminal tail of zDHHC17 is not required for either interaction (-) or S-acylation (-) of Spry2/SPRED3. Figure B includes a schematic representation of zDHHC17 displaying the topological placement of the enzyme within the Golgi membrane. Ankyrin repeat, aa 51-286 (green); DHHC domain (orange), aa 437-487; and transmembrane domains (TMD) (blue): TMD1, aa 305-325; TMD2, aa 326-346; TMD3, aa 358-378; TMD4, aa 382-402; TMD5, aa 481-501, and TMD6, aa 530-550. A schematic representation of Spry2 (315 aa) is also shown displaying the protein main chain (light green), the Sprouty (SPR) domain (yellow), and the zDHHC ankyrin binding motif (zDABM) (light blue). A similar schematic is shown for SPRED3 displaying the protein main chain (light green), the Sprouty (SPR) domain (yellow), and the N-terminal EVH1; Ena/VASP (enabled/vasodilator-stimulated phosphoprotein) homology 1 domain (dark green).*

One of the key findings of this thesis was a novel mechanism of interaction and S-acylation for Spry/SPRED proteins with zDHHC17. This was a surprising observation as these proteins were identified as zDHHC17 substrates based on the presence of a zDABM and yet this conserved motif was found to be dispensable for S-acylation by this enzyme. Thus, a simple zDABM interaction followed by substrate S-acylation, as reported for SNAP25-zDHHC17 interaction and S-acylation (Greaves et al., 2009, Lemonidis et al., 2015a), might not be the main mechanism that determines the wider substrate network of zDHHC17. Furthermore, it was remarkable that the entire Ank domain also appeared to be dispensable for interaction and S-acylation of SPRED3 (which lacks a zDABM). This observation led to the question of where Spry/SPRED proteins bind zDHHC17 to facilitate their subsequent S-acylation. Other conserved regions of zDHHC enzymes that have been shown to be involved in substrate recognition include PDZ domains (Christensen et al., 2019), the DPG motif (Mitchell et al., 2006), the TTXE motif (Mitchell et al., 2006), and the PaCCT motif (González Montoro et al., 2009). Surprisingly, the removal of the C-terminal cytosolic domain of zDHHC17 did not impact SPRED3 binding, apparently ruling out the possibility of interaction with the PDZ domain, TTXE motif, or the PaCCT motif, which are all present in the C-terminal region of zDHHC17.

The finding that neither the AR domain nor the C-terminus of zDHHC17 was required for interaction with SPRED3, suggests that the DHHC-CRD might be involved in this interaction. Although the DPG motif is located within this region, it is unlikely that this motif is responsible for the interaction between zDHHC17 and Spry/SPRED proteins, as this would not explain the selective interaction of SPRED3 with zDHHC17 compared with zDHHC7. Although little is currently known about the exact function of the DPG motif, it has been suggested to be important for structurally stabilising zDHHC enzymes (Malgapo and Linder, 2021). It is possible that SPRED3 is binding to regions of the DHHC-CRD that are not well conserved in other zDHHC enzymes, and it will be interesting to undertake mutational analysis of this region of zDHHC17, including DHHC-CRD chimeric swaps with other enzymes, to further pinpoint the exact site of interaction (as discussed in chapter 4, figure 4.12).

Defining a detailed molecular understanding of zDHHC enzyme-substrate interactions is a key step towards uncovering the substrate networks of individual zDHHC enzymes, and in the development of selective inhibitors against this enzyme family. The development of new and selective zDHHC inhibitors (e.g. that target interaction

mechanisms between specific zDHHC enzymes and their substrates) is a major requirement for the field, as current tool compounds are limited to non-selective and toxic compounds such as 2-bromopalmitate (2-BP) (Davda et al., 2013). While recent studies have reported more selective zDHHC inhibitors, such as the TTZ1/2 compounds that display selectivity over zDHHC2 compared with zDHHC3/7 (Salaun et al., 2022). There is scope to develop peptide-based inhibitors that target specific protein-protein interactions, thereby offering an approach in the development of even better targets for enzyme selectivity.

Therapeutic peptides are an important pharmacological tool that often act as ligands and can bind to targets (often cell surface receptors) to trigger intracellular effects with high affinity and specificity. Peptides also offer other advantages including rapid design flexibility, less immunogenicity, and lower cost (Wang et al., 2022). In addition to binding to cell surface receptors, the development of strategies to allow peptides to pass the cell membrane has opened up huge potential for targeting specific intracellular protein-protein interactions (e.g. by the peptide mimicking the interaction site of one of the binding partners) (Derakhshankhah and Jafari, 2018). For instance, small zDABM containing peptides such as those previously used for SNAP25b (aa 111-GVVASQPARV-120 (Verardi et al., 2017)) could be designed to interact with the Ank repeat of zDHHC17. These peptides would be predicted to perturb the zDABM-mediated interaction of the enzyme and specific substrates. Detailed analysis of the zDABM peptide could also be used to develop peptides with higher affinity and therefore a higher probability of outcompeting the endogenous substrates.

Furthermore, the discovery in this thesis that zDHHC17 has alternative modes of substrate interaction opens up the possibility of targeting distinct substrate interactions of this enzyme using different peptides. Another interesting strategy could be designing zDABM peptides for the proximal delivery of tertiary molecules for the inhibition/promotion of the enzyme (i.e., peptide-based drug delivery) (Wang et al., 2022). In the case of the zDABM, this type of work would benefit crucially from optimising a minimal peptide sequence which can interact with and effect zDHHC17. For instance, it would be useful to generate several small peptides of varying lengths (i.e., 6, 8, 10, 12, & 14 aa) that all contain the zDABM with the addition of a GFP tag (large tag can be used in co-IP) or Myc (small tag to control for bulky GFP). These peptides can be utilised in co-immunoprecipitation assays to show if they are sufficient for zDHHC17 interaction. As well as in click-chemistry assays to examine if they have

an effect on the S-acylation activity of the enzyme towards a model protein such as SNAP25. With the expectation that type of minimal peptide screening can in the future also be conducted if and when an alternative interaction site/motif is uncovered.

As mentioned above, the discovery of different substrate binding modes of zDHHC17 opens up the potential to block a sub-set of substrate interactions. For instance, the overexpression of Spry2 has been implicated in the development and metastasis of both rhabdomyosarcoma and human colonic adenocarcinomas (Holgren et al., 2010, Saini et al., 2018). Where in both cases Spry2 was suggested to interact with, control, and induce the expression of c-MET, which is a RTK which responds to hepatic growth factor and signals. Which in the case of colonic adenocarcinomas, Spry2 increases c-MET activation/signalling resulting in enhanced cell migration and invasion (Saini et al., 2018). Therefore, the modulation/inhibition of Spry2 function, stability, or localisation by targeting zDHHC17 activity/interaction could prove to be a viable therapeutic approach.

In addition to the development of new peptide-based approaches for targeting zDHHC enzymes. The exact knowledge of enzyme-substrate interactions motifs will also inform the identification of novel zDHHC interaction networks. Similar to the study of Lemonidis and colleagues in 2017 (which identified ninety-five human zDABM containing proteins), the use of peptide array-based screening and bioinformatics could also be used to identify a novel set of zDHHC17 substrate proteins that interact with this enzyme in a similar way as seen for Spry/SPRED proteins (Lemonidis et al., 2017a). However, a potential caveat is that the alternative mode of Spry/SPRED binding to zDHHC17 may involve a non-linear motif/conformation, and in this case the use of such peptide-array analysis would be complicated.

The difficulty in pinning down the exact zDHHC17 interaction site on SPRED3 could suggest the presence of cryptic binding sites, a role for specific post-translational modifications, weak and transient interactions, or other tertiary factors (i.e., adaptor proteins or not yet fully understood signalling pathways). For example, Spry2 has already been postulated to contain a cryptic C-terminal proline site that is only exposed after PP2A mediated dephosphorylation of S112. Subsequently leading to the binding and sequestration of Grb2 (via proline site binding), which then prevents Ras activation and MAPK transduction (Lao et al., 2007a). Additionally, in the case of the cardiac Na-K ATPase (Na-pump) it was initially suggested that the inhibitory accessory sub-unit, phospholemman (PLM) formed a direct interaction with zDHHC5.

However, it was subsequently reported that the S-acylation of PLM was indirectly achieved via an interaction between zDHHC5 and the α-subunit of the Na-Pump, which in turn places zDHHC5 in the correct position to S-acylate PLM (which also binds the Na-Pump).

This thesis has also built upon work completed in 2020 which showed that zDHHC17 is able to reduce the turnover of Spry2 (Locatelli et al., 2020). The results of this thesis show for the first time that a substrate of zDHHC17 might also reduce turnover of the enzyme, thus highlighting a unique reciprocal stabilisation between enzyme and substrate. Specifically, evidence was presented that Spry2 (but not other Spry/SPRED proteins) was able to stabilise zDHHC17 in co-expression experiments. Furthermore, this stabilisation was independent of the zDABM of Spry2, implying that the alternative mode of Spry/SPRED interaction is responsible for the dual-stabilisation effect between zDHHC17 and Spry2. However, the effect is unique to Spry2 and not just a ubiquitous function of the SPR domain or even the Spry/SPRED proteins in general. It will be important to investigate how S-acylation effects this reciprocal regulation in more detail. In particular, this could also be achieved by using either CRISPR Cas9 approaches or si/shRNA knockdown techniques to ablate expression of Spry2 or zDHHC17, which will allow the regulatory effects of the endogenously expressed proteins to be confirmed (Marvaldi et al., 2015).

Additionally, Spry2 undergoes a number of post-translational modifications including phosphorylation (Lao et al., 2006, Patel et al., 2013b). Therefore, it would be interesting to test if there is a level of Spry2 phospho-regulation on zDHHC17 activity and/or stability. This could be achieved through the use of site directed mutagenesis to mutate the phosphorylate Y55 residue and/or the poly-serine region of Spry2 between aa 105-119 to alanine. After which specific assays could be utilised such as cycloheximide chase to measure zDHHC17/Spry2 degradation or click-chemistry metabolic labelling to measure S-acylation.

A long-term goal would be to move away from the use of HEK-293T cells and into more relevant cell lines where Spry2 is upregulated such as PC12 cells or RWPE-1 prostate epithelial cells. As discussed above, a neuronal setting such as PC12 cells could provide an interesting system to assess the involvement of these two proteins in both growth factor signalling and neurite outgrowth. Within this thesis, the experiments into FGF/EGF mediated Spry2 inhibition of ERK1/2 were inconclusive in terms of what role zDHHC mediated S-acylation plays. As an alternative, the

prolonged activation of ERK signalling by FGF/NGF leads to neurite outgrowth and differentiation of PC12 cells; whereas, the more transient ERK activation elicited by EGF stimulates cell proliferation (Kao et al., 2001). Therefore, as Spry2 inhibits FGF/NGF mediated neurite outgrowth but stimulates EGF mediate neurite outgrowth, this model may prove viable for examining the effects of S-acylation on Spry2 function. More specifically, through the transfection of Spry2 WT and Spry2 S-acylation deficient mutants into PC12 cells following a designated/optimised period of growth factor stimulation and neurite outgrowth. Neurite outgrowth would be assessed by measuring the length from cell body to the growth cones of the longest neurites (i.e. max distance). These investigations could also run in addition to measurements taken in cells depleted of zDHHC17 i.e., through si/sRNA knockdown.

This thesis also included an investigation of the SARS-CoV-2 accessory protein Orf3d, and its relationship with both zDHHC enzymes and Spry/SPRED proteins. Understanding the molecular mechanisms that underpin viral protein structure, function, or interaction is crucial to discovering druggable targets and developing therapeutics. Whereas other SARS-CoV-2 proteins have been shown to be S-acylated (i.e., the spike protein), research by Dr. Christine Salaun identified that Orf3d is also modified by S-acylation and that this mediates enhanced expression of the Orf3d protein. The focus in this thesis was on the potential regulation of Orf3d S-acylation by Spry/SPRED proteins. Notably Spry2 in particular has been shown in this thesis to have a stabilisation effect on zDHHC17. Initially, an interesting aspect of investigation was into whether or not this increased stability translates to a change in zDHHC17 activity. A viable prospect considering that some zDHHC enzymes are known to have accessory proteins which modulate their activity, such as zDHHC9 and GCP16 (Salaun et al., 2020b, Nguyen et al., 2023, Swarthout et al., 2005).

The main findings of this work showed that both Spry2 and SPRED3 were able to enhance the zDHHC17 mediated increase in Orf3d expression; however, this effect was not seen for SPRED1 and SPRED2. This is interesting in the wider scope of this thesis, owing to the fact that SPRED1 and SPRED2 are not efficiently S-acylated by zDHHC17, whereas Spry2 and SPRED3 are equally well S-acylated. Further to this, when in co-expression with the S-acylation deficient NDK mutant of Spry2, the observed effect of zDHHC17 mediated expression of Orf3d was lost. With the main conclusion, being that the S-acylation of Spry2 is required for any effect it would have on zDHHC17-Orf3d. With the additional finding that the effect of Spry2 does not have

an effect on the normal turnover of Orf3d in the presence of Orf3d active zDHHC enzymes (zDHHC2, 3, 7, & 17). It would also be interesting to examine zDHHC mediated Orf3d expression in the presence of the other Spry2 mutants, as well as the other three Spry proteins (Spry1, 2, & 4), which are all effectively S-acylated by zDHHC17. In addition to this, another finding of the investigation into Orf3d is that the shorter Orf3d-2 isoform is sufficient for both zDHHC17 mediated expression and Spry2 enhanced expression. Furthermore, it was shown that Cys54 and Cys55 are critical for the zDHHC mediated enhancement of Orf3d.

The preliminary data complied within this thesis offers numerous avenues for further investigation into Orf3d. As it is not yet fully known where Orf3d acts with in a cell, immunofluorescent confocal microscopy could be used to observe the localisation of the protein in the presence of both Spry2 and zDHHC enzymes. Utilising immunofluorescent Alexa fluorophore secondary antibodies which conjugate to primary antibodies that recognise the Strep-II tag of Orf3d and the HA-tag of zDHHC enzymes. This is similar to experiments conducted both within figure 4.4 of this thesis and previously published research into Spry2 and zDHHC17 localisation (Locatelli et al., 2020, Lemonidis et al., 2014). Alongside this, other future work would utilise cellular fractionation assays to both support and confirm any findings from the immunofluorescent studies. Fractionation would allow for the separation of lysates into nuclear, cytoplasmic, and membrane compartments/fractions via various steps of homogenisation, centrifugation, and buffer changes (i.e., with non-ionic detergents such as digitonin or NP-40) (Senichkin et al., 2021). With the broad aim to characterise Orf3d as either membrane associated or soluble when in the presence/absence of Spry2 and/or zDHHC enzymes.

An initial difficulty with this type of experiment is that Orf3d appears unstable and would potentially not be visible when not in combination with another stabilising protein such as Spry2/DHHC (figure 5.1). To optimise this, following the results of figure 5.5, if Orf3d is unstable then a short time span cycloheximide protein degradation assay could be conducted. This would be done with Orf3d alone at shorter time points of potentially less than 2 hours, and also in combination with other proteins for longer time points. This would determine the half-life of the protein and give insight into the overall stability of the protein and could also setting parameters for future investigations. Additionally, it is seen in chapter 5 that Orf3d expression can

be stabilised in the presence of Spry2 and zDHHC enzymes but as discussed above the nature of the relationship is currently unclear. Future work into the area of protein-protein binding would be conducted in order to co-immunoprecipitate Orf3d with Spry2, zDHHC enzymes, and other proteins of interest (similar to the GFP-Trap® co-immunoprecipitation assays in this thesis). This will provide a better understanding of where direct interactions may or may not occur.

Overall, this thesis highlights a novel mode of interaction between zDHHC17 and Spry/SPRED proteins that is coupled to S-acylation. Furthermore, it is proposed that the alternative binding mode involves interaction between the conserved SPR domain of the Spry/SPRED proteins and the conserved CRD-DHHC domain of zDHHC17, although this requires further investigation. This thesis has also uncovered a more complex relationship than previously thought between Spry2 and zDHHC enzymes, and it will be important to investigate reciprocal stabilisation of these proteins and its importance for cell signalling and function. In a similar manner, understanding if Spry/SPRED proteins have any impact on Orf3d S-acylation during viral infection will also be an interesting area of future investigation. A key outstanding question remains how S-acylation impacts Spry/SPRED function in cell signalling. Over-expression experiments proved to be unfruitful for investigating this question, but future work could undertake CRISPR to introduce specific cysteine mutations into the CRD of Spry2 and explore how this impacts ERK signalling. A similar approach could be undertaken to investigate how disrupting the distinct binding modes of Spry2 impacts signalling activity (e.g., mutation of the zDABM and/or the novel binding site when it is clearly defined).

*Limitations to this study*

The study has used over-expression analysis in HEK-293T cells throughout. This strategy has proved to be a useful and reliable approach to define zDHHC-substrate interactions and also to map out mechanisms contributing to fatty acid selectivity of zDHHC enzymes (Lemonidis et al., 2015a, Greaves et al., 2017). Indeed, in both these cases the conclusions based on overexpression analysis has been subsequently confirmed by structural (X-ray crystallography) results (Rana et al., 2018a, Verardi et al., 2017). Nevertheless, over-expression has potential to introduce unwanted effects and therefore future work should look to confirm some of the findings of this thesis using knockdown approaches and structure-based analysis.

# CHAPTER 7

# REFERENCES

## Chapter 7 - References


ABLAIN, J., XU, M., ROTHSCHILD, H., JORDAN, R. C., MITO, J. K., DANIELS, B. H., BELL, C. F., JOSEPH, N. M., WU, H., BASTIAN, B. C., ZON, L. I. & YEH, I. 2018. Human tumor genomics and zebrafish modeling identify SPRED1 loss as a driver of mucosal melanoma. *Science,* 362**,** 1055-1060.

ABRAMI, L., AUDAGNOTTO, M., HO, S., MARCAIDA, M. J., MESQUITA, F. S., ANWAR, M. U., SANDOZ, P. A., FONTI, G., POJER, F., DAL PERARO, M. & VAN DER GOOT, F. G. 2021. Palmitoylated acyl protein thioesterase APT2 deforms membranes to extract substrate acyl chains. *Nature Chemical Biology,* 17**,** 438-447.

ABRAMI, L., DALLAVILLA, T., SANDOZ, P. A., DEMIR, M., KUNZ, B., SAVOGLIDIS, G., HATZIMANIKATIS, V. & VAN DER GOOT, F. G. 2017. Identification and dynamics of the human ZDHHC16-ZDHHC6 palmitoylation cascade. *Elife,* 6.

ABRAMI, L., KUNZ, B., DEUQUET, J., BAFICO, A., DAVIDSON, G. & VAN DER GOOT, F. G. 2008a. Functional interactions between anthrax toxin receptors and the WNT signalling protein LRP6. *Cell Microbiol,* 10**,** 2509-19.

ABRAMI, L., KUNZ, B., IACOVACHE, I. & VAN DER GOOT, F. G. 2008b. Palmitoylation and ubiquitination regulate exit of the Wnt signaling protein LRP6 from the endoplasmic reticulum. *Proc Natl Acad Sci U S A,* 105**,** 5384-9.

ABRAMI, L., LEPPLA, S. H. & VAN DER GOOT, F. G. 2006. Receptor palmitoylation and ubiquitination regulate anthrax toxin endocytosis. *J Cell Biol,* 172**,** 309-20.

ADACHI, N., HESS, D. T., MCLAUGHLIN, P. & STAMLER, J. S. 2016. S-Palmitoylation of a Novel Site in the β2-Adrenergic Receptor Associated with a Novel Intracellular Itinerary. *J Biol Chem,* 291**,** 20232-46.

AHTIAINEN, L., VAN DIGGELEN, O. P., JALANKO, A. & KOPRA, O. 2003. Palmitoyl protein thioesterase 1 is targeted to the axons in neurons. *J Comp Neurol,* 455**,** 368-77.

AITKEN, A., COHEN, P., SANTIKARN, S., WILLIAMS, D. H., CALDER, A. G., SMITH, A. & KLEE, C. B. 1982. Identification of the NH2-terminal blocking group of calcineurin B as myristic acid. *FEBS Letters,* 150**,** 314-318.

AIZPURUA-OLAIZOLA, O., SASTRE TORAÑO, J., FALCON-PEREZ, J. M., WILLIAMS, C., REICHARDT, N. & BOONS, G. J. 2018. Mass spectrometry for glycan biomarker discovery. *TrAC Trends in Analytical Chemistry,* 100**,** 7-14.

ARORA, T., MULLANGI, S. & LEKKALA, M. R. 2023. Ovarian Cancer. *StatPearls.* Treasure Island (FL) ineligible companies. Disclosure: Sanjana Mullangi declares no relevant financial relationships with ineligible companies. Disclosure: Manidhar Reddy Lekkala declares no relevant financial relationships with ineligible companies.: StatPearls Publishing



ASHBURNER, M., BALL, C. A., BLAKE, J. A., BOTSTEIN, D., BUTLER, H., CHERRY, J. M., DAVIS, A. P., DOLINSKI, K., DWIGHT, S. S., EPPIG, J. T., HARRIS, M. A., HILL, D. P., ISSEL-TARVER, L., KASARSKIS, A., LEWIS, S., MATESE, J. C., RICHARDSON, J. E., RINGWALD, M., RUBIN, G. M. & SHERLOCK, G. 2000. Gene Ontology: tool for the unification of biology. *Nature Genetics,* 25**,** 25-29.

AULD, D. S. 2013. Zinc-Binding Sites in Proteins. *In:* KRETSINGER, R. H., UVERSKY, V. N. & PERMYAKOV, E. A. (eds.) *Encyclopedia of Metalloproteins.* New York, NY: Springer New York.

BADER, S. M., COONEY, J. P., PELLEGRINI, M. & DOERFLINGER, M. 2022. Programmed cell death: the pathways to severe COVID-19? *Biochem J,* 479**,** 609-628.

BAGDONAS, H., FOGARTY, C. A., FADDA, E. & AGIRRE, J. 2021. The case for post-predictional modifications in the AlphaFold Protein Structure Database. *Nature Structural & Molecular Biology,* 28**,** 869-870.

BAKER, K., ASTLE, D. E., SCERIF, G., BARNES, J., SMITH, J., MOFFAT, G., GILLARD, J., BALDEWEG, T. & RAYMOND, F. L. 2015. Epilepsy, cognitive deficits and neuroanatomy in males with ZDHHC9 mutations. *Ann Clin Transl Neurol,* 2**,** 559-69.

BARMANIA, F. & PEPPER, M. S. 2013. C-C chemokine receptor type five (CCR5): An emerging target for the control of HIV infection. *Appl Transl Genom,* 2**,** 3-16.

BENITEZ, B. A., ALVARADO, D., CAI, Y., MAYO, K., CHAKRAVERTY, S., NORTON, J., MORRIS, J. C., SANDS, M. S., GOATE, A. & CRUCHAGA, C. 2011. Exome-sequencing confirms DNAJC5 mutations as cause of adult neuronal ceroid-lipofuscinosis. *PLoS One,* 6**,** e26741.

BIBLE, E., GUPTA, P., HOFMANN, S. L. & COOPER, J. D. 2004. Regional and cellular neuropathology in the palmitoyl protein thioesterase-1 null mutant mouse model of infantile neuronal ceroid lipofuscinosis. *Neurobiology of Disease,* 16**,** 346-359.

BIONDO, E. D., SPONTARELLI, K., ABABIOH, G., MÉNDEZ, L. & ARTIGAS, P. 2021. Diseases caused by mutations in the Na(+)/K(+) pump α1 gene ATP1A1. *Am J Physiol Cell Physiol,* 321**,** C394-c408.

BLANC, M., DAVID, F., ABRAMI, L., MIGLIOZZI, D., ARMAND, F., BÜRGI, J. & VAN DER GOOT, F. G. 2015. SwissPalm: Protein Palmitoylation database. *F1000Res,* 4**,** 261.

BLANC, M., DAVID, F. P. A. & VAN DER GOOT, F. G. 2019. SwissPalm 2: Protein S-Palmitoylation Database. *Methods Mol Biol,* 2009**,** 203-214.

BLANPAIN, C., WITTAMER, V., VANDERWINDEN, J.-M., BOOM, A., RENNEBOOG, B. T., LEE, B., LE POUL, E., EL ASMAR, L. L., GOVAERTS, C., VASSART, G., DOMS, R. W. & PARMENTIER, M. 2001. Palmitoylation of CCR5 Is Critical for

Receptor Trafficking and Efficient Activation of Intracellular Signaling Pathways *. *Journal of Biological Chemistry,* 276**,** 23795-23804.

BONCOMPAIN, G., HERIT, F., TESSIER, S., LESCURE, A., DEL NERY, E., GESTRAUD, P., STAROPOLI, I., FUKATA, Y., FUKATA, M., BRELOT, A., NIEDERGANG, F. & PEREZ, F. 2019. Targeting CCR5 trafficking to inhibit HIV-1 infection. *Sci Adv,* 5**,** eaax0821.

BONONI, G., TUCCINARDI, T., RIZZOLIO, F. & GRANCHI, C. 2021. α/β-Hydrolase Domain (ABHD) Inhibitors as New Potential Therapeutic Options against Lipid-Related Diseases. *J Med Chem,* 64**,** 9759-9785.

BRIGIDI, G. S., SANTYR, B., SHIMELL, J., JOVELLAR, B. & BAMJI, S. X. 2015. Activity-regulated trafficking of the palmitoyl-acyl transferase DHHC5. *Nature Communications,* 6**,** 8200.

BROWNE, D. L., GANCHER, S. T., NUTT, J. G., BRUNT, E. R., SMITH, E. A., KRAMER, P. & LITT, M. 1994. Episodic ataxia/myokymia syndrome is associated with point mutations in the human potassium channel gene, KCNA1. *Nat Genet,* 8**,** 136-40.

BUCHAN, D. W. A. & JONES, D. T. 2019. The PSIPRED Protein Analysis Workbench: 20 years on. *Nucleic Acids Research,* 47**,** W402-W407.

BUNDSCHU, K., WALTER, U. & SCHUH, K. 2006. The VASP-Spred-Sprouty Domain Puzzle. *Journal of Biological Chemistry,* 281**,** 36477-36481.

BURGOYNE, R. D. & MORGAN, A. 2015. Cysteine string protein (CSP) and its role in preventing neurodegeneration. *Semin Cell Dev Biol,* 40**,** 153-9.

BUSQUETS-HERNÁNDEZ, C. & TRIOLA, G. 2021. Palmitoylation as a Key Regulator of Ras Localization and Function. *Frontiers in Molecular Biosciences,* 8.

BUTLAND, S., SANDERS, S., SCHMIDT, M., RIECHERS, S.-P., LIN, D., MARTIN, D., VAID, K., GRAHAM, R., SINGARAJA, R., WANKER, E., CONIBEAR, E. & HAYDEN, M. 2014. The Palmitoyl acyltransferase HIP14 Shares a High Proportion of

Interactors with Huntingtin: Implications for a Role in the Pathogenesis of Huntington Disease. *Human molecular genetics,* 23.

BUTLER, L., LOCATELLI, C., ALLAGIOTI, D., LOUSA, I., LEMONIDIS, K., TOMKINSON, N. C. O., SALAUN, C. & CHAMBERLAIN, L. H. 2023. S-acylation of Sprouty and SPRED proteins by the S-acyltransferase zDHHC17 involves a novel mode of enzyme–substrate interaction. *Journal of Biological Chemistry,* 299.

CADIEUX-DION, M., ANDERMANN, E., LACHANCE-TOUCHETTE, P., ANSORGE, O., MELOCHE, C., BARNABÉ, A., KUZNIECKY, R., ANDERMANN, F., FAUGHT, E., LEONBERG, S., DAMIANO, J., BERKOVIC, S., ROULEAU, G. & COSSETTE, P. 2013. Recurrent mutations in DNAJC5 cause autosomal dominant Kufs disease. *Clinical Genetics,* 83**,** 571-575.

CALERO, G., GUPTA, P., NONATO, M. C., TANDEL, S., BIEHL, E. R., HOFMANN, S. L. & CLARDY, J. 2003. The Crystal Structure of Palmitoyl Protein Thioesterase-2 (PPT2) Reveals the Basis for Divergent Substrate Specificities of the Two Lysosomal Thioesterases, PPT1 and PPT2 *. *Journal of Biological Chemistry,* 278**,** 37957-37964.

CALZONE, K. A. 2012. Genetic Biomarkers of Cancer Risk. *Seminars in Oncology Nursing,* 28**,** 122-128.

CAMP, L. A. & HOFMANN, S. L. 1993. Purification and properties of a palmitoyl-protein thioesterase that cleaves palmitate from H-Ras. *Journal of Biological Chemistry,* 268**,** 22566-22574.

CARR, S. A., BIEMANN, K., SHOJI, S., PARMELEE, D. C. & TITANI, K. 1982. n-Tetradecanoyl is the NH2-terminal blocking group of the catalytic subunit of cyclic AMP-dependent protein kinase from bovine cardiac muscle. *Proceedings of the National Academy of Sciences,* 79**,** 6128-6131.

CHAMBERLAIN, L. H. & SHIPSTON, M. J. 2015. The Physiology of Protein S-acylation. *Physiological Reviews,* 95**,** 341-376.

CHAN, J. F., YUAN, S., KOK, K. H., TO, K. K., CHU, H., YANG, J., XING, F., LIU, J., YIP, C. C., POON, R. W., TSOI, H. W., LO, S. K., CHAN, K. H., POON, V. K., CHAN,

W. M., IP, J. D., CAI, J. P., CHENG, V. C., CHEN, H., HUI, C. K. & YUEN, K. Y. 2020. A familial cluster of pneumonia associated with the 2019 novel coronavirus indicating person-to-person transmission: a study of a family cluster. *Lancet,* 395**,** 514-523.

CHATURVEDI, U. C. & SHRIVASTAVA, R. 2005. Interaction of viral proteins with metal ions: role in maintaining the structure and functions of viruses. *FEMS Immunol Med Microbiol,* 43**,** 105-14.

CHEN, S., HAN, C., MIAO, X., LI, X., YIN, C., ZOU, J., LIU, M., LI, S., STAWSKI, L., ZHU, B., SHI, Q., XU, Z.-X., LI, C., GODING, C. R., ZHOU, J. & CUI, R. 2019. Targeting MC1R depalmitoylation to prevent melanomagenesis in redheads. *Nature Communications,* 10**,** 877.

CHEN, Y., LI, J., XU, L., GĂMAN, M.-A. & ZOU, Z. 2022. The genesis and evolution of acute myeloid leukemia stem cells in the microenvironment: From biology to therapeutic targeting. *Cell Death Discovery,* 8**,** 397.

CHEUNG, J. Y., ZHANG, X. Q., SONG, J., GAO, E., RABINOWITZ, J. E., CHAN, T. O. & WANG, J. 2010. Phospholemman: a novel cardiac stress protein. *Clin Transl Sci,* 3**,** 189-96.

CHI, L., ITÄRANTA, P., ZHANG, S. & VAINIO, S. 2006. Sprouty2 is involved in male sex organogenesis by controlling fibroblast growth factor 9-induced mesonephric cell migration to the developing testis. *Endocrinology,* 147**,** 3777-88.

CHING, S. T., CUNHA, G. R., BASKIN, L. S., BASSON, M. A. & KLEIN, O. D. 2014. Coordinated activity of Spry1 and Spry2 is required for normal development of the external genitalia. *Developmental Biology,* 386**,** 1-11.

CHRISTENSEN, N. R., ČALYŠEVA, J., FERNANDES, E. F. A., LÜCHOW, S., CLEMMENSEN, L. S., HAUGAARD-KEDSTRÖM, L. M. & STRØMGAARD, K. 2019. PDZ Domains as Drug Targets. *Adv Ther (Weinh),* 2**,** 1800143.

CHU-LAGRAFF, Q., BLANCHETTE, C., O'HERN, P. & DENEFRIO, C. 2010. The Batten disease Palmitoyl Protein Thioesterase 1 gene regulates neural specification

and axon connectivity during Drosophila embryonic development. *PLoS One,* 5**,** e14402.

COHEN, S. 1962. Isolation of a mouse submaxillary gland protein accelerating incisor eruption and eyelid opening in the new-born animal. *The Journal of biological chemistry,* 237**,** 1555-1562.

COLLURA, K. M., NIU, J., SANDERS, S. S., MONTERSINO, A., HOLLAND, S. M. & THOMAS, G. M. 2020. The palmitoyl acyltransferases ZDHHC5 and ZDHHC8 are uniquely present in DRG axons and control retrograde signaling via the Gp130/JAK/STAT3 pathway. *J Biol Chem,* 295**,** 15427-15437.

CONSORTIUM, T. G. O., ALEKSANDER, S. A., BALHOFF, J., CARBON, S., CHERRY, J. M., DRABKIN, H. J., EBERT, D., FEUERMANN, M., GAUDET, P., HARRIS, N. L., HILL, D. P., LEE, R., MI, H., MOXON, S., MUNGALL, C. J., MURUGANUGAN, A., MUSHAYAHAMA, T., STERNBERG, P. W., THOMAS, P. D., VAN AUKEN, K., RAMSEY, J., SIEGELE, D. A., CHISHOLM, R. L., FEY, P., ASPROMONTE, M. C., NUGNES, M. V., QUAGLIA, F., TOSATTO, S., GIGLIO, M., NADENDLA, S., ANTONAZZO, G., ATTRILL, H., DOS SANTOS, G., MARYGOLD, S., STRELETS, V., TABONE, C. J., THURMOND, J., ZHOU, P., AHMED, S. H., ASANITTHONG, P., LUNA BUITRAGO, D., ERDOL, M. N., GAGE, M. C., ALI KADHUM, M., LI, K. Y. C., LONG, M., MICHALAK, A., PESALA, A., PRITAZAHRA, A., SAVERIMUTTU, S. C. C., SU, R., THURLOW, K. E., LOVERING, R. C., LOGIE, C., OLIFERENKO, S., BLAKE, J., CHRISTIE, K., CORBANI, L., DOLAN, M. E., DRABKIN, H. J., HILL, D. P., NI, L., SITNIKOV, D., SMITH, C., CUZICK, A., SEAGER, J., COOPER, L., ELSER, J., JAISWAL, P., GUPTA, P., JAISWAL, P., NAITHANI, S., LERA-RAMIREZ, M., RUTHERFORD, K., WOOD, V., DE PONS, J. L., DWINELL, M. R., HAYMAN, G. T., KALDUNSKI, M. L., KWITEK, A. E., LAULEDERKIND, S. J. F., TUTAJ, M. A., VEDI, M., WANG, S.-J., D'EUSTACHIO, P., AIMO, L., AXELSEN, K., BRIDGE, A., HYKA-NOUSPIKEL, N., MORGAT, A., ALEKSANDER, S. A., CHERRY, J. M., ENGEL, S. R., KARRA, K., MIYASATO, S. R., NASH, R. S., SKRZYPEK, M. S., WENG, S., WONG, E. D., BAKKER, E., et al. 2023. The Gene Ontology knowledgebase in 2023. *Genetics,* 224.

CONSORTIUM, T. U. 2022. UniProt: the Universal Protein Knowledgebase in 2023. *Nucleic Acids Research,* 51**,** D523-D531.

COZZETTO, D., MINNECI, F., CURRANT, H. & JONES, D. T. 2016. FFPred 3: feature-based function prediction for all Gene Ontology domains. *Scientific Reports,* 6**,** 31865.

DANIOTTI, J. L., PEDRO, M. P. & VALDEZ TAUBAS, J. 2017. The role of S-acylation in protein trafficking. *Traffic,* 18**,** 699-710.

DASILVA, J., XU, L., KIM, H. J., MILLER, W. T. & BAR-SAGI, D. 2006. Regulation of sprouty stability by Mnk1-dependent phosphorylation. *Molecular and cellular biology,* 26**,** 1898-1907.

DAVDA, D., EL AZZOUNY, M. A., TOM, C. T., HERNANDEZ, J. L., MAJMUDAR, J. D., KENNEDY, R. T. & MARTIN, B. R. 2013. Profiling targets of the irreversible palmitoylation inhibitor 2-bromopalmitate. *ACS Chem Biol,* 8**,** 1912-7.

DE MAXIMY, A. A., NAKATAKE, Y., MONCADA, S., ITOH, N., THIERY, J. P. & BELLUSCI, S. 1999. Cloning and expression pattern of a mouse homologue of drosophila sprouty in the mouse embryo. *Mech Dev,* 81**,** 213-6.

DEGIRMENCI, U., WANG, M. & HU, J. 2020. Targeting Aberrant RAS/RAF/MEK/ERK Signaling for Cancer Therapy. *Cells,* 9.

DERAKHSHANKHAH, H. & JAFARI, S. 2018. Cell penetrating peptides: A concise review with emphasis on biomedical applications. *Biomedicine & Pharmacotherapy,* 108**,** 1090-1096.

DHILLON, A. S., HAGAN, S., RATH, O. & KOLCH, W. 2007. MAP kinase signalling pathways in cancer. *Oncogene,* 26**,** 3279-3290.

DIEZ-ARDANUY, C., GREAVES, J., MUNRO, K. R., TOMKINSON, N. C. & CHAMBERLAIN, L. H. 2017. A cluster of palmitoylated cysteines are essential for aggregation of cysteine-string protein mutants that cause neuronal ceroid lipofuscinosis. *Sci Rep,* 7**,** 10.

DRAGIC, T., LITWIN, V., ALLAWAY, G. P., MARTIN, S. R., HUANG, Y., NAGASHIMA, K. A., CAYANAN, C., MADDON, P. J., KOUP, R. A., MOORE, J. P. & PAXTON, W. A. 1996. HIV-1 entry into CD4+ cells is mediated by the chemokine receptor CC-CKR-5. *Nature,* 381**,** 667-73.

DRUBIN, D. G., FEINSTEIN, S. C., SHOOTER, E. M. & KIRSCHNER, M. W. 1985. Nerve growth factor-induced neurite outgrowth in PC12 cells involves the coordinate induction of microtubule assembly and assembly-promoting factors. *J Cell Biol,* 101**,** 1799-807.

DU, Z. & LOVLY, C. M. 2018. Mechanisms of receptor tyrosine kinase activation in cancer. *Molecular Cancer,* 17**,** 58.

DUNCAN, J. A. & GILMAN, A. G. 1998a. A cytoplasmic acyl-protein thioesterase that removes palmitate from G protein alpha subunits and p21(RAS). *J Biol Chem,* 273**,** 15830-7.

DUNCAN, J. A. & GILMAN, A. G. 1998b. A Cytoplasmic Acyl-Protein Thioesterase That Removes Palmitate from G Protein α Subunits and p21<sup>RAS</sup>*. *Journal of Biological Chemistry,* 273**,** 15830-15837.

EDWIN, F., ANDERSON, K. & PATEL, T. B. 2010. HECT domain-containing E3 ubiquitin ligase Nedd4 interacts with and ubiquitinates Sprouty2. *J Biol Chem,* 285**,** 255-64.

EDWIN, F., ANDERSON, K., YING, C. & PATEL, T. B. 2009. Intermolecular interactions of Sprouty proteins and their implications in development and disease. *Mol Pharmacol,* 76**,** 679-91.

EL-ZOHAIRY, M. A., ZLOTOS, D. P., BERGER, M. R., ADWAN, H. H. & MANDOUR, Y. M. 2021. Discovery of Novel CCR5 Ligands as Anticolorectal Cancer Agents by Sequential Virtual Screening. *ACS Omega,* 6**,** 10921-10935.

ELLIOT MURPHY, R. & BANERJEE, A. 2022. In vitro reconstitution of substrate S-acylation by the zDHHC family of protein acyltransferases. *Open Biol,* 12**,** 210390.

EMBL-EBI. 2022. *What use cases does AlphaFold not support?* [Online]. AlphaFold Protein Structure Database: EMBL-EBI. Available: https://www.alphafold.ebi.ac.uk/faq#faq-8 [Accessed 13th August 2023].

EVANS, R., O'NEILL, M., PRITZEL, A., ANTROPOVA, N., SENIOR, A., GREEN, T., ŽÍDEK, A., BATES, R., BLACKWELL, S., YIM, J., RONNEBERGER, O., BODENSTEIN, S., ZIELINSKI, M., BRIDGLAND, A., POTAPENKO, A., COWIE, A., TUNYASUVUNAKOOL, K., JAIN, R., CLANCY, E., KOHLI, P., JUMPER, J. & HASSABIS, D. 2022. Protein complex prediction with AlphaFold-Multimer. *bioRxiv***,** 2021.10.04.463034.

FDA, U. S. F. A. D. A.-. 2021. Coronavirus (COVID-19) Update: FDA Authorizes First Oral Antiviral for Treatment of COVID-19. FDA Press Announcements: U.S. Food and Drug Administration - FDA.

FENG, Y.-H., WU, C.-L., TSAO, C.-J., CHANG, J.-G., LU, P.-J., YEH, K.-T., UEN, Y.-H., LEE, J.-C. & SHIAU, A.-L. 2011. Deregulated expression of Sprouty2 and MicroRNA-21 in human colon cancer: Correlation with the clinical stage of the disease. *Cancer biology & therapy,* 11**,** 111-21.

FERNÁNDEZ-HERNANDO, C., FUKATA, M., BERNATCHEZ, P. N., FUKATA, Y., LIN, M. I., BREDT, D. S. & SESSA, W. C. 2006. Identification of Golgi-localized acyl transferases that palmitoylate and regulate endothelial nitric oxide synthase. *The Journal of cell biology,* 174**,** 369-377.

FINKEL, Y., MIZRAHI, O., NACHSHON, A., WEINGARTEN-GABBAY, S., MORGENSTERN, D., YAHALOM-RONEN, Y., TAMIR, H., ACHDOUT, H., STEIN, D., ISRAELI, O., BETH-DIN, A., MELAMED, S., WEISS, S., ISRAELY, T., PARAN, N., SCHWARTZ, M. & STERN-GINOSSAR, N. 2021. The coding capacity of SARS-CoV-2. *Nature,* 589**,** 125-130.

FORRESTER, M. T., HESS, D. T., THOMPSON, J. W., HULTMAN, R., MOSELEY, M. A., STAMLER, J. S. & CASEY, P. J. 2011. Site-specific analysis of protein S-acylation by resin-assisted capture. *J Lipid Res,* 52**,** 393-8.

FUKATA, M., FUKATA, Y., ADESNIK, H., NICOLL, R. A. & BREDT, D. S. 2004. Identification of PSD-95 Palmitoylating Enzymes. *Neuron,* 44**,** 987-996.

GADALLA, M. R., ABRAMI, L., VAN DER GOOT, F. G. & VEIT, M. 2020. Hemagglutinin of Influenza A, but not of Influenza B and C viruses is acylated by ZDHHC2, 8, 15 and 20. *Biochem J,* 477**,** 285-303.

GAGNON, K. B. & DELPIRE, E. 2020. Sodium Transporters in Human Health and Disease. *Front Physiol,* 11**,** 588664.

GAO, W., LIN, S., CHENG, C., ZHU, A., HU, Y., SHI, Z., ZHANG, X. & HONG, Z. 2019. Long non-coding RNA CASC2 regulates Sprouty2 via functioning as a competing endogenous RNA for miR-183 to modulate the sensitivity of prostate cancer cells to docetaxel. *Archives of Biochemistry and Biophysics,* 665**,** 69-78.

GHAZY, R. M., ASHMAWY, R., HAMDY, N. A., ELHADI, Y. A. M., REYAD, O. A., ELMALAWANY, D., ALMAGHRABY, A., SHAABAN, R. & TAHA, S. H. N. 2022. Efficacy and Effectiveness of SARS-CoV-2 Vaccines: A Systematic Review and Meta-Analysis. *Vaccines (Basel),* 10.

GIGLIONE, C., BOULAROT, A. & MEINNEL, T. 2004. Protein N-terminal methionine excision. *Cell Mol Life Sci,* 61**,** 1455-74.

GOEHLER, H., LALOWSKI, M., STELZL, U., WAELTER, S., STROEDICKE, M., WORM, U., DROEGE, A., LINDENBERG, K. S., KNOBLICH, M., HAENIG, C., HERBST, M., SUOPANKI, J., SCHERZINGER, E., ABRAHAM, C., BAUER, B., HASENBANK, R., FRITZSCHE, A., LUDEWIG, A. H., BUESSOW, K., COLEMAN, S. H., GUTEKUNST, C.-A., LANDWEHRMEYER, B. G., LEHRACH, H. & WANKER, E. E. 2004. A Protein Interaction Network Links GIT1, an Enhancer of Huntingtin Aggregation, to Huntington's Disease. *Molecular Cell,* 15**,** 853-865.

GONG, J., YAN, Z. & LIU, Q. 2020. Progress in experimental research on SPRED protein family. *J Int Med Res,* 48**,** 300060520929170.

GONZÁLEZ MONTORO, A., CHUMPEN RAMIREZ, S., VALDEZ TAUBAS, J. & EX 2015. The Canonical DHHC Motif Is Not Absolutely Required for the Activity of the

Yeast S-acyltransferases Swf1 and Pfa4*. *Journal of Biological Chemistry,* 290**,** 22448-22459.

GONZÁLEZ MONTORO, A., QUIROGA, R., MACCIONI, HUGO J. F. & VALDEZ TAUBAS, J. 2009. A novel motif at the C-terminus of palmitoyltransferases is essential for Swf1 and Pfa3 function in vivo. *Biochemical Journal,* 419**,** 301-308.

GORDON, D. E., JANG, G. M., BOUHADDOU, M., XU, J., OBERNIER, K., WHITE, K. M., O'MEARA, M. J., REZELJ, V. V., GUO, J. Z., SWANEY, D. L., TUMMINO, T. A., HÜTTENHAIN, R., KAAKE, R. M., RICHARDS, A. L., TUTUNCUOGLU, B., FOUSSARD, H., BATRA, J., HAAS, K., MODAK, M., KIM, M., HAAS, P., POLACCO, B. J., BRABERG, H., FABIUS, J. M., ECKHARDT, M., SOUCHERAY, M., BENNETT, M. J., CAKIR, M., MCGREGOR, M. J., LI, Q., MEYER, B., ROESCH, F., VALLET, T., MAC KAIN, A., MIORIN, L., MORENO, E., NAING, Z. Z. C., ZHOU, Y., PENG, S., SHI, Y., ZHANG, Z., SHEN, W., KIRBY, I. T., MELNYK, J. E., CHORBA, J. S., LOU, K., DAI, S. A., BARRIO-HERNANDEZ, I., MEMON, D., HERNANDEZ-ARMENTA, C., LYU, J., MATHY, C. J. P., PERICA, T., PILLA, K. B., GANESAN, S. J., SALTZBERG, D. J., RAKESH, R., LIU, X., ROSENTHAL, S. B., CALVIELLO, L., VENKATARAMANAN, S., LIBOY-LUGO, J., LIN, Y., HUANG, X. P., LIU, Y., WANKOWICZ, S. A., BOHN, M., SAFARI, M., UGUR, F. S., KOH, C., SAVAR, N. S., TRAN, Q. D., SHENGJULER, D., FLETCHER, S. J., O'NEAL, M. C., CAI, Y., CHANG, J. C. J., BROADHURST, D. J., KLIPPSTEN, S., SHARP, P. P., WENZELL, N. A., KUZUOGLU-OZTURK, D., WANG, H. Y., TRENKER, R., YOUNG, J. M., CAVERO, D. A., HIATT, J., ROTH, T. L., RATHORE, U., SUBRAMANIAN, A., NOACK, J., HUBERT, M., STROUD, R. M., FRANKEL, A. D., ROSENBERG, O. S., VERBA, K. A., AGARD, D. A., OTT, M., EMERMAN, M., JURA, N., et al. 2020. A SARS-CoV-2 protein interaction map reveals targets for drug repurposing. *Nature,* 583**,** 459-468.

GORLEKU, O. A., BARNS, A. M., PRESCOTT, G. R., GREAVES, J. & CHAMBERLAIN, L. H. 2011. Endoplasmic reticulum localization of DHHC palmitoyltransferases mediated by lysine-based sorting signals. *J Biol Chem,* 286**,** 39573-84.

GOSPODAROWICZ, D., BIALECKI, H. & GREENBURG, G. 1978. Purification of the fibroblast growth factor activity from bovine brain. *The Journal of biological chemistry,* 253**,** 3736-3743.

GOYTAIN, A., HINES, R. M. & QUAMME, G. A. 2008. Huntingtin-interacting proteins, HIP14 and HIP14L, mediate dual functions, palmitoyl acyltransferase and Mg2+ transport. *J Biol Chem,* 283**,** 33365-74.

GREAVES, J. 2021. Deform the membrane, cAPTure the lipid. *Nature Chemical Biology,* 17**,** 371-372.

GREAVES, J., CARMICHAEL, J. A. & CHAMBERLAIN, L. H. 2011. The palmitoyl transferase DHHC2 targets a dynamic membrane cycling pathway: regulation by a C-terminal domain. *Mol Biol Cell,* 22**,** 1887-95.

GREAVES, J. & CHAMBERLAIN, L. H. 2011. Differential palmitoylation regulates intracellular patterning of SNAP25. *J Cell Sci,* 124**,** 1351-60.

GREAVES, J., GORLEKU, O. A., SALAUN, C. & CHAMBERLAIN, L. H. 2010a. Palmitoylation of the SNAP25 protein family: specificity and regulation by DHHC palmitoyl transferases. *J Biol Chem,* 285**,** 24629-38.

GREAVES, J., GORLEKU, O. A., SALAUN, C. & CHAMBERLAIN, L. H. 2010b. Palmitoylation of the SNAP25 Protein Family: SPECIFICITY AND REGULATION BY DHHC PALMITOYL TRANSFERASES*. *Journal of Biological Chemistry,* 285**,** 24629-24638.

GREAVES, J., LEMONIDIS, K., GORLEKU, O. A., CRUCHAGA, C., GREFEN, C. & CHAMBERLAIN, L. H. 2012. Palmitoylation-induced aggregation of cysteine-string protein mutants that cause neuronal ceroid lipofuscinosis. *J Biol Chem,* 287**,** 37330-9.

GREAVES, J., MUNRO, K. R., DAVIDSON, S. C., RIVIERE, M., WOJNO, J., SMITH, T. K., TOMKINSON, N. C. O. & CHAMBERLAIN, L. H. 2017. Molecular basis of fatty acid selectivity in the zDHHC family of S-acyltransferases revealed by click chemistry. *Proceedings of the National Academy of Sciences,* 114**,** E1365-E1374.

GREAVES, J., PRESCOTT, G. R., FUKATA, Y., FUKATA, M., SALAUN, C. & CHAMBERLAIN, L. H. 2009. The hydrophobic cysteine-rich domain of SNAP25 couples with downstream residues to mediate membrane interactions and recognition by DHHC palmitoyl transferases. *Mol Biol Cell,* 20**,** 1845-54.

GU, Y., LIU, X., LIAO, L., GAO, Y., SHI, Y., NI, J. & HE, G. 2021. Relationship between lipid metabolism and Hedgehog signaling pathway. *The Journal of Steroid Biochemistry and Molecular Biology,* 209**,** 105825.

GUNAWARDANA, D. 2016. PDZ Binding Domains, Structural Disorder and Phosphorylation: A Menage-a-trois Tailing Dcp2 mRNA Decapping Enzymes. *Protein Pept Lett,* 23**,** 612-8.

GUO, M. L., XUE, B., JIN, D. Z., MAO, L. M. & WANG, J. Q. 2012. Interactions and phosphorylation of postsynaptic density 93 (PSD-93) by extracellular signal-regulated kinase (ERK). *Brain Res,* 1465**,** 18-25.

GUPTA, P., SOYOMBO, A. A., ATASHBAND, A., WISNIEWSKI, K. E., SHELTON, J. M., RICHARDSON, J. A., HAMMER, R. E. & HOFMANN, S. L. 2001. Disruption of PPT1 or PPT2 causes neuronal ceroid lipofuscinosis in knockout mice. *Proc Natl Acad Sci U S A,* 98**,** 13566-71.

GUPTA, R., JANOSTIAK, R. & WAJAPEYEE, N. 2020. Transcriptional regulators and alterations that drive melanoma initiation and progression. *Oncogene,* 39**,** 7093-7105.

HACHIM, A., KAVIAN, N., COHEN, C. A., CHIN, A. W. H., CHU, D. K. W., MOK, C. K. P., TSANG, O. T. Y., YEUNG, Y. C., PERERA, R., POON, L. L. M., PEIRIS, J. S. M. & VALKENBURG, S. A. 2020. ORF8 and ORF3b antibodies are accurate serological markers of early and late SARS-CoV-2 infection. *Nat Immunol,* 21**,** 1293-1301.

HACOHEN, N., KRAMER, S., SUTHERLAND, D., HIROMI, Y. & KRASNOW, M. A. 1998. sprouty encodes a novel antagonist of FGF signaling that patterns apical branching of the Drosophila airways. *Cell,* 92**,** 253-63.

HANAFUSA, H., TORII, S., YASUNAGA, T. & NISHIDA, E. 2002. Sprouty1 and Sprouty2 provide a control mechanism for the Ras/MAPK signalling pathway. *Nature Cell Biology,* 4**,** 850-858.

HASHIMOTO, S., NAKANO, H., SUGUTA, Y., SINGH, G. & KATYAL, S. L. 2012. Immunolocalization of sprouty-1 and sprouty-2 in developing rat lung. *Pathobiology,* 79**,** 34-44.

HAUSOTT, B. & KLIMASCHEWSKI, L. 2019. Sprouty2-a Novel Therapeutic Target in the Nervous System? *Mol Neurobiol,* 56**,** 3897-3903.

HE, Q., JING, H., LIAW, L., GOWER, L., VARY, C., HUA, S. & YANG, X. 2016. Suppression of Spry1 inhibits triple-negative breast cancer malignancy by decreasing EGF/EGFR mediated mesenchymal phenotype. *Sci Rep,* 6**,** 23216.

HEINONEN, O., KYTTÄLÄ, A., LEHMUS, E., PAUNIO, T., PELTONEN, L. & JALANKO, A. 2000. Expression of palmitoyl protein thioesterase in neurons. *Mol Genet Metab,* 69**,** 123-9.

HENDERSON, M. X., WIRAK, G. S., ZHANG, Y. Q., DAI, F., GINSBERG, S. D., DOLZHANSKAYA, N., STAROPOLI, J. F., NIJSSEN, P. C., LAM, T. T., ROTH, A. F., DAVIS, N. G., DAWSON, G., VELINOV, M. & CHANDRA, S. S. 2016. Neuronal ceroid lipofuscinosis with DNAJC5/CSPα mutation has PPT1 pathology and exhibit aberrant protein palmitoylation. *Acta Neuropathol,* 131**,** 621-37.

HERCEG, Z. & HAINAUT, P. 2007. Genetic and epigenetic alterations as biomarkers for cancer detection, diagnosis and prognosis. *Molecular oncology,* 1**,** 26-41.

HERNANDEZ, J. L., DAVDA, D., KIT, M. C. S., MAJMUDAR, J. D., WON, S. J., GANG, M., PASUPULETI, S. C., CHOI, A. I., BARTKOWIAK, C. M. & MARTIN, B. R. 2017. APT2 inhibition restores scribble localization and S-palmitoylation in snail-transformed cells. *Cell chemical biology,* 24**,** 87-97.

HOBBS, G. A., DER, C. J. & ROSSMAN, K. L. 2016. RAS isoforms and mutations in cancer at a glance. *Journal of Cell Science,* 129**,** 1287-1292.

HOLGREN, C., DOUGHERTY, U., EDWIN, F., CERASI, D., TAYLOR, I., FICHERA, A., JOSEPH, L., BISSONNETTE, M. & KHARE, S. 2010. Sprouty-2 controls c-Met expression and metastatic potential of colon cancer cells: sprouty/c-Met upregulation in human colonic adenocarcinomas. *Oncogene,* 29**,** 5241-53.

HOLLMAN, R., WILD, A., O'LEARY, T., THOMPSON, A., FLIBOTTE, S., POBLETE, T., PENG, A., ROGALSKI, J., GILL, G. & BAMJI, S. 2023. The X-Linked Intellectual Disability gene, ZDHHC9, is important for oligodendrocyte maturation and myelin formation. *bioRxiv***,** 2023.08.08.552342.

HOWIE, J., REILLY, L., FRASER, N. J., VLACHAKI WALKER, J. M., WYPIJEWSKI, K. J., ASHFORD, M. L., CALAGHAN, S. C., MCCLAFFERTY, H., TIAN, L., SHIPSTON, M. J., BOGUSLAVSKYI, A., SHATTOCK, M. J. & FULLER, W. 2014. Substrate recognition by the cell surface palmitoyl transferase DHHC5. *Proc Natl Acad Sci U S A,* 111**,** 17534-9.

HOWIE, J., WYPIJEWSKI, K. J., PLAIN, F., TULLOCH, L. B., FRASER, N. J. & FULLER, W. 2018. Greasing the wheels or a spanner in the works? Regulation of the cardiac sodium pump by palmitoylation. *Critical Reviews in Biochemistry and Molecular Biology,* 53**,** 175-191.

HU, Y., XU, Y., CHEN, W. & QIU, Z. 2021. Stomatin-Like Protein-2: A Potential Target to Treat Mitochondrial Cardiomyopathy. *Heart, Lung and Circulation,* 30**,** 1449-1455.

HUANG, K., SANDERS, S. S., KANG, R., CARROLL, J. B., SUTTON, L., WAN, J., SINGARAJA, R., YOUNG, F. B., LIU, L., EL-HUSSEINI, A., DAVIS, N. G. & HAYDEN, M. R. 2011. Wild-type HTT modulates the enzymatic activity of the neuronal palmitoyl transferase HIP14. *Hum Mol Genet,* 20**,** 3356-65.

HURST, C. H. & HEMSLEY, P. A. 2015. Current perspective on protein S-acylation in plants: more than just a fatty anchor? *Journal of Experimental Botany,* 66**,** 1599-1606.

HURST, C. H., TURNBULL, D., XHELILAJ, K., MYLES, S., PFLUGHAUPT, R. L., KOPISCHKE, M., DAVIES, P., JONES, S., ROBATZEK, S., ZIPFEL, C., GRONNIER, J. & HEMSLEY, P. A. 2023. S-acylation stabilizes ligand-induced receptor kinase

complex formation during plant pattern-triggered immune signaling. *Current Biology,* 33**,** 1588-1596.e6.

HUTTLIN, E. L., TING, L., BRUCKNER, R. J., GEBREAB, F., GYGI, M. P., SZPYT, J., TAM, S., ZARRAGA, G., COLBY, G., BALTIER, K., DONG, R., GUARANI, V., VAITES, L. P., ORDUREAU, A., RAD, R., ERICKSON, B. K., WÜHR, M., CHICK, J., ZHAI, B., KOLIPPAKKAM, D., MINTSERIS, J., OBAR, R. A., HARRIS, T., ARTAVANIS-TSAKONAS, S., SOWA, M. E., DE CAMILLI, P., PAULO, J. A., HARPER, J. W. & GYGI, S. P. 2015. The BioPlex Network: A Systematic Exploration of the Human Interactome. *Cell,* 162**,** 425-440.

IMBRICI, P., D'ADAMO, M. C., KULLMANN, D. M. & PESSIA, M. 2006. Episodic ataxia type 1 mutations in the KCNA1 gene impair the fast inactivation properties of the human potassium channels Kv1.4-1.1/Kvbeta1.1 and Kv1.4-1.1/Kvbeta1.2. *Eur J Neurosci,* 24**,** 3073-83.

IMPAGNATIELLO, M. A., WEITZER, S., GANNON, G., COMPAGNI, A., COTTEN, M. & CHRISTOFORI, G. 2001. Mammalian sprouty-1 and -2 are membrane-anchored phosphoprotein inhibitors of growth factor signaling in endothelial cells. *The Journal of cell biology,* 152**,** 1087-1098.

JANSEN, M. & BEAUMELLE, B. 2022. How palmitoylation affects trafficking and signaling of membrane receptors. *Biol Cell,* 114**,** 61-72.

JEFFRIES, O., GEIGER, N., ROWE, I. C. M., TIAN, L., MCCLAFFERTY, H., CHEN, L., BI, D., KNAUS, H. G., RUTH, P. & SHIPSTON, M. J. 2010. Palmitoylation of the S0-S1 linker regulates cell surface expression of voltage- and calcium-activated potassium (BK) channels. *J Biol Chem,* 285**,** 33307-33314.

JIANG, H., ZHANG, X., CHEN, X., ARAMSANGTIENCHAI, P., TONG, Z. & LIN, H. 2018. Protein Lipidation: Occurrence, Mechanisms, Biological Functions, and Enabling Technologies. *Chem Rev,* 118**,** 919-988.

JIAO, X., VELASCO-VELÁZQUEZ, M. A., WANG, M., LI, Z., RUI, H., PECK, A. R., KORKOLA, J. E., CHEN, X., XU, S., DUHADAWAY, J. B., GUERRERO-RODRIGUEZ, S., ADDYA, S., SICOLI, D., MU, Z., ZHANG, G., STUCKY, A., ZHANG,

X., CRISTOFANILLI, M., FATATIS, A., GRAY, J. W., ZHONG, J. F., PRENDERGAST, G. C. & PESTELL, R. G. 2018. CCR5 Governs DNA Damage Repair and Breast Cancer Stem Cell Expansion. *Cancer Res,* 78**,** 1657-1671.

JIAO, X., WANG, M., ZHANG, Z., LI, Z., NI, D., ASHTON, A. W., TANG, H. Y., SPEICHER, D. W. & PESTELL, R. G. 2021. Leronlimab, a humanized monoclonal antibody to CCR5, blocks breast cancer cellular metastasis and enhances cell death induced by DNA damaging chemotherapy. *Breast Cancer Res,* 23**,** 11.

JIN, M., ZHANG, H., YANG, J., ZHENG, Z. & LIU, K. 2021. Expression mode and prognostic value of FXYD family members in colon cancer. *Aging (Albany NY),* 13**,** 18404-18422.

JONES, D. T. 1999. Protein secondary structure prediction based on position-specific scoring matrices11Edited by G. Von Heijne. *Journal of Molecular Biology,* 292**,** 195-202.

JOY, M. T., BEN ASSAYAG, E., SHABASHOV-STONE, D., LIRAZ-ZALTSMAN, S., MAZZITELLI, J., ARENAS, M., ABDULJAWAD, N., KLIPER, E., KORCZYN, A. D., THAREJA, N. S., KESNER, E. L., ZHOU, M., HUANG, S., SILVA, T. K., KATZ, N., BORNSTEIN, N. M., SILVA, A. J., SHOHAMI, E. & CARMICHAEL, S. T. 2019. CCR5 Is a Therapeutic Target for Recovery after Stroke and Traumatic Brain Injury. *Cell,* 176**,** 1143-1157.e13.

JUMPER, J., EVANS, R., PRITZEL, A., GREEN, T., FIGURNOV, M., RONNEBERGER, O., TUNYASUVUNAKOOL, K., BATES, R., ŽÍDEK, A., POTAPENKO, A., BRIDGLAND, A., MEYER, C., KOHL, S. A. A., BALLARD, A. J., COWIE, A., ROMERA-PAREDES, B., NIKOLOV, S., JAIN, R., ADLER, J., BACK, T., PETERSEN, S., REIMAN, D., CLANCY, E., ZIELINSKI, M., STEINEGGER, M., PACHOLSKA, M., BERGHAMMER, T., BODENSTEIN, S., SILVER, D., VINYALS, O., SENIOR, A. W., KAVUKCUOGLU, K., KOHLI, P. & HASSABIS, D. 2021. Highly accurate protein structure prediction with AlphaFold. *Nature,* 596**,** 583-589.

JUNGREIS, I., NELSON, C. W., ARDERN, Z., FINKEL, Y., KROGAN, N. J., SATO, K., ZIEBUHR, J., STERN-GINOSSAR, N., PAVESI, A., FIRTH, A. E., GORBALENYA,

A. E. & KELLIS, M. 2021. Conflicting and ambiguous names of overlapping ORFs in the SARS-CoV-2 genome: A homology-based resolution. *Virology,* 558**,** 145-151.

KACHROO, N., VALENCIA, T., WARREN, A. Y. & GNANAPRAGASAM, V. J. 2013. Evidence for downregulation of the negative regulator SPRED2 in clinical prostate cancer. *Br J Cancer,* 108**,** 597-601.

KALLEMEIJN, W. W., LANYON-HOGG, T., PANYAIN, N., GOYA GROCIN, A., CIEPLA, P., MORALES-SANFRUTOS, J. & TATE, E. W. 2021. Proteome-wide analysis of protein lipidation using chemical probes: in-gel fluorescence visualization, identification and quantification of N-myristoylation, N- and S-acylation, O-cholesterylation, S-farnesylation and S-geranylgeranylation. *Nature Protocols,* 16**,** 5083-5122.

KALYONCU, S., KESKIN, O. & GURSOY, A. 2010. Interaction prediction and classification of PDZ domains. *BMC Bioinformatics,* 11**,** 357.

KAMIYA, Y., SAKURAI, A., TAMURA, S., TAKAHASHI, N., ABE, K., TSUCHIYA, E., FUKUI, S., KITADA, C. & FUJINO, M. 1978. Structure of rhodotorucine A, a novel lipopeptide, inducing mating tube formation in Rhodosporidiumtoruloides. *Biochemical and Biophysical Research Communications,* 83**,** 1077-1083.

KAO, S.-C., JAISWAL, R. K., KOLCH, W. & LANDRETH, G. E. 2001. Identification of the Mechanisms Regulating the Differential Activation of the MAPK Cascade by Epidermal Growth Factor and Nerve Growth Factor in PC12 Cells*. *The Journal of Biological Chemistry,* 276**,** 18169 - 18177.

KATO, R., NONAMI, A., TAKETOMI, T., WAKIOKA, T., KUROIWA, A., MATSUDA, Y. & YOSHIMURA, A. 2003. Molecular cloning of mammalian Spred-3 which suppresses tyrosine kinase-mediated Erk activation. *Biochemical and Biophysical Research Communications,* 302**,** 767-772.

KAWAZOE, T. & TANIGUCHI, K. 2019. The Sprouty/Spred family as tumor suppressors: Coming of age. *Cancer Sci,* 110**,** 1525-1535.

KIELAR, C., MADDOX, L., BIBLE, E., PONTIKIS, C. C., MACAULEY, S. L., GRIFFEY, M. A., WONG, M., SANDS, M. S. & COOPER, J. D. 2007. Successive neuron loss in the thalamus and cortex in a mouse model of infantile neuronal ceroid lipofuscinosis. *Neurobiol Dis,* 25**,** 150-62.

KIM, E. K. & CHOI, E.-J. 2010. Pathological roles of MAPK signaling pathways in human diseases. *Biochimica et Biophysica Acta (BBA) - Molecular Basis of Disease,* 1802**,** 396-405.

KIM, Y.-M. & SHIN, E.-C. 2021. Type I and III interferon responses in SARS-CoV-2 infection. *Experimental & Molecular Medicine,* 53**,** 750-760.

KING, J. A., STRAFFON, A. F., D'ABACO, G. M., POON, C. L., I, S. T., SMITH, C. M., BUCHERT, M., CORCORAN, N. M., HALL, N. E., CALLUS, B. A., SARCEVIC, B., MARTIN, D., LOCK, P. & HOVENS, C. M. 2005. Distinct requirements for the Sprouty domain for functional activity of Spred proteins. *Biochem J,* 388**,** 445-54.

KO, P.-J., WOODROW, C., DUBREUIL, M. M., MARTIN, B. R., SKOUTA, R., BASSIK, M. C. & DIXON, S. J. 2019. A ZDHHC5-GOLGA7 Protein Acyltransferase Complex Promotes Nonapoptotic Cell Death. *Cell Chemical Biology,* 26**,** 1716-1724.e9.

KO, P. J. & DIXON, S. J. 2018. Protein palmitoylation and cancer. *EMBO Rep,* 19.

KONG, E., PENG, S., CHANDRA, G., SARKAR, C., ZHANG, Z., BAGH, M. B. & MUKHERJEE, A. B. 2013. Dynamic palmitoylation links cytosol-membrane shuttling of acyl-protein thioesterase-1 and acyl-protein thioesterase-2 with that of proto-oncogene H-ras product and growth-associated protein-43. *J Biol Chem,* 288**,** 9112-25.

KORDYUKOVA, L., KRABBEN, L., SEREBRYAKOVA, M. & VEIT, M. 2019. S-Acylation of Proteins. *In:* KANNICHT, C. (ed.) *Post-Translational Modification of Proteins: Tools for Functional Proteomics.* New York, NY: Springer New York.

KORYCKA, J., ŁACH, A., HEGER, E., BOGUSŁAWSKA, D. M., WOLNY, M., TOPORKIEWICZ, M., AUGOFF, K., KORZENIEWSKI, J. & SIKORSKI, A. F. 2012.

Human DHHC proteins: A spotlight on the hidden player of palmitoylation. *European Journal of Cell Biology,* 91**,** 107-117.

KOSTER, K. P., FRANCESCONI, W., BERTON, F., ALAHMADI, S., SRINIVAS, R. & YOSHII, A. 2019. Developmental NMDA receptor dysregulation in the infantile neuronal ceroid lipofuscinosis mouse model. *Elife,* 8.

KOSTER, K. P. & YOSHII, A. 2019. Depalmitoylation by Palmitoyl-Protein Thioesterase 1 in Neuronal Health and Degeneration. *Front Synaptic Neurosci,* 11**,** 25.

KOUSKOU, M., THOMSON, D. M., BRETT, R. R., WHEELER, L., TATE, R. J., PRATT, J. A. & CHAMBERLAIN, L. H. 2018. Disruption of the Zdhhc9 intellectual disability gene leads to behavioural abnormalities in a mouse model. *Exp Neurol,* 308**,** 35-46.

KRAFT, K., OLBRICH, H., MAJOUL, I., MACK, M., PROUDFOOT, A. & OPPERMANN, M. 2001. Characterization of Sequence Determinants within the Carboxyl-terminal Domain of Chemokine Receptor CCR5 That Regulate Signaling and Receptor Internalization *. *Journal of Biological Chemistry,* 276**,** 34408-34418.

KYTE, J. & DOOLITTLE, R. F. 1982. A simple method for displaying the hydropathic character of a protein. *Journal of Molecular Biology,* 157**,** 105-132.

LAKKARAJU, A. K., ABRAMI, L., LEMMIN, T., BLASKOVIC, S., KUNZ, B., KIHARA, A., DAL PERARO, M. & VAN DER GOOT, F. G. 2012. Palmitoylated calnexin is a key component of the ribosome-translocon complex. *Embo j,* 31**,** 1823-35.

LAM, J. Y., YUEN, C. K., IP, J. D., WONG, W. M., TO, K. K., YUEN, K. Y. & KOK, K. H. 2020. Loss of orf3b in the circulating SARS-CoV-2 strains. *Emerg Microbes Infect,* 9**,** 2685-2696.

LAO, D.-H., CHANDRAMOULI, S., YUSOFF, P., FONG, C. W., SAW, T. Y., TAI, L. P., YU, C. Y., LEONG, H. F. & GUY, G. R. 2006. A Src Homology 3-binding Sequence on the C Terminus of Sprouty2 Is Necessary for Inhibition of the Ras/ERK Pathway

Downstream of Fibroblast Growth Factor Receptor Stimulation *<sup></sup>. *Journal of Biological Chemistry,* 281**,** 29993-30000.

LAO, D.-H., YUSOFF, P., CHANDRAMOULI, S., PHILP, R. J., FONG, C. W., JACKSON, R. A., SAW, T. Y., YU, C. Y. & GUY, G. R. 2007a. Direct Binding of PP2A to Sprouty2 and Phosphorylation Changes Are a Prerequisite for ERK Inhibition Downstream of Fibroblast Growth Factor Receptor Stimulation *. *Journal of Biological Chemistry,* 282**,** 9117-9126.

LAO, D.-H., YUSOFF, P., CHANDRAMOULI, S., PHILP, R. J., FONG, C. W., JACKSON, R. A., SAW, T. Y., YU, C. Y. & GUY, G. R. 2007b. Direct Binding of PP2A to Sprouty2 and Phosphorylation Changes Are a Prerequisite for ERK Inhibition Downstream of Fibroblast Growth Factor Receptor Stimulation*. *Journal of Biological Chemistry,* 282**,** 9117-9126.

LAVOIE, H., GAGNON, J. & THERRIEN, M. 2020. ERK signalling: a master regulator of cell behaviour, life and fate. *Nature Reviews Molecular Cell Biology,* 21**,** 607-632.

LAZARUS, J. V., WYKA, K., WHITE, T. M., PICCHIO, C. A., GOSTIN, L. O., LARSON, H. J., RABIN, K., RATZAN, S. C., KAMARULZAMAN, A. & EL-MOHANDES, A. 2023. A survey of COVID-19 vaccine acceptance across 23 countries in 2022. *Nature Medicine,* 29**,** 366-375.

LEE, H. J. & ZHENG, J. J. 2010. PDZ domains and their binding partners: structure, specificity, and modification. *Cell Commun Signal,* 8**,** 8.

LEE, T. C., POGUE, J. M., MCCREARY, E. K. & MORRIS, A. M. 2022. What is the place in therapy for nirmatrelvir/ritonavir? *BMJ Evidence-Based Medicine***,** bmjebm-2022-112064.

LEEKSMA, O. C., VAN ACHTERBERG, T. A., TSUMURA, Y., TOSHIMA, J., ELDERING, E., KROES, W. G., MELLINK, C., SPAARGAREN, M., MIZUNO, K., PANNEKOEK, H. & DE VRIES, C. J. 2002. Human sprouty 4, a new ras antagonist on 5q31, interacts with the dual specificity kinase TESK1. *Eur J Biochem,* 269**,** 2546-56.

LEHTONEN, A., HOWIE, E., TRUMP, D. & HUSON, S. M. 2013. Behaviour in children with neurofibromatosis type 1: cognition, executive function, attention, emotion, and social competence. *Dev Med Child Neurol,* 55**,** 111-125.

LEHTOVIRTA, M., KYTTÄLÄ, A., ESKELINEN, E.-L., HESS, M., HEINONEN, O. & JALANKO, A. 2001. Palmitoyl protein thioesterase (PPT) localizes into synaptosomes and synaptic vesicles in neurons: implications for infantile neuronal ceroid lipofuscinosis (INCL). *Human Molecular Genetics,* 10**,** 69-75.

LEMMON, M. A. & SCHLESSINGER, J. 2010. Cell signaling by receptor tyrosine kinases. *Cell,* 141**,** 1117-1134.

LEMONIDIS, SANCHEZ-PEREZ, M. C. & CHAMBERLAIN, L. H. 2015a. Identification of a Novel Sequence Motif Recognized by the Ankyrin Repeat Domain of zDHHC17/13 S-Acyltransferases. *Journal of Biological Chemistry,* 290**,** 21939-21950.

LEMONIDIS, K., GORLEKU, O. A., SANCHEZ-PEREZ, M. C., GREFEN, C. & CHAMBERLAIN, L. H. 2014. The Golgi S-acylation machinery comprises zDHHC enzymes with major differences in substrate affinity and S-acylation activity. *Mol Biol Cell,* 25**,** 3870-83.

LEMONIDIS, K., MACLEOD, R., BAILLIE, G. S. & CHAMBERLAIN, L. H. 2017a. Peptide array-based screening reveals a large number of proteins interacting with the ankyrin-repeat domain of the zDHHC17 S-acyltransferase. *J Biol Chem,* 292**,** 17190-17202.

LEMONIDIS, K., SALAUN, C., KOUSKOU, M., DIEZ-ARDANUY, C., CHAMBERLAIN, L. H. & GREAVES, J. 2017b. Substrate selectivity in the zDHHC family of S-acyltransferases. *Biochem Soc Trans,* 45**,** 751-758.

LEMONIDIS, K., SANCHEZ-PEREZ, M. C. & CHAMBERLAIN, L. H. 2015b. Identification of a Novel Sequence Motif Recognized by the Ankyrin Repeat Domain of zDHHC17/13 S-Acyltransferases. *Journal of Biological Chemistry,* 290**,** 21939-21950.

LEMONIDIS, K., WERNO, MARTIN W., GREAVES, J., DIEZ-ARDANUY, C., SANCHEZ-PEREZ, MARIA C., SALAUN, C., THOMSON, DAVID M. & CHAMBERLAIN, LUKE H. 2015c. The zDHHC family of S-acyltransferases. *Biochemical Society Transactions,* 43**,** 217-221.

LEVI-MONTALCINI, R. & BOOKER, B. 1960. EXCESSIVE GROWTH OF THE SYMPATHETIC GANGLIA EVOKED BY A PROTEIN ISOLATED FROM MOUSE SALIVARY GLANDS. *Proceedings of the National Academy of Sciences of the United States of America,* 46**,** 373-384.

LI, D., LIU, Y., LU, Y., GAO, S. & ZHANG, L. 2022a. Palmitoylation of SARS-CoV-2 S protein is critical for S-mediated syncytia formation and virus entry. *J Med Virol,* 94**,** 342-348.

LI, Q., LIU, Y. & ZHANG, L. 2022b. Cytoplasmic tail determines the membrane trafficking and localization of SARS-CoV-2 spike protein. *Frontiers in Molecular Biosciences,* 9.

LIM, J., WONG, E. S. M., ONG, S. H., YUSOFF, P., LOW, B. C. & GUY, G. R. 2000. Sprouty Proteins Are Targeted to Membrane Ruffles upon Growth Factor Receptor Tyrosine Kinase Activation: IDENTIFICATION OF A NOVEL TRANSLOCATION DOMAIN. *Journal of Biological Chemistry,* 275**,** 32837-32845.

LIM, J., YUSOFF, P., WONG, E. S. M., CHANDRAMOULI, S., LAO, D.-H., FONG, C. W. & GUY, G. R. 2002. The Cysteine-Rich Sprouty Translocation Domain Targets Mitogen-Activated Protein Kinase Inhibitory Proteins to Phosphatidylinositol 4,5-Bisphosphate in Plasma Membranes. *Molecular and Cellular Biology,* 22**,** 7953-7966.

LIN, D. T. & CONIBEAR, E. 2015. ABHD17 proteins are novel protein depalmitoylases that regulate N-Ras palmitate turnover and subcellular localization. *Elife,* 4**,** e11306.

LINDER, M. E. & DESCHENES, R. J. 2007. Palmitoylation: policing protein stability and traffic. *Nat Rev Mol Cell Biol,* 8**,** 74-84.

LOBO, S., GREENTREE, W. K., LINDER, M. E. & DESCHENES, R. J. 2002. Identification of a Ras palmitoyltransferase in Saccharomyces cerevisiae. *J Biol Chem,* 277**,** 41268-73.

LOCATELLI, C. 2021. *Investigating the mechanisms and outcomes of Sprouty-2 S-acylation.*

LOCATELLI, C., LEMONIDIS, K., SALAUN, C., TOMKINSON, N. C. O. & CHAMBERLAIN, L. H. 2020. Identification of key features required for efficient S-acylation and plasma membrane targeting of sprouty-2. *Journal of cell science,* 133**,** jcs249664.

LORD, C. C., THOMAS, G. & BROWN, J. M. 2013. Mammalian alpha beta hydrolase domain (ABHD) proteins: Lipid metabolizing enzymes at the interface of cell signaling and energy metabolism. *Biochim Biophys Acta,* 1831**,** 792-802.

LORENZO, C. & MCCORMICK, F. 2020. SPRED proteins and their roles in signal transduction, development, and malignancy. *Genes Dev,* 34**,** 1410-1421.

LOVE, I. M., SHI, D. & GROSSMAN, S. R. 2013. p53 Ubiquitination and proteasomal degradation. *Methods Mol Biol,* 962**,** 63-73.

MA, B., ELKAYAM, T., WOLFSON, H. & NUSSINOV, R. 2003. Protein–protein interactions: Structurally conserved residues distinguish between binding sites and exposed protein surfaces. *Proceedings of the National Academy of Sciences,* 100**,** 5772-5777.

MACHHI, J., HERSKOVITZ, J., SENAN, A. M., DUTTA, D., NATH, B., OLEYNIKOV, M. D., BLOMBERG, W. R., MEIGS, D. D., HASAN, M., PATEL, M., KLINE, P., CHANG, R. C., CHANG, L., GENDELMAN, H. E. & KEVADIYA, B. D. 2020. The Natural History, Pathobiology, and Clinical Manifestations of SARS-CoV-2 Infections. *J Neuroimmune Pharmacol,* 15**,** 359-386.

MADEIRA, F., PEARCE, M., TIVEY, A. R. N., BASUTKAR, P., LEE, J., EDBALI, O., MADHUSOODANAN, N., KOLESNIKOV, A. & LOPEZ, R. 2022. Search and

sequence analysis tools services from EMBL-EBI in 2022. *Nucleic Acids Research,* 50**,** W276-W279.

MALGAPO, M. I. P. & LINDER, M. E. 2021. Substrate recruitment by zDHHC protein acyltransferases. *Open Biol,* 11**,** 210026.

MALONE, B., URAKOVA, N., SNIJDER, E. J. & CAMPBELL, E. A. 2022. Structures and functions of coronavirus replication–transcription complexes and their relevance for SARS-CoV-2 drug design. *Nature Reviews Molecular Cell Biology,* 23**,** 21-39.

MANSOURI, M. R., MARKLUND, L., GUSTAVSSON, P., DAVEY, E., CARLSSON, B., LARSSON, C., WHITE, I., GUSTAVSON, K.-H. & DAHL, N. 2005. Loss of ZDHHC15 expression in a woman with a balanced translocation t(X;15)(q13.3;cen) and severe mental retardation. *European Journal of Human Genetics,* 13**,** 970-977.

MARKOV, P. V., GHAFARI, M., BEER, M., LYTHGOE, K., SIMMONDS, P., STILIANAKIS, N. I. & KATZOURAKIS, A. 2023. The evolution of SARS-CoV-2. *Nature Reviews Microbiology,* 21**,** 361-379.

MARTIN, B. R. & CRAVATT, B. F. 2009. Large-scale profiling of protein palmitoylation in mammalian cells. *Nat Methods,* 6**,** 135-8.

MARTIN, D. D. O., BEAUCHAMP, E. & BERTHIAUME, L. G. 2011. Post-translational myristoylation: Fat matters in cellular life and death. *Biochimie,* 93**,** 18-31.

MARTÍNEZ, N., GRAGERA, T., DE LUCAS, M. P., CÁMARA, A. B., BALLESTER, A., ANTA, B., FERNÁNDEZ-MEDARDE, A., LÓPEZ-BRIONES, T., ORTEGA, J., PEÑA-JIMÉNEZ, D., BARBÁCHANO, A., MONTERO-CALLE, A., CORDERO, V., BARDERAS, R., IGLESIAS, T., YUNTA, M., OLIVA, J. L., MUÑOZ, A., SANTOS, E., ZARICH, N. & ROJAS-CABAÑEROS, J. M. 2023. PKD phosphorylation and COP9/Signalosome modulate intracellular Spry2 protein stability. *Oncogenesis,* 12**,** 20.

MARVALDI, L., THONGRONG, S., KOZŁOWSKA, A., IRSCHICK, R., PRITZ, C. O., BÄUMER, B., RONCHI, G., GEUNA, S., HAUSOTT, B. & KLIMASCHEWSKI, L. 2015.

Enhanced axon outgrowth and improved long-distance axon regeneration in sprouty2 deficient mice. *Developmental Neurobiology,* 75**,** 217-231.

MASOUMI-MOGHADDAM, S., AMINI, A., EHTEDA, A., WEI, A. Q. & MORRIS, D. L. 2014a. The expression of the Sprouty 1 protein inversely correlates with growth, proliferation, migration and invasion of ovarian cancer cells. *J Ovarian Res,* 7**,** 61.

MASOUMI-MOGHADDAM, S., AMINI, A. & MORRIS, D. L. 2014b. The developing story of Sprouty and cancer. *Cancer and Metastasis Reviews,* 33**,** 695-720.

MASOUMI-MOGHADDAM, S., AMINI, A., WEI, A.-Q., ROBERTSON, G. & MORRIS, D. L. 2015a. Sprouty2 protein in prediction of post-treatment ascites in epithelial ovarian cancer treated with adjuvant carbotaxol chemotherapy. *American journal of cancer research,* 5**,** 2498-2507.

MASOUMI-MOGHADDAM, S., AMINI, A., WEI, A. Q., ROBERTSON, G. & MORRIS, D. L. 2015b. Sprouty 1 predicts prognosis in human epithelial ovarian cancer. *Am J Cancer Res,* 5**,** 1531-41.

MCCOLGAN, P. & TABRIZI, S. J. 2018. Huntington's disease: a clinical review. *Eur J Neurol,* 25**,** 24-34.

MESQUITA, F. S., ABRAMI, L., BRACQ, L., PANYAIN, N., MERCIER, V., KUNZ, B., CHUAT, A., CARLEVARO-FITA, J., TRONO, D. & GOOT, F. G. V. D. 2023. SARS-CoV-2 shifts transcription of host gene to increase Spike acylation and boost infectivity. *bioRxiv***,** 2023.04.15.537011.

MESQUITA, F. S., ABRAMI, L., SERGEEVA, O., TURELLI, P., QING, E., KUNZ, B., RACLOT, C., PAZ MONTOYA, J., ABRIATA, L. A., GALLAGHER, T., DAL PERARO, M., TRONO, D., D'ANGELO, G. & VAN DER GOOT, F. G. 2021. S-acylation controls SARS-CoV-2 membrane lipid organization and enhances infectivity. *Dev Cell,* 56**,** 2790-2807.e8.

MILNERWOOD, A. J., PARSONS, M. P., YOUNG, F. B., SINGARAJA, R. R., FRANCIOSI, S., VOLTA, M., BERGERON, S., HAYDEN, M. R. & RAYMOND, L. A.

2013. Memory and synaptic deficits in Hip14/DHHC17 knockout mice. *Proc Natl Acad Sci U S A,* 110**,** 20296-301.

MIRAOUI, H., DWYER, A. A., SYKIOTIS, G. P., PLUMMER, L., CHUNG, W., FENG, B., BEENKEN, A., CLARKE, J., PERS, T. H., DWORZYNSKI, P., KEEFE, K., NIEDZIELA, M., RAIVIO, T., CROWLEY, W. F., JR., SEMINARA, S. B., QUINTON, R., HUGHES, V. A., KUMANOV, P., YOUNG, J., YIALAMAS, M. A., HALL, J. E., VAN VLIET, G., CHANOINE, J. P., RUBENSTEIN, J., MOHAMMADI, M., TSAI, P. S., SIDIS, Y., LAGE, K. & PITTELOUD, N. 2013. Mutations in FGF17, IL17RD, DUSP6, SPRY4, and FLRT3 are identified in individuals with congenital hypogonadotropic hypogonadism. *Am J Hum Genet,* 92**,** 725-43.

MITCHELL, D. A., HAMEL, L. D., REDDY, K. D., FARH, L., RETTEW, L. M., SANCHEZ, P. R. & DESCHENES, R. J. 2014. Mutations in the X-linked Intellectual Disability Gene, zDHHC9, Alter Autopalmitoylation Activity by Distinct Mechanisms *. *Journal of Biological Chemistry,* 289**,** 18582-18592.

MITCHELL, D. A., MITCHELL, G., LING, Y., BUDDE, C. & DESCHENES, R. J. 2010. Mutational Analysis of Saccharomyces cerevisiae Erf2 Reveals a Two-step Reaction Mechanism for Protein Palmitoylation by DHHC Enzymes*, ♦. *Journal of Biological Chemistry,* 285**,** 38104-38114.

MITCHELL, D. A., VASUDEVAN, A., LINDER, M. E. & DESCHENES, R. J. 2006. Thematic review series: Lipid Posttranslational Modifications. Protein palmitoylation by a family of DHHC protein S-acyltransferases. *Journal of Lipid Research,* 47**,** 1118-1127.

MIYOSHI, K., WAKIOKA, T., NISHINAKAMURA, H., KAMIO, M., YANG, L., INOUE, M., HASEGAWA, M., YONEMITSU, Y., KOMIYA, S. & YOSHIMURA, A. 2004. The Sprouty-related protein, Spred, inhibits cell motility, metastasis, and Rho-mediated actin reorganization. *Oncogene,* 23**,** 5567-76.

MOLE, S. E. & COTMAN, S. L. 2015. Genetics of the neuronal ceroid lipofuscinoses (Batten disease). *Biochim Biophys Acta,* 1852**,** 2237-41.

MOLL, U. M. & PETRENKO, O. 2003. The MDM2-p53 Interaction. *Molecular Cancer Research,* 1**,** 1001-1008.

MORETTO, E. & PASSAFARO, M. 2018. Recent Findings on AMPA Receptor Recycling. *Front Cell Neurosci,* 12**,** 286.

MUKAI, J., LIU, H., BURT, R. A., SWOR, D. E., LAI, W.-S., KARAYIORGOU, M. & GOGOS, J. A. 2004. Evidence that the gene encoding ZDHHC8 contributes to the risk of schizophrenia. *Nature Genetics,* 36**,** 725-731.

MURUGAN, A. K., GRIECO, M. & TSUCHIDA, N. 2019. RAS mutations in human cancers: Roles in precision medicine. *Semin Cancer Biol,* 59**,** 23-35.

MÓL, A. R., CASTRO, M. S. & FONTES, W. 2018. NetWheels: A web application to create high quality peptide helical wheel and net projections. *bioRxiv***,** 416347.

NELSON, C. W., ARDERN, Z., GOLDBERG, T. L., MENG, C., KUO, C.-H., LUDWIG, C., KOLOKOTRONIS, S.-O. & WEI, X. 2020. Dynamically evolving novel overlapping gene as a factor in the SARS-CoV-2 pandemic. *eLife,* 9**,** e59633.

NG, C., JACKSON, R. A., BUSCHDORF, J. P., SUN, Q., GUY, G. R. & SIVARAMAN, J. 2008. Structural basis for a novel intrapeptidyl H-bond and reverse binding of c-Cbl-TKB domain substrates. *The EMBO Journal,* 27**,** 804-816.

NGUYEN, P. L., GREENTREE, W. K., KAWATE, T. & LINDER, M. E. 2023. GCP16 stabilizes the DHHC9 subfamily of protein acyltransferases through a conserved C-terminal cysteine motif. *Frontiers in Physiology,* 14.

NORITAKE, J., FUKATA, Y., IWANAGA, T., HOSOMI, N., TSUTSUMI, R., MATSUDA, N., TANI, H., IWANARI, H., MOCHIZUKI, Y., KODAMA, T., MATSUURA, Y., BREDT, D. S., HAMAKUBO, T. & FUKATA, M. 2009. Mobile DHHC palmitoylating enzyme mediates activity-sensitive synaptic targeting of PSD-95. *J Cell Biol,* 186**,** 147-60.

NORMANNO, N., DE LUCA, A., BIANCO, C., STRIZZI, L., MANCINO, M., MAIELLO, M. R., CAROTENUTO, A., DE FEO, G., CAPONIGRO, F. & SALOMON, D. S. 2006. Epidermal growth factor receptor (EGFR) signaling in cancer. *Gene,* 366**,** 2-16.

NOSKOVÁ, L., STRÁNECKÝ, V., HARTMANNOVÁ, H., PŘISTOUPILOVÁ, A., BAREŠOVÁ, V., IVÁNEK, R., HŮLKOVÁ, H., JAHNOVÁ, H., VAN DER ZEE, J., STAROPOLI, J. F., SIMS, K. B., TYYNELÄ, J., VAN BROECKHOVEN, C., NIJSSEN, P. C., MOLE, S. E., ELLEDER, M. & KMOCH, S. 2011. Mutations in DNAJC5, encoding cysteine-string protein alpha, cause autosomal-dominant adult-onset neuronal ceroid lipofuscinosis. *Am J Hum Genet,* 89**,** 241-52.

ODENIYIDE, P., YOHE, M. E., POLLARD, K., VASEVA, A. V., CALIZO, A., ZHANG, L., RODRIGUEZ, F. J., GROSS, J. M., ALLEN, A. N., WAN, X., SOMWAR, R., SCHRECK, K. C., KESSLER, L., WANG, J. & PRATILAS, C. A. 2022. Targeting farnesylation as a novel therapeutic approach in HRAS-mutant rhabdomyosarcoma. *Oncogene,* 41**,** 2973-2983.

OHNO, Y., KIHARA, A., SANO, T. & IGARASHI, Y. 2006. Intracellular localization and tissue-specific distribution of human and yeast DHHC cysteine-rich domain-containing proteins. *Biochimica et biophysica acta,* 1761**,** 474-83.

OHTA, E., MISUMI, Y., SOHDA, M., FUJIWARA, T., YANO, A. & IKEHARA, Y. 2003. Identification and Characterization of GCP16, a Novel Acylated Golgi Protein That Interacts with GCP170 *. *Journal of Biological Chemistry,* 278**,** 51957-51967.

OKAMOTO, M., SCHOCH, S. & SÜDHOF, T. C. 1999. EHSH1/Intersectin, a Protein That Contains EH and SH3 Domains and Binds to Dynamin and SNAP-25: A PROTEIN CONNECTION BETWEEN EXOCYTOSIS AND ENDOCYTOSIS?*. *Journal of Biological Chemistry,* 274**,** 18446-18454.

OKUR, M. N., OOI, J., FONG, C. W., MARTINEZ, N., GARCIA-DOMINGUEZ, C., ROJAS, J. M., GUY, G. & O'BRYAN, J. P. 2012. Intersectin 1 Enhances Cbl Ubiquitylation of Epidermal Growth Factor Receptor through Regulation of Sprouty2-Cbl Interaction. *Molecular and Cellular Biology,* 32**,** 817-825.

OLIVEIRA-PAULA, G. H., LACCHINI, R. & TANUS-SANTOS, J. E. 2016. Endothelial nitric oxide synthase: From biochemistry and gene structure to clinical implications of NOS3 polymorphisms. *Gene,* 575**,** 584-99.

OO, H. Z., SENTANI, K., SAKAMOTO, N., ANAMI, K., NAITO, Y., URAOKA, N., OSHIMA, T., YANAGIHARA, K., OUE, N. & YASUI, W. 2014. Overexpression of ZDHHC14 promotes migration and invasion of scirrhous type gastric cancer. *Oncol Rep,* 32**,** 403-410.

PALSULEDESAI, C. C. & DISTEFANO, M. D. 2015. Protein prenylation: enzymes, therapeutics, and biotechnology applications. *ACS Chem Biol,* 10**,** 51-62.

PANCHARIYA, L., KHAN, W. A., KUILA, S., SONKAR, K., SAHOO, S., GHOSHAL, A., KUMAR, A., VERMA, D. K., HASAN, A., KHAN, M. A., JAIN, N., MOHAPATRA, A. K., DAS, S., THAKUR, J. K., MAITI, S., NANDA, R. K., HALDER, R., SUNIL, S. & AROCKIASAMY, A. 2021. Zinc(2+) ion inhibits SARS-CoV-2 main protease and viral replication in vitro. *Chem Commun (Camb),* 57**,** 10083-10086.

PARK, H. L., BAI, C., PLATT, K. A., MATISE, M. P., BEEGHLY, A., HUI, C. C., NAKASHIMA, M. & JOYNER, A. L. 2000. Mouse Gli1 mutants are viable but have defects in SHH signaling in combination with a Gli2 mutation. *Development,* 127**,** 1593-1605.

PASMANT, E., GILBERT-DUSSARDIER, B., PETIT, A., DE LAVAL, B., LUSCAN, A., GRUBER, A., LAPILLONNE, H., DESWARTE, C., GOUSSARD, P., LAURENDEAU, I., UZAN, B., PFLUMIO, F., BRIZARD, F., VABRES, P., NAGUIBVENA, I., FASOLA, S., MILLOT, F., PORTEU, F., VIDAUD, D., LANDMAN-PARKER, J. & BALLERINI, P. 2015. SPRED1, a RAS MAPK pathway inhibitor that causes Legius syndrome, is a tumour suppressor downregulated in paediatric acute myeloblastic leukaemia. *Oncogene,* 34**,** 631-8.

PATEL, R., GAO, M., AHMAD, I., FLEMING, J., SINGH, L. B., RAI, T. S., MCKIE, A. B., SEYWRIGHT, M., BARNETSON, R. J., EDWARDS, J., SANSOM, O. J. & LEUNG, H. Y. 2013a. Sprouty2, PTEN, and PP2A interact to regulate prostate cancer progression. *J Clin Invest,* 123**,** 1157-75.

PATEL, R., GAO, M., AHMAD, I., FLEMING, J., SINGH, L. B., RAI, T. S., MCKIE, A. B., SEYWRIGHT, M., BARNETSON, R. J., EDWARDS, J., SANSOM, O. J. & LEUNG, H. Y. 2013b. Sprouty2, PTEN, and PP2A interact to regulate prostate cancer progression. *The Journal of clinical investigation,* 123**,** 1157-1175.

PEDRAM, A., RAZANDI, M., DESCHENES, R. J. & LEVIN, E. R. 2012. DHHC-7 and -21 are palmitoylacyltransferases for sex steroid receptors. *Mol Biol Cell,* 23**,** 188-99.

PELTONEN, S., KALLIONPÄÄ, R. A. & PELTONEN, J. 2017. Neurofibromatosis type 1 (NF1) gene: Beyond café au lait spots and dermal neurofibromas. *Experimental Dermatology,* 26**,** 645-648.

PETERSON, F. C. & VOLKMAN, B. F. 2009. Diversity of polyproline recognition by EVH1 domains. *Front Biosci (Landmark Ed),* 14**,** 833-46.

PETIT, C. M., CHOULJENKO, V. N., IYER, A., COLGROVE, R., FARZAN, M., KNIPE, D. M. & KOUSOULAS, K. G. 2007. Palmitoylation of the cysteine-rich endodomain of the SARS-coronavirus spike glycoprotein is important for spike-mediated cell fusion. *Virology,* 360**,** 264-74.

PIPEK, O., VIZKELETI, L., DOMA, V., ALPÁR, D., BÖDÖR, C., KÁRPÁTI, S. & TIMAR, J. 2023. The Driverless Triple-Wild-Type (BRAF, RAS, KIT) Cutaneous Melanoma: Whole Genome Sequencing Discoveries. *Cancers,* 15**,** 1712.

PLAIN, F., HOWIE, J., KENNEDY, J., BROWN, E., SHATTOCK, M. J., FRASER, N. J. & FULLER, W. 2020. Control of protein palmitoylation by regulating substrate recruitment to a zDHHC-protein acyltransferase. *Commun Biol,* 3**,** 411.

PORMOHAMMAD, A., MONYCH, N. K. & TURNER, R. J. 2021. Zinc and SARS-CoV-2: A molecular modeling study of Zn interactions with RNA-dependent RNA-polymerase and 3C-like proteinase enzymes. *Int J Mol Med,* 47**,** 326-334.

PRIOR, I. A., HOOD, F. E. & HARTLEY, J. L. 2020. The Frequency of Ras Mutations in Cancer. *Cancer Research,* 80**,** 2969-2974.

PUTHENVEETIL, R., LUN, C. M., MURPHY, R. E., HEALY, L. B., VILMEN, G., CHRISTENSON, E. T., FREED, E. O. & BANERJEE, A. 2021. S-acylation of SARS-CoV-2 spike protein: Mechanistic dissection, in vitro reconstitution and role in viral infectivity. *J Biol Chem,* 297**,** 101112.

QUACH, T. T., STRATTON, H. J., KHANNA, R., KOLATTUKUDY, P. E., HONNORAT, J., MEYER, K. & DUCHEMIN, A.-M. 2021. Intellectual disability: dendritic anomalies and emerging genetic perspectives. *Acta Neuropathologica,* 141**,** 139-158.

RADTKE, H. B., BERGER, A., SKELTON, T. & GOETSCH WEISMAN, A. 2023. Neurofibromatosis Type 1 (NF1): Addressing the Transition from Pediatric to Adult Care. *Pediatric Health Med Ther,* 14**,** 19-32.

RAKHA, E. A., EL-SHEIKH, S. E., KANDIL, M. A., EL-SAYED, M. E., GREEN, A. R. & ELLIS, I. O. 2008. Expression of BRCA1 protein in breast cancer and its prognostic significance. *Hum Pathol,* 39**,** 857-65.

RAMADAN, A. A., MAYILSAMY, K., MCGILL, A. R., GHOSH, A., GIULIANOTTI, M. A., DONOW, H. M., MOHAPATRA, S. S., MOHAPATRA, S., CHANDRAN, B., DESCHENES, R. J. & ROY, A. 2022. Identification of SARS-CoV-2 Spike Palmitoylation Inhibitors That Results in Release of Attenuated Virus with Reduced Infectivity. *Viruses,* 14.

RAMAZI, S. & ZAHIRI, J. 2021. Posttranslational modifications in proteins: resources, tools and prediction methods. *Database (Oxford),* 2021.

RANA, M. S., KUMAR, P., LEE, C. J., VERARDI, R., RAJASHANKAR, K. R. & BANERJEE, A. 2018a. Fatty acyl recognition and transfer by an integral membrane S-acyltransferase. *Science,* 359.

RANA, M. S., LEE, C.-J. & BANERJEE, A. 2018b. The molecular mechanism of DHHC protein acyltransferases. *Biochemical Society Transactions,* 47**,** 157-167.

RAYMOND, F. L., TARPEY, P. S., EDKINS, S., TOFTS, C., O'MEARA, S., TEAGUE, J., BUTLER, A., STEVENS, C., BARTHORPE, S., BUCK, G., COLE, J., DICKS, E.,

GRAY, K., HALLIDAY, K., HILLS, K., HINTON, J., JONES, D., MENZIES, A., PERRY, J., RAINE, K., SHEPHERD, R., SMALL, A., VARIAN, J., WIDAA, S., MALLYA, U., MOON, J., LUO, Y., SHAW, M., BOYLE, J., KERR, B., TURNER, G., QUARRELL, O., COLE, T., EASTON, D. F., WOOSTER, R., BOBROW, M., SCHWARTZ, C. E., GECZ, J., STRATTON, M. R. & FUTREAL, P. A. 2007. Mutations in ZDHHC9, which encodes a palmitoyltransferase of NRAS and HRAS, cause X-linked mental retardation associated with a Marfanoid habitus. *Am J Hum Genet,* 80**,** 982-7.

REDONDO, N., ZALDÍVAR-LÓPEZ, S., GARRIDO, J. J. & MONTOYA, M. 2021. SARS-CoV-2 Accessory Proteins in Viral Pathogenesis: Knowns and Unknowns. *Frontiers in Immunology,* 12.

REMSBERG, J. R., SUCIU, R. M., ZAMBETTI, N. A., HANIGAN, T. W., FIRESTONE, A. J., INGUVA, A., LONG, A., NGO, N., LUM, K. M., HENRY, C. L., RICHARDSON, S. K., PREDOVIC, M., HUANG, B., DIX, M. M., HOWELL, A. R., NIPHAKIS, M. J., SHANNON, K. & CRAVATT, B. F. 2021. ABHD17 regulation of plasma membrane palmitoylation and N-Ras-dependent cancer growth. *Nature Chemical Biology,* 17**,** 856-864.

ROBINSON, P. J. & BULLEID, N. J. 2020. Mechanisms of Disulfide Bond Formation in Nascent Polypeptides Entering the Secretory Pathway. *Cells,* 9**,** 1994.

ROCKS, O., GERAUER, M., VARTAK, N., KOCH, S., HUANG, Z.-P., PECHLIVANIS, M., KUHLMANN, J., BRUNSVELD, L., CHANDRA, A., ELLINGER, B., WALDMANN, H. & BASTIAENS, P. I. H. 2010. The Palmitoylation Machinery Is a Spatially Organizing System for Peripheral Membrane Proteins. *Cell,* 141**,** 458-471.

ROCKS, O., PEYKER, A. & BASTIAENS, P. I. H. 2006. Spatio-temporal segregation of Ras signals: one ship, three anchors, many harbors. *Current Opinion in Cell Biology,* 18**,** 351-357.

ROTH, A. F., FENG, Y., CHEN, L. & DAVIS, N. G. 2002. The yeast DHHC cysteine-rich domain protein Akr1p is a palmitoyl transferase. *The Journal of cell biology,* 159**,** 23-28.

SAINI, M., VERMA, A. & MATHEW, S. J. 2018. SPRY2 is a novel MET interactor that regulates metastatic potential and differentiation in rhabdomyosarcoma. *Cell Death & Disease,* 9**,** 237.

SAITOU, N. & NEI, M. 1987. The neighbor-joining method: a new method for reconstructing phylogenetic trees. *Molecular biology and evolution,* 4**,** 406-425.

SALAUN, C., GREAVES, J., TOMKINSON, N. C. O. & CHAMBERLAIN, L. H. 2020a. The linker domain of the SNARE protein SNAP25 acts as a flexible molecular spacer that ensures efficient S-acylation. *Journal of Biological Chemistry,* 295**,** 7501-7515.

SALAUN, C., LOCATELLI, C., ZMUDA, F., CABRERA GONZÁLEZ, J. & CHAMBERLAIN, L. H. 2020b. Accessory proteins of the zDHHC family of S-acylation enzymes. *Journal of Cell Science,* 133.

SALAUN, C., RITCHIE, L., GREAVES, J., BUSHELL, T. J. & CHAMBERLAIN, L. H. 2017. The C-terminal domain of zDHHC2 contains distinct sorting signals that regulate intracellular localisation in neurons and neuroendocrine cells. *Mol Cell Neurosci,* 85**,** 235-246.

SALAUN, C., TAKIZAWA, H., GALINDO, A., MUNRO, K. R., MCLELLAN, J., SUGIMOTO, I., OKINO, T., TOMKINSON, N. C. O. & CHAMBERLAIN, L. H. 2022. Development of a novel high-throughput screen for the identification of new inhibitors of protein S-acylation. *J Biol Chem,* 298**,** 102469.

SALAUN, C., TOMKINSON, N. C. O. & CHAMBERLAIN, L. H. 2023. The endoplasmic reticulum–localized enzyme zDHHC6 mediates S-acylation of short transmembrane constructs from multiple type I and II membrane proteins. *Journal of Biological Chemistry,* 299**,** 105201.

SALAÜN, C., GOULD, G. W. & CHAMBERLAIN, L. H. 2005a. Lipid raft association of SNARE proteins regulates exocytosis in PC12 cells. *J Biol Chem,* 280**,** 19449-53.

SALAÜN, C., GOULD, G. W. & CHAMBERLAIN, L. H. 2005b. The SNARE proteins SNAP-25 and SNAP-23 display different affinities for lipid rafts in PC12 cells. Regulation by distinct cysteine-rich domains. *J Biol Chem,* 280**,** 1236-40.

SANDERS, D. W., JUMPER, C. C., ACKERMAN, P. J., BRACHA, D., DONLIC, A., KIM, H., KENNEY, D., CASTELLO-SERRANO, I., SUZUKI, S., TAMURA, T., TAVARES, A. H., SAEED, M., HOLEHOUSE, A. S., PLOSS, A., LEVENTAL, I., DOUAM, F., PADERA, R. F., LEVY, B. D. & BRANGWYNNE, C. P. 2021. SARS-CoV-2 requires cholesterol for viral entry and pathological syncytia formation. *Elife,* 10.

SANDERS, S. S., HERNANDEZ, L. M., SOH, H., KARNAM, S., WALIKONIS, R. S., TZINGOUNIS, A. V. & THOMAS, G. M. 2020. The palmitoyl acyltransferase ZDHHC14 controls Kv1-family potassium channel clustering at the axon initial segment. *Elife,* 9.

SANDERS, S. S., MARTIN, D. D. O., BUTLAND, S. L., LAVALLÉE-ADAM, M., CALZOLARI, D., KAY, C., YATES, J. R., III & HAYDEN, M. R. 2015. Curation of the Mammalian Palmitoylome Indicates a Pivotal Role for Palmitoylation in Diseases and Disorders of the Nervous System and Cancers. *PLOS Computational Biology,* 11**,** e1004405.

SANDERS, S. S., MUI, K. K., SUTTON, L. M. & HAYDEN, M. R. 2014. Identification of binding sites in Huntingtin for the Huntingtin Interacting Proteins HIP14 and HIP14L. *PLoS One,* 9**,** e90669.

SANTOPOLO, S., RICCIO, A. & SANTORO, M. G. 2021. The biogenesis of SARS-CoV-2 spike glycoprotein: multiple targets for host-directed antiviral therapy. *Biochem Biophys Res Commun,* 538**,** 80-87.

SASAKI, T., HIROKI, K. & YAMASHITA, Y. 2013. The role of epidermal growth factor receptor in cancer metastasis and microenvironment. *BioMed research international,* 2013**,** 546318-546318.

SCHLESSINGER, J. 2014. Receptor tyrosine kinases: legacy of the first two decades. *Cold Spring Harbor perspectives in biology,* 6**,** a008912.

SCHMIDT, M. F. & SCHLESINGER, M. J. 1979. Fatty acid binding to vesicular stomatitis virus glycoprotein: a new type of post-translational modification of the viral glycoprotein. *Cell,* 17**,** 813-9.

SCHWARTZ, C. E., LOUIE, R. J., TOUTAIN, A., SKINNER, C., FRIEZ, M. J. & STEVENSON, R. E. 2023. X-Linked intellectual disability update 2022. *American Journal of Medical Genetics Part A,* 191**,** 144-159.

SEHNAL, D., BITTRICH, S., DESHPANDE, M., SVOBODOVÁ, R., BERKA, K., BAZGIER, V., VELANKAR, S., BURLEY, S. K., KOČA, J. & ROSE, A. S. 2021. Mol* Viewer: modern web app for 3D visualization and analysis of large biomolecular structures. *Nucleic Acids Research,* 49**,** W431-W437.

SENICHKIN, V. V., PROKHOROVA, E. A., ZHIVOTOVSKY, B. & KOPEINA, G. S. 2021. Simple and Efficient Protocol for Subcellular Fractionation of Normal and Apoptotic Cells. *Cells,* 10.

SEZGIN, E., LEVENTAL, I., MAYOR, S. & EGGELING, C. 2017. The mystery of membrane organization: composition, regulation and roles of lipid rafts. *Nature Reviews Molecular Cell Biology,* 18**,** 361-374.

SHAH, B. S., SHIMELL, J. J. & BAMJI, S. X. 2019. Regulation of dendrite morphology and excitatory synapse formation by zDHHC15. *J Cell Sci,* 132.

SHARMA, C., YANG, X. H. & HEMLER, M. E. 2008. DHHC2 affects palmitoylation, stability, and functions of tetraspanins CD9 and CD151. *Mol Biol Cell,* 19**,** 3415-25.

SHARMA, P., SARAYA, A. & SHARMA, R. 2016. Potential diagnostic implications of miR-144 overexpression in human oesophageal cancer. *Indian J Med Res,* 143**,** S91-s103.

SHEIKH, E., TRAN, T., VRANIC, S., LEVY, A. & BONFIL, R. D. 2022. Role and significance of c-KIT receptor tyrosine kinase in cancer: A review. *Bosn J Basic Med Sci,* 22**,** 683-698.

SHI, W., WANG, F., GAO, M., YANG, Y., DU, Z., WANG, C., YAO, Y., HE, K., CHEN, X. & HAO, A. 2015. ZDHHC17 promotes axon outgrowth by regulating TrkA–tubulin complex formation. *Molecular and Cellular Neuroscience,* 68**,** 194-202.

SHIMELL, J. J., GLOBA, A., SEPERS, M. D., WILD, A. R., MATIN, N., RAYMOND, L. A. & BAMJI, S. X. 2021. Regulation of hippocampal excitatory synapses by the Zdhhc5 palmitoyl acyltransferase. *J Cell Sci,* 134.

SHIMELL, J. J., SHAH, B. S., CAIN, S. M., THOUTA, S., KUHLMANN, N., TATARNIKOV, I., JOVELLAR, D. B., BRIGIDI, G. S., KASS, J., MILNERWOOD, A. J., SNUTCH, T. P. & BAMJI, S. X. 2019. The X-Linked Intellectual Disability Gene Zdhhc9 Is Essential for Dendrite Outgrowth and Inhibitory Synapse Formation. *Cell Rep,* 29**,** 2422-2437.e8.

SHIN, E. H., ZHAO, G., WANG, Q. & LOVICU, F. J. 2015. Sprouty gain of function disrupts lens cellular processes and growth by restricting RTK signaling. *Developmental Biology,* 406**,** 129-146.

SIMONATI, A. & WILLIAMS, R. E. 2022. Neuronal Ceroid Lipofuscinosis: The Multifaceted Approach to the Clinical Issues, an Overview. *Front Neurol,* 13**,** 811686.

SINGARAJA, R. R., HADANO, S., METZLER, M., GIVAN, S., WELLINGTON, C. L., WARBY, S., YANAI, A., GUTEKUNST, C.-A., LEAVITT, B. R., YI, H., FICHTER, K., GAN, L., MCCUTCHEON, K., CHOPRA, V., MICHEL, J., HERSCH, S. M., IKEDA, J.-E. & HAYDEN, M. R. 2002. HIP14, a novel ankyrin domain-containing protein, links huntingtin to intracellular trafficking and endocytosis. *Human Molecular Genetics,* 11**,** 2815-2828.

SINGARAJA, R. R., HUANG, K., SANDERS, S. S., MILNERWOOD, A. J., HINES, R., LERCH, J. P., FRANCIOSI, S., DRISDEL, R. C., VAID, K., YOUNG, F. B., DOTY, C., WAN, J., BISSADA, N., HENKELMAN, R. M., GREEN, W. N., DAVIS, N. G., RAYMOND, L. A. & HAYDEN, M. R. 2011. Altered palmitoylation and neuropathological deficits in mice lacking HIP14. *Hum Mol Genet,* 20**,** 3899-909.

SIRIVATANAUKSORN, Y., SIRIVATANAUKSORN, V., SRISAWAT, C., KHONGMANEE, A. & TONGKHAM, C. 2012. Differential expression of sprouty genes in hepatocellular carcinoma. *Journal of Surgical Oncology,* 105**,** 273-276.

SOBOCIŃSKA, J., ROSZCZENKO-JASIŃSKA, P., CIESIELSKA, A. & KWIATKOWSKA, K. 2017. Protein Palmitoylation and Its Role in Bacterial and Viral Infections. *Front Immunol,* 8**,** 2003.

SONG, L. & LUO, Z. Q. 2019. Post-translational regulation of ubiquitin signaling. *J Cell Biol,* 218**,** 1776-1786.

SOYOMBO, A. A. & HOFMANN, S. L. 1997. Molecular cloning and expression of palmitoyl-protein thioesterase 2 (PPT2), a homolog of lysosomal palmitoyl-protein thioesterase with a distinct substrate specificity. *J Biol Chem,* 272**,** 27456-63.

SPURLOCK, G., BENNETT, E., CHUZHANOVA, N., THOMAS, N., JIM, H.-P., SIDE, L., DAVIES, S., HAAN, E., KERR, B., HUSON, S. M. & UPADHYAYA, M. 2009. SPRED1 mutations (Legius syndrome): another clinically useful genotype for dissecting the neurofibromatosis type 1 phenotype. *Journal of Medical Genetics,* 46**,** 431-437.

ST-GERMAIN, J. R., ASTORI, A., SAMAVARCHI-TEHRANI, P., ABDOUNI, H., MACWAN, V., KIM, D.-K., KNAPP, J. J., ROTH, F. P., GINGRAS, A.-C. & RAUGHT, B. 2020. A SARS-CoV-2 BioID-based virus-host membrane protein interactome and virus peptide compendium: new proteomics resources for COVID-19 research. *bioRxiv***,** 2020.08.28.269175.

STARK, C., BREITKREUTZ, B. J., REGULY, T., BOUCHER, L., BREITKREUTZ, A. & TYERS, M. 2006. BioGRID: a general repository for interaction datasets. *Nucleic Acids Res,* 34**,** D535-9.

STOWE, I. B., MERCADO, E. L., STOWE, T. R., BELL, E. L., OSES-PRIETO, J. A., HERNÁNDEZ, H., BURLINGAME, A. L. & MCCORMICK, F. 2012. A shared molecular mechanism underlies the human rasopathies Legius syndrome and Neurofibromatosis-1. *Genes Dev,* 26**,** 1421-6.

STOWERS, R. S. & ISACOFF, E. Y. 2007. Drosophila huntingtin-interacting protein 14 is a presynaptic protein required for photoreceptor synaptic transmission and expression of the palmitoylated proteins synaptosome-associated protein 25 and cysteine string protein. *J Neurosci,* 27**,** 12874-83.

SUN, S., KARKI, C., AGUILERA, J., LOPEZ HERNANDEZ, A. E., SUN, J. & LI, L. 2021. Computational Study on the Function of Palmitoylation on the Envelope Protein in SARS-CoV-2. *J Chem Theory Comput,* 17**,** 6483-6490.

SUNG, H., FERLAY, J., SIEGEL, R. L., LAVERSANNE, M., SOERJOMATARAM, I., JEMAL, A. & BRAY, F. 2021. Global Cancer Statistics 2020: GLOBOCAN Estimates of Incidence and Mortality Worldwide for 36 Cancers in 185 Countries. *CA: A Cancer Journal for Clinicians,* 71**,** 209-249.

SUTHERLAND, D., SAMAKOVLIS, C. & KRASNOW, M. A. 1996. branchless Encodes a Drosophila FGF Homolog That Controls Tracheal Cell Migration and the Pattern of Branching. *Cell,* 87**,** 1091-1101.

SUTTON, L. M., SANDERS, S. S., BUTLAND, S. L., SINGARAJA, R. R., FRANCIOSI, S., SOUTHWELL, A. L., DOTY, C. N., SCHMIDT, M. E., MUI, K. K., KOVALIK, V., YOUNG, F. B., ZHANG, W. & HAYDEN, M. R. 2013. Hip14l-deficient mice develop neuropathological and behavioural features of Huntington disease. *Hum Mol Genet,* 22**,** 452-65.

SVIRIDOV, D., MUKHAMEDOVA, N. & MILLER, Y. I. 2020. Lipid rafts as a therapeutic target. *J Lipid Res,* 61**,** 687-695.

SWARBRICK, C. M. D., NANSON, J. D., PATTERSON, E. I. & FORWOOD, J. K. 2020. Structure, function, and regulation of thioesterases. *Progress in Lipid Research,* 79**,** 101036.

SWARTHOUT, J. T., LOBO, S., FARH, L., CROKE, M. R., GREENTREE, W. K., DESCHENES, R. J. & LINDER, M. E. 2005. DHHC9 and GCP16 constitute a human protein fatty acyltransferase with specificity for H- and N-Ras. *J Biol Chem,* 280**,** 31141-8.

SZKLARCZYK, D., GABLE, A. L., LYON, D., JUNGE, A., WYDER, S., HUERTA-CEPAS, J., SIMONOVIC, M., DONCHEVA, N. T., MORRIS, J. H., BORK, P., JENSEN, L. J. & MERING, C. V. 2019. STRING v11: protein-protein association networks with increased coverage, supporting functional discovery in genome-wide experimental datasets. *Nucleic Acids Res,* 47**,** D607-d613.

TAN, E., CHIN, C. S. H., LIM, Z. F. S. & NG, S. K. 2021. HEK293 Cell Line as a Platform to Produce Recombinant Proteins and Viral Vectors. *Front Bioeng Biotechnol,* 9**,** 796991.

TAYLOR, J. K., COLEMAN, C. M., POSTEL, S., SISK, J. M., BERNBAUM, J. G., VENKATARAMAN, T., SUNDBERG, E. J. & FRIEMAN, M. B. 2015. Severe Acute Respiratory Syndrome Coronavirus ORF7a Inhibits Bone Marrow Stromal Antigen 2 Virion Tethering through a Novel Mechanism of Glycosylation Interference. *J Virol,* 89**,** 11820-33.

TENNIS, M. A., VAN SCOYK, M. M., FREEMAN, S. V., VANDERVEST, K. M., NEMENOFF, R. A. & WINN, R. A. 2010. Sprouty-4 Inhibits Transformed Cell Growth, Migration and Invasion, and Epithelial-Mesenchymal Transition, and Is Regulated by Wnt7A through PPARγ in Non–Small Cell Lung Cancer. *Molecular Cancer Research,* 8**,** 833-843.

THOMAS, GARETH M., HAYASHI, T., CHIU, S.-L., CHEN, C.-M. & HUGANIR, RICHARD L. 2012. Palmitoylation by DHHC5/8 Targets GRIP1 to Dendritic Endosomes to Regulate AMPA-R Trafficking. *Neuron,* 73**,** 482-496.

TIAN, L., JEFFRIES, O., MCCLAFFERTY, H., MOLYVDAS, A., ROWE, I. C., SALEEM, F., CHEN, L., GREAVES, J., CHAMBERLAIN, L. H., KNAUS, H. G., RUTH, P. & SHIPSTON, M. J. 2008. Palmitoylation gates phosphorylation-dependent regulation of BK potassium channels. *Proc Natl Acad Sci U S A,* 105**,** 21006-11.

TIAN, L., MCCLAFFERTY, H., JEFFRIES, O. & SHIPSTON, M. J. 2010. Multiple palmitoyltransferases are required for palmitoylation-dependent regulation of large conductance calcium- and voltage-activated potassium channels. *J Biol Chem,* 285**,** 23954-62.

TIAN, L., MCCLAFFERTY, H., KNAUS, H. G., RUTH, P. & SHIPSTON, M. J. 2012. Distinct acyl protein transferases and thioesterases control surface expression of calcium-activated potassium channels. *J Biol Chem,* 287**,** 14718-25.

TIASH, S. & CHOWDHURY, E. H. 2015. Growth factor receptors: promising drug targets in cancer. *Journal of Cancer Metastasis and Treatment,* 1**,** 190-200.

TO, K. K., SRIDHAR, S., CHIU, K. H., HUNG, D. L., LI, X., HUNG, I. F., TAM, A. R., CHUNG, T. W., CHAN, J. F., ZHANG, A. J., CHENG, V. C. & YUEN, K. Y. 2021. Lessons learned 1 year after SARS-CoV-2 emergence leading to COVID-19 pandemic. *Emerg Microbes Infect,* 10**,** 507-535.

TOMATIS, V. M., TRENCHI, A., GOMEZ, G. A. & DANIOTTI, J. L. 2010. Acyl-protein thioesterase 2 catalyzes the deacylation of peripheral membrane-associated GAP-43. *PLoS One,* 5**,** e15045.

TORTOSA, E., ADOLFS, Y., FUKATA, M., PASTERKAMP, R. J., KAPITEIN, L. C. & HOOGENRAAD, C. C. 2017. Dynamic Palmitoylation Targets MAP6 to the Axon to Promote Microtubule Stabilization during Neuronal Polarization. *Neuron,* 94**,** 809-825.e7.

TOYODA, T., SUGIMOTO, H. & YAMASHITA, S. 1999. Sequence, expression in Escherichia coli, and characterization of lysophospholipase II1The nucleotide sequence data reported in this paper have been submitted to the GenBank/EMBL/DDBJ Nucleotide Sequence Databases under the accession number AB009653.1. *Biochimica et Biophysica Acta (BBA) - Molecular and Cell Biology of Lipids,* 1437**,** 182-193.

UDENWOBELE, D. I., SU, R.-C., GOOD, S. V., BALL, T. B., VARMA SHRIVASTAV, S. & SHRIVASTAV, A. 2017. Myristoylation: An Important Protein Modification in the Immune Response. *Frontiers in Immunology,* 8.

VARADI, M., ANYANGO, S., DESHPANDE, M., NAIR, S., NATASSIA, C., YORDANOVA, G., YUAN, D., STROE, O., WOOD, G., LAYDON, A., ŽÍDEK, A., GREEN, T., TUNYASUVUNAKOOL, K., PETERSEN, S., JUMPER, J., CLANCY, E., GREEN, R., VORA, A., LUTFI, M., FIGURNOV, M., COWIE, A., HOBBS, N., KOHLI, P., KLEYWEGT, G., BIRNEY, E., HASSABIS, D. & VELANKAR, S. 2022. AlphaFold Protein Structure Database: massively expanding the structural coverage of protein-sequence space with high-accuracy models. *Nucleic Acids Res,* 50**,** D439-d444.

VARTAK, N., PAPKE, B., GRECCO, HERNAN E., ROSSMANNEK, L., WALDMANN, H., HEDBERG, C. & BASTIAENS, PHILIPPE I. H. 2014. The Autodepalmitoylating

Activity of APT Maintains the Spatial Organization of Palmitoylated Membrane Proteins. *Biophysical Journal,* 106**,** 93-105.

VELINOV, M., DOLZHANSKAYA, N., GONZALEZ, M., POWELL, E., KONIDARI, I., HULME, W., STAROPOLI, J. F., XIN, W., WEN, G. Y., BARONE, R., COPPEL, S. H., SIMS, K., BROWN, W. T. & ZÜCHNER, S. 2012. Mutations in the gene DNAJC5 cause autosomal dominant Kufs disease in a proportion of cases: study of the Parry family and 8 other families. *PLoS One,* 7**,** e29729.

VELTMAN, D. M. & INSALL, R. H. 2010. WASP Family Proteins: Their Evolution and Its Physiological Implications. *Molecular Biology of the Cell,* 21**,** 2880-2893.

VERARDI, R., KIM, J.-S., GHIRLANDO, R., BANERJEE, A. & BANERJEE, A. 2017. Structural Basis for Substrate Recognition by the Ankyrin Repeat Domain of Human DHHC17 Palmitoyltransferase. *Structure (London, England : 1993),* 25**,** 1337-1347.e6.

VERKRUYSE, L. A. & HOFMANN, S. L. 1996. Lysosomal targeting of palmitoyl-protein thioesterase. *J Biol Chem,* 271**,** 15831-6.

VESA, J., HELLSTEN, E., VERKRUYSE, L. A., CAMP, L. A., RAPOLA, J., SANTAVUORI, P., HOFMANN, S. L. & PELTONEN, L. 1995. Mutations in the palmitoyl protein thioesterase gene causing infantile neuronal ceroid lipofuscinosis. *Nature,* 376**,** 584-7.

VILMEN, G., BANERJEE, A. & FREED, E. O. 2021. Rafting through the palms: S-acylation of SARS-CoV-2 spike protein induces lipid reorganization. *Dev Cell,* 56**,** 2787-2789.

VOGEL, K. & ROCHE, P. A. 1999. SNAP-23 and SNAP-25 Are Palmitoylatedin Vivo. *Biochemical and Biophysical Research Communications,* 258**,** 407-410.

WAKIOKA, T., SASAKI, A., KATO, R., SHOUDA, T., MATSUMOTO, A., MIYOSHI, K., TSUNEOKA, M., KOMIYA, S., BARON, R. & YOSHIMURA, A. 2001. Spred is a Sprouty-related suppressor of Ras signalling. *Nature,* 412**,** 647-651.

WALKER, D. J. & LAND, S. C. 2018. Regulation of vascular signalling by nuclear Sprouty2 in fetal lung epithelial cells: Implications for co-ordinated airway and vascular branching in lung development. *Comp Biochem Physiol B Biochem Mol Biol,* 224**,** 105-114.

WALSH, A. M. & LAZZARA, M. J. 2013. Regulation of EGFR trafficking and cell signaling by Sprouty2 and MIG6 in lung cancer cells. *Journal of Cell Science,* 126**,** 4339.

WANG, B., DAI, T., SUN, W., WEI, Y., REN, J., ZHANG, L., ZHANG, M. & ZHOU, F. 2021a. Protein N-myristoylation: functions and mechanisms in control of innate immunity. *Cellular & Molecular Immunology,* 18**,** 878-888.

WANG, C., DELOGU, S., HO, C., LEE, S. A., GUI, B., JIANG, L., LADU, S., CIGLIANO, A., DOMBROWSKI, F., EVERT, M., CALVISI, D. F. & CHEN, X. 2012. Inactivation of Spry2 accelerates AKT-driven hepatocarcinogenesis via activation of MAPK and PKM2 pathways. *J Hepatol,* 57**,** 577-83.

WANG, L., WANG, N., ZHANG, W., CHENG, X., YAN, Z., SHAO, G., WANG, X., WANG, R. & FU, C. 2022. Therapeutic peptides: current applications and future directions. *Signal Transduction and Targeted Therapy,* 7**,** 48.

WANG, M. & CASEY, P. J. 2016. Protein prenylation: unique fats make their mark on biology. *Nature Reviews Molecular Cell Biology,* 17**,** 110-122.

WANG, W., BEIRD, H., KROLL, C. J., HU, S., BUESO-RAMOS, C. E., FANG, H., TANG, G., TANG, Z., WANG, F., TAKAHASHI, K., YOU, M. J., KHOURY, J. D., MEDEIROS, L. J. & FUTREAL, P. A. 2020. T(6;14)(q25;q32) involves BCL11B and is highly associated with mixed-phenotype acute leukemia, T/myeloid. *Leukemia,* 34**,** 2509-2512.

WANG, Y., GUO, S., ZHUANG, Y., YUN, Y., XU, P., HE, X., GUO, J., YIN, W., XU, H. E., XIE, X. & JIANG, Y. 2021b. Molecular recognition of an acyl-peptide hormone and activation of ghrelin receptor. *Nature Communications,* 12**,** 5064.

WANG, Y.-H. & BECK, C. W. 2014. Distal expression of sprouty (spry) genes during Xenopus laevis limb development and regeneration. *Gene Expression Patterns,* 15**,** 61-66.

WEST, S. J., BOEHNING, D. & AKIMZHANOV, A. M. 2022. Regulation of T cell function by protein S-acylation. *Frontiers in Physiology,* 13.

WILKINS, M. R., GASTEIGER, E., BAIROCH, A., SANCHEZ, J. C., WILLIAMS, K. L., APPEL, R. D. & HOCHSTRASSER, D. F. 1999. Protein identification and analysis tools in the ExPASy server. *Methods Mol Biol,* 112**,** 531-52.

WON, S. J., CHEUNG SEE KIT, M. & MARTIN, B. R. 2018. Protein depalmitoylases. *Critical Reviews in Biochemistry and Molecular Biology,* 53**,** 83-98.

WONG, E. S., FONG, C. W., LIM, J., YUSOFF, P., LOW, B. C., LANGDON, W. Y. & GUY, G. R. 2002. Sprouty2 attenuates epidermal growth factor receptor ubiquitylation and endocytosis, and consequently enhances Ras/ERK signalling. *Embo j,* 21**,** 4796-808.

WU, C., LIU, Y., YANG, Y., ZHANG, P., ZHONG, W., WANG, Y., WANG, Q., XU, Y., LI, M., LI, X., ZHENG, M., CHEN, L. & LI, H. 2020. Analysis of therapeutic targets for SARS-CoV-2 and discovery of potential drugs by computational methods. *Acta Pharm Sin B,* 10**,** 766-788.

WU, Z., ZHANG, Z., WANG, X., ZHANG, J., REN, C., LI, Y., GAO, L., LIANG, X., WANG, P. & MA, C. 2021. Palmitoylation of SARS-CoV-2 S protein is essential for viral infectivity. *Signal Transduction and Targeted Therapy,* 6**,** 231.

XU, Y. F., LIU, H. D., LIU, Z. L., PAN, C., YANG, X. Q., NING, S. L., ZHANG, Z. L., GUO, S. & YU, J. M. 2018. Sprouty2 suppresses progression and correlates to favourable prognosis of intrahepatic cholangiocarcinoma via antagonizing FGFR2 signalling. *J Cell Mol Med,* 22**,** 5596-5606.

YANAI, A., HUANG, K., KANG, R., SINGARAJA, R. R., ARSTIKAITIS, P., GAN, L., ORBAN, P. C., MULLARD, A., COWAN, C. M., RAYMOND, L. A., DRISDEL, R. C., GREEN, W. N., RAVIKUMAR, B., RUBINSZTEIN, D. C., EL-HUSSEINI, A. &

HAYDEN, M. R. 2006. Palmitoylation of huntingtin by HIP14 is essential for its trafficking and function. *Nature neuroscience,* 9**,** 824-831.

YANG, G. & CYNADER, M. S. 2011. Palmitoyl acyltransferase zD17 mediates neuronal responses in acute ischemic brain injury by regulating JNK activation in a signaling module. *J Neurosci,* 31**,** 11980-91.

YANG, H., ZHANG, G. & CUI, J. 2015. BK channels: multiple sensors, one activation gate. *Front Physiol,* 6**,** 29.

YANG, Q., ZHENG, F., HU, Y., YANG, Y., LI, Y., CHEN, G., WANG, W., HE, M., ZHOU, R., MA, Y., XU, D., TIAN, X., GAO, X., WANG, Q. & WANG, X. 2018. ZDHHC8 critically regulates seizure susceptibility in epilepsy. *Cell Death & Disease,* 9**,** 795.

YANG, Z. R., JIANG, Y. W., LI, F. X., LIU, D., LIN, T. F., ZHAO, Z. Y., WEI, C., JIN, Q. Y., LI, X. M., JIA, Y. X., ZHU, F. C., YANG, Z. Y., SHA, F., FENG, Z. J. & TANG, J. L. 2023. Efficacy of SARS-CoV-2 vaccines and the dose-response relationship with three major antibodies: a systematic review and meta-analysis of randomised controlled trials. *Lancet Microbe,* 4**,** e236-e246.

YARDEN, Y., KUANG, W. J., YANG-FENG, T., COUSSENS, L., MUNEMITSU, S., DULL, T. J., CHEN, E., SCHLESSINGER, J., FRANCKE, U. & ULLRICH, A. 1987. Human proto-oncogene c-kit: a new cell surface receptor tyrosine kinase for an unidentified ligand. *Embo j,* 6**,** 3341-51.

YEH, D. C., DUNCAN, J. A., YAMASHITA, S. & MICHEL, T. 1999. Depalmitoylation of endothelial nitric-oxide synthase by acyl-protein thioesterase 1 is potentiated by Ca(2+)-calmodulin. *J Biol Chem,* 274**,** 33148-54.

YESTE-VELASCO, M., LINDER, M. E. & LU, Y. J. 2015. Protein S-palmitoylation and cancer. *Biochim Biophys Acta,* 1856**,** 107-20.

YESTE-VELASCO, M., MAO, X., GROSE, R., KUDAHETTI, S. C., LIN, D., MARZEC, J., VASILJEVIĆ, N., CHAPLIN, T., XUE, L., XU, M., FOSTER, J. M., KARNAM, S. S., JAMES, S. Y., CHIONI, A.-M., GOULD, D., LORINCZ, A. T., OLIVER, R. T. D., CHELALA, C., THOMAS, G. M., SHIPLEY, J. M., MATHER, S. J., BERNEY, D. M.,

YOUNG, B. D. & LU, Y.-J. 2014. Identification of ZDHHC14 as a novel human tumour suppressor gene. *The Journal of Pathology,* 232**,** 566-577.

YIGZAW, Y., CARTIN, L., PIERRE, S., SCHOLICH, K. & PATEL, T. B. 2001. The C Terminus of Sprouty Is Important for Modulation of Cellular Migration and Proliferation*. *Journal of Biological Chemistry,* 276**,** 22742-22747.

YIM, D. G., GHOSH, S., GUY, G. R. & VIRSHUP, D. M. 2015. Casein kinase 1 regulates Sprouty2 in FGF-ERK signaling. *Oncogene,* 34**,** 474-84.

YOON, J. W., LIU, C. Z., YANG, J. T., SWART, R., IANNACCONE, P. & WALTERHOUSE, D. 1998. GLI Activates Transcription through a Herpes Simplex Viral Protein 16-Like Activation Domain *. *Journal of Biological Chemistry,* 273**,** 3496-3501.

YOUNG, J., XU, C., PAPADAKIS, G. E., ACIERNO, J. S., MAIONE, L., HIETAMÄKI, J., RAIVIO, T. & PITTELOUD, N. 2019. Clinical Management of Congenital Hypogonadotropic Hypogonadism. *Endocrine Reviews,* 40**,** 669-710.

YOUSAF, R., AHMED, Z. M., GIESE, A. P., MORELL, R. J., LAGZIEL, A., DABDOUB, A., WILCOX, E. R., RIAZUDDIN, S., FRIEDMAN, T. B. & RIAZUDDIN, S. 2018. Modifier variant of METTL13 suppresses human GAB1-associated profound deafness. *The Journal of clinical investigation,* 128**,** 1509-1522.

YU, L., READER, J. C., CHEN, C., ZHAO, X. F., HA, J. S., LEE, C., YORK, T., GOJO, I., BAER, M. R. & NING, Y. 2011. Activation of a novel palmitoyltransferase ZDHHC14 in acute biphenotypic leukemia and subsets of acute myeloid leukemia. *Leukemia,* 25**,** 367-371.

ZANETTI, L., REGONI, M., RATTI, E., VALTORTA, F. & SASSONE, J. 2021. Presynaptic AMPA Receptors in Health and Disease. *Cells,* 10.

ZHA, J., WEILER, S., OH, K. J., WEI, M. C. & KORSMEYER, S. J. 2000. Posttranslational N-Myristoylation of BID as a Molecular Switch for Targeting Mitochondria and Apoptosis. *Science,* 290**,** 1761-1765.

ZHANG, M. M. & HANG, H. C. 2017. Protein S-palmitoylation in cellular differentiation. *Biochem Soc Trans,* 45**,** 275-285.

ZINGLER, P., SÄRCHEN, V., GLATTER, T., CANING, L., SAGGAU, C., KATHAYAT, R. S., DICKINSON, B. C., ADAM, D., SCHNEIDER-BRACHERT, W., SCHÜTZE, S. & FRITSCH, J. 2019. Palmitoylation is required for TNF-R1 signaling. *Cell Communication and Signaling,* 17**,** 90.

ZINSMAIER, K. E., HOFBAUER, A., HEIMBECK, G., PFLUGFELDER, G. O., BUCHNER, S. & BUCHNER, E. 1990. A Cysteine-String Protein is Expressed in Retina and Brain of Drosophila. *Journal of Neurogenetics,* 7**,** 15-29.

ZMUDA, F. & CHAMBERLAIN, L. H. 2020. Regulatory effects of post-translational modifications on zDHHC S-acyltransferases. *J Biol Chem,* 295**,** 14640-14652.

# Appendix I

## FORMING THE CONNECTION BETWEEN ZDHHC17 AND SPROUTY/SPRED PROTEINS

[1]Strathclyde Institute of Pharmacy and Biomedical Sciences, University of Strathclyde, Glasgow, Scotland, UK

[1]Liam Butler, [1]Carolina Locatelli, [1]Christine Salaun, [1]Desponia Alligioti and [1]Luke Chamberlain

University of Strathclyde Glasgow

### BACKGROUND

**Relevance** Sprouty (Spry)/SPRED proteins are important regulators of the MAPK/ERK signaling pathway, and dysregulation of this pathway is known to contribute to the progression of cancer.

**Concept** The defining feature of Spry/SPRED proteins is a highly conserved SPR domain/cysteine-rich domain (CRD); which for Spry2 contains 26 cysteine residues. Recent work has shown that this domain in Spry2 and SPRED3 is S-acylated (palmitoylated) by zDHHC17. However, the mechanism of action does not follow typical binding to the known zDHHC17 ankyrin binding consensus motif (VIAP)(VIT)XXQP (known as zDABM)

**Aim** The aim of the current research is to identify and understand the interaction between zDHHC17 and Spry/SPRED proteins, and to uncover the functional consequences of this interaction.

### WORKFLOW OF MAIN TECHNIQUES

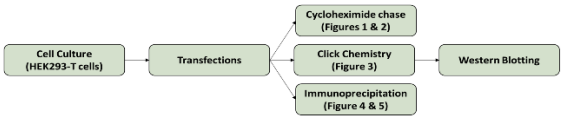


### RESULTS 1

**Figure 1: The zDHHC17 acyltransferase is more stable in the presence of Spry2 protein**

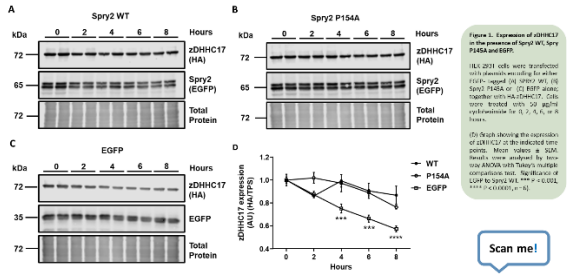


Whats going on?

Cycloheximide inhibits protein synthesis and less stable proteins will degrade faster than more stable ones.

In the top panels (HA-zD17) of **figures 1 & 2.** The band intensity relates to the expression of zDHHC17. The quicker the band disappears, then the less stable the protein is!

Scan me!

Check out our previously published work on this topic! Including the results which show the role of NDK in the stabilisation and S-acylation of Spry2 (Figure 7)

**Figure 2: zDHHC17 stability is not affected by SPRED proteins and the stabilisation effect of Spry2 is abrogated by the tripeptide NDK mutation**

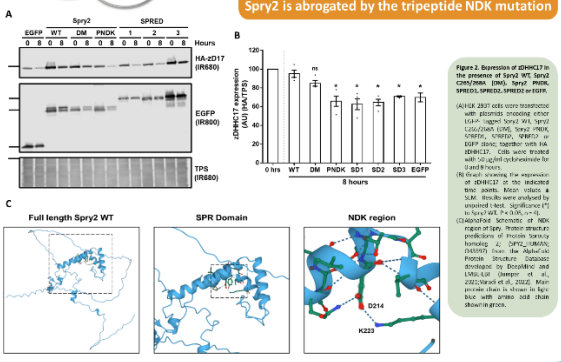


### RESULTS 2

**Figure 3: The S-acylation of SPRED3 by zDHHC17 occurs in the SPR domain**

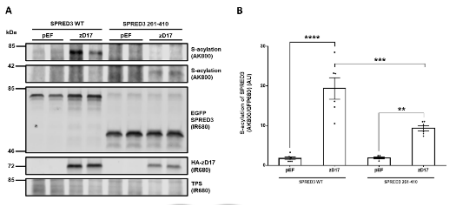


Whats going on?

Cu(I)-catalysed azide-alkyne click chemistry reaction for the fluorescent detection of S-acylated proteins.

In the top panel (S-acylation) of figure 3A. The band intensity relates to the S-acylation of SPRED3 protein. The more intense the band, then the more S-acylation that has occurred!

**Figure 4: The SPR domain of SPRED3 is sufficient to bind to zDHHC17**

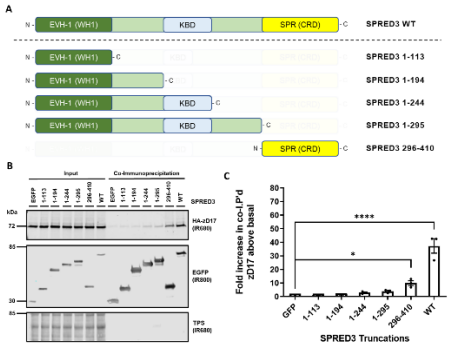


Whats going on?

GFP-trap co-immunoprecipitation allows for the indirect capture of proteins that bind to GFP-tagged proteins. In this case, the level of zDHHC17 captured is being investigated

In the top (HA-zD17) panels of figures 4 & 5. Band intensity relates to the expression of co-immunoprecipitated zD17. The more intense the HA-band, then the more zD17 that binds to its relative GFP band (Spry/SPRED)

**Figure 5: SPRED3 does not bind to zDHHC17 via the Ank repeat domain**

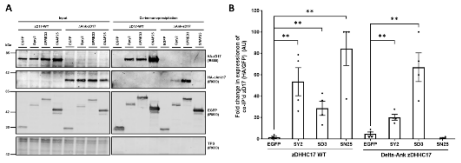


liambutler4
Connect
@LiamButler49
l.butler@strath.ac.uk

### MAIN CONCLUSIONS

1. Spry2 specifically has a more complex interaction with zD17 than similar SPRED proteins. The designated "NDK region" within the SPR domain is crucial for both the S-acylation and stabilisation of Spry2; but also has a reciprocal stabilisation for the stability of zD17.
2. The zD17-SPRED3 binding site coupled to interaction and/or S-acylation; occurs between the conserved SPR domain of SPRED3 and a region of zD17, not contained within the Ankyrin repeat domain.

# Appendix II

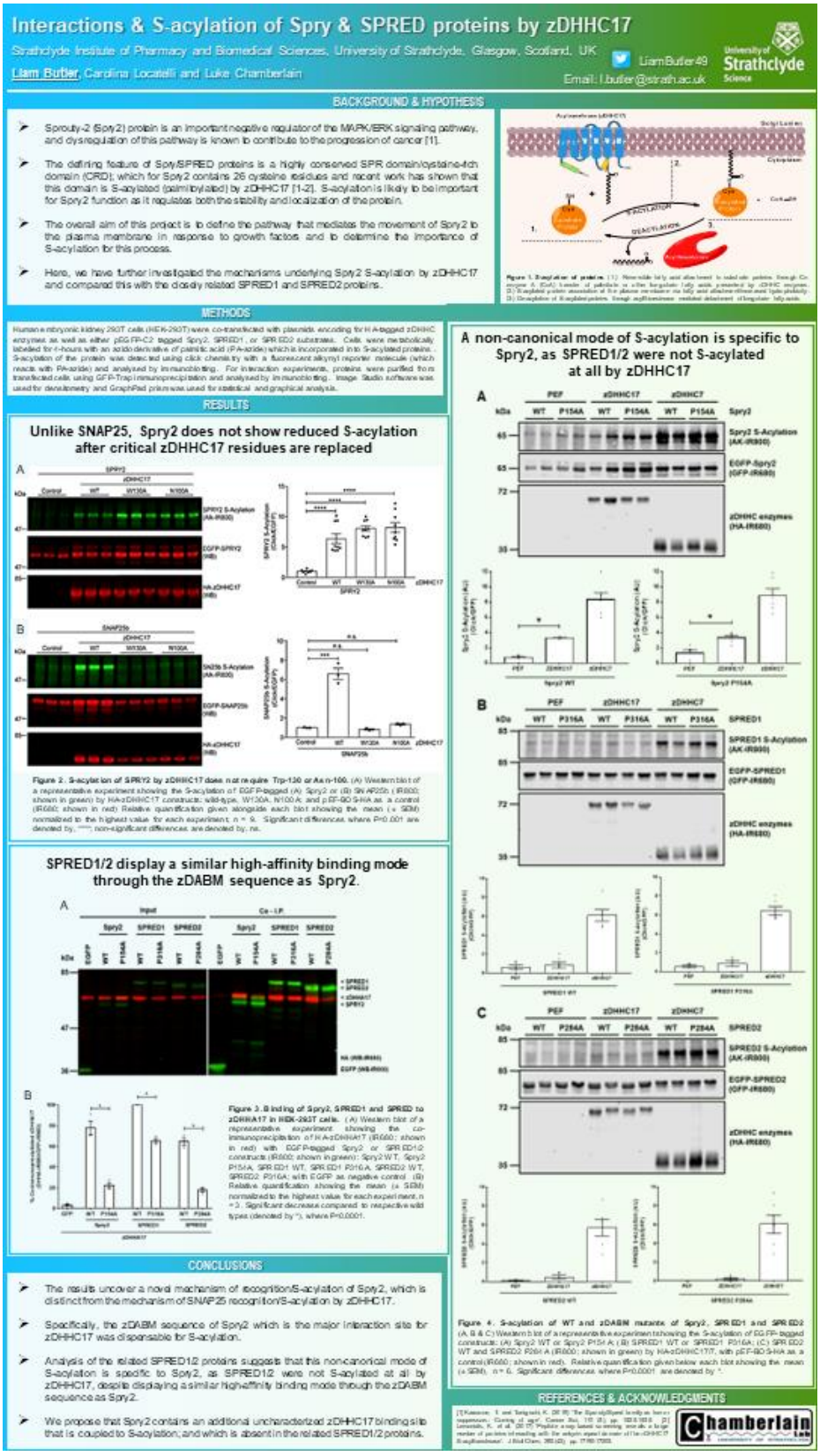
Interactions & S-acylation of Spry & SPRED proteins by zDHHC17
Strathclyde Institute of Pharmacy and Biomedical Sciences, University of Strathclyde, Glasgow, Scotland, UK
Liam Butler, Cardina Locatelli and Luke Chamberlain
LiamButler49
Email: l.butler@strath.ac.uk
University of Strathclyde
BACKGROUND & HYPOTHESIS
Sprouty-2 (Spry2) protein is an important negative regulator of the MAPK/ERK signaling pathway, and dysregulation of this pathway is known to contribute to the progression of cancer [1].
The defining feature of Spry/SPRED proteins is a highly conserved SPR domain/cysteine-rich domain (CRD), which for Spry2 contains 26 cysteine residues and recent work has shown that this domain is S-acylated (palmitoylated) by zDHHC17 [1-2]. S-acylation is likely to be important for Spry2 function as it regulates both the stability and localization of the protein.
The overall aim of this project is to define the pathway that mediates the movement of Spry2 to the plasma membrane in response to growth factors and to determine the importance of S-acylation for this process.
Here, we have further investigated the mechanisms underlying Spry2 S-acylation by zDHHC17 and compared this with the closely related SPRED1 and SPRED2 proteins.
METHODS
RESULTS
Unlike SNAP25, Spry2 does not show reduced S-acylation after critical zDHHC17 residues are replaced
SPRED1/2 display a similar high-affinity binding mode through the zDABM sequence as Spry2.
CONCLUSIONS
The results uncover a novel mechanism of recognition/S-acylation of Spry2, which is distinct from the mechanism of SNAP25 recognition/S-acylation by zDHHC17.
Specifically, the zDABM sequence of Spry2 which is the major interaction site for zDHHC17 was dispensable for S-acylation.
Analysis of the related SPRED1/2 proteins suggests that this non-canonical mode of S-acylation is specific to Spry2, as SPRED1/2 were not S-acylated at all by zDHHC17, despite displaying a similar high-affinity binding mode through the zDABM sequence as Spry2.
We propose that Spry2 contains an additional uncharacterized zDHHC17 binding site that is coupled to S-acylation, and which is absent in the related SPRED1/2 proteins.
A non-canonical mode of S-acylation is specific to Spry2, as SPRED1/2 were not S-acylated at all by zDHHC17
REFERENCES & ACKNOWLEDGMENTS
Chamberlain Lab